# DIFFRACTION OF ANTI-PLANE (SH) WAVES BY SURFACE ELLIPTICAL TOPOGRAPHIES IN AN ELASTIC HALF-SPACE

by

Alongkorn Amornwongpaibun

---

A Dissertation Presented to the
FACULTY OF THE USC GRADUATE SCHOOL
UNIVERSITY OF SOUTHERN CALIFORNIA
In Partial Fulfillment of the
Requirements for the Degree
DOCTOR OF PHILOSOPHY
(CIVIL ENGINEERING)

December 2011





ProQuest LLC.
789 East Eisenhower Parkway
P.O. Box 1346
Ann Arbor, MI 48106 - 1346

# ACKNOWLEDGEMENTS

The time I spent at University of Southern California “USC” was very fruitful and memorable. First and foremost, I would like to acknowledge the steady guidance and encouragement of my research adviser Professor V.W. Lee, who treated me like family and took very good care of me. His intuition on scientific problems is incredible. At every stage of this work, he provided timely and insightful advice and made sure that I was in the right direction. I thank him for being an excellent adviser and am already looking forward to working with him after I leave USC.

I am also deeply grateful to my dissertation committee members Professor H.L. Wong, and Professor F.E. Udwadia who have provided kind encouragement over the years. As well I am thankful to my various faculties at USC, particularly Professor J.C. Anderson, Professor J.J. Lee, Professor M.D. Trifunac and Professor Y. Xiao. I would also like to thank my uncle Dr. Phuvadol Songprasert of Kasetsart University for being a childhood role model; Dr. Suvimol Sujjawanich of Kasetsart University for great advice and words of encouragement while I was pursuing a Master’s degree there; Dr.Somboon Pornpinatepong of Prince of Songkla University for his guidance during my undergraduate; all my early-day teachers for their patience with a very stubborn student like me.

Last but not least, I would like to thank you for seeing the potential inside of me and helping me drag that out. None of this would have been possible without your love and support; I really love you guys “Dad, Mum, Aunty Leng and Bua”. The voyage to the completion of this dissertation would have been much harder without this group of people in my life. So, I dedicate this dissertation to them and their life-long hard work.

# TABLE OF CONTENTS

# LIST OF FIGURES

# ABSTRACT

The study presented in this dissertation aims at the ground motion assessment of various two-dimensional hill models subjected to incident plane SH waves in an elastic half-space. The exact, analytic solutions to the boundary-valued problem, based on method of wave function expansion in elliptical coordinate are presented. These require the technique of angular half-range expansion in elliptical coordinate to deal with mixed-boundary condition arisen during mathematical implementation of all hill models; the traction-free boundary condition at the surface of the elliptical hill and the continuity of displacement and stress at the semi-elliptical interface.

In the study we found out that the existence of a hill results in complex pattern of surface displacement. Generally for nearly grazing angle, a hill shields the propagating waves, resulting in a standing wave pattern in the coming direction and the focusing of the amplitude at the far edge of the hill. In addition the presence of full-elliptical tunnels resulted in more prominent standing waves, and amplitudes of ground motion in the neighborhood of unity or less on the far end may be monitored without the abrupt jump at that edge of the. We discovered that the presence of a full-elliptical tunnel amplifies maximum displacement by 30%-70% from corresponding value of reference (inexistence of a tunnel) for the horizontal incidence and de-amplifies maximum displacement in the range of 1%-

15% for the vertical incidence; note that these amplifying and de-amplifying effects are dependent on the size of tunnels. The bigger the tunnel is, the stronger the effects are.

We also found out that the effect of the semi-elliptical tunnels on ground surface motion is dissimilar to the effect of the full-elliptical ones. Since horizontal incidences are able to slip underneath semi-tunnels, the weaker standing waves on the left side and weaker shadow zones associated with high jumps of the displacement amplitude at the far edge of the hill are observed. However, when the incident waves are nearly vertical, the stronger shielding effect due to semi-elliptical tunnels than to full-elliptical ones are detected. It could be said that the hinder efficiency of an elliptical tunnel depends on the direction of wave passage; the tunnel becomes better obstruction when the incidence is propagating normal to its major axis.

# CHAPTER 1: INTRODUCTION

## 1.1 General Introduction

In boundless media, a wave maintains its path of travel with constant velocity if there is no disturbance. However, when a wave encounters an obstacle, its propagating path is altered due to the interference between the incident waves and those which are emitted by the obstacle acting as a secondary source. The emission of these secondary waves from an obstacle is called “scattering”. (Mow and Pao, 1971)

In the seventeenth century, the study of scattering effects of obstacles upon the wave passage started first in the field of optics and later in fields of electromagnetic, seismology and earthquake engineering, respectively. During this period, computational methods have been developed and implemented in order to deal with mathematical difficulty and physical complication of the problems. Researchers have developed two major schemes to examine this phenomenon: numerical methods, and analytical methods.

Normally when dealing with sophisticated problems such as arbitrary shape of obstacles, geometric irregularities and material nonlinearities, numerical schemes such as finite difference, boundary element, or finite element methods seem to be a better choice. However, numerically there is a major drawback for

resolving wave scattering problem. A full-scale analysis is a tedious process and requires hardware with huge storage even though nowadays computer technology is continuously upgrading and becomes more advanced. In addition, numerical schemes are restrictive in only a finite domain. Hence, numerous procedures such as absorbing boundary (Clayton and Engquist, 1977; Fuyuki and Matsumoto, 1980; Emerman and Stephen, 1983), silent boundary (Cohen and Jennings, 1983), nesting grids (Wolf and Song, 1996), and infinite element using mapping functions (Zienkiewicz and Taylor, 2000) have been implemented to account for the reduction of the problem's scale. Yet, these procedures always produce some errors in the solutions (Kawase, 1988; Fu and Bouchon, 2004).

In contrast to numerical schemes, analytical schemes such as the method of integral equation, the integral transform, and the method of wave function expansion provide more accurate results and offer relatively simple implementation. However, the major limitation of the analytical schemes is that only linearly-elastic or visco-elastic media with a simple geometric obstacle such as circles or ellipses can be solved analytically. In spite of what has just been mentioned, analytical solutions provide more physical insight into the problems than the numerical schemes by investigating the significance of various physical parameters in an economical way and a short time manner. Furthermore, analytical solutions offer the best benchmarks to test and verify other approximate solutions obtained by numerical schemes. It is noteworthy that both

numerical and analytical schemes can generate ‘numerical results’, and need numerical processes.

The objective of this study is to investigate the scattering effect of a semi-elliptical hill with/without a full-elliptical tunnel or a semi-elliptical tunnel in a two-dimensional elastic half-space subjected to anti-plane (SH) waves. The exact infinite series solutions by the method of wave function expansion are presented in this study. The results obtained in the analysis are compared with available existing results. Complicated analytical infinite series solutions via the method of wave function expansion must be determined and solved numerically on a digital computer.

## 1.2 Literature Reviews

Earthquakes have been severe and terrifying disasters since the early history of mankind and the development of civilization. Usual locations of civilization, which have been normally located along shores of bodies of water or in alluvial valleys, are now known as risk regions susceptible to earthquakes (Milne, 1880). Various field measurements have shown that intensity of ground motions are influenced by variation of topography and subsurface configuration (Kanai and Suzuki, 1953; Kanai et al, 1955; Gutenberg, 1957; Kanai et al, 1958; Alcock, 1969; Borcherdt, 1970; Hudson, 1972).

To be aware of the behavior of ground shaking under the influence of geologic and topographic variation, numerous mathematical models and assumptions were developed and implemented. The first model was horizontally stratified surface layers overlying an elastic half-space which was the prime model for various seismologists to study the pattern of wave propagation in the outer regions of the Earth; a suitable earth-flattening transformation can provide a useful quantitative result even though there is some distortion introduced by flattening (Ewing et al, 1957; Biswas and Knopoff, 1970; Hill, 1972). By considering the wave equation of shear wave analytically, Kanai (1950) and Kanai et al (1953) discovered that soft subsoil was most likely to produce large amplitude which was in agreement with the conclusion made by Tsai later in 1969.

Even though the amplification of ground motion may be explained by the model of stratified surface layers of alluvium, other behaviors caused by the variation of topography and geology such as focusing of seismic waves and standing waves could be better recognized by two-dimensional models. Considering scattering wave of SH waves around a semi-cylindrical alluvial valley, Trifunac (1971) was able to explain these behaviors analytically; he successfully used the method of wave function expansion by the utilization of Bessel functions in polar coordinate and obtained a close-form solution. In 1973 Trifunac provided another exact solution of scattering of SH waves by a semi-cylindrical canyon, and applied this

solution to the realistic case of Pacoima ground motion data in which he suggested that the record was not affected by variation topography.

Later in 1974 Wong and Trifunac extended the valley and canyon models to the elliptical coordinate. The influence of geometric aspect ratio of canyons and valleys on the ground motion could be examined. Moeen-Vaziri and Trifunac (1981) studied the vibration of a semi-circular canal with lining and found out that a rigid liner is more efficient in transmitting the energy of incident wave to medium behind the canal, and subjected to higher stress than a flexible liner. In their following paper published in 1985, Moeen-Vaziri and Trifunac extended their canal model to arbitrary shape by the utilization of mean square error; they started by the utilization of wave expansion in the series of Bessel functions for incident wave and assumed sets of linearly independent scattering waves. Later in 1988 Moeen-Vaziri and Trifunac applied again the concept of mean square error to obtain results for scattering and diffraction of plane P and SV waves by two dimensional inhomogeneities.

Lee and Cao (1989) studied the scattering effect of plane SH waves by shallow circular canyons. They replaced the horizontal ground surface of the half-space by a circular-arc with very large radius and successfully obtained an approximate analytical solution by the employment of Graf’s addition formula. Later on, Lee and many other researchers employed this approximation method to obtain a set

of analytic solutions for P, SV and Rayleigh incident waves to canyon and valley models (Cao and Lee, 1989; Cao and Lee, 1990; Todorovska and Lee, 1990; Todorovska and Lee, 1991a; Todorovska and Lee, 1991b; Jian-wen et al, 2001). In 1994, Yuan and Liao presented an improved analytical solution to a shallow circular-arc canyon problem without large arc approximation and later in 1995 to a valley problem for incident plane SH waves.

The investigation of scattering effect due to topographic variations before 1990s mostly focused on subsurface inhomogeneities even though it has been mentioned that structures built on mountains or hills were rocked by the stronger ground motions than structures situated on a plain (Milne, 1880; Griffiths and Bollinger, 1979). Sánchez-Sesma et al (1982) and Sánchez-Sesma (1985) applied Boundary method and Green's functions respectively to wedge-like hill model subjected to SH incident waves. Mostaghel and Nowroozi (1985) treated a hill as a linearly elastic shear cantilever beam subjected to ground motion at its fixed-support; they found very reasonable approximation for horizontal motion having wavelengths somewhat greater than the width of the hill. Later Gilbert and Knopoff (1960) successfully utilized perturbation scheme and treated the scattered phenomenon as secondary waves generated by localized source or body force which is now classified as Bulk (body) scattering (Mow and Pao, 1971) to get scattering motion from mountain.

In 1992 Yuan and Men purposed a closed-form solution to a semi-circular hill sitting on a half-space by applying the Fourier expansion to stress/displacement auxiliary functions. Later this solution was extended to arbitrary shallow hill case in 1996 again by Yuan and Liao. Hayir et al (2001) and Todorovska et al (2001) studied the anti plane response of a dike subjected to incident SH waves and found that at the vertex of dike the surface amplitude was larger than at the top of circular hill; however their analytical result does not agree with work done numerically by Sánchez-Sesma et al (1982). Quiu and Liu (2005) revisited the same problem as that of Hayir et al (2001), yet utilized conjunction technique to obtain the standing wave equation in the hill region which satisfied both wave equation and zero-stress condition on the wedges; they also mentioned that equation of the standing wave purposed by Hayir et al (2001) can not satisfy zero-stress condition on the wedges. Jian-wen et al (2004) extended the auxiliary functions technique by Yuan and Men (1996) to get an analytical solution for a circular arc hill with circular tunnel subjected to incident SH waves. However as mentioned by Yuan and Men (1996) about the accuracies of solution near rims of the circular hill, Lee et al (2006) revisited this model and adopted a cosine half-range expansion to obtain a more accurate analytical solution without any overshoot of amplitudes at the rims.

## 1.3 Organization

The semi-elliptical hill with/without a tunnel models studies in this work are within the framework of linear elastodynamic theory in two-dimensional elastic half-space. The presentation is organized into the following parts:

(1) In the first part (Chapter II), the wave equation in elliptical coordinate and its solution are presented. In addition the derivation of anti-plane (SH) waves in elliptical coordinate is demonstrated. Next the series expansions of Mathieu functions in an angular half-range domain are elaborated herein.

(2) The second part (Chapter III) deals with the exact solution to scattering of plane SH waves by a shallow semi-elliptical hill. The interference due to the presence of the hill is investigated. To test accuracy of solutions, some numerical results when semi-elliptical tends to semi-circular were compared with the existing results presented by Lee et al (2006).

(3) In the third part (Chapter IV), the exact solution to scattering of plane SH waves by a deep semi-elliptical hill is presented. Again numerical results when semi-elliptical tends to semi-circular were compared with the existing results presented by Lee et al (2006) and results presented in Chapter III. The effects of frequency of the incident waves, incident angle, and the aspect ratio of elliptical hills on ground motion are demonstrated and discussed.

(4) The fourth part (Chapter V) deals with the exact solution to scattering of plane SH waves by a shallow semi-elliptical hill with an elliptical concentric tunnel. The interference due to the presence of the elliptical concentric tunnel is investigated and compared to the results from Chapter IV.

(5) In the fifth part (Chapter VI), the exact solution to scattering of plane SH waves by a deep semi-elliptical hill with an elliptical concentric tunnel is presented. The effects of frequency of the incident waves, incident angle, and the aspect ratios of both elliptical hill and tunnel on ground motion are investigated.

(6) The sixth part (Chapter VII) deals with the exact solution to scattering of plane SH waves by a shallow semi-elliptical hill with a semi-elliptical tunnel. The scattering due to the presence of the semi-elliptical tunnel is studied and compared to the results from Chapter IV and V.

(7) In the seventh part (Chapter VIII), the exact solution to scattering of plane SH waves by a deep semi-elliptical hill with a semi-elliptical tunnel is presented. The effect of frequency of the incident waves, incident angle, and the presence of the semi-elliptical tunnel on ground motion are illustrated and discussed.

(8) The last part (Chapter IX) gives a summary of the above studies of the scattering of anti-plane (SH) waves. Some comparisons among above models are discussed and summarized.

# CHAPTER 2: WAVE EQUATION

## 2.1 The Wave Equation in Elliptical Coordinate

To facilitate the geometries presented in this study, it is more convenient to describe quantities of interest in the elliptical coordinate $(\rho, \vartheta, z)$ system, which is shown in Figure 2.1; a is a focal length, and x, y axes in the corresponding Cartesian coordinate system are along $\vartheta = 0$ and $\pi/2$ respectively. Furthermore z-axe in both coordinate systems is normal to the paper face. Normally we call $\rho$ the radial coordinate, and $\vartheta$ the angular coordinate. The relationship between $(x, y)$ in Cartesian and $(\rho, \vartheta)$ in elliptical coordinate systems are $x = \mathrm{a}\cosh\rho\cos\vartheta$ and $y = \mathrm{a}\sinh\rho\sin\vartheta$.

Given a displacement function $\tilde{u}(\tilde{r}, t)$ of space and time and $c$ is a wave velocity, the wave equation can be expressed in elliptical coordinate as

$$c^2\nabla^2\tilde{u} - \partial^2\tilde{u}/\partial t^2 = 0 \qquad (2.1)$$

In addition the gradient ∇ and Jacobian J are defined by

$$\nabla(\quad) = \frac{1}{aJ}\left(\frac{\partial(\quad)}{\partial\rho}\tilde{e}_\rho + \frac{\partial(\quad)}{\partial\vartheta}\tilde{e}_\vartheta\right) + \frac{\partial(\quad)}{\partial z}\tilde{e}_\rho \qquad (2.2)$$

$$J^2 = \frac{1}{2}(cosh^2\rho - cos^2\vartheta) = \frac{1}{2}(cosh2\rho - cos2\vartheta) \qquad (2.3)$$

where $\tilde{e}_\rho$, $\tilde{e}_\vartheta, \tilde{e}_\rho$ are unit vectors in elliptical coordinate. Since a vector may be represented by a summation of an irrotational vector field "$\phi$" and rotational

vector field "$\tilde{\psi} = \left(\psi_\rho, \psi_\vartheta, \psi_z\right)^{\mathrm{T}}$", then we set the displacement vector

$$\tilde{u} = \nabla\phi + \nabla \cdot \tilde{\psi} \tag{2.4}$$

Since the problem of interest is two-dimensional anti-plane, any derivatives respect to the z-axis or out-of-plane direction become zero. Hence the displacement vector becomes

$$\tilde{u} = (u, v, w)^{\mathrm{T}} = \frac{1}{aJ}\left(\frac{\partial\phi}{\partial\rho} + \frac{\partial\psi_z}{\partial\vartheta}, \frac{\partial\phi}{\partial\vartheta} - \frac{\partial\psi_z}{\partial\rho}, \frac{1}{aJ}\left[\frac{\partial}{\partial\rho}(aJ\psi_\vartheta) + \frac{\partial}{\partial\vartheta}(aJ\psi_\rho)\right]\right)^{\mathrm{T}} \tag{2.5}$$

Figure 2.1: Family of Con-focal Ellipses and Hyperbolas

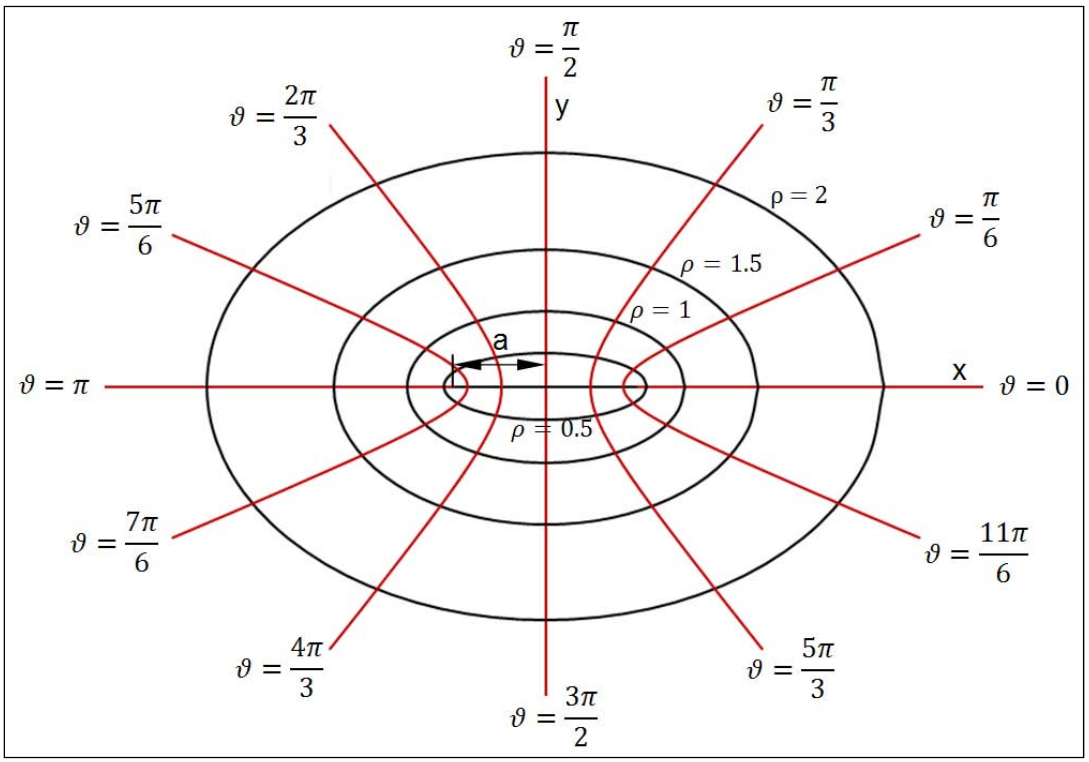

The displacement components in radial and angular coordinates of Equation (2.5) are coupling since they are function of $\psi_z$, whereas the anti-plane displacements "$w$" are independent to previous two components, and of function of $\rho$ and $\vartheta$.

Hence all models in this study subjected to incident plane SH waves are governed by the scalar wave equation

$$c^2\nabla^2 w - \partial^2 w/\partial t^2 = 0 \quad (2.6)$$

Since an arbitrary time variation can be represented by Fourier analysis in terms of harmonic components, it is possible to consider only the harmonic equation of the form

$$w(\rho,\vartheta,t) = w(\rho,\vartheta)e^{i\omega t} \quad (2.7)$$

where $i = \sqrt{-1}$, $\omega$ is the harmonic frequency.

In addition $w(\rho,\vartheta)$ satisfies the following Helmholtz equation

$$\nabla^2 w + k^2 w = 0 \quad (2.8)$$

where $k = \omega/c$ is a wave number.

The solution to Equation (2.8) can be solved by the method of separation of variables. So the displacement $w(\rho,\vartheta)$ may be expressed in the form

$$w(\rho,\vartheta) = \sum_{n=0}^{n} H_n(\rho)\cdot Z_n(\vartheta) \quad (2.9)$$

Later the partial differential equations, Equation (2.8) can be separated into two ordinary differential equations as shown in the following page

$$\frac{d^2H_n}{d\rho^2} - (b - 2qcos2\rho)H_n = 0$$
$$\frac{d^2H_n}{d\rho^2} - (b - qcos^2\rho)H_n = 0 \quad (2.10)$$

$$\frac{d^2Z_n}{d\vartheta^2} + (b - 2qcosh2\vartheta)Z_n = 0$$
$$\frac{d^2Z_n}{d\vartheta^2} + (b - qcosh^2\vartheta)Z_n = 0 \quad (2.11)$$

where

$$q = \frac{a^2k^2}{4} = \frac{a^2\omega^2}{4c^2} \quad (2.12)$$

and b is separation constant or characteristic number. The solutions to Equation (2.11) is called the Mathieu functions while the solution to Equation (2.10) is called Modified Mathieu functions; Equation (2.10) can be transformed to the latter by writing $i\vartheta$ for $\rho$.

Generally for the study of wave scattering, the solutions to angular differential equation, Equation (2.11), must be periodic with period either $\pi$ or $2\pi$. Later $Z_n$ could be written as

$$Z_n = \begin{cases} ce_{2n}(\vartheta, q) = \sum_{s=0}^{\infty} A_{2s}^{(2n)}(q)\ cos2s\vartheta\ , b = be_{2n} \\ ce_{2n+1}(\vartheta, q) = \sum_{s=0}^{\infty} A_{2s+1}^{(2n+1)}(q)\ cos(2s+1)\vartheta\ , b = be_{2n+1} \\ se_{2n+1}(\vartheta, q) = \sum_{s=0}^{\infty} B_{2s+1}^{(2n+1)}(q)\ sin(2s+1)\vartheta\ , b = bo_{2n+1} \\ se_{2n+2}(\vartheta, q) = \sum_{s=0}^{\infty} B_{2s+2}^{(2n+2)}(q)\ sin(2s+2)\vartheta\ , b = bo_{2n+2} \end{cases} \quad (2.13)$$

The first two are known as even Mathieu functions (even angular Mathieu functions or elliptical cosine functions) with period $\pi$ correspondent to the characteristic number $be_{2n}$ and $be_{2n+1}$ respectively, whereas the latter are odd Mathieu functions (odd angular Mathieu functions or elliptical sine functions) with

period $2\pi$ correspondent to the characteristic number $bo_{2n+2}$ and $bo_{2n+1}$ respectively.

There are many possibilities to find the characteristic number b. However the procedure in this study is started by substitution Equation (2.13) into (2.11), which leads to a homogeneous linear system of equations for the Fourier coefficients $A_{2s}^{(2n)}$, $A_{2s+1}^{(2n+1)}$, $B_{2s+1}^{(2n+1)}$, and $B_{2s+2}^{(2n+2)}$. The characteristic number may be evaluated by the truncation of the matrix and solving for the Eigen value. More details of other methods are available in textbooks by McLachlan (1947), Abramowitz and Stegun (1972). In addition the values of $A_{2s}^{(2n)}$, $A_{2s+1}^{(2n+1)}$, $B_{2s+1}^{(2n+1)}$, and $B_{2s+2}^{(2n+2)}$ depend on the rule of normalization; in this study we set

$$\int_0^{2\pi} ce_n^2(\vartheta, q)d\eta = \int_0^{2\pi} se_n^2(\vartheta, q)d\eta = \pi \qquad (2.14)$$

Hence we obtain

$$\sum_{s=0}^{\infty} \frac{2}{\delta_s}\left[A_{2s}^{(2n)}\right]^2 = \sum_{s=0}^{\infty}\left[A_{2s+1}^{(2n+1)}\right]^2 = \sum_{s=0}^{\infty}\left[B_{2s+1}^{(2n+1)}\right]^2 = \sum_{s=0}^{\infty}\left[B_{2s+2}^{(2n+2)}\right]^2 = 1 \qquad (2.15)$$

where

$$\delta_s = \begin{cases} 1 \ ; \ s = 0 \\ 2 \ ; \ s \neq 0 \end{cases} \qquad (2.16)$$

The solutions to radial differential equation, Equation (2.10), have several forms (McLachlan, 1947; Abramowitz and Stegun, 1972; Mechel, 1997). However because of their asymptotic behaviors and rates of convergence, the preferable forms are in forms of the series of the products of Bessel functions

$$H_n = \begin{cases} Mc_{2n}^{(i)}(\rho,q) = & \frac{\delta_s}{2A_{2s}^{(2n)}} \sum_{t=0}^{\infty} (-1)^{n+t} A_{2t}^{(2n)}(q) \cdot \\ & \cdot \left[ J_{t-s}(w_1) Z_{t+s}^{(i)}(w_2) + J_{t+s}(w_1) Z_{t-s}^{(i)}(w_2) \right] \\ Mc_{2n+1}^{(i)}(\rho,q) = & \frac{1}{A_{2s+1}^{(2n+1)}} \sum_{t=0}^{\infty} (-1)^{n+t} A_{2t+1}^{(2n+1)}(q) \cdot \\ & \cdot \left[ J_{t-s}(w_1) Z_{t+s+1}^{(i)}(w_2) + J_{t+s+1}(w_1) Z_{t-s}^{(i)}(w_2) \right] \\ Ms_{2n+1}^{(i)}(\rho,q) = & \frac{1}{B_{2s+1}^{(2n+1)}} \sum_{t=0}^{\infty} (-1)^{n+t} B_{2t+1}^{(2n+1)}(q) \cdot \\ & \cdot \left[ J_{t-s}(w_1) Z_{t+s+1}^{(i)}(w_2) - J_{t+s+1}(w_1) Z_{t-s}^{(i)}(w_2) \right] \\ Ms_{2n+2}^{(i)}(\rho,q) = & \frac{1}{B_{2s+2}^{(2n+2)}} \sum_{t=0}^{\infty} (-1)^{n+t} B_{2t+2}^{(2n+2)}(q) \cdot \\ & \cdot \left[ J_{t-s}(w_1) Z_{t+s+2}^{(i)}(w_2) - J_{t+s+2}(w_1) Z_{t-s}^{(i)}(w_2) \right] \end{cases} \quad (2.17)$$

where $\delta_s$ is defined earlier, $w_1 = \sqrt{q}e^{-\rho}$, $w_2 = \sqrt{q}e^{\rho}$, $Z_n^{(1)} = J_n$, $Z_n^{(2)} = Y_n$, $Z_n^{(3)} = H_n^{(1)}$ and $Z_n^{(4)} = H_n^{(2)}$. The first two are known as even Modified Mathieu functions (even Radial Mathieu functions) of the ***"ith"*** kind, whereas the latter are odd Modified Mathieu functions (odd Radial functions) of the ***"ith"*** kind. Furthermore the asymptotical behavior of ***"ith"*** Radial Mathieu functions is similar to function $Z_n^{(i)}$ in their series expression.

In order to have a meaningful solution to Helmholtz equation, characteristic number b of $H_n(\rho)$ must be identical to $Z_n(\vartheta, q)$. Then $ce_{2n}(\vartheta, q)$, $ce_{2n+1}(\vartheta, q)$, $se_{2n+1}(\vartheta, q)$, and $se_{2n+2}(\vartheta, q)$ must pair with $Mc_{2n}^{(i)}(\rho, q)$, $Mc_{2n+1}^{(i)}(\rho, q)$, $Ms_{2n+1}^{(i)}(\rho, q)$ and $Ms_{2n+2}^{(i)}(\rho, q)$ respectively.

## 2.2 Plane Wave Function in Elliptical Coordinate

The expansion the plane wave function in a series of product of Mathieu functions and Mathieu Modified functions may be carried out by consideration of line source as if it is located at large distance from origin. The line source function in elliptical cylindrical coordinate can be specified as follows

$$H_0^{(1)}(kR) = 2\left\{\sum_{n=0}^{\infty} ce_n(\vartheta', q)ce_n(\vartheta, q)\begin{cases} Mc_n^{(1)}(\rho, q)Mc_n^{(3)}(\rho', q)\ ;\ \rho \le \rho' \\ Mc_n^{(1)}(\rho', q)Mc_n^{(3)}(\rho, q)\ ;\ \rho' < \rho \end{cases}\right. \\ \left. + \sum_{n=1}^{\infty} se_n(\vartheta', q)se_n(\eta, q)\begin{cases} Ms_n^{(1)}(\rho, q)Ms_n^{(3)}(\rho', q)\ ;\ \rho \le \rho' \\ Ms_n^{(1)}(\rho', q)Ms_n^{(3)}(\rho, q)\ ;\ \rho' < \rho \end{cases}\right\} \tag{2.18}$$

It is noteworthy that Equation (2.18) represents the cylindrical line source located at $(\rho', \vartheta')$ in elliptical coordinate system; see Appendix A for more detail. Next if we set the source point at very large distance from origin in a direction $\gamma + \pi$ to the positive x axis, the radial domain of interest is $\rho \le \rho'$. Then Equation (2.18) may be reduced to

$$H_0^{(1)}(kR) = 2\left\{\sum_{n=0}^{\infty} ce_n(\vartheta', q)ce_n(\vartheta, q)Mc_n^{(1)}(\rho, q)Mc_n^{(3)}(\rho', q) \right. \\ \left. + \sum_{n=1}^{\infty} se_n(\vartheta', q)se_n(\eta, q)Ms_n^{(1)}(\rho, q)Ms_n^{(3)}(\rho', q)\right\} \tag{2.19}$$

In addition the amplitude of $R$ in Figure A.1 turns out to be $r' + r\cos(\gamma - \theta)$ as $r' \gg r$. In addition $\vartheta'$ becomes $\gamma + \pi$ and $kr'$ may asymptotically equal to $a\cosh\rho'$. Since we have

$$H_0^{(1)}(kR) \to \sqrt{\frac{2}{\pi a\cosh\rho'}}\, e^{i\left(kr' + kr\cos(\gamma-\theta) - \frac{\pi}{4}\right)}$$

$$Mc_n^{(3)}(\rho', q) \to \sqrt{\frac{2}{\pi a \cosh \rho'}}\, e^{i\left(a \cosh \rho' - \frac{\pi}{4} - \frac{n\pi}{2}\right)}$$

$$Ms_n^{(3)}(\rho', q) \to (-1)^n \sqrt{\frac{2}{\pi a \cosh \rho'}}\, e^{i\left(a \cosh \rho' - \frac{\pi}{4} + \frac{n\pi}{2}\right)}$$

together with $ce_n(\gamma + \pi, q) = (-1)^n ce_n(\gamma, q)$ and $se_n(\gamma + \pi, q) = (-1)^n se_n(\gamma, q)$ (McLachlan, 1947), Equation (2.19) can be transformed to

$$e^{ikr\cos(\gamma-\theta)} = 2\left\{\sum_{n=0}^{\infty} i^n ce_n(\gamma, q) ce_n(\vartheta, q) Mc_n^{(1)}(\rho, q) + \sum_{n=1}^{\infty} i^n se_n(\gamma, q) se_n(\eta, q) Ms_n^{(1)}(\rho, q)\right\} \qquad (2.20)$$

Figure 2.2: Anti-Plane (SH) Waves in Elastic Full-Space

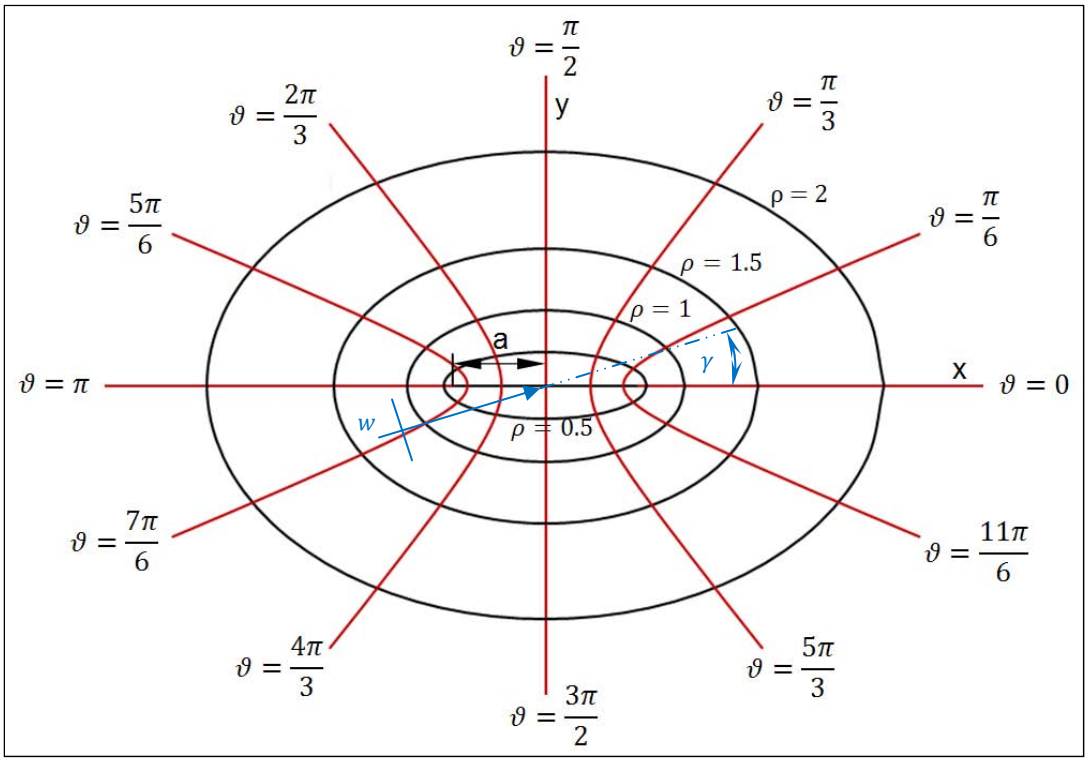

The previous equation represents the excitation $w$**,** consisting of an infinite train of plane SH waves with incident angle $\gamma$ as shown in Figure 2.2, since

$$w = e^{ik(xcos\gamma + ysin\gamma)} = e^{ikrcos(\gamma-\theta)} \quad (2.21)$$

## 2.3 Half-Range Expansion of Angular Mathieu Functions

**Generalized Fourier series:**

If a set of real-valued functions $\{g_1(\xi), g_2(\xi), \dots, g_n(\xi)\}$, when n = 1,2,3,… , is defined on an interval $a \le \xi \le b$ and is such that the following integral product of any pair $g_m(\xi)$, $g_n(\xi)$ in the set do exist. The prescribed set of functions is said to be orthogonal if the product of

$$\left(g_m(\xi), g_n(\xi)\right) = \int_a^b g_m(\xi) g_n(\xi) d\xi \quad (2.22)$$

for any distinct functions $g_m(\xi)$ and $g_n(\xi)$ over interval $a \le \xi \le b$ is always zero. (Kreyszig, 1983); the nonzero product of the integral occurs only when $m = n$.

This orthogonal property is very important because any real-valued function $f(\xi)$ over the prescribed interval may be expressed in terms of $g_n(\xi)$'s

$$f(\xi) = \sum_{n=1}^{\infty} f_n g_n(\xi) = f_1 g_1(\xi) + f_2 g_2(\xi) + \cdots \quad (2.23)$$

Employing the orthogonality together with the concept of L2-norm

$$\|g_n\| = \sqrt{\left(g_n(\xi), g_n(\xi)\right)} = \sqrt{\int_a^b g_n(\xi) g_n(\xi) d\xi} \quad (2.24)$$

the constants $f_n$ can be determined easily. Multiplying Equation (2.23) with $g_m(\xi)$ and integrating the product over an interval $a \le \xi \le b$ yield

$$f_n = \frac{\left(f(\xi), g_n(\xi)\right)}{\|g_n\|^2} = \frac{1}{\|g_n\|^2}\int_a^b f(\xi) g_n(\xi) d\xi \quad (2.25)$$

The series in Equation (2.23) is called a generalized Fourier series while the constants $f_n$, Equation (2.25), are called the Fourier constants.

**Series expansion of Mathieu function in the ranges $[0, \pi]$ and $[-\pi, 0]$ :**

In the angular half-range $[0, \pi]$ or $[-\pi, 0]$, either the set of elliptical cosine functions $\{ce_n(\vartheta, q);\ n = 0, 1, 2 \ldots\}$ or the set of elliptical sine functions $\{se_n(\vartheta, q);\ n = 1, 2, 3 \ldots\}$ forms a complete orthogonal set. However in this study we select the set of elliptical cosine functions as the orthogonal set over the prescribed ranges. Utilizing the concept of the generalized Fourier series demonstrated previously together with the rule of normalization Equation (2.14), any function $f(\vartheta)$ over the range $[0, \pi]$ can have an elliptical cosine series expansion

$$f(\vartheta) = \sum_{n=0}^{\infty} f_n ce_n(\vartheta, q) \quad (2.26)$$

where

$$f_n = \frac{\left(f(\vartheta), ce_n(\vartheta, q)\right)}{\|ce_n\|^2} = \frac{2}{\pi}\int_0^{\pi} f(\vartheta) ce_n(\vartheta, q)\, d\vartheta \quad (2.27)$$

Utilizing Equations (2.26) and (2.27) together with Equation (2.13), $se_m(\vartheta, q)$ can be expanded over the range $[0, \pi]$ as follows

$$se_m(\vartheta, q) = \sum_{n=0}^{\infty} \mathfrak{C}_{mn}\, ce_n(\vartheta, q); \quad (2.28)$$

where

$$\mathfrak{C}_{mn} = \frac{4}{\pi}\sum_{\substack{r=1,s=0 \\ r+s\ odd}}^{\infty}\left(\frac{r}{r^2-s^2}\right)A_s^{(n)}B_r^{(m)};\ 0 \le \vartheta \le \pi \tag{2.29}$$

Similarly, over the range $[-\pi, 0]$ Equation (2.28) is still valid except

$$\mathfrak{C}_{mn} = -\frac{4}{\pi}\sum_{\substack{r=1,s=0 \\ r+s\ odd}}^{\infty}\left(\frac{r}{r^2-s^2}\right)A_s^{(n)}B_r^{(m)};\ -\pi \le \vartheta \le 0 \tag{2.30}$$

**Series expansion of Mathieu function in the ranges $\left[-\frac{\pi}{2}, \frac{\pi}{2}\right]$ and $\left[\frac{\pi}{2}, -\frac{\pi}{2}\right]$:**

In the angular half-range $[-\pi/2\,, \pi/2]$ or $[\pi/2\,, -\pi/2]$, we select the set of elliptical cosine functions of even order and elliptical sine functions of odd order $\{ce_{2n}(\vartheta, q), se_{2n+1}(\vartheta, q);\ n = 0, 1, 2, \ldots\}$ to form an complete orthogonal set; the set of elliptical cosine functions of odd order and elliptical sine functions of even order $\{ce_{2n+1}(\vartheta, q), se_{2n+2}(\vartheta, q);\ n = 0, 1, 2, \ldots\}$ is also an orthogonal set. Again employing the concept of the generalized Fourier series demonstrated previously together with the rule of normalization for $ce_{2n}$ and $se_{2n+1}$, Equation (2.14), any function $f(\vartheta)$ over the range $[-\pi/2\,, \pi/2]$ can be expanded into the series form of

$$f(\vartheta) = \sum_{n=0}^{\infty}[f_{2n}ce_{2n}(\vartheta, q) + f_{2n+1}se_{2n+1}(\vartheta, q)] \tag{2.31}$$

where

$$f_{2n} = \frac{(f(\vartheta), ce_{2n}(\vartheta, q))}{\|ce_{2n}\|^2} = \frac{2}{\pi}\int_{-\pi/2}^{\pi/2} f(\vartheta)ce_{2n}(\vartheta, q)\, d\vartheta \tag{2.32}$$

$$f_{2n+1} = \frac{(f(\vartheta), se_{2n+1}(\vartheta, q))}{\|se_{2n+1}\|^2} = \frac{2}{\pi}\int_{-\pi/2}^{\pi/2} f(\vartheta)se_{2n+1}(\vartheta, q)\, d\vartheta \tag{2.33}$$

Employing Equations (2.31), (2.32) and (2.33) together with Equation (2.13) an

the orthogonal property between any elliptical cosine and elliptical sine, $ce_{2m+1}(\vartheta, q)$ for $m = 0, 1, 2, \ldots$ can be expressed over the range $[-\pi/2\,, \pi/2]$ as follows

$$ce_{2m+1}(\vartheta, q) = \sum_{n=0}^{\infty} \mathfrak{M}_{mn}\, ce_{2n}(\vartheta, q) \tag{2.34}$$

where

$$\mathfrak{M}_{mn} = \frac{2}{\pi}\sum_{r=0}^{\infty}\sum_{s=0}^{\infty}\left[\frac{(-1)^{r-s}}{2r-2s+1} + \frac{(-1)^{r+s}}{2r+2s+1}\right] A_{2r+1}^{(2m+1)} A_{2s}^{(2n)}\,;\ -\pi/2 \le \vartheta \le \pi/2 \tag{2.35}$$

Similarly, over the range $[\pi/2\,, -\pi/2]$ Equation (2.34) is still valid except

$$\mathfrak{M}_{mn} = -\frac{2}{\pi}\sum_{r=0}^{\infty}\sum_{s=0}^{\infty}\left[\frac{(-1)^{r-s}}{2r-2s+1} + \frac{(-1)^{r+s}}{2r+2s+1}\right] A_{2r+1}^{(2m+1)} A_{2s}^{(2n)}\,;\ \pi/2 \le \vartheta \le -\pi/2 \tag{2.36}$$

Same orthogonal set of functions developed earlier are applicable to $se_{2m+2}(\vartheta, q)$ in the prescribed half-ranges; $se_{2m+2}(\vartheta, q)$ can be written in the following form as

$$se_{2m+2}(\vartheta, q) = \sum_{n=0}^{\infty} \mathfrak{N}_{mn}\, se_{2n+1}(\vartheta, q) \tag{2.37}$$

where

$$\mathfrak{N}_{mn} = \frac{2}{\pi}\sum_{r=0}^{\infty}\sum_{s=0}^{\infty}\left[\frac{(-1)^{r-s}}{2r-2s+1} + \frac{(-1)^{r+s}}{2r+2s+3}\right] B_{2r+2}^{(2m+2)} B_{2s+1}^{(2n+1)}\,;\ -\pi/2 \le \vartheta \le \pi/2 \tag{2.38}$$

and

$$\mathfrak{N}_{mn} = -\frac{2}{\pi}\sum_{r=0}^{\infty}\sum_{s=0}^{\infty}\left[\frac{(-1)^{r-s}}{2r-2s+1} + \frac{(-1)^{r+s}}{2r+2s+3}\right] B_{2r+2}^{(2m+2)} B_{2s+1}^{(2n+1)}\,;\ \pi/2 \le \vartheta \le -\pi/2 \tag{2.39}$$

It is noteworthy that elliptical sine functions are always orthogonal to elliptical cosine functions over the half ranges $[-\pi/2\,, \pi/2]$ and $[\pi/2\,, -\pi/2]$, yet $[-\pi, \pi]$ and $[\pi, -\pi]$. In addition proof of all series expansions of Mathieu functions and orthogonal sets are shown in Appendix B and C.

# CHAPTER 3: SCATTERING OF PLANE (SH) WAVES BY A SHALLOW SEMI-ELLIPTICAL HILL

In this Chapter, an exact, analytic solution to the boundary-valued problem of the two-dimensional scattering of anti-plane (SH) waves by a shallow semi-elliptical hill is presented. It is based on method of wave function expansion in elliptical coordinate and elliptical cosine half-range expansion. In addition the comparison between our results when semi-elliptical tends to semi-circular and the existing solutions of circular hill offered by Lee et al (2006) are demonstrated. Scattering effects due to the existence of elliptical hill and angles of wave incidence on ground motion are investigated.

## 3.1 The Shallow Semi-Elliptical Hill Model

The cross-section of two-dimensional model is shown in Figure 3.1; it represents an elastic, isotropic, and homogeneous half-space with a semi-elliptical hill. The material properties are given by the rigidity $\mu$ and the velocity of shear wave $\beta$. The elliptical coordinate $(\rho, \vartheta)$ system is as defined in the figure whereas *x* and *y* axes in the corresponding Cartesian coordinate system are along $\vartheta = 0$ and $\pi/2$ respectively. To facilitate the analysis of a shallow hill, we defined the half-space by $y \geq 0$.

Figure 3.1: Shallow Semi-Elliptical Hill Model

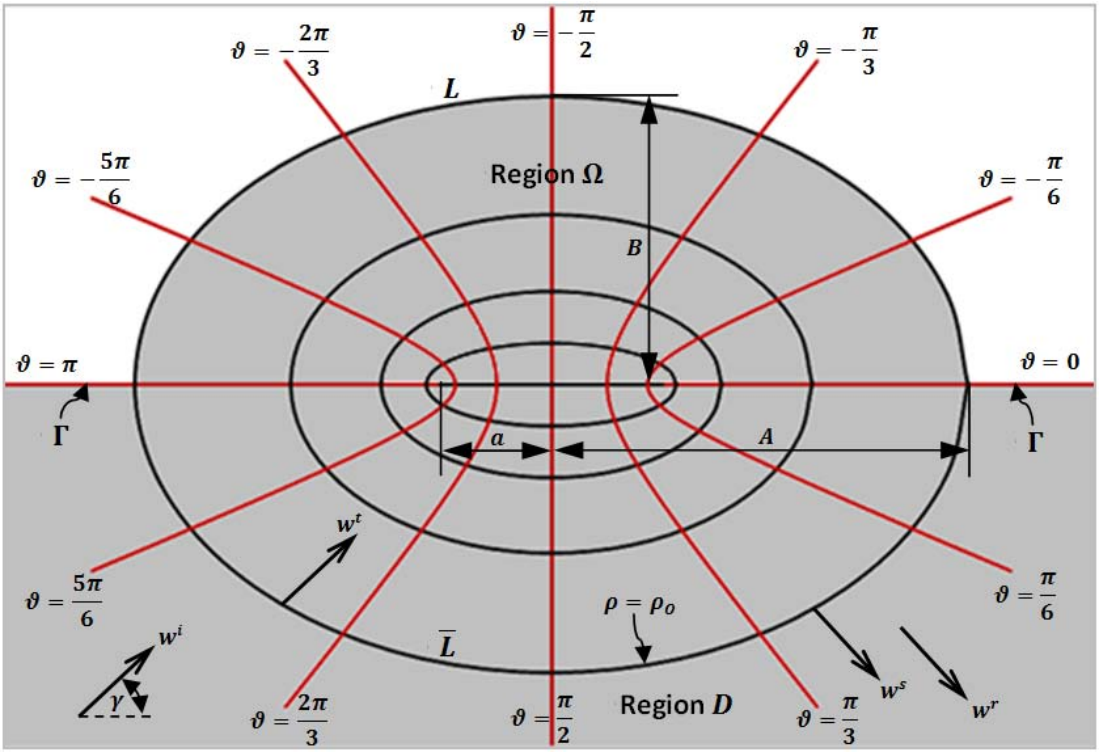


The model consists of the regions $\Omega$ and *D.* The interior regions $\Omega$ is the full elliptical region which has the boundary *L* along surface of the semi-elliptical hill, $\rho = \rho_0$ and $-\pi \leq \vartheta \leq 0$, and the boundary $\bar{L}$ between the regions $\Omega$ and *D*, $\rho = \rho_0$ and $0 \leq \vartheta \leq \pi$. The exterior region *D* consists of the half-space bounded by $\bar{L}$ along interface $\rho = \rho_0$ and the flat surface of the half-space beyond the hill denoted by $\Gamma$ along $\vartheta = 0$ and $\pi$. The half-width and height of the semi-elliptical hill are denoted by A and B. In addition $a$ is the focal length.

## 3.2 Series Expansion of Wave Functions

**Incident and Reflected Waves:**

The excitation $w^i$ consists of infinite trains of plane SH waves, (anti-plane) particle moving in z direction only, with frequency $\omega$ and incident angle $\gamma$ with respect to the positive x axis. It satisfies wave equation, Equation (2.6), and can be represented in the Cartesian coordinate system by

$$w^i = w_0 e^{ik(x\cos\gamma - y\sin\gamma) - i\omega t} \tag{3.1}$$

where $w_0 =$ amplitude of the incident wave, and $k = k_\beta = \omega/\beta =$ shear wave number. However since the time factor $e^{-i\omega t}$ representing the steady-state harmonic motions exists in the incident and all resulting waves, it will be omitted on all subsequent wave expressions from here on.

In the absence of the hill, the incident waves would reflect at the flat surface $\Gamma$. Later the reflected plane waves $w^r$ can be expressed as

$$w^r = w_0 e^{ik(x\cos\gamma + y\sin\gamma)} \tag{3.2}$$

Far from the hill, the interference of the incident and reflected waves yields the free field waves, $w^{ff} = w^i + w^r$; applying Equation (2.20), $w^{ff}$ can be expressed in elliptical coordinate, to facilitate the geography shown in Figure 3.1, as follows

$$w^{ff} = w^i + w^r = 4w_0 \sum_{n=0}^{\infty} \left[ i^n M c_n^{(1)}(\rho, q) ce_n(\vartheta, q) ce_n(\gamma, q) \right] \tag{3.3}$$

where $q$, $Mc_n^{(1)}(\cdot)$, and $ce_n(\cdot)$ are Mathieu parameter defined by Equation (2.12), Modified Mathieu function of the first kind and Mathieu function respectively; the expression of both function are given by Equations (2.13) and (2.17).

**Scattered and Transmitted Waves:**

After the incident plane waves hit the interface between regions $\Omega$ and *D*, two more plane waves are generated. The first waves are the scattered and diffracted outgoing waves $w^s$ in the exterior region *D*, whereas the second ones are the standing transmitted waves $w^t$ inside the elliptical region $\Omega$. Both scattered and transmitted waves can be written as an elliptical wave function series which takes the form

$$w^s = \sum_{n=0}^{\infty}\left[A_n Mc_n^{(3)}(\rho,q)ce_n(\vartheta,q)\right];\ \rho \geq \rho_0 \quad (3.4)$$

$$w^t = \sum_{n=0}^{\infty}\left[B_n Mc_n^{(1)}(\rho,q)ce_n(\vartheta,q)\right] + \sum_{n=1}^{\infty}\left[C_n Ms_n^{(1)}(\rho,q)se_n(\vartheta,q)\right];\ \rho \leq \rho_0 \quad (3.5)$$

where $A_n$, $B_n$ and $C_n$ are the unknown coefficients of the new waves to be determined. Moreover $Mc_n^{(3)}(\cdot)$, $Ms_n^{(1)}(\cdot)$ and $se_n(\cdot)$ are even Modified Mathieu function of the third kind, odd Modified Mathieu function of the first kind and odd Mathieu function, respectively, while $Mc_n^{(1)}(\cdot)$ and $ce_n(\cdot)$ are defined previously. The scattered waves in the region *D* ($\rho \geq \rho_0, 0 \leq \vartheta \leq \pi$) have $Mc_n^{(3)}(\cdot)$ as radial wave functions since the asymptotic behavior of this function is of Hankel function of the first kind which automatically satisfies Sommerfeld's far field

condition. Furthermore only $ce_n(\cdot)$ are used to form angular wave functions because they form a complete orthogonal set of functions in the angular domain $0 \leq \vartheta \leq \pi$; see Appendix C for more information.

Since the radial wave functions of transmitted waves in the interior region $\Omega$ must be finite everywhere in the full elliptical region $\Omega$, $Mc_n^{(1)}(\cdot)$ and $Ms_n^{(1)}(\cdot)$, which have asymptotic behavior of Bessel function of the first kind, are used. (Pao and Mow, 1973) In addition we utilize both $ce_n(\cdot)$ and $se_n(\cdot)$ to form a complete orthogonal set of functions in the full angular domain of the region $\Omega$.

**Solution of the Problem using Angular Half-range Expansion**

The wave functions of the total displacement, $w = w^{ff} + w^s$, in the exterior region *D* and of the transmitted wave, $w^t$, in the elliptical region $\Omega$ must satisfy the Helmholtz equation, Equation (2.8), and the following boundary conditions:

1. The traction-free boundary condition at the surface of the flat half-space $\Gamma$ $(\rho \geq \rho_0, \vartheta = 0, \pi)$

$$\tau_{yz}\big|_{y=0} = \tau_{\vartheta z}|_{\vartheta=0,\pi} = \frac{\mu}{aJ}\frac{\partial(w^{ff}+w^s)}{\partial\vartheta} = 0 \qquad (3.6)$$

2. The traction-free boundary condition at the surface of the elliptical hill *L* $(\rho = \rho_0, -\pi \leq \vartheta \leq 0)$

$$\tau_{\rho z}\big|_{\rho=\rho_0} = \frac{\mu}{aJ}\frac{\partial w^t}{\partial \rho}\Big|_{\rho=\rho_0} = 0 \tag{3.7}$$

3. The continuity of displacement and radial stress at the interface $\overline{L}$ $(\rho = \rho_0, 0 \leq \vartheta \leq \pi)$

$$\begin{aligned} &(w^{ff} + w^s)\big|_{\rho=\rho_0} = w^t|_{\rho=\rho_0} \\ &\tau_{\rho z}\big|_{\rho=\rho_0} = \frac{\mu}{aJ}\frac{\partial (w^{ff}+w^s)}{\partial \rho}\Big|_{\rho=\rho_0} = \frac{\mu}{aJ}\frac{\partial w^t}{\partial \rho}\Big|_{\rho=\rho_0} \end{aligned} \tag{3.8}$$

Since $w^{ff}$ and $w^s$ in Equations (3.3) and (3.4) content elliptical cosine functions, they automatically satisfy the traction-free boundary condition at the surface of the flat half-space $\Gamma$, Equation (3.6). Hence to determine the unknown coefficients of the scattered and transmitted waves, Equations (3.4) and (3.5), boundary conditions of Equations (3.7) and (3.8) are employed.

Here the mathematical difficulty arises since along the circumference of the full elliptical region the transmitted waves expressing the displacement motion in the full elliptical region must satisfy two disjoint sets of boundary conditions, one set for traction-free boundary condition at the surface of the elliptical hill *L*, $-\pi \leq \vartheta \leq 0$ and another set for the continuity of displacement and stress at the interface $\overline{L}$, $0 \leq \vartheta \leq \pi$. In addition as the transmitted waves compose of both elliptical cosine

and sine, those boundary conditions could not be separately imposed without any modification. Later utilizing the orthogonality of angular Mathieu functions in the half-range $[0,\pi]$ (and similarly in $[-\pi,0]$), $se_m(\vartheta,q)$ for $m=1,2,3\ldots$ can be expanded as a series of elliptical cosine. Recalling Equation (2.28), the transmitted waves $w^t$ and the corresponding radial stress becomes

$$w^t=\sum_{n=0}^{\infty}\left[B_n Mc_n^{(1)}(\rho,q)\mp\sum_{m=1}^{\infty}\mathfrak{C}_{mn}C_m Ms_m^{(1)}(\rho,q)\right]ce_n(\vartheta,q) \tag{3.9}$$

$$\tau_{\rho z}^t=\frac{\mu}{aJ}\sum_{n=0}^{\infty}\left[B_n Mc_n^{(1)\prime}(\rho,q)\mp\sum_{m=1}^{\infty}\mathfrak{C}_{mn}C_m Ms_m^{(1)\prime}(\rho,q)\right]ce_n(\vartheta,q) \tag{3.10}$$

where –ve above and +ve below are assigned for $-\pi\le\vartheta\le 0$ and $0\le\vartheta\le\pi$ respectively; $\mathfrak{C}_{mn}$ is given by Equation (2.29). Moreover " ' " designates the derivative of a function with respect to $\rho$ from here on. Since all correspondent displacement and stress functions are in the form of elliptical cosine series, boundary conditions are convenient to apply.

Applying Equation (3.7), the traction-free along surface *L*, yields

$$B_n=\frac{1}{Mc_n^{(1)\prime}(\rho_0,q)}\sum_{m=1}^{\infty}\mathfrak{C}_{mn}Ms_m^{(1)\prime}(\rho_0,q)C_m \tag{3.11}$$

Then applying the continuity of displacement and stress at the interface $\overline{L}$ yields

$$\begin{aligned}4w_0 i^n Mc_n^{(1)}(\rho_0,q)ce_n(\gamma,q)+Mc_n^{(3)}(\rho_0,q)A_n\\ =Mc_n^{(1)}(\rho_0,q)B_n+\sum_{m=1}^{\infty}\mathfrak{C}_{mn}Ms_m^{(1)}(\rho_0,q)C_m\end{aligned} \tag{3.12}$$

$$\begin{aligned}4w_0 i^n Mc_n^{(1)'}(\rho_0,q)ce_n(\gamma,q)+Mc_n^{(3)'}(\rho_0,q)A_n\\ =Mc_n^{(1)\prime}(\rho_0,q)B_n+\sum_{m=1}^{\infty}\mathfrak{C}_{mn}Ms_m^{(1)\prime}(\rho_0,q)C_m\end{aligned} \tag{3.13}$$

There are many schemes to solve for the unknowns. One of them is first to plug in Equation (3.11) into Equations (3.12) and (3.13), and later to eliminate $A_n$ by setting

$$A_n = \frac{1}{Mc_n^{(3)}(\rho_0,q)}\left\{\sum_{m=1}^{\infty} \mathfrak{C}_{mn}\left[\left(\frac{Mc_n^{(1)}(\rho_0,q)}{Mc_n^{(1)\prime}(\rho_0,q)}\right) Ms_m^{(1)\prime}(\rho_0,q) + Ms_m^{(1)}(\rho_0,q)\right] C_m - 4w_0 i^n Mc_n^{(1)}(\rho_0,q)ce_n(\gamma,q)\right\} \quad (3.14)$$

The linear equation of infinite order is formulated and takes the form

$$\sum_{m=1}^{\infty} \mathbb{C}_{mn}C_m = 4w_0 i^n \left[Mc_n^{(1)\prime}(\rho_0,q) - \left(\frac{Mc_n^{(3)\prime}(\rho_0,q)}{Mc_n^{(3)}(\rho_0,q)}\right) Mc_n^{(1)}(\rho_0,q)\right] ce_n(\gamma,q) \quad (3.15)$$

where

$$\mathbb{C}_{mn} = \mathfrak{C}_{mn}\left\{2Ms_m^{(1)'}(\rho_0,q) - \left(\frac{Mc_n^{(3)'}(\rho_0,q)}{Mc_n^{(3)}(\rho_0,q)}\right)\left[\left(\frac{Mc_n^{(1)}(\rho_0,q)}{Mc_n^{(1)'}(\rho_0,q)}\right) Ms_m^{(1)'}(\rho_0,q) + Ms_m^{(1)}(\rho_0,q)\right]\right\}$$

Here $C_m$'s may be solved by truncation of infinite matrix as shown in Equation (3.15). Later $A_n$'s and $B_n$'s can be solved by inserting $C_m$'s back into Equations (3.11) and (3.14).

## 3.3 Results and Analysis

To study scattering effects due to locally topographic irregularities, amplitudes of ground motions at various points are of importance. Since we may assume the infinite train of SH incident wave with unity amplitude, hence in the absence of a hill the amplitude of the ground motion is equal to 2. Due to the presence of the

hill, the scattered waves interfere with the incident and reflected waves in the exterior region *D* beyond the hill, and the transmitted waves in the interior region $\Omega$; the amplitude of the ground motion different from 2 is expected. Similar to previous works by Wong and Trifunac in 1974, we display the results in term of the dimensionless parameter $\eta$ defined as

$$\eta = \frac{2A}{\lambda} = \frac{A\omega}{\pi\beta} = q^{1/2}\left(\frac{2A}{\pi a}\right) \tag{3.16}$$

where $\lambda$ is the wave length and $a$ is the focal length expressed in term of A and B, the half-width and height of the hill correspondingly, as follows

$$a = \frac{A}{cosh\left(tanh^{-1}(B/A)\right)} \tag{3.17}$$

In addition in order to study the shape effect of a semi-elliptical hill, the aspect ratio *R* is defined

$$R = \frac{B}{A} \tag{3.18}$$

It is noteworthy that the maximum aspect ratio R of a semi-elliptical hill is limited to that of semi-circular one.

**Comparison with the Previous Work:**

The numerical results when semi-elliptical tends to semi-circular $(R = 0.9999)$ at $\eta = 5$ and $10$ are compared with the existing results of semi-circular hill (Lee et al, 2006). In the general trend, the comparisons between Figures 3.2a and 3.2b and Figures 3.3a and 3.3b show that our results agree with results presented by Lee et al (2006). Only slight differences, less than 1%, between those do exist as

shown by the discrepancy of maximum values of the displacements. The above difference may come from the different functions used in each problem, Bessel and Hankel functions for the semi-circular hill and Mathieu elliptical sine and cosine functions for the semi-elliptical hill.

Figure 3.2: Displacement Amplitudes of Ground Motion at $\eta = 5$

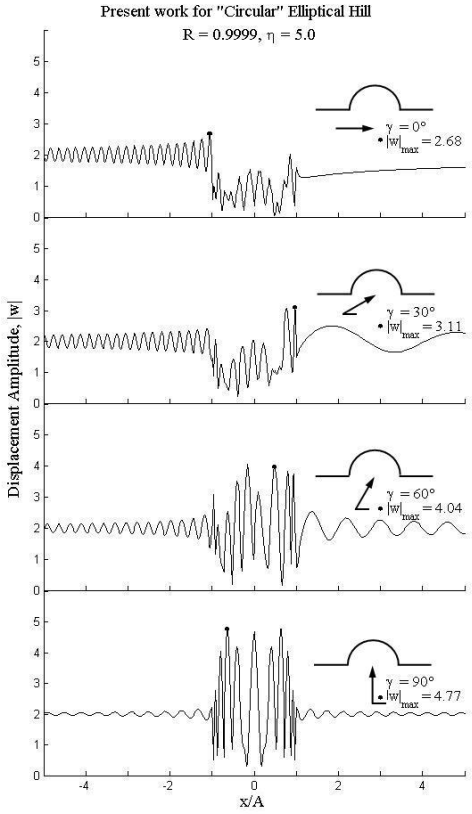


(a) "Almost-Circular" Elliptical Hill ($R = 0.9999$)

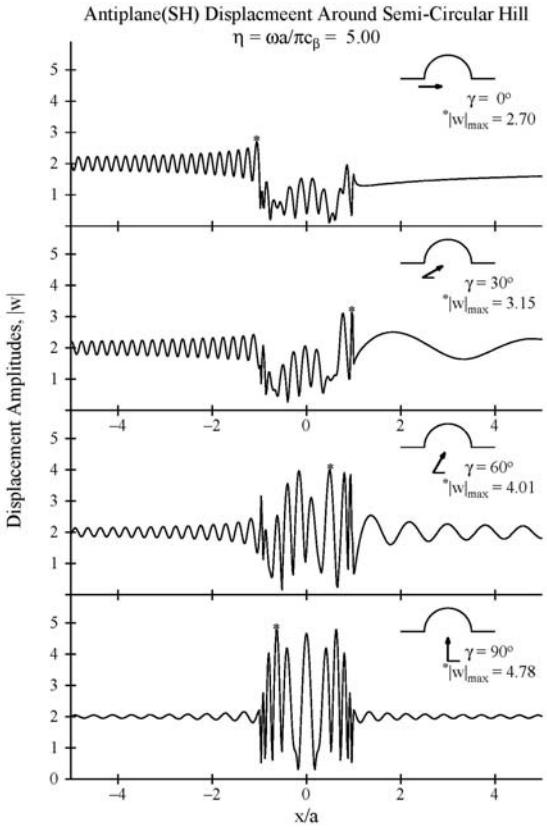


(b) Semi-Circular Hill (Courtesy of Lee et al, 2006)

Figure 3.3: Displacement Amplitudes of Ground Motion at $\eta = 10$

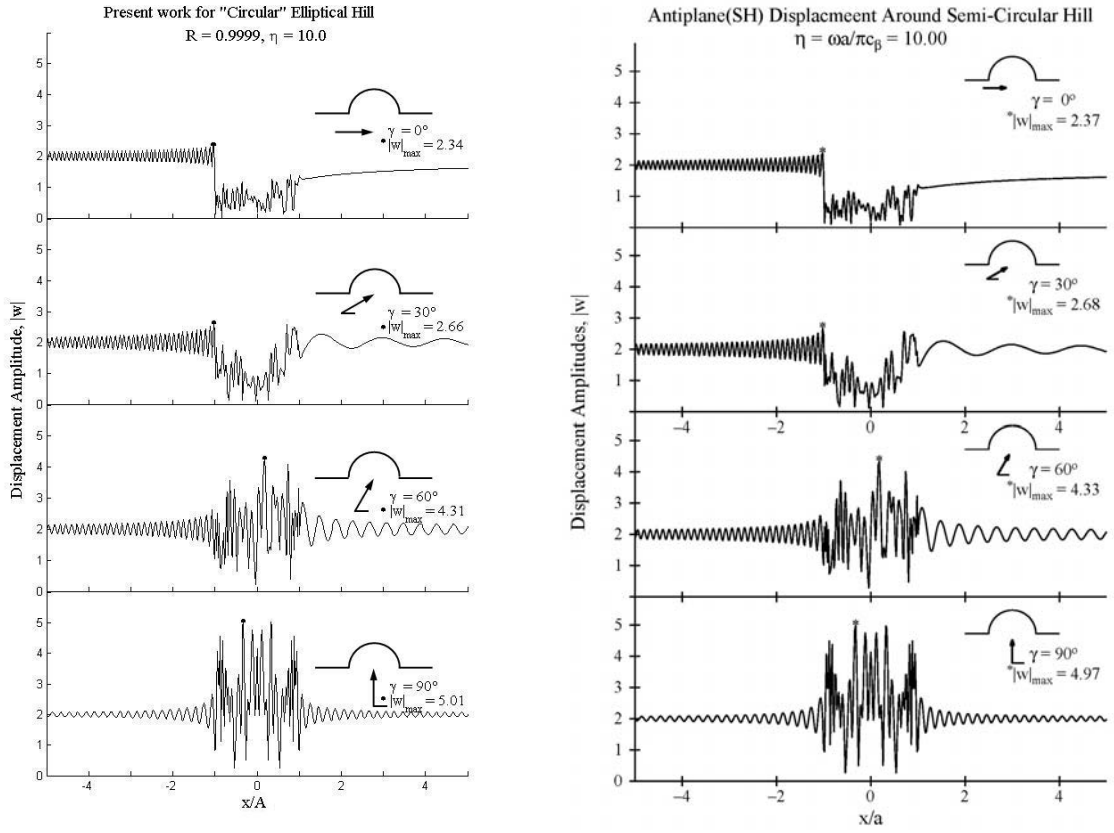


(a) "Almost-Circular" Elliptical Hill ($R = 0.9999$)

(b) Semi-Circular Hill (Courtesy of Lee et al, 2006)

**Effects of Height-to-Width Ratio of Elliptical Hills, and of Incident Angle:**

Figures 3.4 to 3.23 illustrate amplitudes of surface displacements for $R = 0.1$, 0.3, 0.5, 0.7 and 0.9 which are equivalent to the height-to-width ratios of 0.05, 0.15, 0.25, 0.35 and 0.45 respectively. Each figure shows three-dimensional plots of displacement amplitudes at one of four different incident angles of $\gamma = 0°$, 30°, 60° and 90° versus the distance *x/A* on and around the hill and the

dimensionless frequency $\eta$ in the range of 0.5 to 10. In addition the amplitudes in the range of *x/A* in $[-1,1]$ are those on the elliptical surface of the hill.

Figures 3.4 through 3.7 show the displacement amplitudes for R = 0.1 which are slightly different from the uniform half-space amplitudes. In particular when $\eta$ is small, an incident angle is of irrelevance on the displacement amplitudes. This confirms the fact that the long waves do not feel any undersized topographic irregularity and only minor changes into the uniform half-space amplitudes may be introduced. In addition as shown in following Figures 3.8 through 3.23, the pattern of surface displacement becomes progressively more complicated when an elliptical hill gets steeper. Moreover for nearly grazing angle ($\gamma = 0°$ and $30°$) the hill acts like a barrier shielding the propagating waves coming from the left, resulting in a standing wave pattern in the front of the hill. Besides that, with $\eta$ larger than 3 we also observed more prominent and more abrupt jumps of the displacement amplitudes at the right edge of the hill $(x/A = 1)$. This may be due to the fact that the right rim reflects the incoming waves back into the elliptical hill. Shortly these reflected waves would bounce at the surface of hills, resulting in the superimposition of the overall wave propagation and the localized concentration at the right rim. It is also notable that for nearly vertical incidences ($60°$ and $90°$) the similar pattern to the case of semi-circular hill has been observed here. Lee et al (2006) mentioned that displacement is large and oscillates on the hill surface.

Figure 3.4: Displacement Amplitude for $R = 0.1$ when $\gamma = 0°$

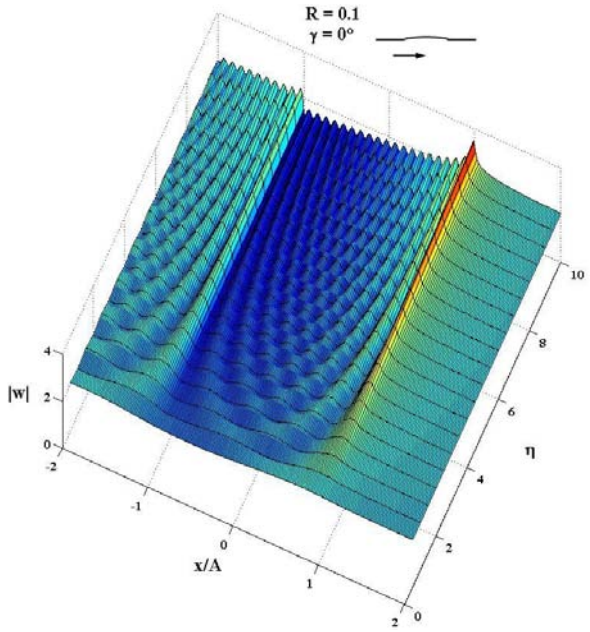


Figure 3.5: Displacement Amplitude for $R = 0.1$ when $\gamma = 30°$

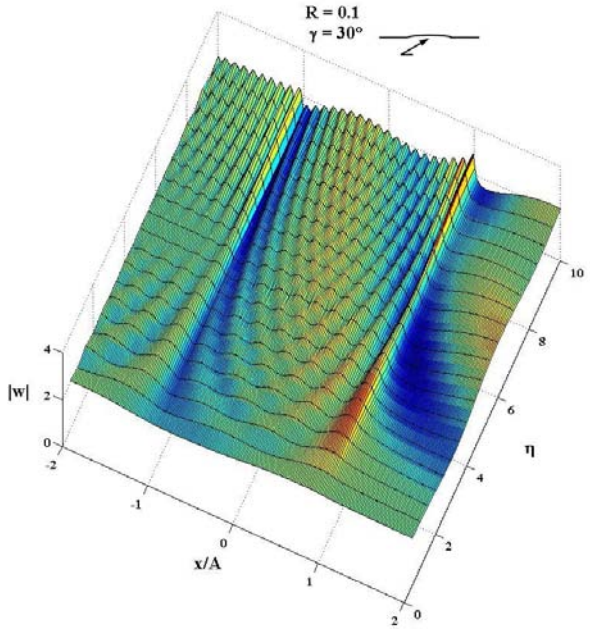

Figure 3.6: Displacement Amplitude for $R = 0.1$ when $\gamma = 60°$

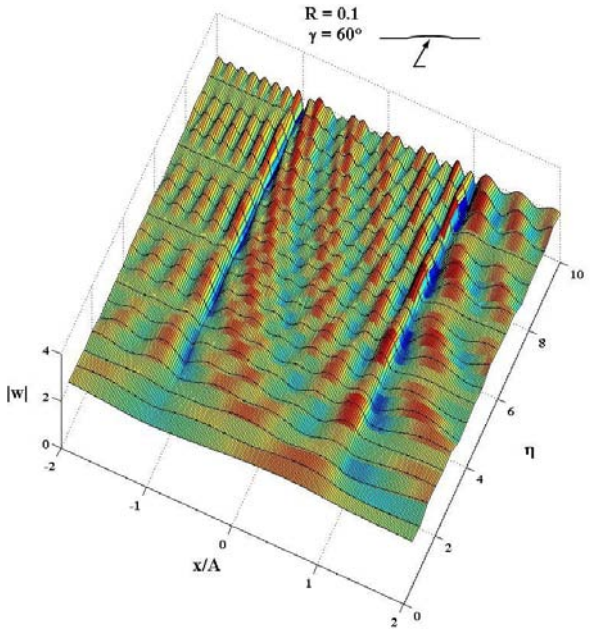


Figure 3.7: Displacement Amplitude for $R = 0.1$ when $\gamma = 90°$

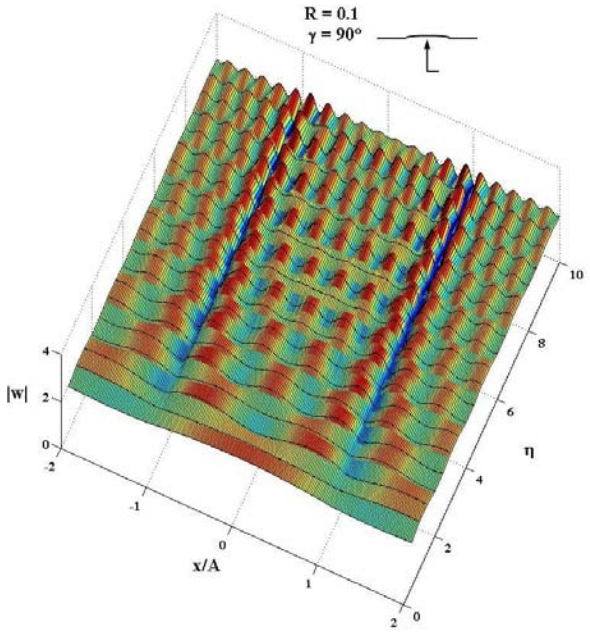

Figure 3.8: Displacement Amplitude for $R = 0.3$ when $\gamma = 0°$

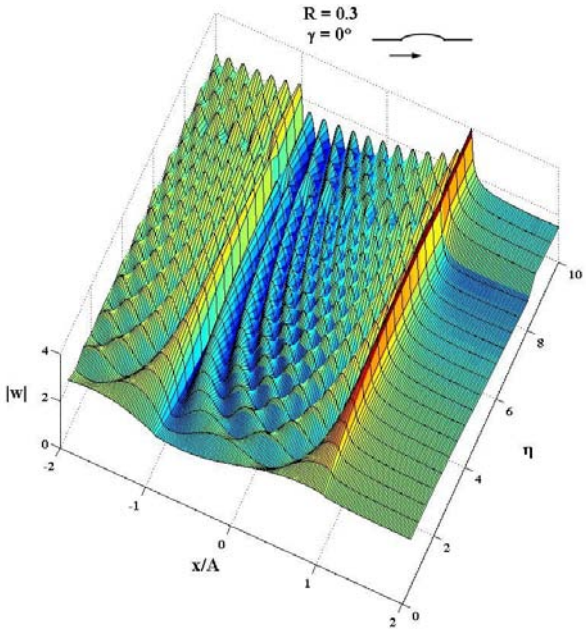


Figure 3.9: Displacement Amplitude for $R = 0.3$ when $\gamma = 30°$

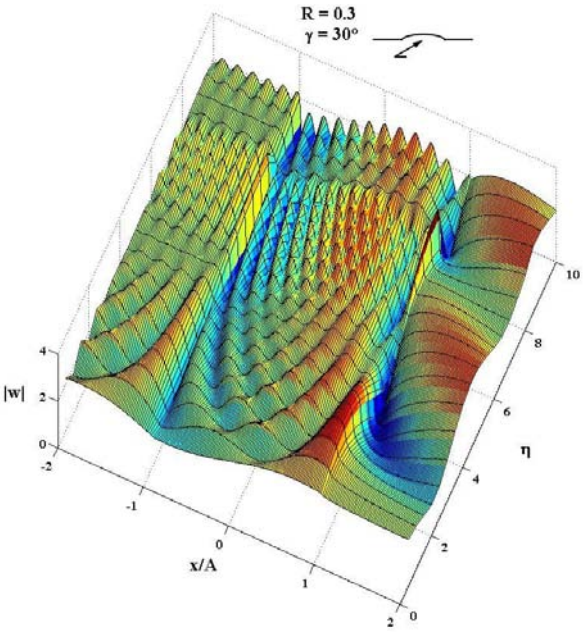

Figure 3.10: Displacement Amplitude for $R = 0.3$ when $\gamma = 60°$

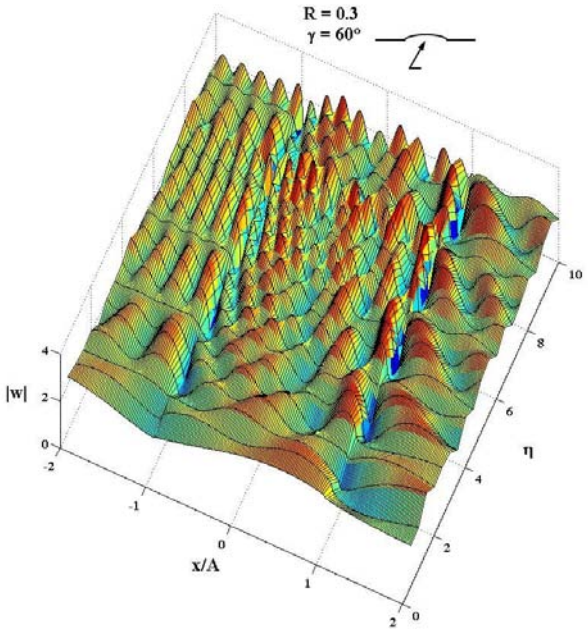


Figure 3.11: Displacement Amplitude for $R = 0.3$ when $\gamma = 90°$

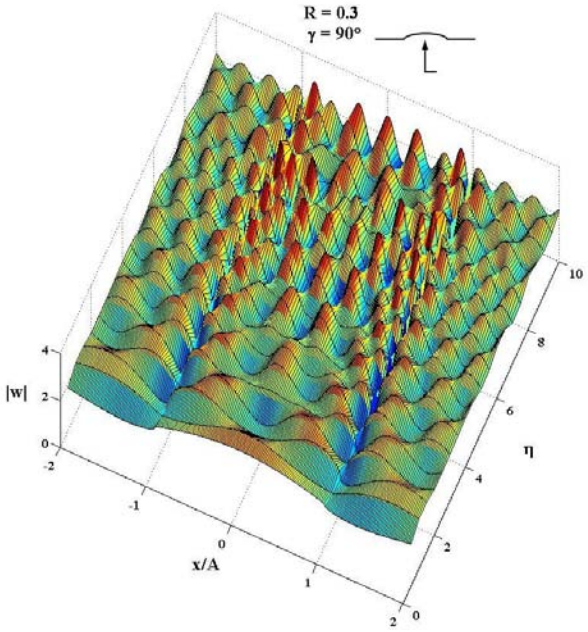

Figure 3.12: Displacement Amplitude for $R = 0.5$ when $\gamma = 0°$

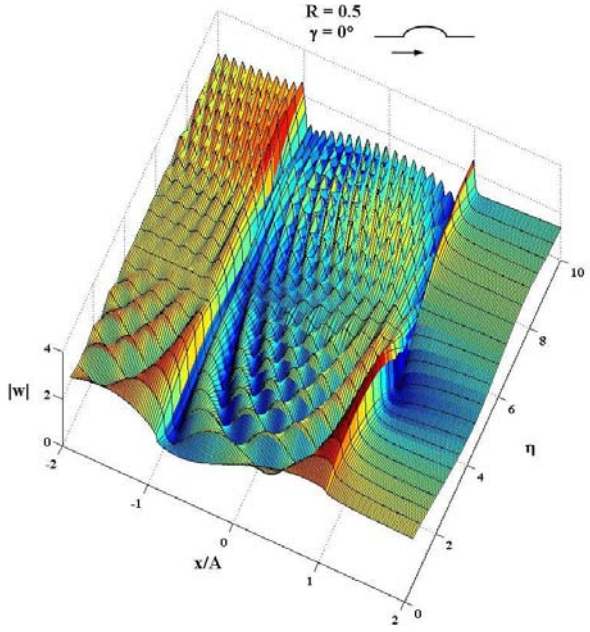


Figure 3.13: Displacement Amplitude for $R = 0.5$ when $\gamma = 30°$

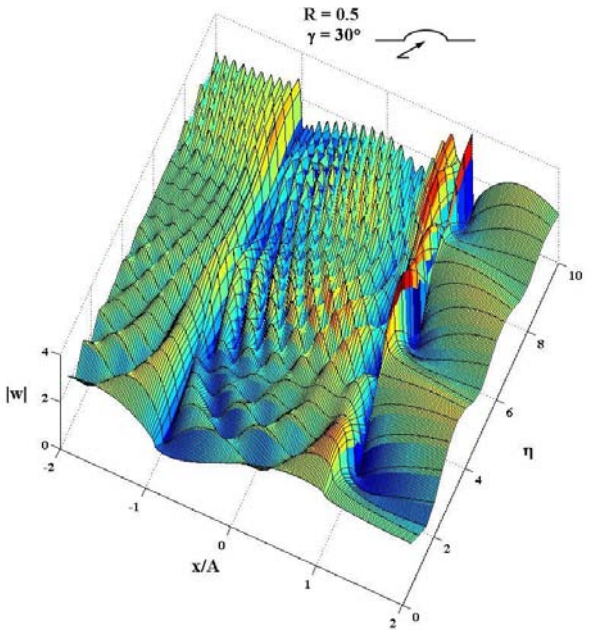

Figure 3.14: Displacement Amplitude for $R = 0.5$ when $\gamma = 60°$

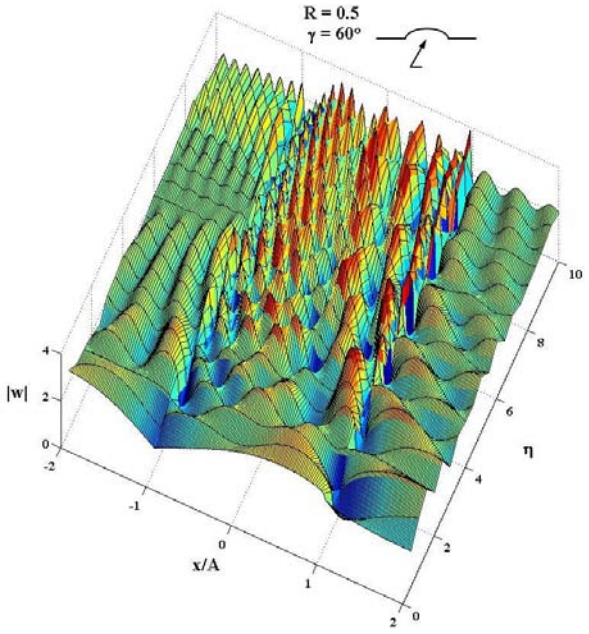


Figure 3.15: Displacement Amplitude for $R = 0.5$ when $\gamma = 90°$

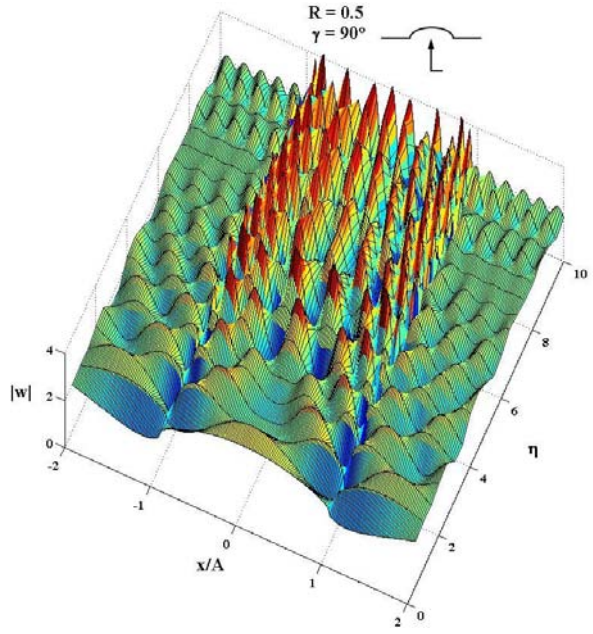

Figure 3.16: Displacement Amplitude for $R = 0.7$ when $\gamma = 0°$

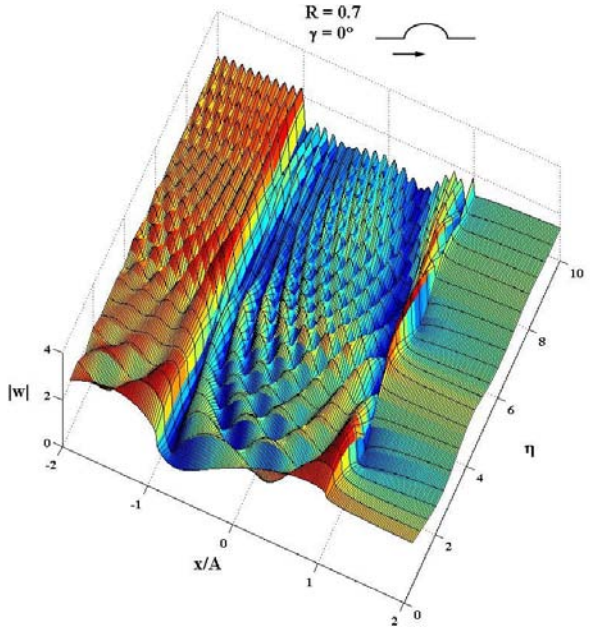


Figure 3.17: Displacement Amplitude for $R = 0.7$ when $\gamma = 30°$

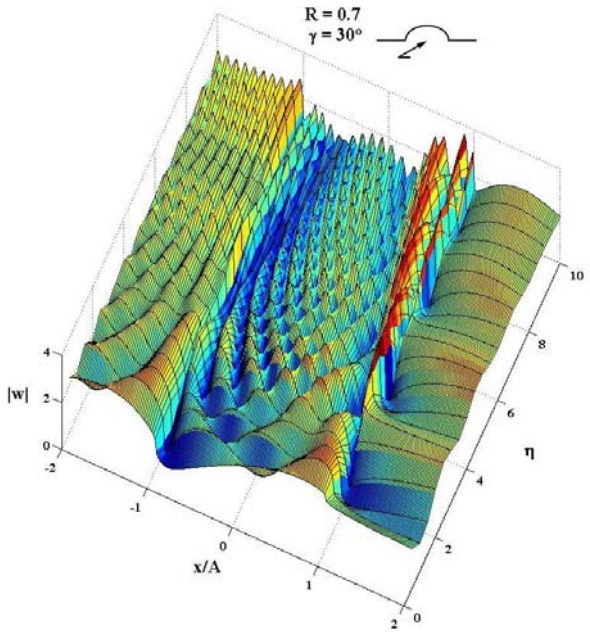

Figure 3.18: Displacement Amplitude for $R = 0.7$ when $\gamma = 60°$

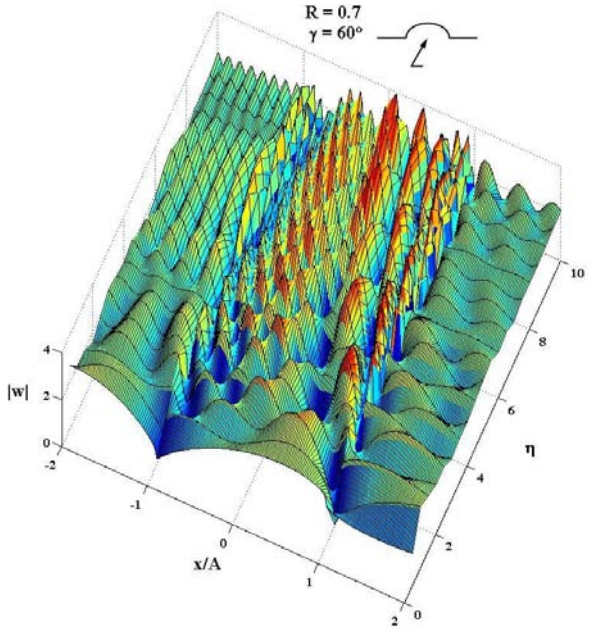


Figure 3.19: Displacement Amplitude for $R = 0.7$ when $\gamma = 90°$

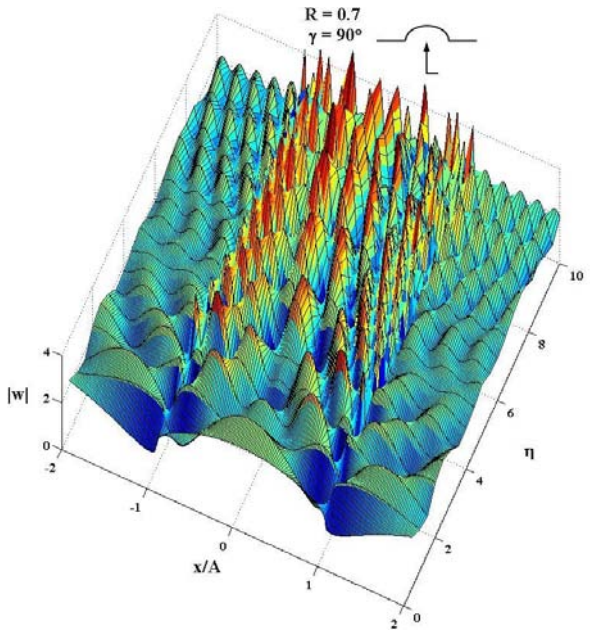

Figure 3.20: Displacement Amplitude for $R = 0.9$ when $\gamma = 0°$

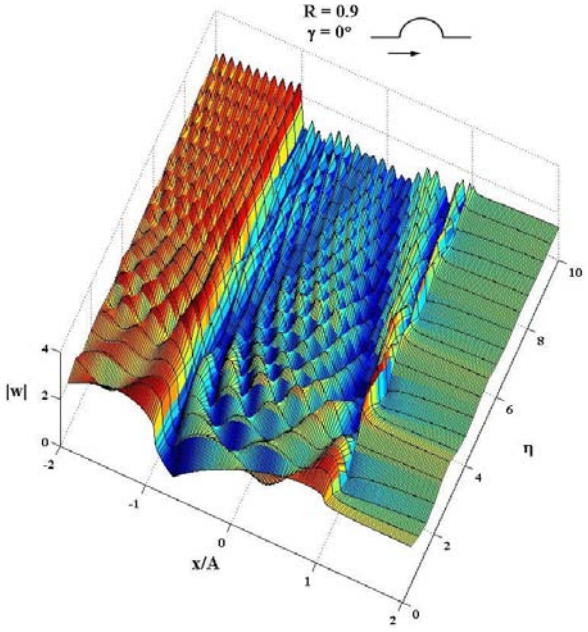


Figure 3.21: Displacement Amplitude for $R = 0.9$ when $\gamma = 30°$

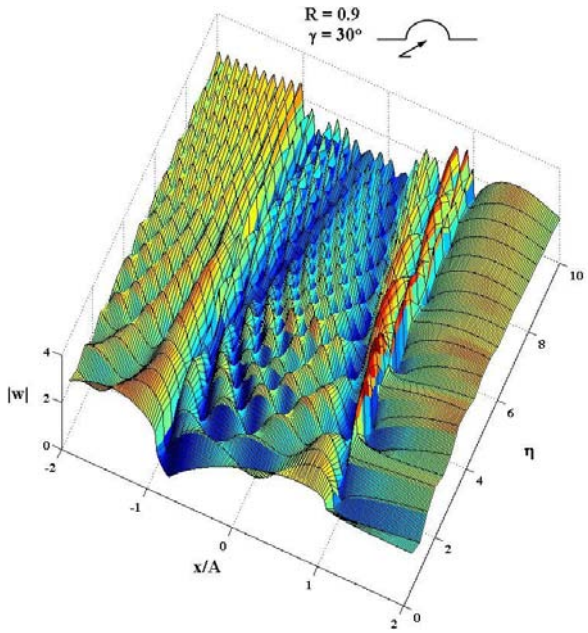

Figure 3.22: Displacement Amplitude for $R = 0.9$ when $\gamma = 60°$

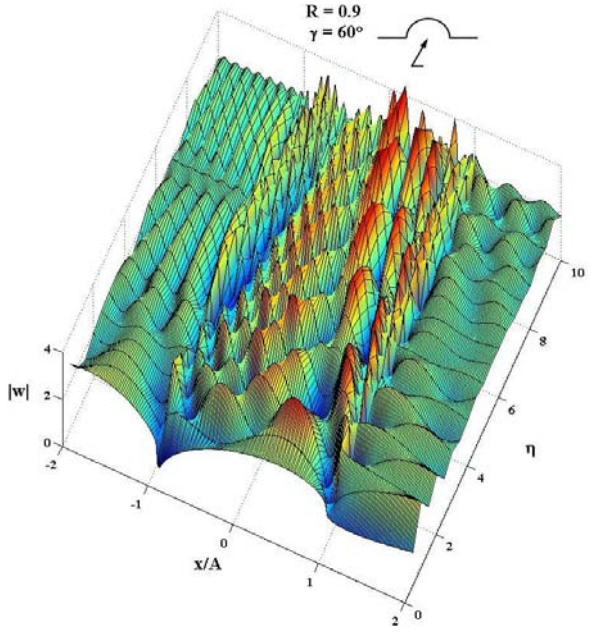


Figure 3.23: Displacement Amplitude for $R = 0.9$ when $\gamma = 90°$

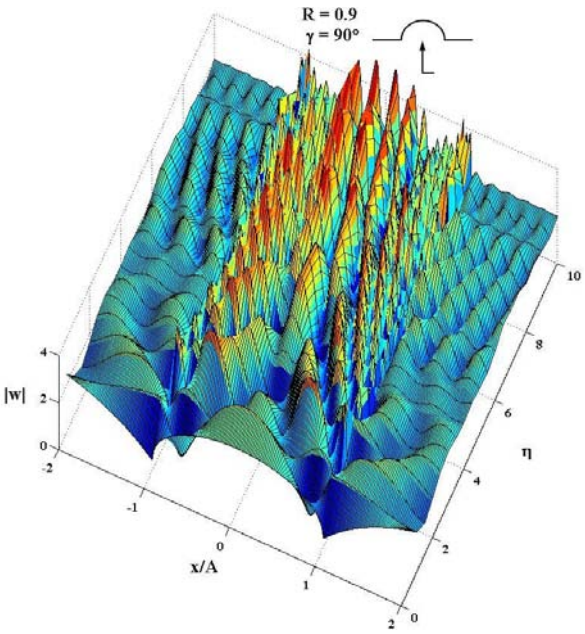

# CHAPTER 4: SCATTERING OF PLANE (SH) WAVES BY A DEEP SEMI-ELLIPTICAL HILL

In this Chapter, the ground motion and wave propagation resulted from the scattering of anti-plane (SH) waves by a deep semi-elliptical hill on an elastic half-space is studied and explained by the closed-form solution, based on method of wave function expansion, and the expansion of elliptical sine and cosine over the half-range $[-\pi/2, \pi/2]$. Similar to Chaper 3 shallow semi-elliptical hill, numerical results when semi-elliptical tends to semi-circular are compared with the work by Lee et al (2006). The analysis shows the interference on ground motion depends on several factors such as frequency of the incident waves, incident angle, and the aspect ratio of elliptical hills

## 4.1 The Deep Semi-Elliptical Hill Model

The cross-section of two-dimensional model studied in this paper is shown in Figure 4.1; it represents an elastic, isotropic, and homogeneous half-space with a semi-elliptical hill. Its material properties are given by the rigidity $\mu$ and the velocity of shear wave $\beta$. Similar coordinate systems to Chapter 3 are utilized, except the half-space which is defined by $x \geq 0$ in order to facilitate the analysis of the deep semi-elliptical hill. In addition the lower bound to which our solution applies is limited to that of semi-circular hill.

Figure 4.1: Deep Semi-Elliptical Hill Model

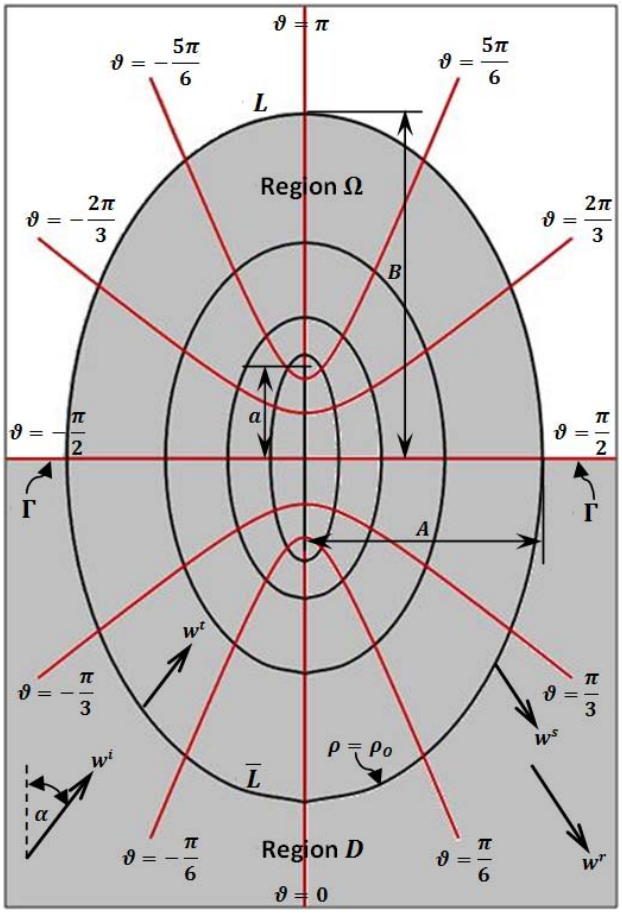


The model consists of the regions $\Omega$ and *D.* The interior regions $\Omega$ is the full elliptical region which has the boundary *L* along surface of the semi-elliptical hill, $\rho = \rho_0$ and $\pi/2 \leq \vartheta \leq -\pi/2$, and the boundary $\overline{L}$ between the regions $\Omega$ and *D*, $\rho = \rho_0$ and $-\pi/2 \leq \vartheta \leq \pi/2$. The exterior region *D* consists of the half-space bounded by $\overline{L}$ along interface $\rho = \rho_0$ and the flat surface of the half-space beyond the hill denoted by $\Gamma$ along $\vartheta = -\pi/2$ and $\pi/2$. Again the half-width and height of the semi-elliptical hill are denoted by A and B, and $a$ is the focal length.

## 4.2 Series Expansion of Wave Functions

**Incident and Reflected Waves:**

In the absence of the hill, the plane incident SH waves $w^i$ travelling in the direction $\pi - \gamma$ would reflect at the flat surface $\Gamma$ and therefore generate the reflected plane waves, $w^r$, moving with angle $\gamma$. Later the incident plane waves interfere with the reflected plane waves, and yield the free field waves $w^{ff}$ which can be expressed by the series of Mathieu functions after applying Equation (2.20).

$$\begin{aligned} w^{ff} = \quad & 4w_0 \sum_{n=0}^{\infty}\left[(-1)^n Mc_{2n}^{(1)}(\rho, q)ce_{2n}(\vartheta, q)ce_{2n}(\gamma, q)\right] \\ & + 4iw_0 \sum_{n=0}^{\infty}\left[(-1)^n Ms_{2n+1}^{(1)}(\rho, q)se_{2n+1}(\vartheta, q)se_{2n+1}(\gamma, q)\right] \end{aligned} \tag{4.1}$$

where $w_0 =$ amplitude of the incident wave.

In addition $q$, $Mc_{2n}^{(1)}(\cdot)$, $Ms_{2n+1}^{(1)}(\cdot)$, $ce_{2n}(\cdot)$ and $se_{2n+1}(\cdot)$ are Mathieu parameter, even and odd Modified Mathieu function of the first kind, and even and odd Mathieu function respectively; the expression of these functions are given by Equations (2.13) and (2.17). It is worth mentioning that shown in Equation (4.1) only even order of Mathieu functions appears in the first series whereas the odd order solely does in the second series since

$$ce_n(\pi - \gamma, q) = (-1)^n ce_n(\gamma, q)$$

$$se_n(\pi - \gamma, q) = (-1)^{n+1} se_n(\gamma, q)$$

**Scattered and Transmitted Waves:**

Two more plane SH waves are generated as the incident plane waves strike the crossing point between regions $\Omega$ and *D*. The first waves are the scattered and diffracted outgoing waves $w^s$ in the exterior region *D*, whereas the second ones are the standing transmitted waves $w^t$ inside the elliptical region $\Omega$; they can be expressed in the forms of elliptical wave functions

$$w^s = \sum_{n=0}^{\infty}\left[A_{2n}Mc_{2n}^{(3)}(\rho,q)ce_{2n}(\vartheta,q) + A_{2n+1}Ms_{2n+1}^{(3)}(\rho,q)se_{2n+1}(\vartheta,q)\right]; \rho \geq \rho_0 \quad (4.2)$$

$$w^t = \sum_{n=0}^{\infty}\left[B_nMc_n^{(1)}(\rho,q)ce_n(\vartheta,q)\right] + \sum_{n=1}^{\infty}\left[C_nMs_n^{(1)}(\rho,q)se_n(\vartheta,q)\right]; \rho \leq \rho_0 \quad (4.3)$$

where $A_n$, $B_n$ and $C_n$ are the unknown coefficients of the new plane waves to be determined. Moreover $Mc_{2n}^{(3)}(\cdot)$ and $Ms_{2n+1}^{(3)}(\cdot)$ are even and odd modified Mathieu function of the third kind respectively, while others are defined previously. The scattered waves in the region *D* $(\rho \geq \rho_0, -\pi/2 \leq \vartheta \leq \pi/2)$ have $Mc_{2n}^{(3)}(\cdot)$ and $Ms_{2n+1}^{(3)}(\cdot)$ as radial wave functions since they have asymptotic behavior of Hankel function of the first kind which satisfies Sommerfeld's far field condition. Furthermore $ce_{2n}(\cdot)$ and $se_{2n+1}(\cdot)$ are used to form angular wave functions because they form a complete orthogonal set of functions in the angular domain $-\pi/2 \leq \vartheta \leq \pi/2$. The transmitted waves in the interior region $\Omega$ $(\rho \leq \rho_0, 0 \leq \vartheta \leq 2\pi)$ have $Mc_n^{(1)}(\cdot)$ and $Ms_n^{(1)}(\cdot)$ as radial wave functions since they have asymptotic behavior of Bessel function of the first kind which are finite everywhere in the full elliptical region $\Omega$ (Pao and Mow, 1973). In addition in the

full angular domain of the region $\Omega$, $ce_n(\cdot)$ and $se_n(\cdot)$ form a complete orthogonal set of functions.

**Solution of the Problem using Angular Half-range Expansion**

The wave functions of the total displacement, $w = w^{ff} + w^s$, in the exterior region *D* and of the transmitted wave, $w^t$, in the elliptical region $\Omega$ must satisfy the Helmholtz equation, Equation (2.8), and the following boundary conditions:

1. The traction-free boundary condition at the flat half-space $\Gamma$
   $(\rho \geq \rho_0, \vartheta = -\pi/2\,, \pi/2)$

$$\tau_{yz}\big|_{y=0} = \tau_{\vartheta z}|_{\vartheta=-\pi/2,\pi/2} = \frac{\mu}{aJ}\frac{\partial(w^{ff}+w^s)}{\partial\vartheta} = 0 \tag{4.4}$$

2. The traction-free boundary condition at the surface of the elliptical hill *L*
   $(\rho = \rho_0, \pi/2 \leq \vartheta \leq -\pi/2)$

$$\tau_{\rho z}\big|_{\rho=\rho_0} = \frac{\mu}{aJ}\frac{\partial w^t}{\partial\rho}\Big|_{\xi=\xi_0} = 0 \tag{4.5}$$

3. The continuity of displacement and radial stress at the interface $\overline{L}$
   $(\rho = \rho_0, -\pi/2 \leq \vartheta \leq \pi/2)$

$$\begin{aligned}(w^{ff} + w^s)\big|_{\rho=\rho_0} &= w^t|_{\rho=\rho_0} \\ \tau_{\rho z}\big|_{\rho=\rho_0} = \frac{\mu}{aJ}\frac{\partial(w^{ff}+w^s)}{\partial\rho}\Big|_{\rho=\rho_0} &= \frac{\mu}{aJ}\frac{\partial w^t}{\partial\rho}\Big|_{\rho=\rho_0}\end{aligned} \tag{4.6}$$

Each term of $w^{ff}$ and $w^s$, Equations (4.1) and (4.2), contents an elliptical cosine function of even order and an elliptical sine function of odd order; hence they

automatically satisfy the traction-free boundary condition at the surface of the flat half-space $\Gamma$, Equation (4.4).

Boundary conditions of Equations (4.5) and (4.6) are applied to determine the unknown coefficients of both scattered and transmitted waves. Similar to the case of shallow elliptical hill, the transmitted waves $w^t$ in the full elliptical region must satisfy two disjoint sets of boundary conditions, one set for traction-free boundary condition at the free surface of the elliptical hill *L*, and another set for the continuity of displacement and stress at the interface $\overline{L}$. In addition as the transmitted waves $w^t$ contain elliptical cosine and sine of both even and odd orders, those boundary conditions could not be separately imposed directly. Later utilizing the complete orthogonal set $\{ce_{2n}(\vartheta,q), se_{2n+1}(\vartheta,q);\ n=0,1,2\ldots\}$ in the half-range $[-\pi/2\,,\pi/2]$ (and similarly in $[\pi/2\,,-\pi/2]$), the transmitted waves $w^t$ and the corresponding radial stress becomes

$$\begin{aligned} w^t \quad &= \sum_{n=0}^{\infty}\left[B_{2n}Mc_{2n}^{(1)}(\rho,q) \mp \sum_{m=0}^{\infty}\mathfrak{M}_{mn}B_{2m+1}Mc_{2m+1}^{(1)}(\rho,q)\right]ce_{2n}(\vartheta,q) \\ &\quad + \sum_{n=0}^{\infty}\left[C_{2n+1}Ms_{2n+1}^{(1)}(\rho,q) \mp \sum_{m=0}^{\infty}\mathfrak{N}_{mn}C_{2m+2}Ms_{2m+2}^{(1)}(\rho,q)\right]se_{2n+1}(\vartheta,q) \end{aligned} \tag{4.7}$$

$$\begin{aligned} \tau_{\rho z} \quad &= \frac{\mu}{aJ}\sum_{n=0}^{\infty}\left[B_{2n}Mc_{2n}^{(1)'}(\rho,q) \mp \sum_{m=0}^{\infty}\mathfrak{M}_{mn}B_{2m+1}Mc_{2m+1}^{(1)'}(\rho,q)\right]ce_{2n}(\eta,q) \\ &\quad + \frac{\mu}{aJ}\sum_{n=0}^{\infty}\left[C_{2n+1}Ms_{2n+1}^{(1)'}(\rho,q) \mp \sum_{m=0}^{\infty}\mathfrak{N}_{mn}C_{2m+2}Ms_{2m+2}^{(1)'}(\rho,q)\right]se_{2n+1}(\vartheta,q) \end{aligned} \tag{4.8}$$

where –ve above and +ve below are assigned for $\pi/2 \le \vartheta \le -\pi/2$ and $-\pi/2 \le \vartheta \le \pi/2$; $\mathfrak{M}_{mn}$ and $\mathfrak{N}_{mn}$ are given by Equations (2.35) and (2.38). As all displacement and stress functions of far-field, scattered and transmitted waves

are in the forms of elliptical cosine series with order 2n and of elliptical sine series with order 2n+1, boundary conditions are convenient to apply. Similar procedure to the case of the shallow semi-elliptical hill is performed, yet two linear equations of infinite order are formulated

$$\sum_{m=0}^{\infty} \mathbb{D}_{mn} B_{2m+1} = 4w_0(-1)^n \left[ Mc_{2n}^{(1)'}(\rho_0, q) - \left( \frac{Mc_{2n}^{(3)'}(\rho_0,q)}{Mc_{2n}^{(3)}(\rho_0,q)} \right) Mc_{2n}^{(1)}(\rho_0, q) \right] ce_{2n}(\gamma, q) \tag{4.9}$$

$$\sum_{m=0}^{\infty} \mathbb{E}_{mn} C_{2m+2} = 4w_0 i(-1)^n \left[ Ms_{2n+1}^{(1)'}(\rho_0, q) - \left( \frac{Ms_{2n+1}^{(3)'}(\rho_0,q)}{Ms_{2n+1}^{(3)}(\rho_0,q)} \right) Ms_{2n+1}^{(1)}(\rho_0, q) \right] se_{2n+1}(\gamma, q) \tag{4.10}$$

where

$$\mathbb{D}_{mn} = \mathfrak{M}_{mn} \left\{ 2Mc_{2m+1}^{(1)'}(\rho_0, q) - \left( \frac{Mc_{2n}^{(3)'}(\rho_0,q)}{Mc_{2n}^{(3)}(\rho_0,q)} \right) \left[ \left( \frac{Mc_{2n}^{(1)}(\rho_0,q)}{Mc_{2n}^{(1)'}(\rho_0,q)} \right) Mc_{2m+1}^{(1)'}(\rho_0, q) + Mc_{2m+1}^{(1)}(\rho_0, q) \right] \right\}$$

$$\mathbb{E}_{mn} = \mathfrak{N}_{mn} \left\{ 2Ms_{2m+2}^{(1)'}(\rho_0, q) - \left( \frac{Ms_{2n+1}^{(3)'}(\rho_0,q)}{Ms_{2n+1}^{(3)}(\rho_0,q)} \right) \left[ \left( \frac{Ms_{2n+1}^{(1)}(\rho_0,q)}{Ms_{2n+1}^{(1)'}(\rho_0,q)} \right) Ms_{2m+2}^{(1)'}(\rho_0, q) + Ms_{2m+2}^{(1)}(\rho_0, q) \right] \right\}$$

Here $B_{2m+1}$'s and $C_{2m+1}$'s could be calculated first by truncation of the above infinite matrices. Later other coefficients are determined through the equations

$$A_{2n} = \frac{1}{Mc_{2n}^{(3)}(\rho_0,q)} \left\{ \sum_{m=0}^{\infty} \mathfrak{M}_{mn} \left[ \left( \frac{Mc_{2n}^{(1)}(\rho_0,q)}{Mc_{2n}^{(1)'}(\rho_0,q)} \right) Mc_{2m+1}^{(1)'}(\rho_0, q) + Mc_{2m+1}^{(1)}(\rho_0, q) \right] B_{2m+1} - 4w_0(-1)^n Mc_{2n}^{(1)}(\rho_0, q) ce_{2n}(\gamma, q) \right\}$$

$$A_{2n+1} = \frac{1}{Ms^{(3)}_{2n+1}(\rho_0,q)}\left\{\sum_{m=0}^{\infty} \mathfrak{R}_{mn}\left[\left(\frac{Ms^{(1)}_{2n+1}(\rho_0,q)}{Ms^{(1)\prime}_{2n+1}(\rho_0,q)}\right) Ms^{(1)\prime}_{2m+2}(\rho_0,q) + Ms^{(1)}_{2m+2}(\rho_0,q)\right] C_{2m+2} \right.$$
$$\left. -4iw_0(-1)^n Ms^{(1)}_{2n+1}(\rho_0,q)se_{2n+1}(\gamma,q)\right\}$$

$$B_{2n} = \frac{1}{Mc^{(1)'}_{2n}(\rho_0,q)}\sum_{m=0}^{\infty} \mathfrak{M}_{mn} Mc^{(1)'}_{2m+1}(\rho_0,q) B_{2m+1}$$

$$C_{2n+1} = \frac{1}{Ms^{(1)\prime}_{2n+1}(\rho_0,q)}\sum_{m=0}^{\infty} \mathfrak{R}_{mn} Ms^{(1)\prime}_{2m+2}(\rho_0,q) C_{2m+2}$$

## 4.3 Results and Analysis

Amplitudes of ground motions at various points are analyzed. Similar to Chapter 3 we assume the excitation consists of an infinite train of SH wave with amplitude 1, and present the results in term of the dimensionless parameter $\eta$ which is defined as Equation (3.16), except the focal length which is expressed in term of A and B, the half-width and height of the hill respectively, as follows

$$c = \frac{A}{sinh\left(tanh^{-1}(A/B)\right)} \tag{4.11}$$

Moreover the aspect ratio *R*, Equation (3.18), is employed to study the shape effect of a semi-elliptical hill; the minimum aspect ratio $R$ of a deep semi-elliptical hill is limited to that of semi-circular one.

As noted by Wong and Trifunac (1974**b**), the required number of terms in series representation of Mathieu functions increases with increasing $|y|$ and $q$; for example, increasing $R$ and $\eta$. The utilization of the half-range expansion in the elliptical hill model even requires more number of terms than semi-elliptical

canyon/alluvial model, and cause a numerical problem; asymptotic approximation for modified Mathieu functions may be needed. In addition the applicable range of proposed solution also depends on the availability of program package (Mechel, 1997). Hence we restrict and calculate the amplitude of displacement only in the range $|y/A| \leq 2.0$ for all $R$, even though amplitude of displacement may be evaluated while $|y/A|$ in the range up to 4.0 without any numerical problem for smaller $R$ with the dimensionless parameter $\eta$ up to 10.

**Comparison with the Previous Work:**

The proposed solution are implemented and tested by modeling a semi-elliptical hill for the “Almost-Circular”, $R$ =1.0001. Previously published result for a semi-circular hill (Lee et al; 2006) are used for comparison purpose. The dimensionless frequency $\eta = 5$ and $10$ are selected for the evaluation.

The Figures 4.2 and 4.3 illustrated the comparison of displacement amplitude of ground surface at 4 angles of incidence $\gamma$ for the “almost-circular” elliptical hill and Circular hill; however note that we define angle of incidence for both cases differently, an angle of incidence measures from the vertical axis for elliptical hill while from the horizontal axis for circular hill. A remarkable agreement between these results has been observed. Particularly around two sharp edges of hill at $y = \pm A$ for elliptical hill and at $x = \pm a$ for circular one, the displacements demonstrate identical patterns. However some minor departures are observed

such as the discrepancies of the displacement at the right rim for the incident wave travelling parallel to flat surface, and of maximum values of the displacements. These variations possible are explained by the utilization of different wave functions in each problem, Angular and Radial Mathieu functions for the semi-elliptical hill and Bessel, Hankel, Sine and Cosine functions for the semi-circular hill.

Figure 4.2: Displacement Amplitudes of Ground Motion at $\eta = 5$

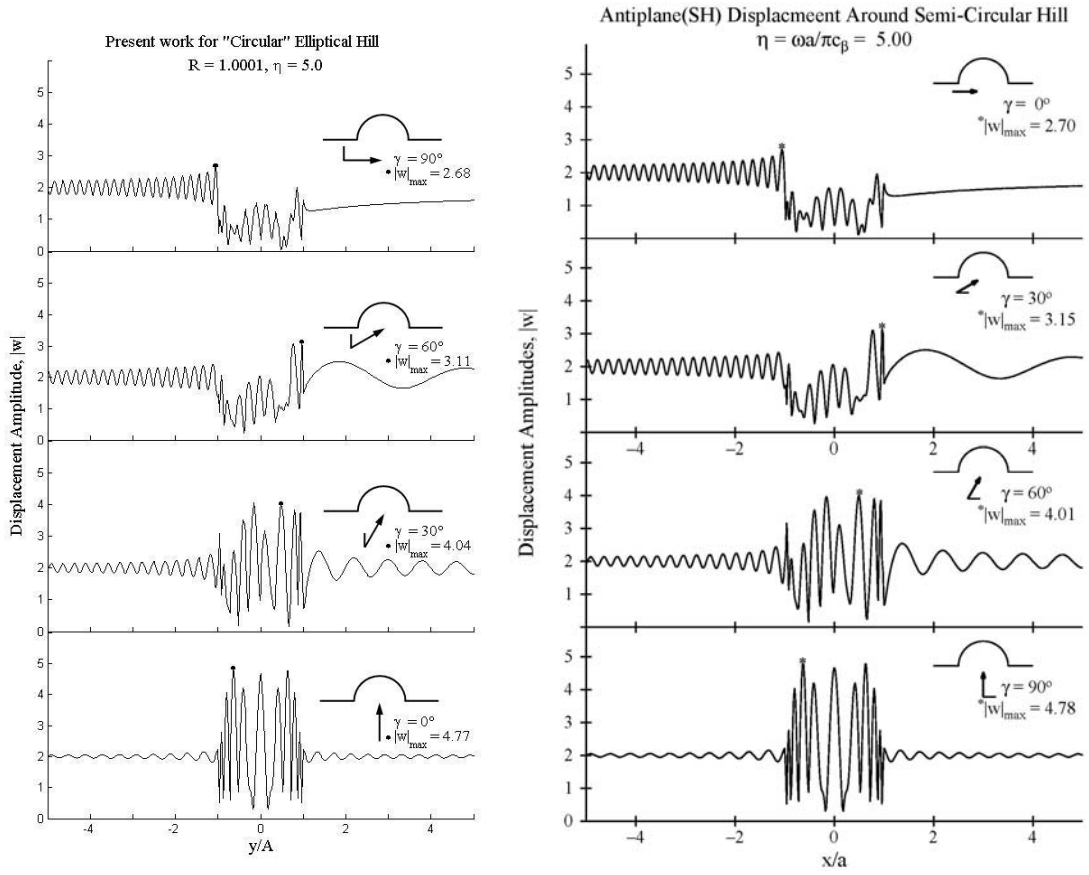


(a) "Almost-Circular" Elliptical Hill ($R = 1.0001$)

(b) Semi-Circular Hill (Courtesy of Lee et al, 2006)

Figure 4.3: Displacement Amplitudes of Ground Motion at $\eta = 10$

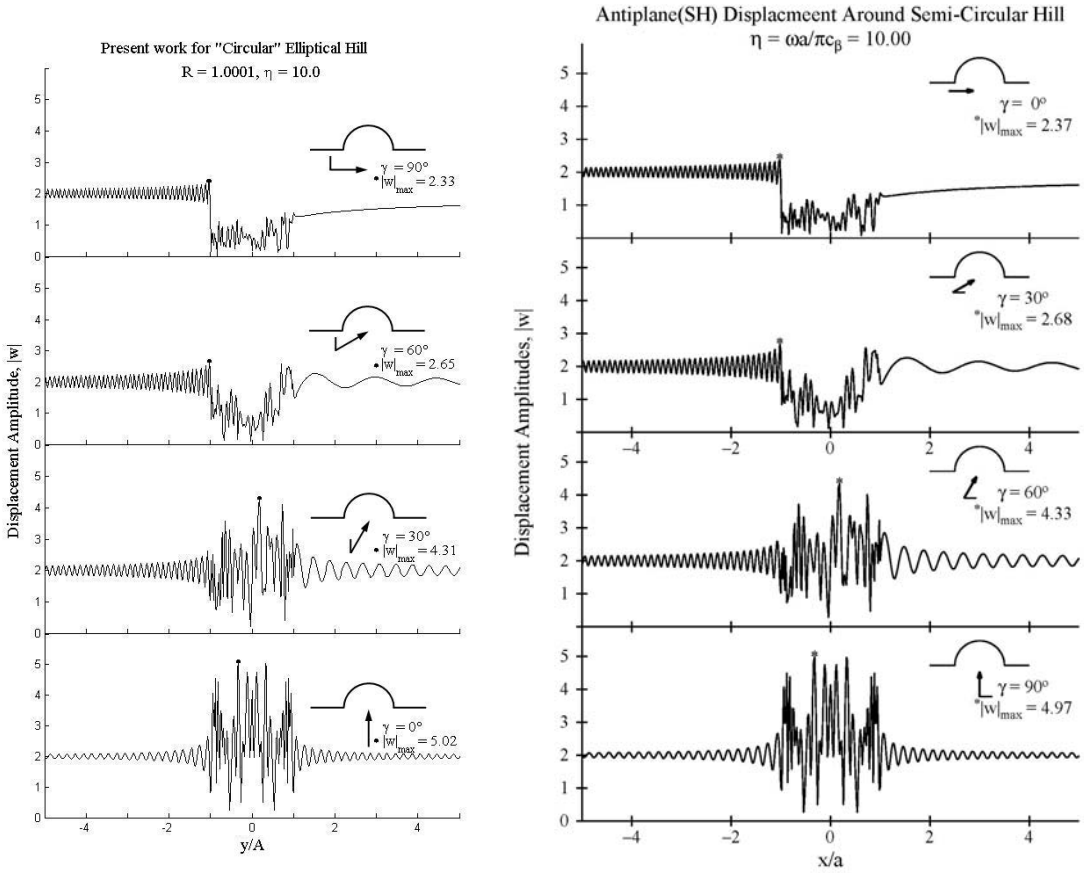


(a) "Almost-Circular" Elliptical Hill ($R = 0.9999$)

(b) Semi-Circular Hill (Courtesy of Lee et al, 2006)

Beside the above comparison with the existing work by Lee et al, 2006, our proposed solutions for both shallow and deep semi-elliptical hills demonstrate very consistent numerical results as we evaluate Figure 3.2a against 4.2a and 3.3a against 4.3a; this may confirm the reliability of the angular half-range expansions.

**Effects of Height-to-Width Ratio of Elliptical Hills, and of Incident Angle:**

Amplitudes of surface displacements for $R = 1.1, 1.3, 1.5, 1.7$ and 1.9, equivalent to height-to-width ratio of 0.55, 0.65, 0.75, 0.85 and 0.95 respectively, are shown in Figures 4.4 through 4.23. They are the three-dimensional plots of displacement amplitudes at one of four incident angles of $\gamma = 0°, 30°, 60°$ and 90° versus the distance *y/A* on and around the hill and the dimensionless frequency $\eta$ in the range of 0.5 to 10. In addition the amplitudes in the range of *y/A* in $[-1,1]$ are those on the elliptical surface of the hill. However it is noted that an angle of incidence measures from the vertical axis.

As the aspect ratio $R$ becomes bigger, the surface displacement demonstrates more complex pattern, which also depends on the angle of incidence. For nearly horizontal angles of incidence $(\gamma = 60°$ and $90°)$, the ground surface in a neighborhood of the zenith experiences smaller disturbance. As aspect ratio $R$ and the frequency of incidence become larger, the displacement amplitudes in the vicinity of unity may possibly occur (for example; R = 1.9 and $\eta \geq 3$). Similar to semi-circular and shallow semi-elliptical hills, the shielding effect of the incoming waves from the left is noticeable, resulting in a standing wave pattern in the front of the hill and minor deviation of the displacement amplitude from the uniform half-space amplitude ($|w| = 2$) in the back of the hill. The sudden jump of the displacement amplitude, which normally is the maximum value, at the right edge of the hill $(y/A = 1)$ is also observed for the glazing angles since the right

rim causes the reflection and diffraction of the incoming waves in the elliptical hill, and the hill becomes a wave trap resulting in the destructive/constructive interferences between the incident, reflected and diffracted waves and the focusing of the amplitude at this edge. While possibly maximum amplitudes of surface displacement for the horizontal angles of incidence are about 4, the maximum amplitudes of 5 or larger are perhaps monitored for vertical incidence.

Figure 4.4: Displacement Amplitude for $R = 0.11$ when $\gamma = 0°$

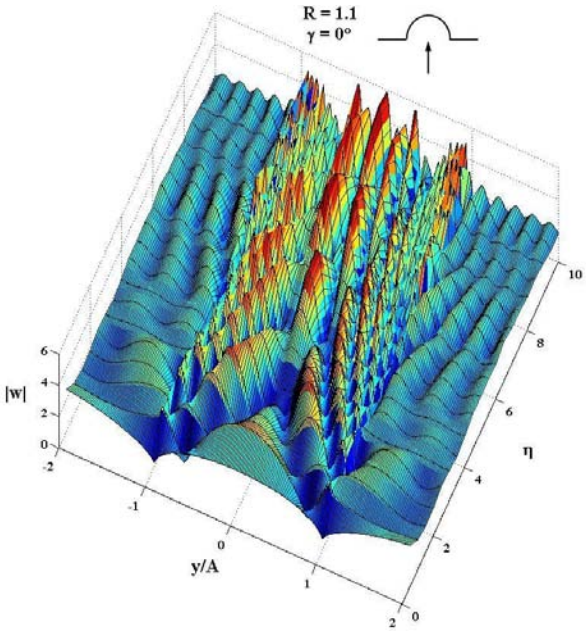

Figure 4.5: Displacement Amplitude for $R = 1.1$ when $\gamma = 30°$

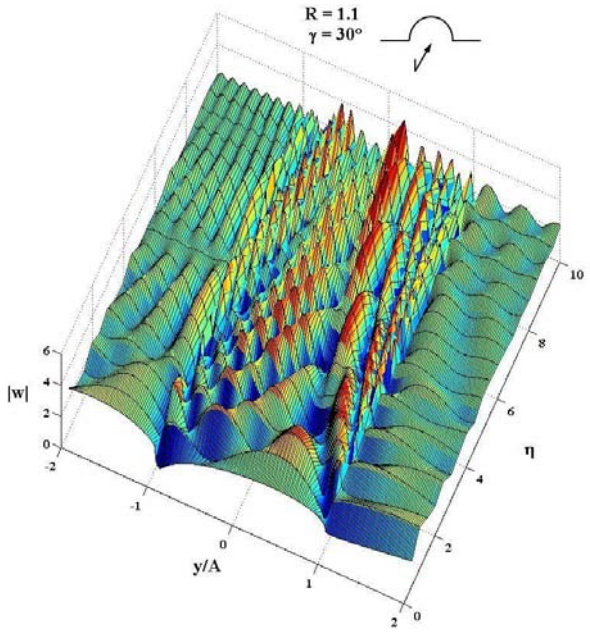


Figure 4.6: Displacement Amplitude for $R = 1.1$ when $\gamma = 60°$

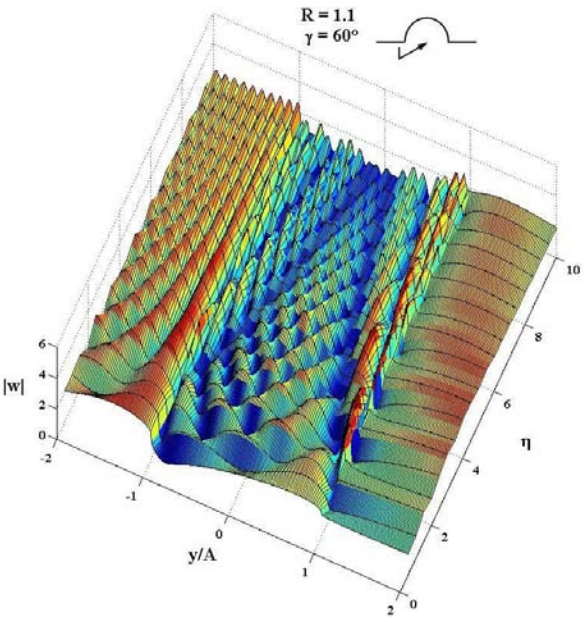

Figure 4.7: Displacement Amplitude for $R = 1.1$ when $\gamma = 90°$

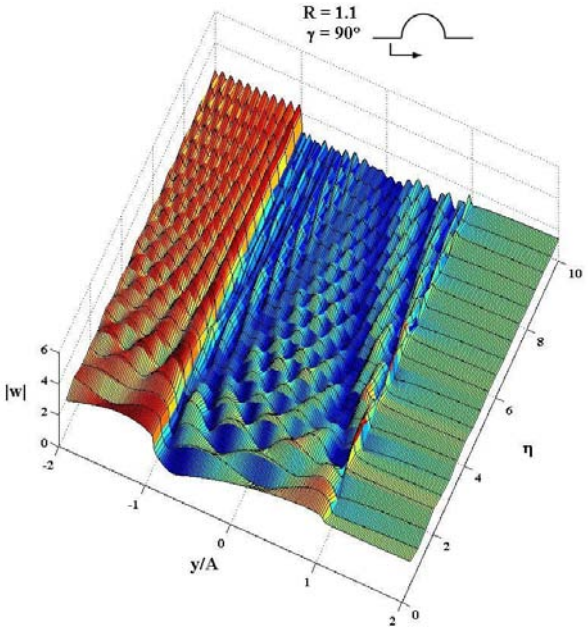


Figure 4.8: Displacement Amplitude for $R = 1.3$ when $\gamma = 0°$

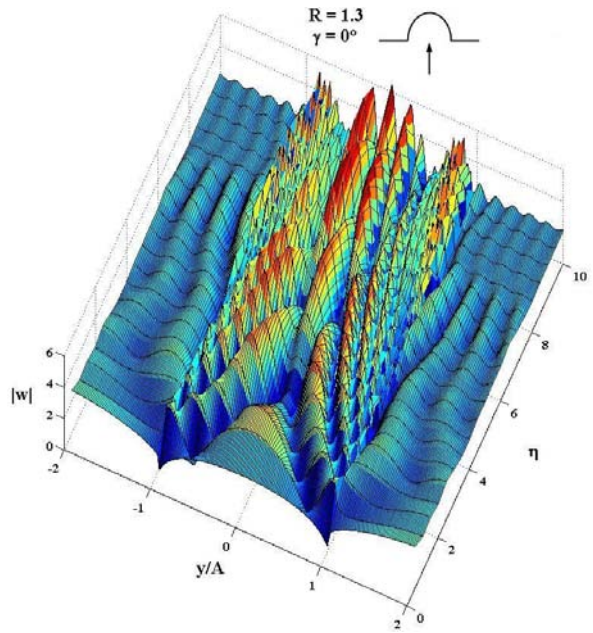

Figure 4.9: Displacement Amplitude for $R = 1.3$ when $\gamma = 30°$

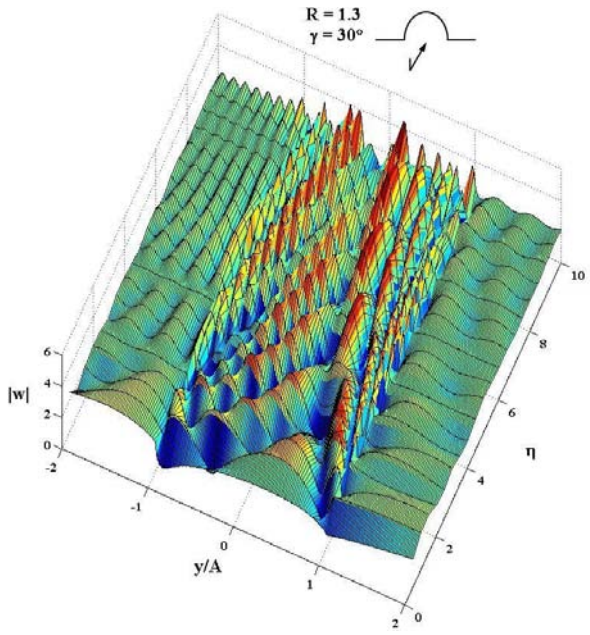


Figure 4.10: Displacement Amplitude for $R = 1.3$ when $\gamma = 60°$

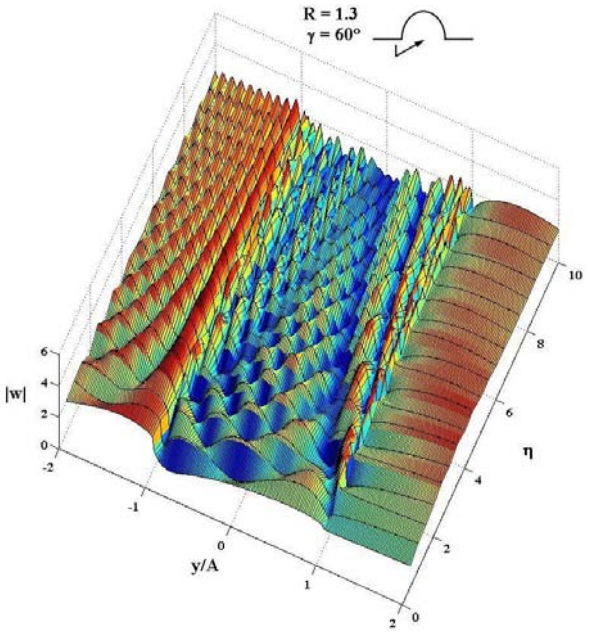

Figure 4.11: Displacement Amplitude for $R = 1.3$ when $\gamma = 90°$

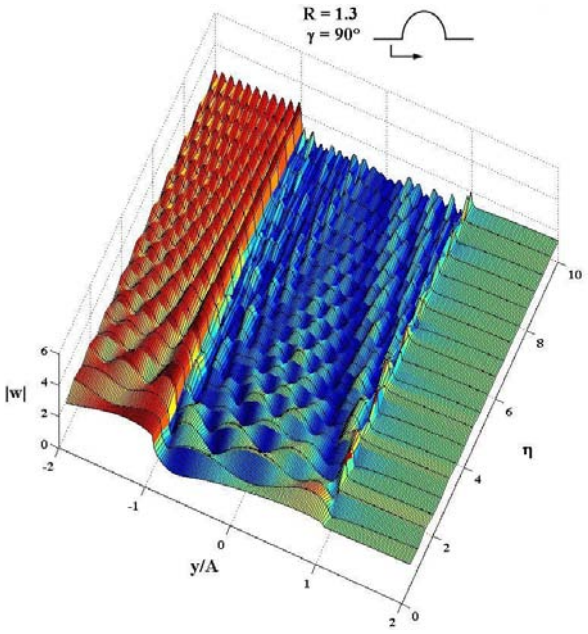


Figure 4.12: Displacement Amplitude for $R = 1.5$ when $\gamma = 0°$

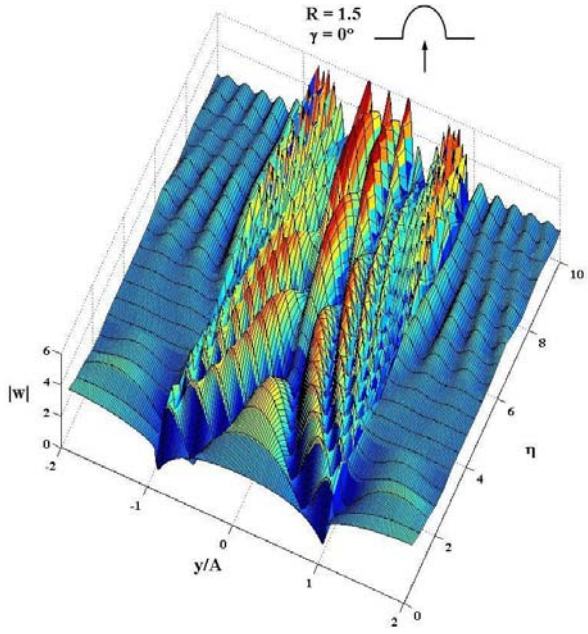

Figure 4.13: Displacement Amplitude for $R = 1.5$ when $\gamma = 30°$

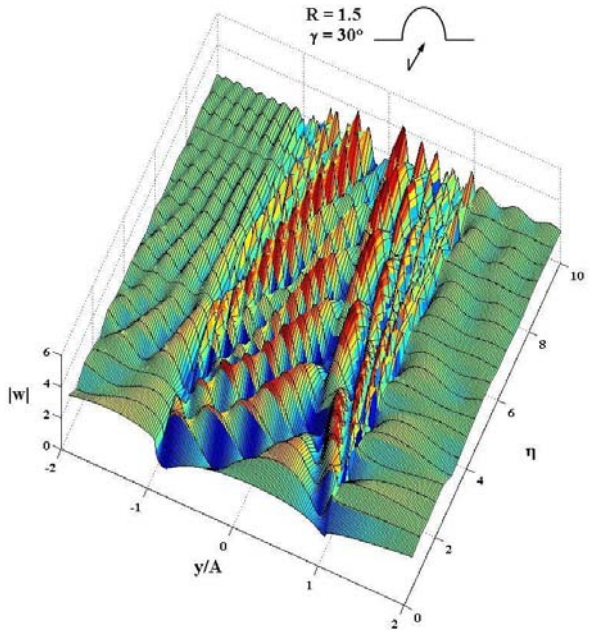


Figure 4.14: Displacement Amplitude for $R = 1.5$ when $\gamma = 60°$

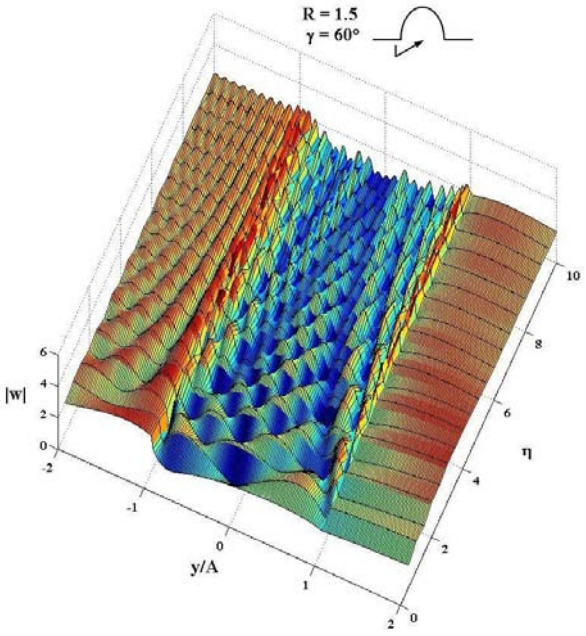

Figure 4.15: Displacement Amplitude for $R = 1.5$ when $\gamma = 90°$

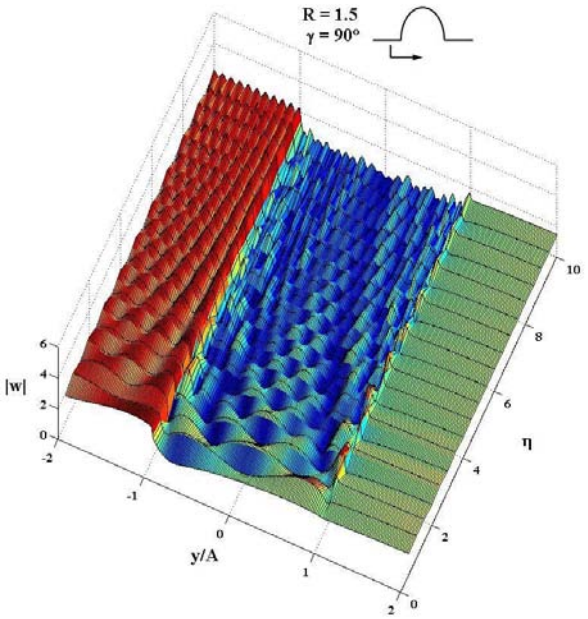


Figure 4.16: Displacement Amplitude for $R = 1.7$ when $\gamma = 0°$

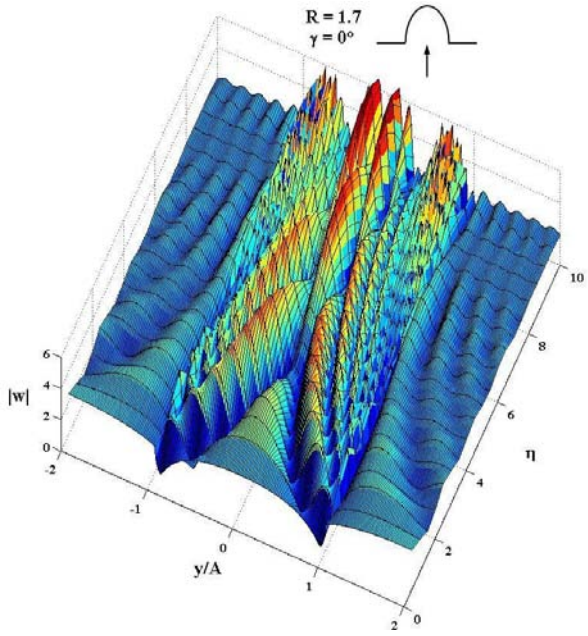

Figure 4.17: Displacement Amplitude for $R = 1.7$ when $\gamma = 30°$

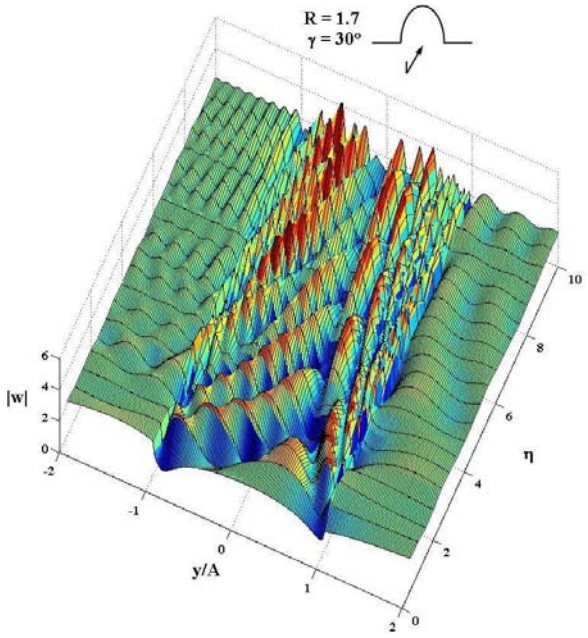


Figure 4.18: Displacement Amplitude for $R = 1.7$ when $\gamma = 60°$

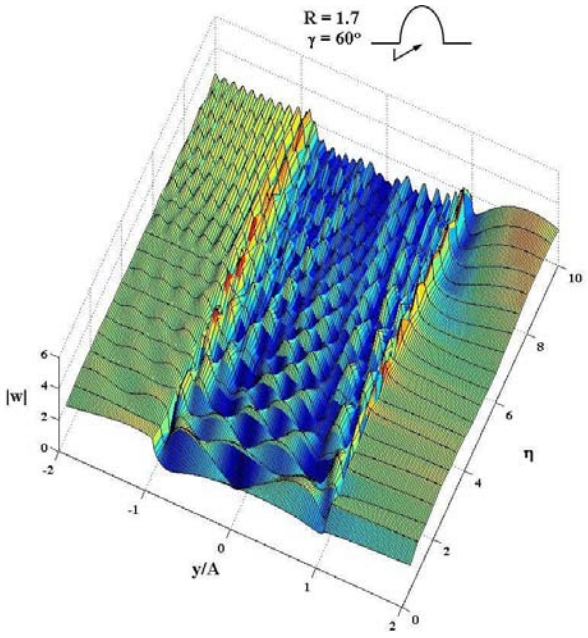

Figure 4.19: Displacement Amplitude for $R = 1.7$ when $\gamma = 90°$

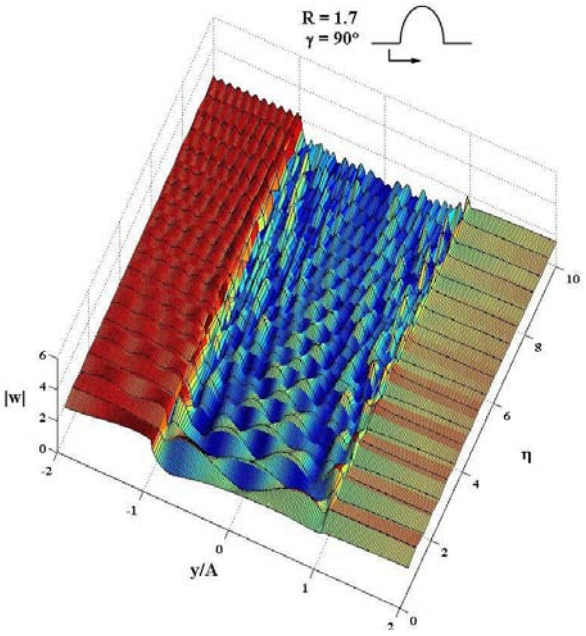


Figure 4.20: Displacement Amplitude for $R = 1.9$ when $\gamma = 0°$

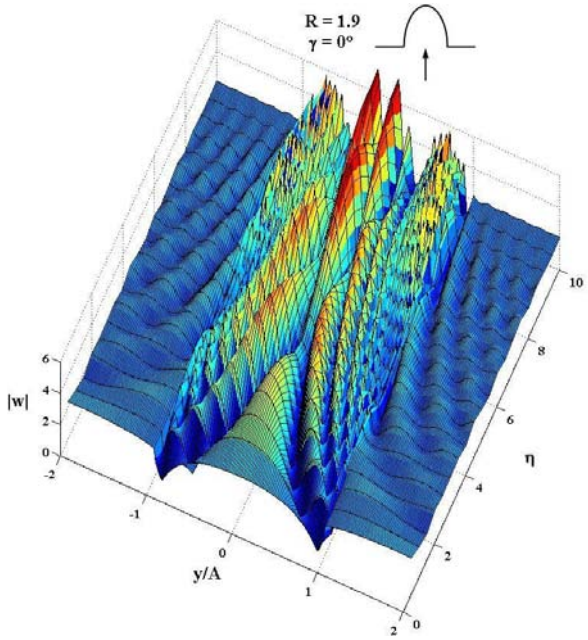

Figure 4.21: Displacement Amplitude for $R = 1.9$ when $\gamma = 30°$

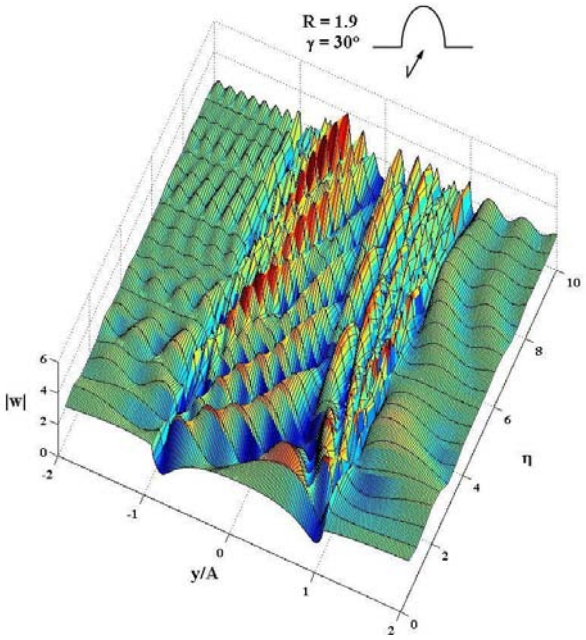


Figure 4.22: Displacement Amplitude for $R = 1.9$ when $\gamma = 60°$

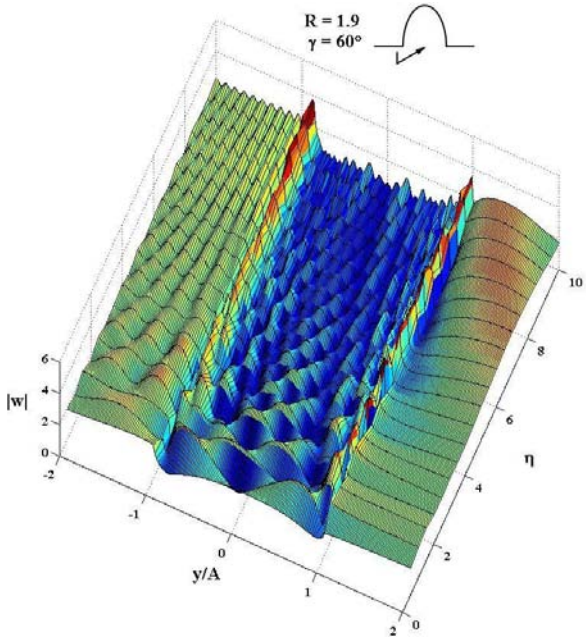

Figure 4.23: Displacement Amplitude for $R = 1.9$ when $\gamma = 90°$

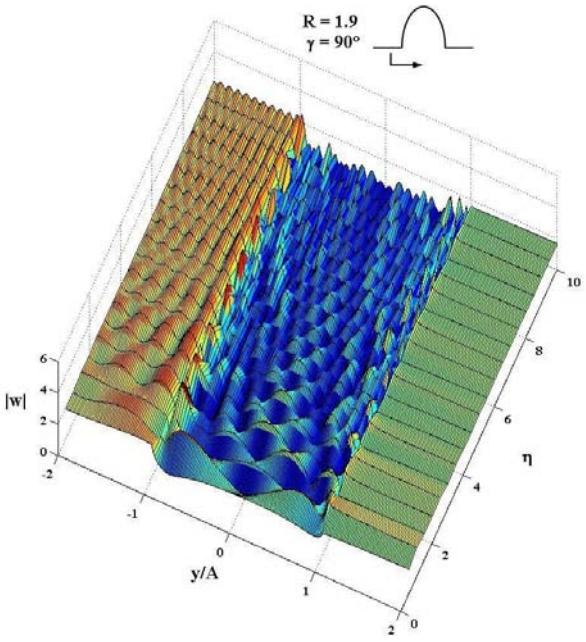

# CHAPTER 5: SCATTERING OF PLANE (SH) WAVES BY A SHALLOW SEMI-ELLIPTICAL HILL WITH AN ELLIPTICAL TUNNEL

As a matter of fact, the presence of a tunnel, cave or cavern is very common in mountain area. It is necessary to consider their influence to a site in seismic regions. In this chapter, an analytic solution to the boundary-valued problem of the two-dimensional scattering of anti-plane (SH) waves by a shallow semi-elliptical hill with a concentric tunnel is presented. Scattering effects due to the existence of elliptical tunnel in the hill are studied and compared with the results of Chapter 3, the scattering effects due to the shallow semi-elliptical hill.

## 5.1 The Shallow Semi-Elliptical Hill with an Elliptical Tunnel Model

The cross-section of two-dimensional model is shown in Figure 5.1. Similar configuration, material properties, and coordinate systems to what we have in Chapter 3 are employed here, but with the presence of a concentric tunnel; A, B and $a$ are expressed as in Chapter 3, while T is the half-width of the tunnel. The model consists of the two regions. The exterior region *D* consists of and extends over the same domain and boundaries as shown in section 3.1, while the regions $\Omega$ is the full-elliptical ring which has the outer boundaries $L$ and $\overline{L}$ and the inner boundary $M$, $\rho = \rho_I$.

Figure 5.1: Shallow Semi-Elliptical Hill with an Elliptical Tunnel Model

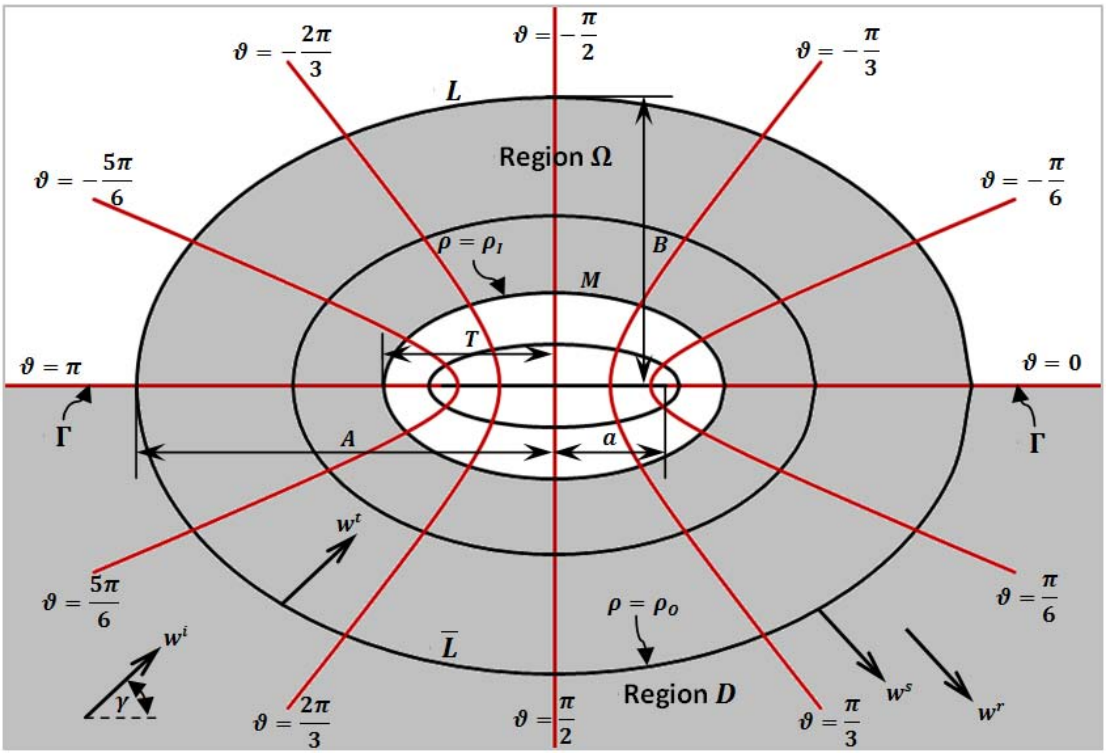


## 5.2 Series Expansion of Wave Functions

**Incident and Reflected Waves:**

The same excitation $w^i$**,** consisting of infinite trains of plane SH waves and travelling in the direction $\gamma$ to positive x axis, as shown in Chapter 3 is applied. Moreover in the free field, no existence of the hill and tunnel, the incident waves strike the flat surface $\Gamma$ and create the reflected plane waves $w^r$; their summation yields the free field waves which can be expressed in elliptical coordinate as Equation (3.3).

**Scattered and Transmitted Waves:**

The expression of the scattered and diffracted outgoing waves $w^s$ in the exterior region *D*, Equation (3.4), once more is applicable here, but we need the different expression of transmitted waves to Equation (3.5); therefore the transmitted waves may take the form

$$w^t = \sum_{n=0}^{\infty}\left[B_n Mc_n^{(3)}(\rho,q) + D_n Mc_n^{(4)}(\rho,q)\right]ce_n(\vartheta,q) + \sum_{n=1}^{\infty}\left[C_n Ms_n^{(3)}(\rho,q) + E_n Ms_n^{(4)}(\rho,q)\right]se_n(\vartheta,q)\,;\ \rho_I \le \rho \le \rho_O \tag{5.1}$$

where $B_n$, $C_n$, $D_n$, and $E_n$, beside $A_n$ in Equation (3.4), are additional unknown coefficients to be calculated. The transmitted waves in the interior region $\Omega$ $(\rho_O \le \rho \le \rho_0, 0 \le \vartheta \le 2\pi)$ have $Mc_n^{(3)}(\cdot)$, $Ms_n^{(3)}(\cdot)$, $Mc_n^{(4)}(\cdot)$ and $Ms_n^{(4)}(\cdot)$ as radial wave functions since their asymptotic behaviors are Hankel functions of the first kind and of second kind, representing outgoing and incoming waves in the full elliptical region $\Omega$ (Pao and Mow, 1973). Furthermore both $ce_n(\cdot)$ and $se_n(\cdot)$ are employed since they form a complete orthogonal set of angular domain in the region $\Omega$, $0 \le \vartheta \le 2\pi$.

**Solution of the Problem using Angular Half-range Expansion**

The wave functions of the total displacement, $w = w^{ff} + w^s$, in the exterior region *D* and the transmitted wave, $w^t$, in the elliptical region $\Omega$ must satisfy the Helmholtz equation, Equation (2.8), and the additional boundary condition,

beside those in Chapter 3; the traction-free boundary condition at the surface of the elliptical tunnel $(\rho = \rho_I, 0 \le \vartheta \le 2\pi)$

$$\tau_{\rho z}\big|_{\rho=\rho_I} = \frac{\mu}{aJ}\frac{\partial w^t}{\partial \rho}\Big|_{\rho=\rho_I} = 0 \tag{5.2}$$

Applying the above condition and utilizing orthogonality of elliptical sine and cosine functions, therefore we obtain $B_n = -\left[Mc_n^{(3)'}(\rho_I, q)/Mc_n^{(4)'}(\rho_I, q)\right]D_n$ and $C_n = -\left[Ms_n^{(3)'}(\rho_I, q)/Ms_n^{(4)'}(\rho_I, q)\right]E_n$. Hence unknowns $D_n$ and $E_n$ could be eliminated and previous Equation (5.1) can be rewritten as

$$\begin{aligned} w^t = &\sum_{n=0}^{\infty}\left[Mc_n^{(3)}(\rho, q) - \frac{Mc_n^{(3)\prime}(\rho_I, q)}{Mc_n^{(4)\prime}(\rho_I, q)}Mc_n^{(4)}(\rho, q)\right]B_n ce_n(\vartheta, q) \\ &+ \sum_{n=1}^{\infty}\left[Ms_n^{(3)}(\rho, q) - \frac{Ms_n^{(3)\prime}(\rho_I, q)}{Ms_n^{(4)\prime}(\rho_I, q)}Ms_n^{(4)}(\rho, q)\right]C_n se_n(\vartheta, q)\,;\ \rho_I \le \rho \le \rho_O \end{aligned} \tag{5.3}$$

Later to determine other unknowns of the wave functions, boundary conditions, Equations (3.6) through (3.8), along the interface $\rho = \rho_O$ are applied. Again the transmitted waves $w^t$ consisting of both elliptical cosine and sine must satisfy two disjoint sets of boundary conditions, the continuity of displacement and radial stress along the interface $\overline{L}$, Equations (3.8). Similar treatment we developed in the previous Hill model must be utilized; $se_m(\vartheta, q)$ can be expanded as the elliptical cosine series in the half-ranges. As a result the transmitted waves $w^t$ and the corresponding radial stress become

$$\begin{aligned} w^t = &\sum_{n=0}^{\infty}\left[Mc_n^{(3)}(\rho, q) - \frac{Mc_n^{(3)\prime}(\rho_I, q)}{Mc_n^{(4)\prime}(\rho_I, q)}Mc_n^{(4)}(\rho, q)\right]B_n ce_n(\vartheta, q) \\ &\mp \sum_{n=0}^{\infty}\sum_{m=1}^{\infty}\mathfrak{C}_{mn}\left[Ms_m^{(3)}(\rho, q) - \frac{Ms_n^{(3)\prime}(\rho_I, q)}{Ms_n^{(4)\prime}(\rho_I, q)}Ms_m^{(4)}(\rho, q)\right]C_m ce_n(\vartheta, q) \end{aligned} \tag{5.4}$$

$$\tau_{\rho z}^{t} = \frac{\mu}{cJ}\sum_{n=0}^{\infty}\left[Mc_n^{(3)\prime}(\rho,q) - \frac{Mc_n^{(3)\prime}(\rho_I,q)}{Mc_n^{(4)\prime}(\rho_I,q)}Mc_n^{(4)\prime}(\rho,q)\right]B_n ce_n(\vartheta,q)$$
$$\mp\frac{\mu}{cJ}\sum_{n=0}^{\infty}\sum_{m=1}^{\infty}\mathfrak{C}_{mn}\left[Ms_m^{(3)\prime}(\rho,q) - \frac{Ms_n^{(3)\prime}(\rho_I,q)}{Ms_n^{(4)\prime}(\rho_I,q)}Ms_m^{(4)\prime}(\rho,q)\right]C_m ce_n(\vartheta,q) \quad (5.5)$$

where –ve above and +ve below are assigned for $-\pi \le \vartheta \le 0$ and $0 \le \vartheta \le \pi$ respectively; $\mathfrak{C}_{mn}$ is given by Equation (2.29). Then displacement and stress functions of far-field, scattered and transmitted waves are in the form of elliptical cosine series, boundary conditions are convenient to apply. These wave functions routinely satisfy the traction-free boundary, Equation (3.6). Applying the traction-free at the surface of the elliptical hill, Equation (3.7), yields

$$B_n = \frac{\sum_{m=1}^{\infty}\mathfrak{C}_{mn}C_m\left(Ms_m^{(3)\prime}(\rho_O,q) - \frac{Ms_n^{(3)\prime}(\rho_I,q)}{Ms_n^{(4)\prime}(\rho_I,q)}Ms_m^{(4)\prime}(\rho_O,q)\right)}{Mc_n^{(3)\prime}(\rho_O,q) - \frac{Mc_n^{(3)\prime}(\rho_I,q)}{Mc_n^{(4)\prime}(\rho_I,q)}Mc_n^{(4)\prime}(\rho_O,q)} \quad (5.6)$$

Then applying the continuity of displacement and stress at the interface $\overline{L}$ yields

$$\begin{Bmatrix} 4w_0 i^n Mc_n^{(1)}(\rho_O,q)ce_n(\gamma,q) \\ + \; Mc_n^{(3)}(\rho_O,q)A_n \end{Bmatrix} = \begin{Bmatrix} \sum_{m=1}^{\infty}\mathfrak{C}_{mn}\left[Ms_m^{(3)}(\rho_0,q) - \frac{Ms_n^{(3)\prime}(\rho_I,q)}{Ms_n^{(4)\prime}(\rho_I,q)}Ms_m^{(4)}(\rho_0,q)\right]C_m \\ + \left[Mc_n^{(3)}(\rho_0,q) - \frac{Mc_n^{(3)\prime}(\rho_I,q)}{Mc_n^{(4)\prime}(\rho_I,q)}Mc_n^{(4)}(\rho_0,q)\right]B_n \end{Bmatrix} \quad (5.7)$$

$$\begin{Bmatrix} 4w_0 i^n Mc_n^{(1)\prime}(\rho_O,q)ce_n(\gamma,q) \\ + \; Mc_n^{(3)\prime}(\rho_O,q)A_n \end{Bmatrix} = \begin{Bmatrix} \sum_{m=1}^{\infty}\mathfrak{C}_{mn}\left[Ms_m^{(3)\prime}(\rho_0,q) - \frac{Ms_n^{(3)\prime}(\rho_I,q)}{Ms_n^{(4)\prime}(\rho_I,q)}Ms_m^{(4)\prime}(\rho_0,q)\right]C_m \\ + \left[Mc_n^{(3)\prime}(\rho_0,q) - \frac{Mc_n^{(3)\prime}(\rho_I,q)}{Mc_n^{(4)\prime}(\rho_I,q)}Mc_n^{(4)\prime}(\rho_0,q)\right]B_n \end{Bmatrix} \quad (5.8)$$

Equations (5.6), (5.7) and (5.8) establish three sets of infinite equations for the three sets of unknowns $A_n$, $B_n$ and $C_n$. To solve this numerically can be done by first plugging $B_n$, which is in term of $C_n$, from Equation (5.6) into Equations (5.7) and (5.8). Next $A_n$ can be eliminated by setting in term of $C_n$, and afterward the

infinite linear equation in $C_n$ would be formulated. By matrix truncation, we can solve for some first terms of $C_n$. Lastly $A_n$ and $B_n$ could be determined by back substitution of $C_n$ into their relationships.

## 5.3 Results and Analysis

Amplitudes of ground motions are analyzed. Similar to Chapters 3 and 4 we assume the excitation with amplitude 1, and present the results in term of the dimensionless parameters $\eta$ and *R* which are defined by Equations (3.16) and (3.18); the focal length is also given by Equation (3.17). Furthermore to investigate the scattering effect due to the presence of an elliptical tunnel, dimensionless parameter $\eta_T$ is introduced and expressed as

$$\eta_T = \frac{2T}{\lambda} = \frac{T}{A}\eta \tag{5.9}$$

where $T$ is the half-width of the tunnel. For each aspect ratio *R*, its minimum value of $T$ is equal to the focal length;

$$a = \frac{A}{cosh\left(tanh^{-1}(B/A)\right)} \tag{3.17}$$

Due to numerical constraint, we limit $T$ to $0.8A$. As a result, 0.6 is the minimum aspect ratio $R$ in this chapter. Table 3.1 shows the minimum ratio $T/A$ for the corresponding the aspect ratio $R$; noted that $R$ less than 0.6 would yield the ratio $T/A$ greater than 0.8.

Table 5.1: The Minimum Ratio $T/A$ of the Aspect Ratio $R$

| $R$ | Minimum $T/A$ |
|---|---|
| 0.6 | 0.8 |
| 0.8 | 0.6 |
| 0.9999 | 0.0006 |

**Comparison with the Solutions of "Circular" Semi-Elliptical Hill:**

When a concentric tunnel is really tiny in comparison to the hill, wave functions derived previously must be in agreement with those of semi-elliptical hill without tunnel. Theoretically this can be verified by the consideration of asymptotic values of $\frac{Mc_n^{(3)'}(\rho_I,q)}{Mc_n^{(4)'}(\rho_I,q)}$ and $\frac{Ms_n^{(3)'}(\rho_I,q)}{Ms_n^{(4)'}(\rho_I,q)}$ when $\rho_I$ approaches zero; however this is only applicable to *R* = 0.9999 since the tunnel may be assigned to be so small without becoming a slit-like. Since we know that $Mc_n^{(1)'}(0,q) = Ms_n^{(1)'}(0,q) = 0$ (Mechel, 1997), we obtain $\lim_{\rho_I\to 0}\left[\frac{Mc_n^{(3)'}(\rho_I,q)}{Mc_n^{(4)'}(\rho_I,q)}\right] = \lim_{\rho_I\to 0}\left[\frac{Ms_n^{(3)'}(\rho_I,q)}{Ms_n^{(4)'}(\rho_I,q)}\right] = -1$ .

Therefore

$$\lim_{\rho_I\to 0}\left[Mc_n^{(3)}(\rho,q) - \frac{Mc_n^{(3)'}(\rho_I,q)}{Mc_n^{(4)'}(\rho_I,q)}Mc_n^{(4)}(\rho,q)\right] = Mc_n^{(1)}(\rho,q)$$

$$\lim_{\rho_I\to 0}\left[Mc_n^{(3)'}(\rho,q) - \frac{Mc_n^{(3)'}(\rho_I,q)}{Mc_n^{(4)'}(\rho_I,q)}Mc_n^{(4)'}(\rho,q)\right] = Mc_n^{(1)'}(\rho,q)$$

$$\lim_{\rho_I\to 0}\left[Ms_m^{(3)}(\rho,q) - \frac{Ms_n^{(3)'}(\rho_I,q)}{Ms_n^{(4)'}(\rho_I,q)}Ms_m^{(4)}(\rho,q)\right] = Ms_n^{(1)}(\rho,q)$$

$$\lim_{\rho_I \to 0} \left[ Ms_m^{(3)'}(\rho, q) - \frac{Ms_n^{(3)'}(\rho_I, q)}{Ms_n^{(4)'}(\rho_I, q)} Ms_m^{(4)'}(\rho, q) \right] = Ms_n^{(1)'}(\rho, q)$$

After inserting the above asymptotic values back to Equations (5.3) through (5.8), we obtain the identical equations to those of the semi-elliptical hill model without tunnel.

Figure 5.2: Displacement Amplitudes of Ground Motion at $\eta = 1$

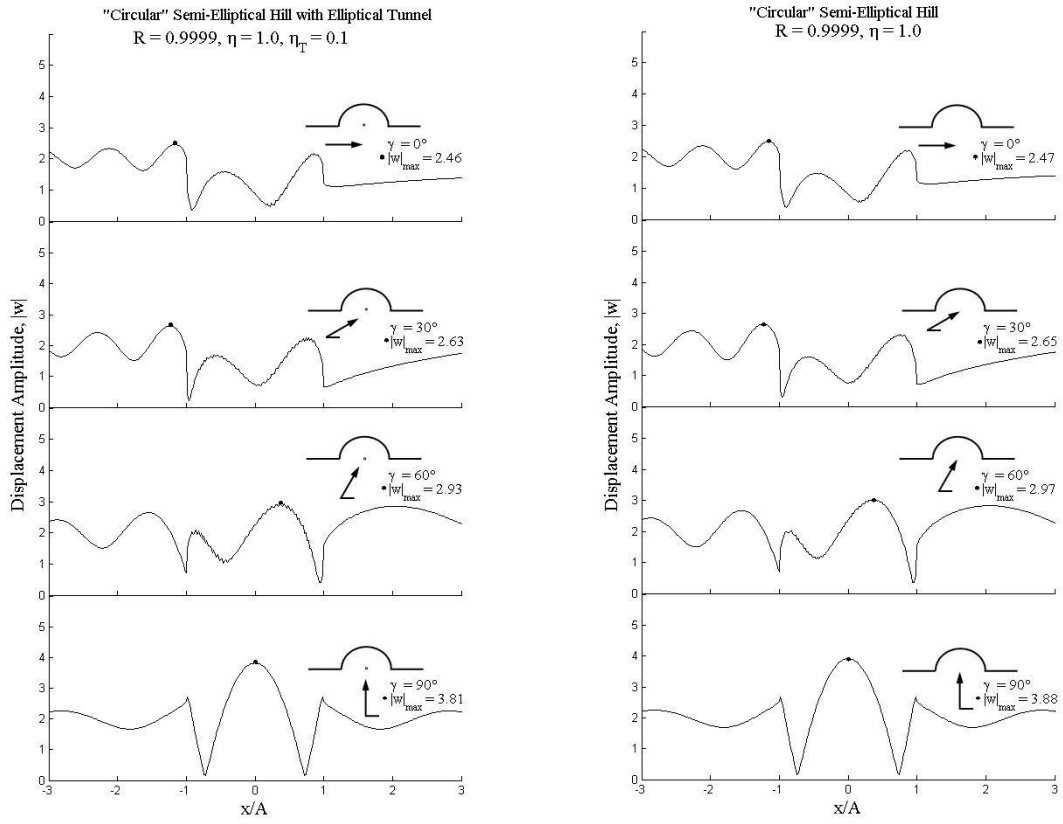


(a) "Circular " Semi-Elliptical Hill with an elliptical tunnel $\eta_T = 0.1$

(b) Semi-Circular Hill

The previous Figure (5.2) illustrates the similarity for both semi-elliptical hills with and without a concentric tunnel when semi-elliptical tends to semi-circular $(R = 0.9999)$ at $\eta = 1$; $\eta_T = 0.1$ is assigned for the case of tunnel. As expected their trends are in agreement with 2% difference at large for the maximum values; this validates the fact that the long waves do not feel any undersized topographic irregularity.

Figure 5.3: Displacement Amplitude for $R = 0.6$ at $\eta = 5$

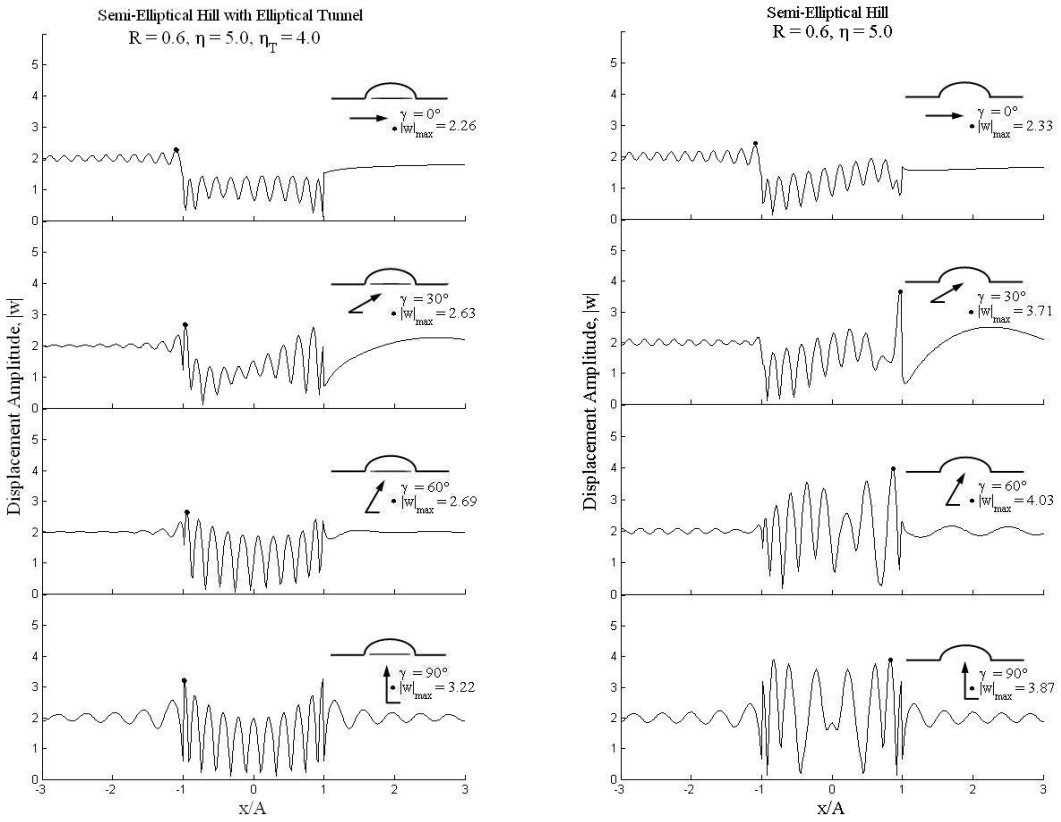


(a) with Tunnel; $T = 0.8A$ (b) without Tunnel

**Effects of Tunnel, and Incident Angle to Semi-Elliptical Hill:**

To study the effect of the existence of an elliptical tunnel, we consider only three aspect ratios $R$; 0.6, 0.8 and 0.9999. In addition per limitation shown in Table 3.1, we investigate the effect of the tunnel by assuming $T = 0.8A$ only for $R = 0.6$ and 0.8, and $T = 0.2A$, $0.5A$ and $0.8A$ for $R = 0.9999$ "**circular**" elliptical tunnel. Once more we consider the effect of incident angle by assuming four different incident angles of $\gamma = 0°$, 30°, 60° and 90° for each case of study.

Figure 5.4: Displacement Amplitude for $R = 0.6$ at $\eta = 10$

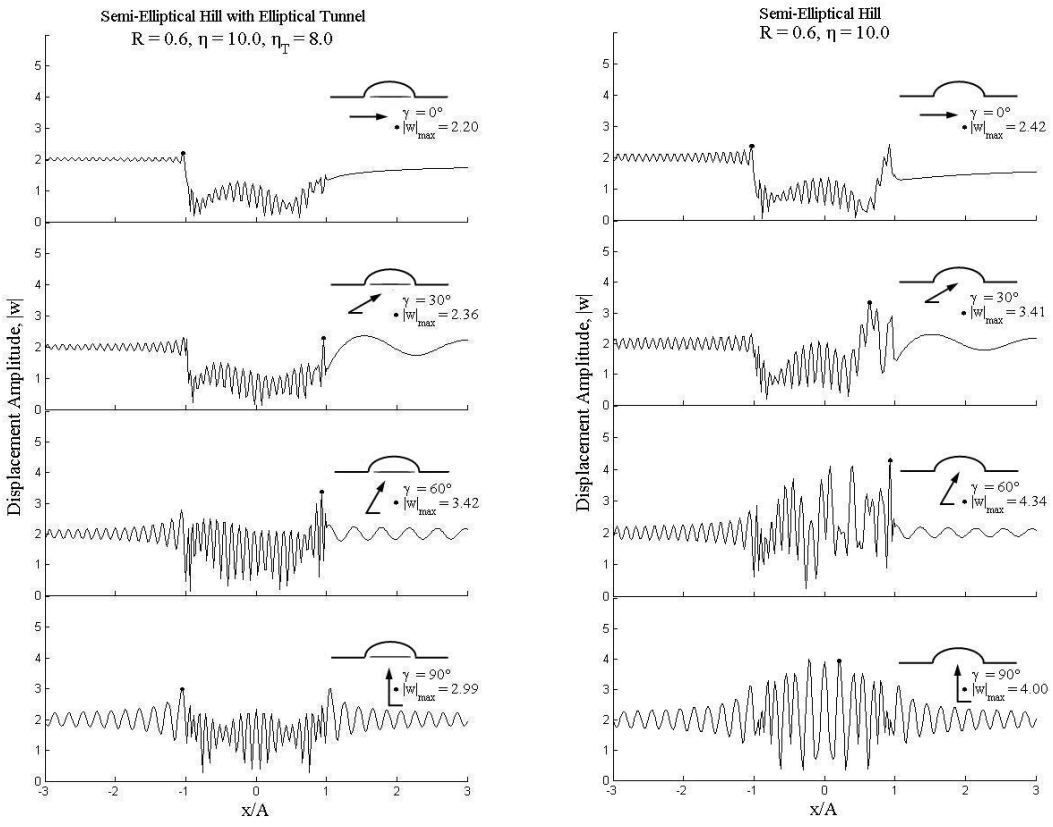


(a) with Tunnel; $T = 0.8A$ (b) without Tunnel

Figures 5.3 to 5.4 illustrate amplitudes of surface displacements at four prescribed incidences versus the distance *x/A* on and around the hill with the dimensionless frequency $\eta = 5$ and 10 for the semi-elliptical hill $R = 0.6$ with an elliptical tunnel $T = 0.8A$; their corresponding plots of surface displacement for the semi-elliptical hill without a tunnel are shown on their right-hand side.

Figure 5.5: Displacement Amplitude for $R = 0.8$ at $\eta = 5$

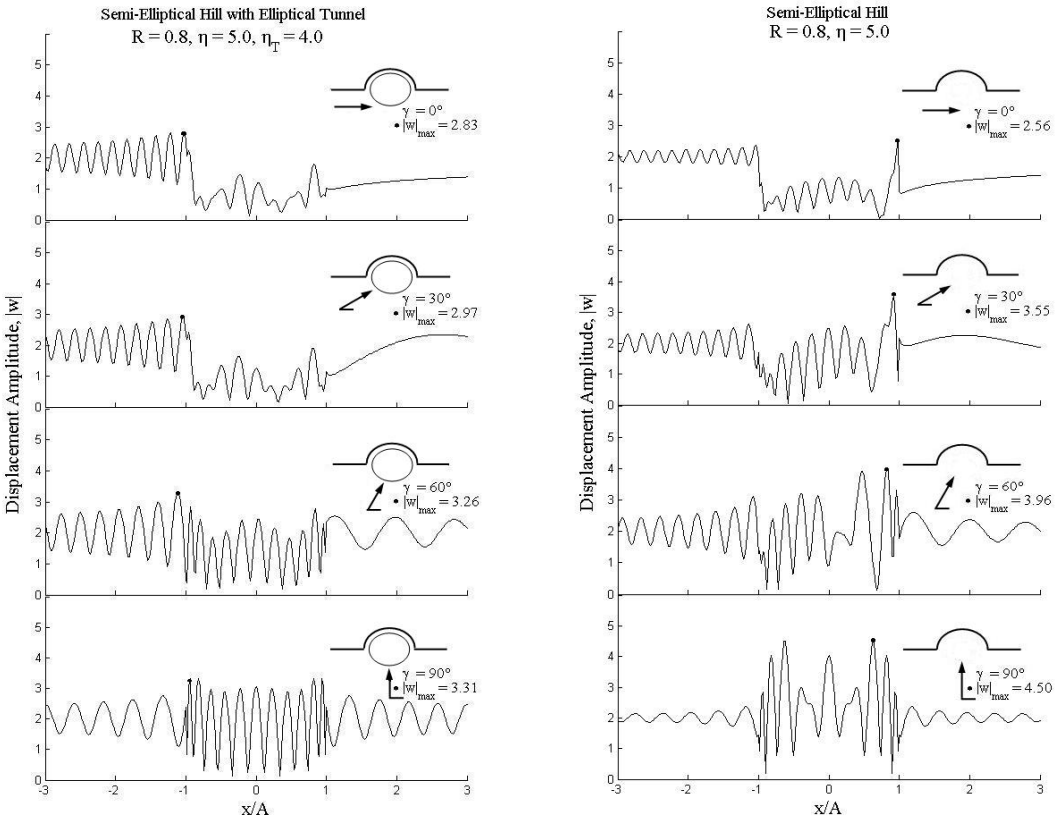


(a) with Tunnel; $T = 0.8A$ (b) without Tunnel

We found that the existence of the tunnels has significant effect on the amplitude of ground motion. In general the presence of the tunnels makes maximum values of the displacement lower; except at $\gamma = 0°$ for $\eta = 5$. Their corresponding locations are shifted for $\gamma = 30°$ and 60°. The shielding effect of tunnel becomes stronger for the surface in its vicinity. An incident angle seems rather irrelevant on the displacement amplitudes of points vertically above tunnel; these amplitude values are about to or less than 2.

Figure 5.6: Displacement Amplitude for $R = 0.8$ at $\eta = 10$

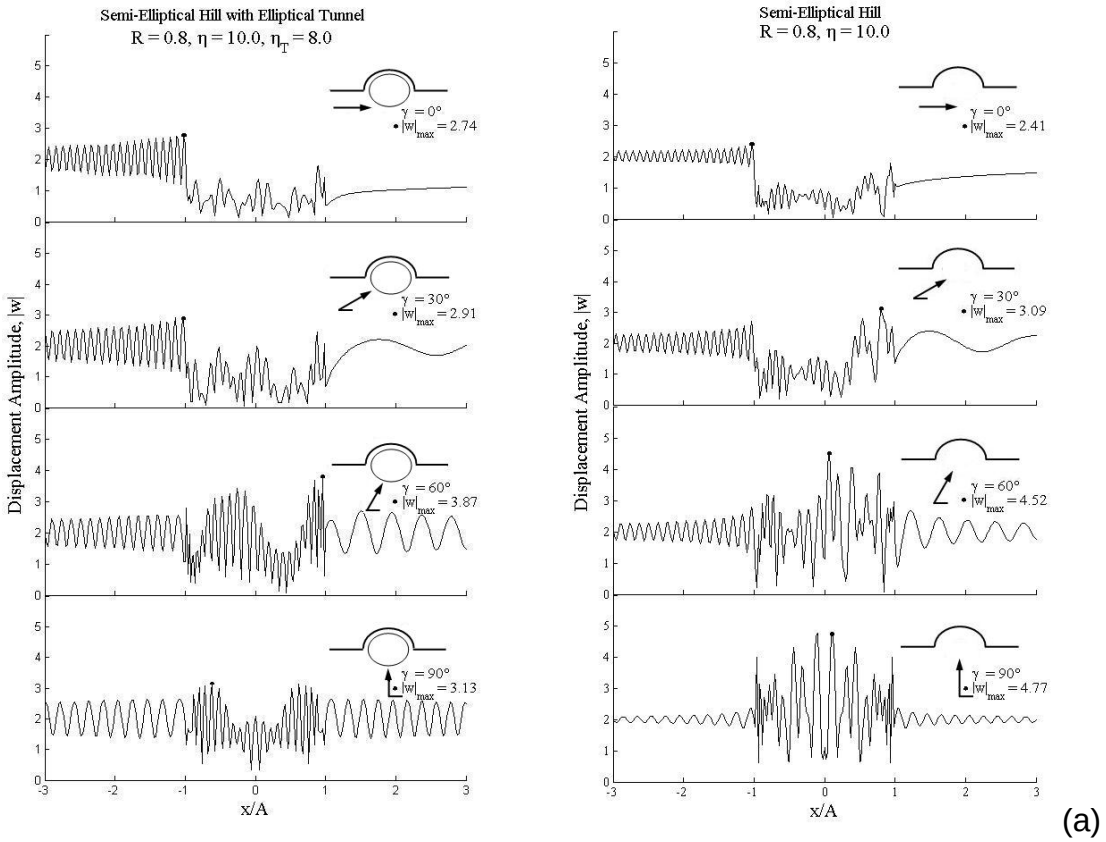


(a) with Tunnel; $T = 0.8A$ (b) without Tunnel

Next let consider the semi-elliptical hill $R = 0.8$ with the same tunnel-size ratio as previous case $T = 0.8A$. Figures 5.5 and 5.6 illustrate amplitudes of surface displacements at four prescribed incident angles with the dimensionless frequency $\eta = 5$ and 10; again their corresponding plots for the semi-elliptical hill without a tunnel are also shown on their right-hand side. Similar tendency to previous case of $R = 0.6$ is spotted. The surface displacements on the hill are obviously lower with the existence of the tunnel.

Figure 5.7: Displacement Amplitude for $R = 0.9999$ with Tunnel $T = 0.8A$

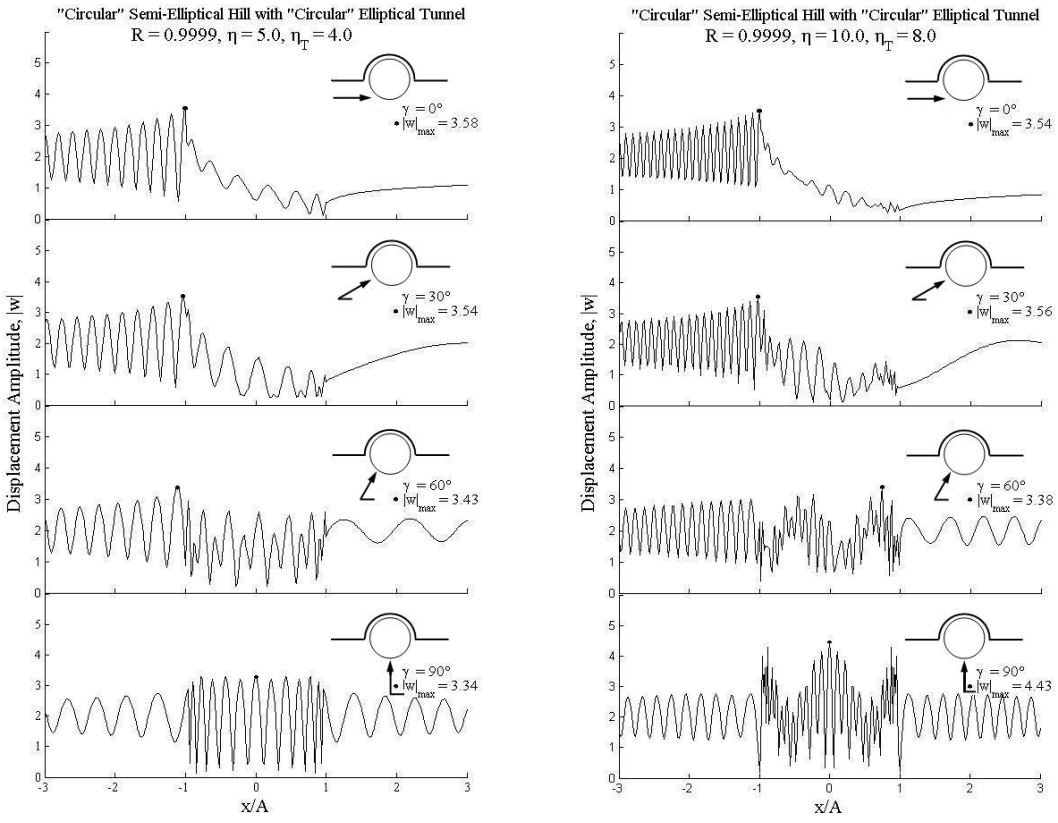


(a) $\eta = 5$ (b) $\eta = 10$

There are two major differences in wave patterns for the slit-like tunnel in comparison to elliptical tunnel; it may be considered as the shape effect. First, stronger pattern of standing waves is observed for the case of the elliptical tunnel with, especially, nearly grazing incidence. Second the slit-like tunnel is more effective in shielding the incoming waves in nearly vertical direction; their surface displacements are less than ones of the elliptical tunnel.

Figure 5.8: Displacement Amplitude for $R = 0.9999$ with Tunnel $T = 0.2A$

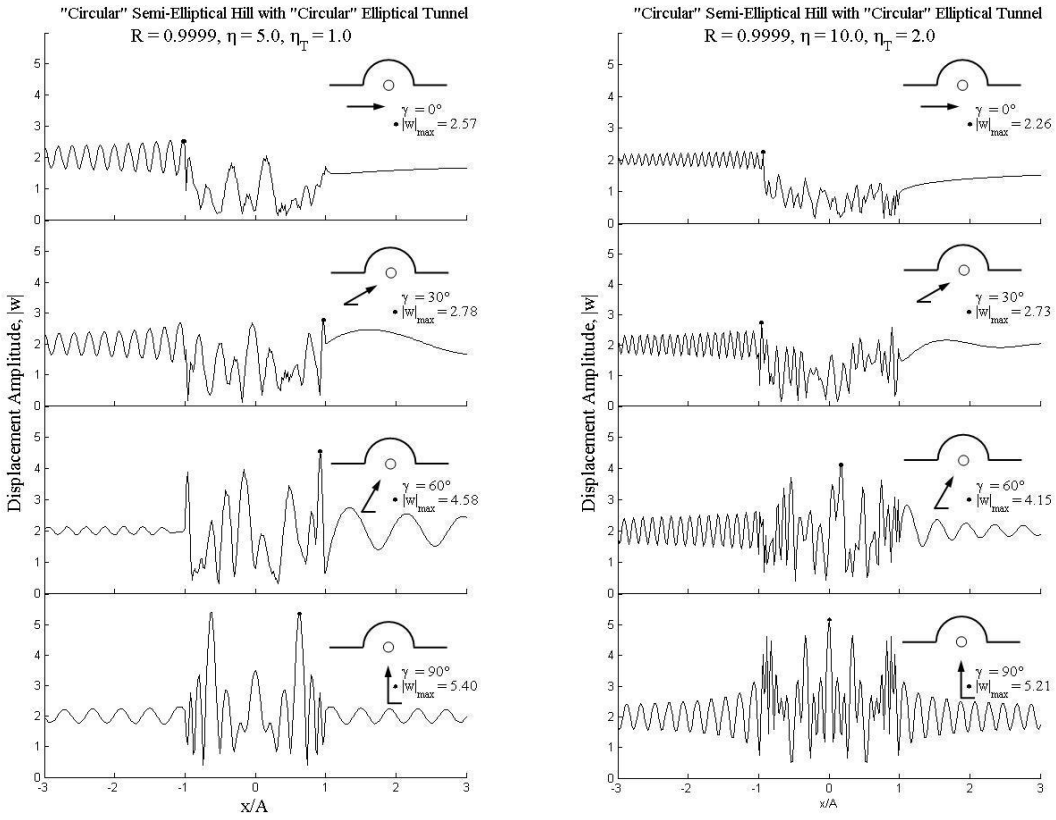


(a) $\eta = 5$ (b) $\eta = 10$

To further elaborate the shape effect of tunnel, we may compare Figure 5.7, the surface displacements due to “circular” elliptical tunnel with the same tunnel-size ratio $T = 0.8A$, with Figures 5.3 through 5.6. For $\gamma = 0°$, the circular-like tunnel creates stronger shadow zone on the right-side of the hill; their amplitudes are in the neighborhood of unity or less. Still this tunnel is less efficient in shielding the vertical waves than other tunnels as expected; their maximum surface displacements are higher than other cases.

Figure 5.9: Displacement Amplitude for $R = 0.9999$ with Tunnel $T = 0.5A$

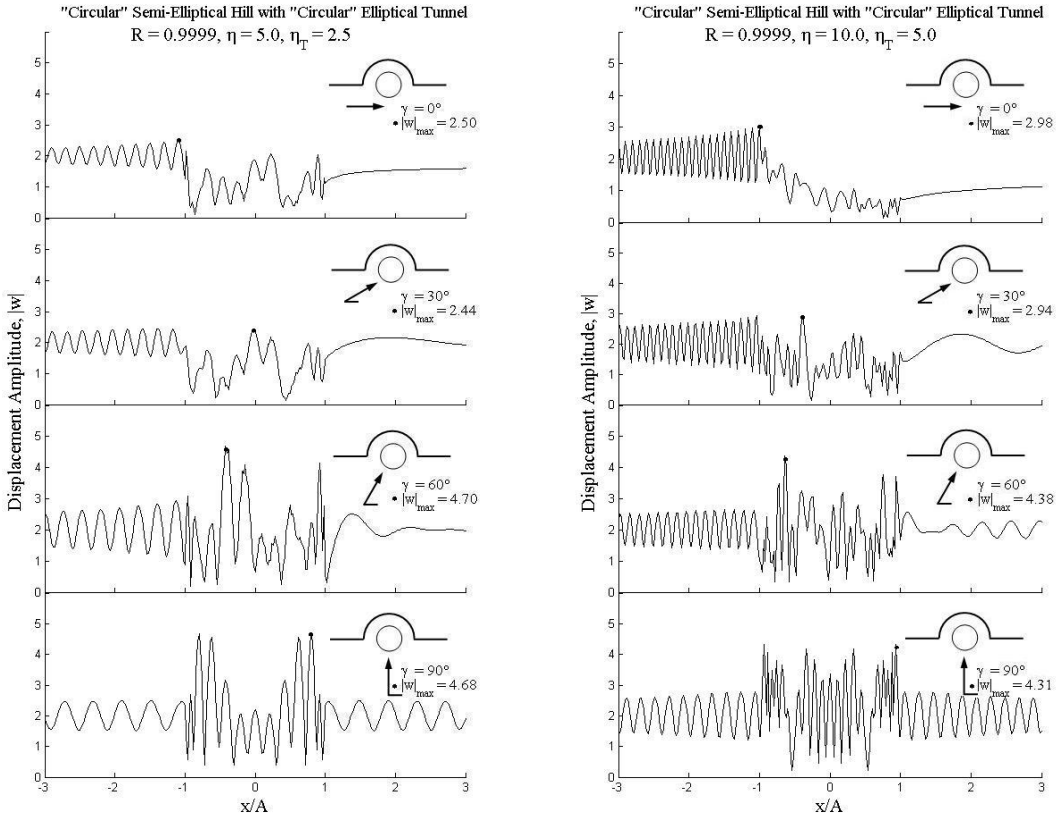


(a) $\eta = 5$ (b) $\eta = 10$

To study the influence of tunnel-size, we consider only “circular” semi-elliptical hill with a “circular” elliptical tunnel due to the limitation of the formulation previously mentioned. After evaluating Figures 5.8 and 5.9 of “circular” tunnels $T = 0.2A$ and $0.5A$ against the above figure, it may be said that for nearly horizontal angle the standing waves on the left-side become more prominent as the tunnel is getting larger. In addition for vertical angle, the maximum value of surface displacement is noticeably less when the elliptical obstacle gets bigger. Besides that, the surface displacements on both sides of the hill become progressively more fluctuated as the obstacle become larger apparently for all angles.

Figures 5.10 through 5.29 show three-dimensional plots of surface displacements for $R = 0.6$, 0.8, and 0.9999, equivalent to the height-to-width ratios of 0.3, 0.4, and 0.4999 respectively; the values of $T$ for particular $R$ are as at the beginning of this section. Each figure illustrates the plots at four incident angles, $\gamma = 0°$, 30°, 60° and 90°, versus the distance *x/A* on and around the hill and the dimensionless frequency $\eta$ in the range of 0.5 to 10; the amplitudes in the range of *x/A* in $[-1,1]$ are those on the elliptical surface of the hill.

Figures 5.10 through 5.17 show that the presence of a tunnel and direction of incident waves have great effect on surface displacement. For nearly horizontal angles, the local jump of surface displacement in the neighborhood of the right edge of the hill $(x/A = 1)$ common for all cases of semi-elliptical hill is not

Figure 5.10: Displacement Amplitude for $R = 0.6$, $T = 0.8A$ when $\gamma = 0°$

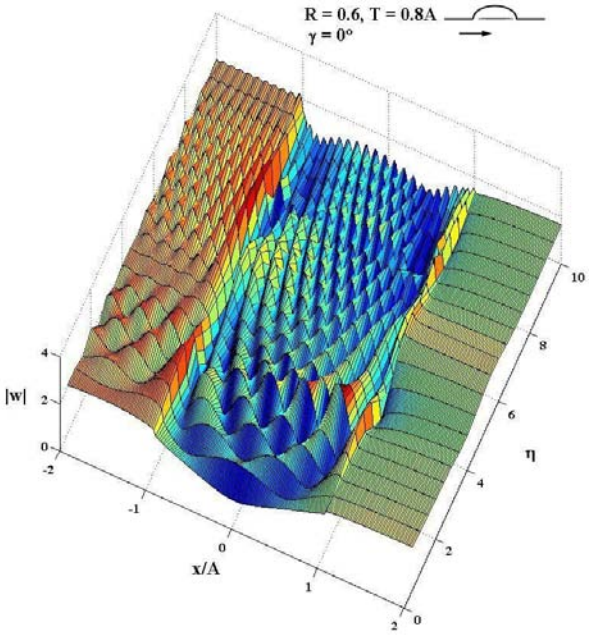


Figure 5.11: Displacement Amplitude for $R = 0.6$, $T = 0.8A$ when $\gamma = 30°$

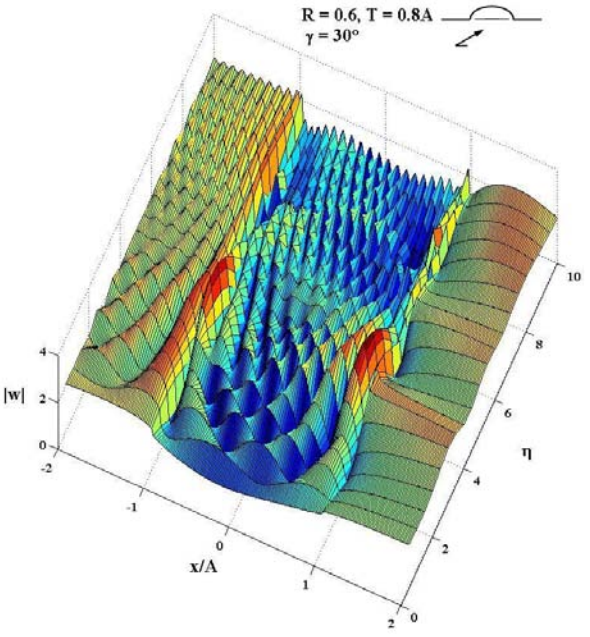

detected due to shadow zone formed by a tunnel; surface displacement on a hill is typically in vicinity of 2 or less with the exception of some particular values of $\eta$. This phenomenon may be explained by the fact that a tunnel easily reflects some input waves back and forth with the hill surface. For nearly vertical angles of incidence, in general surface displacement is greatly hindered by a tunnel.

Clearly, Figures 5.18 through 5.29 also validate what we have mentioned earlier about the shape and size effects of tunnels; moreover pattern of all surface displacement turn out to be increasingly more complicated when the incident waves become shorter.

Figure 5.12: Displacement Amplitude for $R = 0.6$, $T = 0.8A$ when $\gamma = 60°$

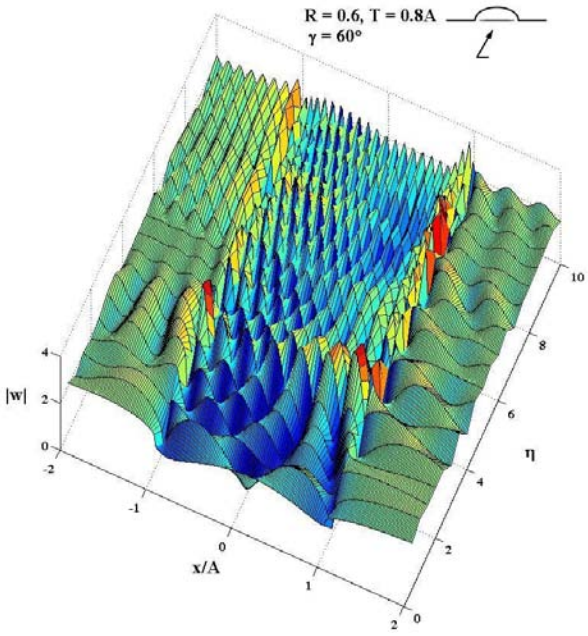

Figure 5.13: Displacement Amplitude for $R = 0.6$, $T = 0.8A$ when $\gamma = 90°$

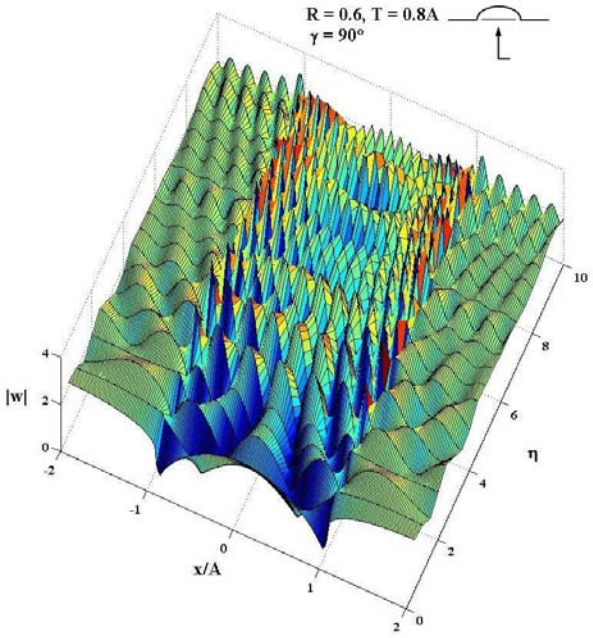


Figure 5.14: Displacement Amplitude for $R = 0.8$, $T = 0.8A$ when $\gamma = 0°$

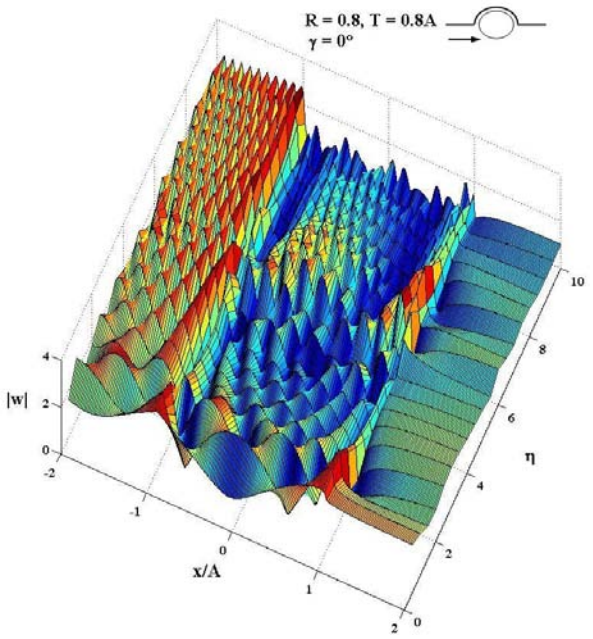

Figure 5.15: Displacement Amplitude for $R = 0.8$, $T = 0.8A$ when $\gamma = 30°$

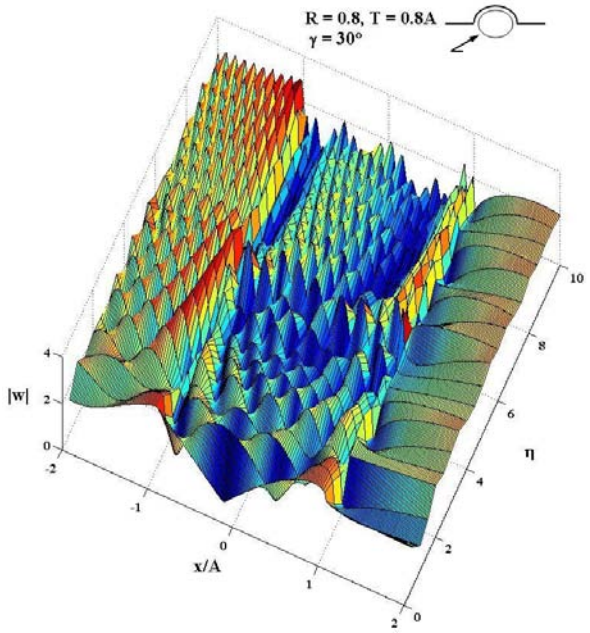


Figure 5.16: Displacement Amplitude for $R = 0.8$, $T = 0.8A$ when $\gamma = 60°$

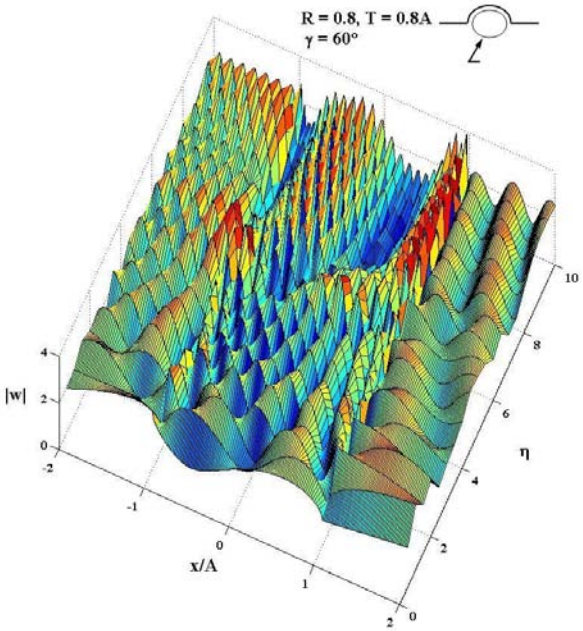

Figure 5.17: Displacement Amplitude for $R = 0.8$, $T = 0.8A$ when $\gamma = 90°$

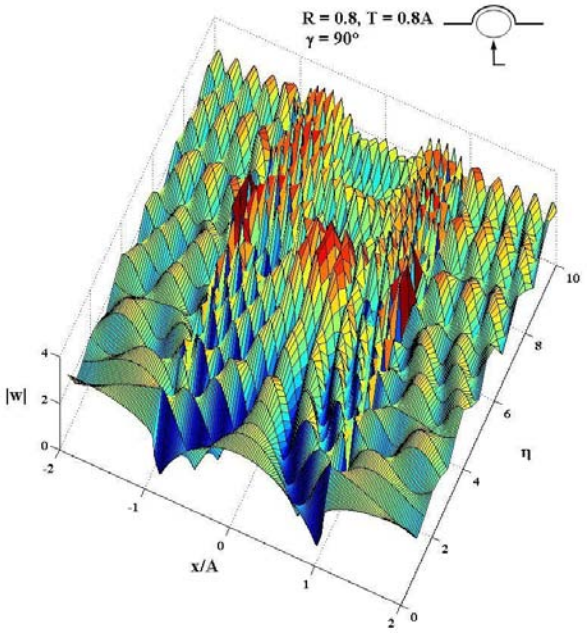


Figure 5.18: Displacement Amplitude for $R = 0.9999$, $T = 0.2A$ when $\gamma = 0°$

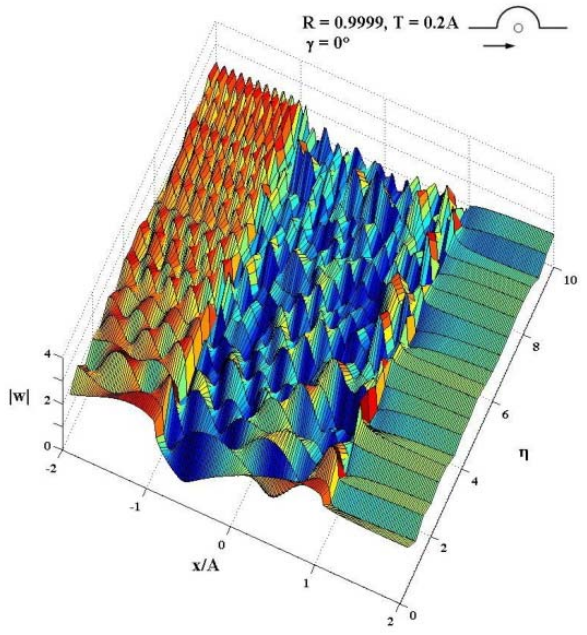

Figure 5.19: Displacement Amplitude for $R = 0.9999$, $T = 0.2A$ when $\gamma = 30°$

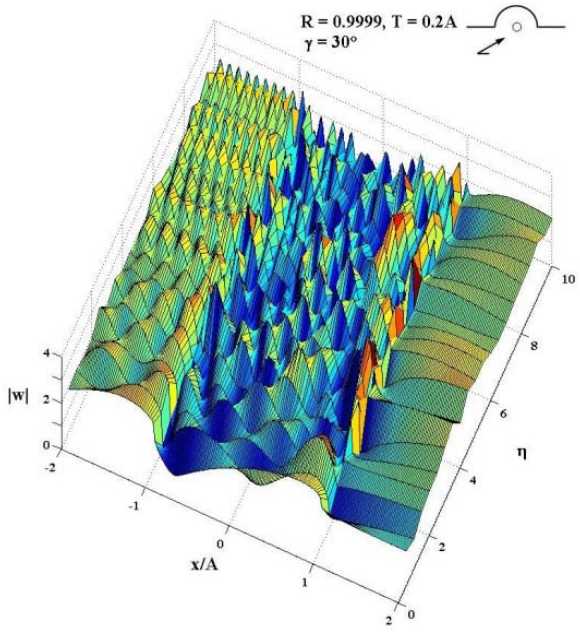


Figure 5.20: Displacement Amplitude for $R = 0.9999$, $T = 0.2A$ when $\gamma = 60°$

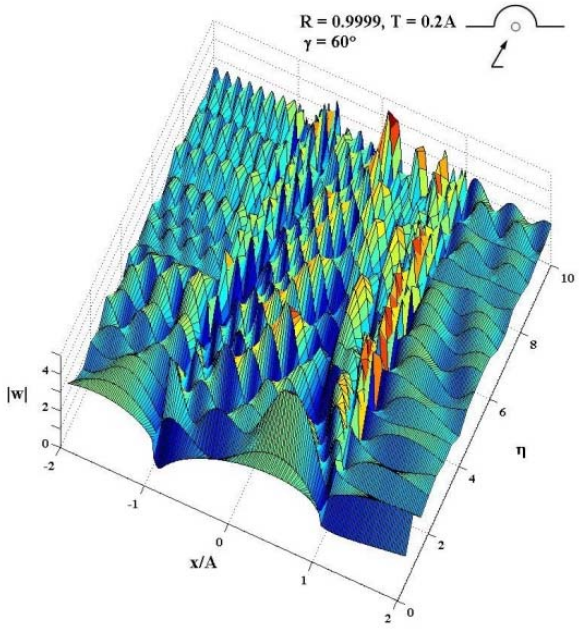

Figure 5.21: Displacement Amplitude for $R = 0.9999$, $T = 0.2A$ when $\gamma = 90°$

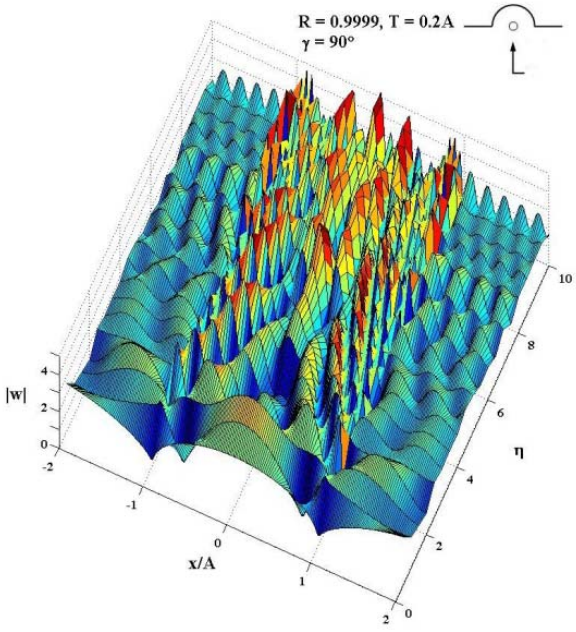


Figure 5.22: Displacement Amplitude for $R = 0.9999$, $T = 0.5A$ when $\gamma = 0°$

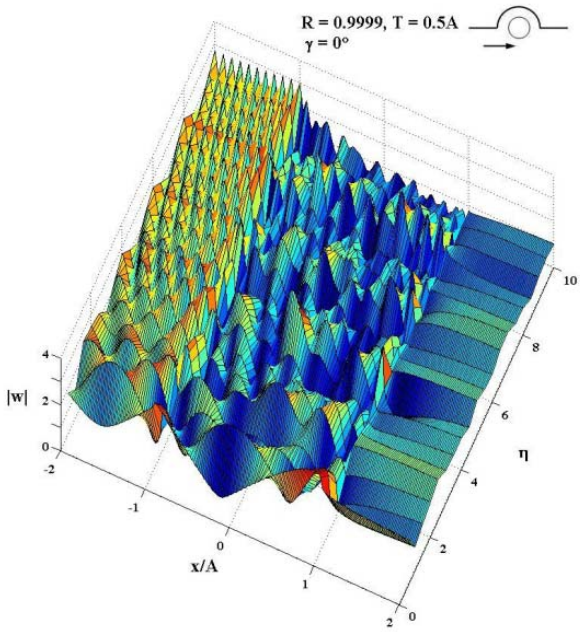

Figure 5.23: Displacement Amplitude for $R = 0.9999$, $T = 0.5A$ when $\gamma = 30°$

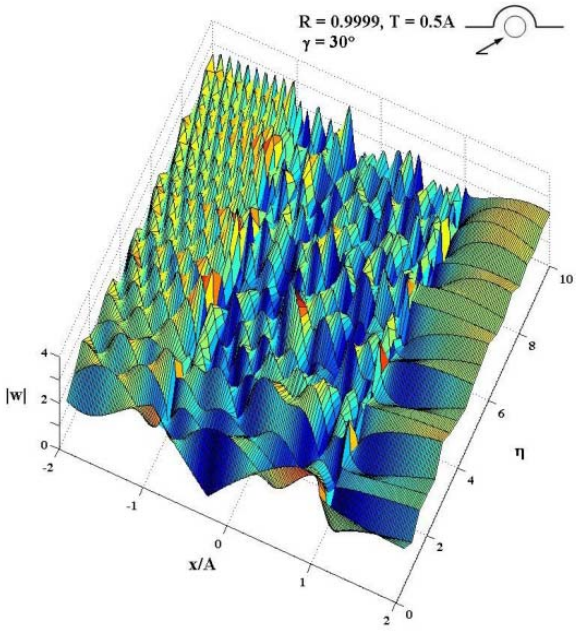


Figure 5.24: Displacement Amplitude for $R = 0.9999$, $T = 0.5A$ when $\gamma = 60°$

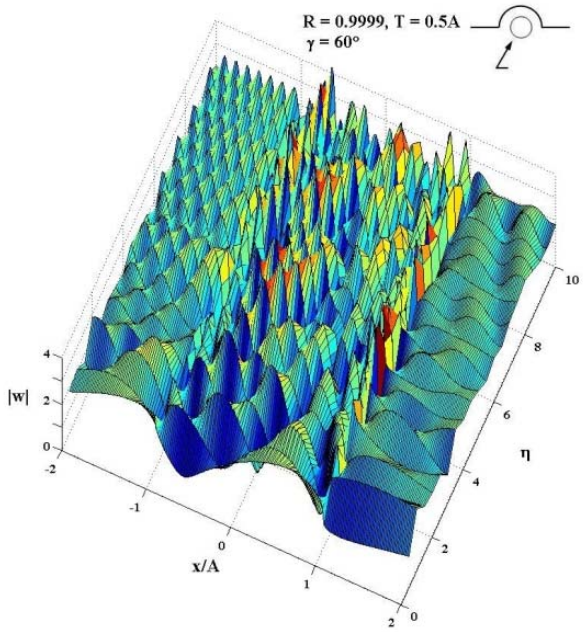

Figure 5.25: Displacement Amplitude for $R = 0.9999$, $T = 0.5A$ when $\gamma = 90°$

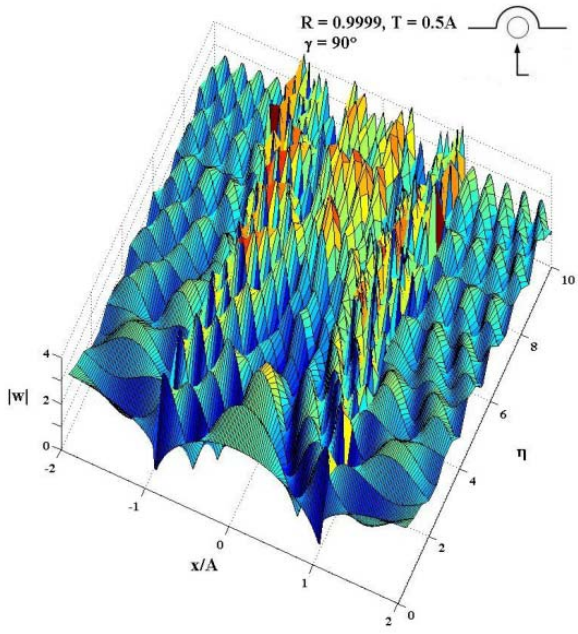


Figure 5.26: Displacement Amplitude for $R = 0.9999$, $T = 0.8A$ when $\gamma = 0°$

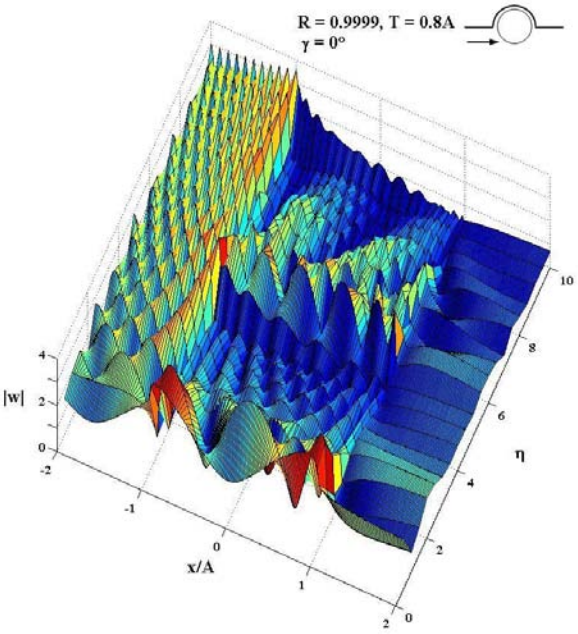

Figure 5.27: Displacement Amplitude for $R = 0.9999$, $T = 0.8A$ when $\gamma = 30°$

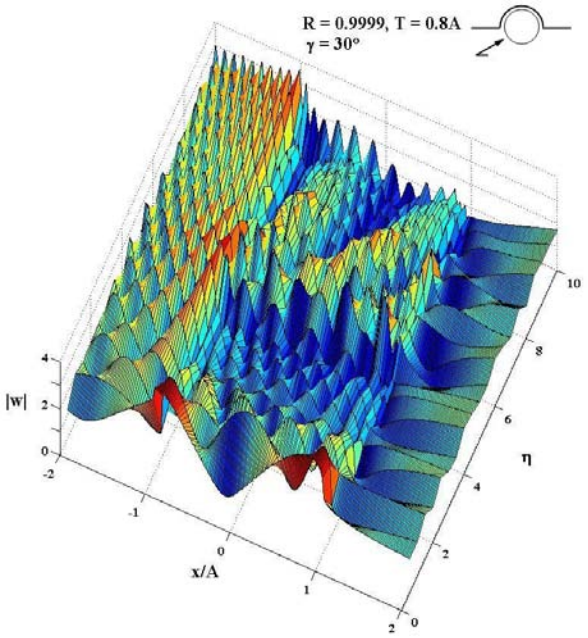


Figure 5.28: Displacement Amplitude for $R = 0.9999$, $T = 0.8A$ when $\gamma = 60°$

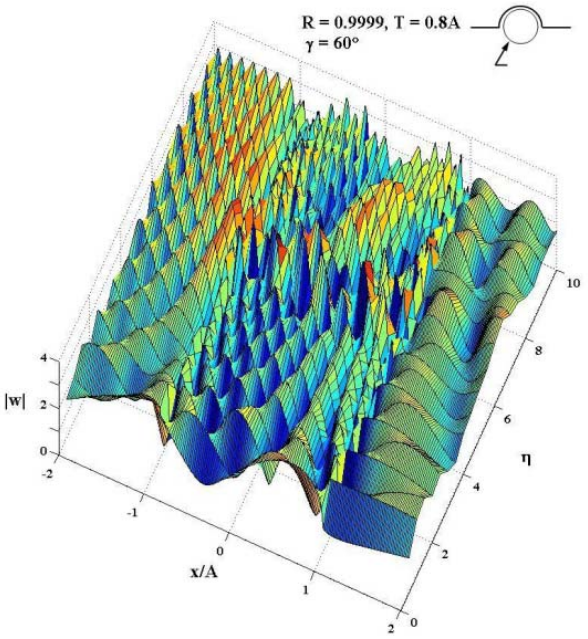

Figure 5.29: Displacement Amplitude for $R = 0.9999$, $T = 0.8A$ when $\gamma = 90°$

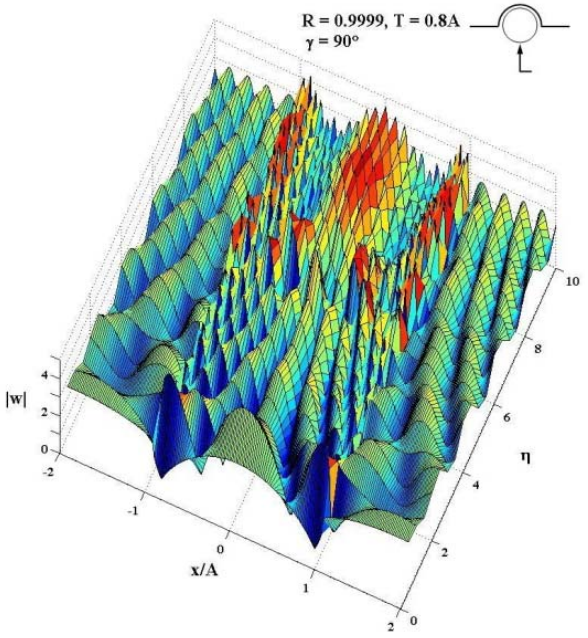

# CHAPTER 6: SCATTERING OF PLANE (SH) WAVES BY A DEEP SEMI-ELLIPTICAL HILL WITH AN ELLIPTICAL TUNNEL

In this chapter, an analytic solution to the boundary-valued problem of the two-dimensional scattering of anti-plane (SH) waves by a deep semi-elliptical hill with a concentric tunnel is presented. Scattering effects due to the existence of elliptical tunnel in the hill are studied and compared with the results of Chapter 4, the scattering effects due to the presence of deep semi-elliptical hill.

## 6.1 The Deep Semi-Elliptical Hill with an Elliptical Tunnel Model

The cross-section of two-dimensional model is shown in Figure 6.1; identical configuration, material properties, and coordinate systems to what we have in Chapter 4 are employed here, but with the presence of a concentric tunnel; A, B and $a$ are expressed as in Chapter 4, while T is the half-width of the tunnel. The model consists of the two regions. The exterior region *D* expands over the similar domain and boundaries to section 4.1, while the regions $\Omega$ is the complete elliptical ring which has the outer boundaries $L$ and $\overline{L}$ and the inner boundary $M$, $\rho = \rho_I$.

Figure 6.1: Deep Semi-Elliptical Hill with an Elliptical Tunnel Model

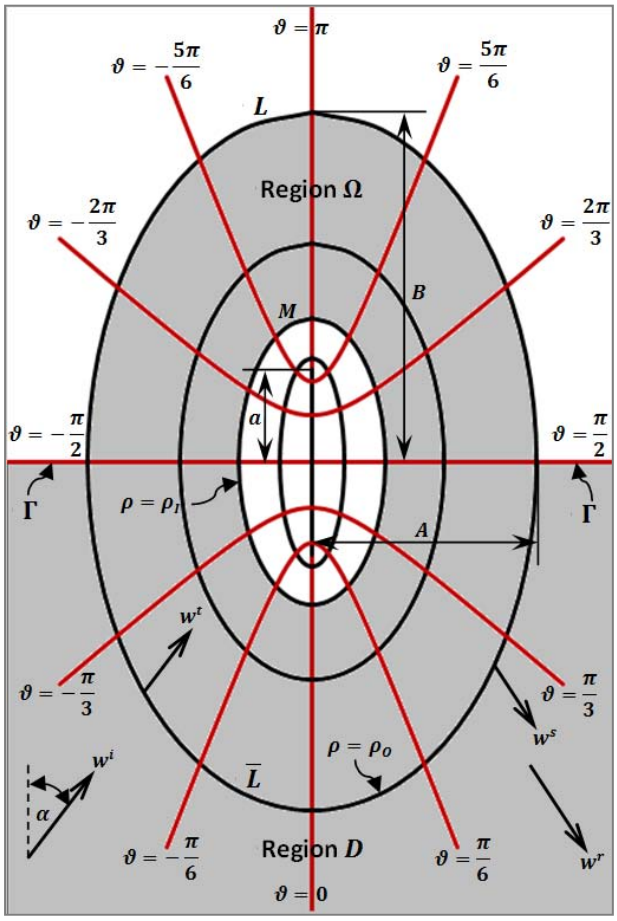


## 6.2 Series Expansion of Wave Functions

**Incident and Reflected Waves:**

The same excitation $w^i$ and reflected waves**,** infinite trains of plane SH waves travelling in the directions $\pi - \gamma$ and $\gamma$ to positive x axis, as shown in Chapter 4 are applied. Moreover in the free field, no existence of the hill and tunnel, their summation yields the free field waves which can be expressed as Equation (4.1) in elliptical coordinate system.

**Scattered and Transmitted Waves:**

The expression of the scattered and diffracted outgoing waves $w^s$ in the exterior region *D*, Equation (4.2), is valid here. Even though we utilize different model to one of Chapter 5, identical expression of transmitted waves to Equation (5.1) is applicable too since we require asymptotic behaviors of Hankel functions of the first kind and of second kind, representing outgoing and incoming waves in the full elliptical region $\Omega$. In addition to form the complete orthogonal set of angular domain in the region $\Omega$, both elliptical cosine and sine functions must be employed.

**Solution of the Problem using Angular Half-range Expansion**

The total displacement $w = w^{ff} + w^s$ in the exterior region *D* and the transmitted displacement $w^t$ in the ring region $\Omega$ must satisfy the Helmholtz equation, Equation (2.8), and the extra boundary condition, the traction-free boundary condition at the inner surface of the elliptical tunnel, Equation (4.2), in addition to Equations (4.4) through (4.6) in Chapter 4. After applying this traction-free boundary condition at the inner surface and orthogonality of elliptical sine and cosine functions, unknowns $D_n$ and $E_n$ could be eliminated and same expression of the transmitted wave function as Equation (5.3) has been reached.

Other unknowns of the wave functions can be obtained after applying boundary conditions along the interface $\rho = \rho_O$, Equations (4.4) through (4.6). Again the transmitted waves $w^t$ consisting of both elliptical cosine and sine must satisfy two disjoint sets of boundary conditions, the continuity of displacement and radial stress along the interface $\overline{L}$, Equations (4.6). The expansion technique we developed in the Hill model must be utilized; $ce_{2m+1}(\vartheta, q)$ and $se_{2m+2}(\vartheta, q)$ must be expanded as the series of elliptical cosine functions of odd order and elliptical sine functions of even order $\{ce_{2n+1}(\vartheta, q), se_{2n+2}(\vartheta, q);\ n = 0, 1, 2, \ldots\}$ in the half-range $[-\pi/2\,, \pi/2]$ (and similarly in $[\pi/2\,, -\pi/2]$). As a result the transmitted waves $w^t$ and the corresponding radial stress become

$$
\begin{aligned}
w^t = {} & \sum_{n=0}^{\infty}\left[Mc_{2n}^{(3)}(\rho,q) - \frac{Mc_{2n}^{(3)\prime}(\rho_I,q)}{Mc_{2n}^{(4)\prime}(\rho_I,q)} Mc_{2n}^{(4)}(\rho,q)\right] B_{2n} ce_{2n}(\vartheta,q) \\
& \mp \sum_{m,n=0}^{\infty} \mathfrak{M}_{mn}\left[Mc_{2m+1}^{(3)}(\rho,q) - \frac{Mc_{2m+1}^{(3)\prime}(\rho_I,q)}{Mc_{2m+1}^{(4)\prime}(\rho_I,q)} Mc_{2m+1}^{(4)}(\rho,q)\right] B_{2m+1} ce_{2n}(\vartheta,q) \\
& + \sum_{n=0}^{\infty}\left[Ms_{2n+1}^{(3)}(\rho,q) - \frac{Ms_{2n+1}^{(3)\prime}(\rho_I,q)}{Ms_{2n+1}^{(4)\prime}(\rho_I,q)} Ms_{2n+1}^{(4)}(\rho,q)\right] C_{2n+1} se_{2n+1}(\vartheta,q) \\
& \mp \sum_{m,n=0}^{\infty} \mathfrak{N}_{mn}\left[Ms_{2m+2}^{(3)}(\rho,q) - \frac{Ms_{2m+2}^{(3)\prime}(\rho_I,q)}{Ms_{2m+2}^{(4)\prime}(\rho_I,q)} Ms_{2m+2}^{(4)}(\rho,q)\right] C_{2m+2} se_{2n+1}(\vartheta,q)
\end{aligned}
\tag{6.1}
$$

$$
\begin{aligned}
\tau_{\rho z} = {} & \frac{\mu}{aJ}\sum_{n=0}^{\infty}\left[Mc_{2n}^{(3)\prime}(\rho,q) - \frac{Mc_{2n}^{(3)\prime}(\rho_I,q)}{Mc_{2n}^{(4)\prime}(\rho_I,q)} Mc_{2n}^{(4)\prime}(\rho,q)\right] B_{2n} ce_{2n}(\vartheta,q) \\
& \mp \frac{\mu}{aJ}\sum_{m,n=0}^{\infty} \mathfrak{M}_{mn}\left[Mc_{2m+1}^{(3)\prime}(\rho,q) - \frac{Mc_{2m+1}^{(3)\prime}(\rho_I,q)}{Mc_{2m+1}^{(4)\prime}(\rho_I,q)} Mc_{2m+1}^{(4)\prime}(\rho,q)\right] B_{2m+1} ce_{2n}(\vartheta,q) \\
& + \frac{\mu}{aJ}\sum_{n=0}^{\infty}\left[Ms_{2n+1}^{(3)\prime}(\rho,q) - \frac{Ms_{2n+1}^{(3)\prime}(\rho_I,q)}{Ms_{2n+1}^{(4)\prime}(\rho_I,q)} Ms_{2n+1}^{(4)\prime}(\rho,q)\right] C_{2n+1} se_{2n+1}(\vartheta,q) \\
& \mp \frac{\mu}{aJ}\sum_{m,n=0}^{\infty} \mathfrak{N}_{mn}\left[Ms_{2m+2}^{(3)\prime}(\rho,q) - \frac{Ms_{2m+2}^{(3)\prime}(\rho_I,q)}{Ms_{2m+2}^{(4)\prime}(\rho_I,q)} Ms_{2m+2}^{(4)\prime}(\rho,q)\right] C_{2m+2} se_{2n+1}(\vartheta,q)
\end{aligned}
\tag{6.2}
$$

where –ve above and +ve below are assigned for $\pi/2 \le \vartheta \le -\pi/2$ and $-\pi/2 \le \vartheta \le \pi/2$; $\mathfrak{M}_{mn}$ and $\mathfrak{N}_{mn}$ are given by Equations (2.35) and (2.38). As all

displacement and stress functions of far-field, scattered and transmitted waves are the series of elliptical cosine series with order 2n and of elliptical sine series with order 2n+1, these wave functions customarily satisfy the traction-free boundary, Equation (4.4), and other conditions can be applied by utilization of orthogonality of elliptical cosine and sine functions. Applying the traction-free condition at the surface of the elliptical hill, Equation (4.5), yields

$$B_{2n} = \frac{\sum_{m=0}^{\infty} \mathfrak{M}_{mn} B_{2m+1} \left( Mc_{2m+1}^{(3)\prime}(\rho_O,q) - \frac{Mc_{2m+1}^{(3)\prime}(\rho_I,q)}{Mc_{2m+1}^{(4)\prime}(\rho_I,q)} Mc_{2m+1}^{(4)\prime}(\rho_O,q) \right)}{Mc_{2n}^{(3)\prime}(\rho_O,q) - \frac{Mc_{2n}^{(3)\prime}(\rho_I,q)}{Mc_{2n}^{(4)\prime}(\rho_I,q)} Mc_{2n}^{(4)\prime}(\rho_O,q)} \tag{6.3}$$

$$C_{2n+1} = \frac{\sum_{m=0}^{\infty} \mathfrak{N}_{mn} C_{2m+2} \left( Ms_{2m+2}^{(3)}(\rho_O,q) - \frac{Ms_{2m+2}^{(3)\prime}(\rho_I,q)}{Ms_{2m+2}^{(4)\prime}(\rho_I,q)} Ms_{2m+2}^{(4)}(\rho_O,q) \right)}{Ms_{2n+1}^{(3)}(\rho_O,q) - \frac{Ms_{2n+1}^{(3)\prime}(\rho_I,q)}{Ms_{2n+1}^{(4)\prime}(\rho_I,q)} Ms_{2n+1}^{(4)}(\rho_O,q)} \tag{6.4}$$

Then applying the continuity of displacement and stress at the interface $\overline{L}$ yields

$$\begin{Bmatrix} 4w_0(-1)^n Mc_{2n}^{(1)}(\rho_O,q) ce_{2n}(\gamma,q) \\ + Mc_{2n}^{(3)}(\rho_O,q) A_{2n} \end{Bmatrix} = \begin{Bmatrix} \sum_{m=0}^{\infty} \mathfrak{M}_{mn} \left[ Mc_{2m+1}^{(3)}(\rho_O,q) - \frac{Mc_{2m+1}^{(3)\prime}(\rho_I,q)}{Mc_{2m+1}^{(4)\prime}(\rho_I,q)} Mc_{2m+1}^{(4)}(\rho_O,q) \right] B_{2m+1} \\ + \left[ Mc_{2n}^{(3)}(\rho_O,q) - \frac{Mc_{2n}^{(3)\prime}(\rho_I,q)}{Mc_{2n}^{(4)\prime}(\rho_I,q)} Mc_{2n}^{(4)}(\rho_O,q) \right] B_{2n} \end{Bmatrix} \tag{6.5}$$

$$\begin{Bmatrix} 4w_0(-1)^n Mc_{2n}^{(1)\prime}(\rho_O,q) ce_{2n}(\gamma,q) \\ + (\rho_O,q) A_{2n} \end{Bmatrix} = \begin{Bmatrix} \sum_{m=0}^{\infty} \mathfrak{M}_{mn} \left[ Mc_{2m+1}^{(3)\prime}(\rho_O,q) - \frac{Mc_{2m+1}^{(3)\prime}(\rho_I,q)}{Mc_{2m+1}^{(4)\prime}(\rho_I,q)} Mc_{2m+1}^{(4)\prime}(\rho_O,q) \right] B_{2m+1} \\ + \left[ Mc_{2n}^{(3)\prime}(\rho_O,q) - \frac{Mc_{2n}^{(3)\prime}(\rho_I,q)}{Mc_{2n}^{(4)\prime}(\rho_I,q)} Mc_{2n}^{(4)\prime}(\rho_O,q) \right] B_{2n} \end{Bmatrix} \tag{6.6}$$

$$\begin{Bmatrix} 4iw_0(-1)^n Ms_{2n+1}^{(1)}(\rho_O,q) se_{2n+1}(\gamma,q) \\ + Ms_{2n+1}^{(3)}(\rho_O,q) A_{2n+1} \end{Bmatrix} = \begin{Bmatrix} \sum_{m=0}^{\infty} \mathfrak{N}_{mn} \left[ Ms_{2m+2}^{(3)}(\rho_O,q) - \frac{Ms_{2m+2}^{(3)\prime}(\rho_I,q)}{Ms_{2m+2}^{(4)\prime}(\rho_I,q)} Ms_{2m+2}^{(4)}(\rho_O,q) \right] C_{2m+2} \\ + \left[ Ms_{2n+1}^{(3)}(\rho_O,q) - \frac{Ms_{2n+1}^{(3)\prime}(\rho_I,q)}{Ms_{2n+1}^{(4)\prime}(\rho_I,q)} Ms_{2n+1}^{(4)}(\rho_O,q) \right] C_{2n+1} \end{Bmatrix} \tag{6.7}$$

$$\begin{Bmatrix} 4iw_0(-1)^n Ms_{2n+1}^{(1)\prime}(\rho_O,q) se_{2n+1}(\gamma,q) \\ + Ms_{2n+1}^{(3)\prime}(\rho_O,q) A_{2n+1} \end{Bmatrix} = \begin{Bmatrix} \sum_{m=0}^{\infty} \mathfrak{N}_{mn} \left[ Ms_{2m+2}^{(3)\prime}(\rho_O,q) - \frac{Ms_{2m+2}^{(3)\prime}(\rho_I,q)}{Ms_{2m+2}^{(4)\prime}(\rho_I,q)} Ms_{2m+2}^{(4)\prime}(\rho_O,q) \right] C_{2m+2} \\ + \left[ Ms_{2n+1}^{(3)\prime}(\rho_O,q) - \frac{Ms_{2n+1}^{(3)\prime}(\rho_I,q)}{Ms_{2n+1}^{(4)\prime}(\rho_I,q)} Ms_{2n+1}^{(4)\prime}(\rho_O,q) \right] C_{2n+1} \end{Bmatrix} \tag{6.8}$$

Equations (6.3), (6.5) and (6.6) establish three sets of infinite equations for the three sets of unknowns $A_{2n}$, $B_{2n}$ and $B_{2n+1}$, where Equations (6.4), (6.7) and (6.8) found other three sets for $A_{2n+1}$, $C_{2n}$ and $C_{2n+2}$; on each set we have three groups of unknown, we can solve them by doing matrix truncation. Similar procedure to Chapter 5 can apply here.

## 6.3 Results and Analysis

Assuming the excitation with unity amplitude, the influence of tunnel and incident angle on ground surface are investigated and the results are presented in term of the dimensionless parameters $\eta$, $\eta_T$, and *R* prescribed by Equations (3.16), (3.18) and (5.9) respectively. We restrict values of $R$ to 1.00002, 1.2, 1.4, and 1.6, which are equivalent the height-to-width ratios of 0.50001, 0.6, 0.7, and 0.8 respectively. We also restrict values of $T$, width of tunnel, to 0.2$A$, 0.5$A$ and 0.8$A$; these apply to every value of *R*.

**Comparison with the Solutions of "Circular" Elliptical Case:**

If, in comparison to the hill, a tunnel is really small and wave length of input waves is comparably long, the above wave functions must be identical to those of semi-elliptical hill without tunnel; however this is applicable to *R* = 1.00002 since the tunnel could be assigned to be so small without becoming a line.

Applying asymptotic values of $\frac{Mc_n^{(3)'}(\rho_I,q)}{Mc_n^{(4)'}(\rho_I,q)}$ and $\frac{Ms_n^{(3)'}(\rho_I,q)}{Ms_n^{(4)'}(\rho_I,q)}$ when $\rho_I$ approaches zero, we obtain the identical equations to those of the semi-elliptical hill model without tunnel in Chapter 4.

Figure 6.2: Displacement Amplitudes of Ground Motion at $\eta = 1$

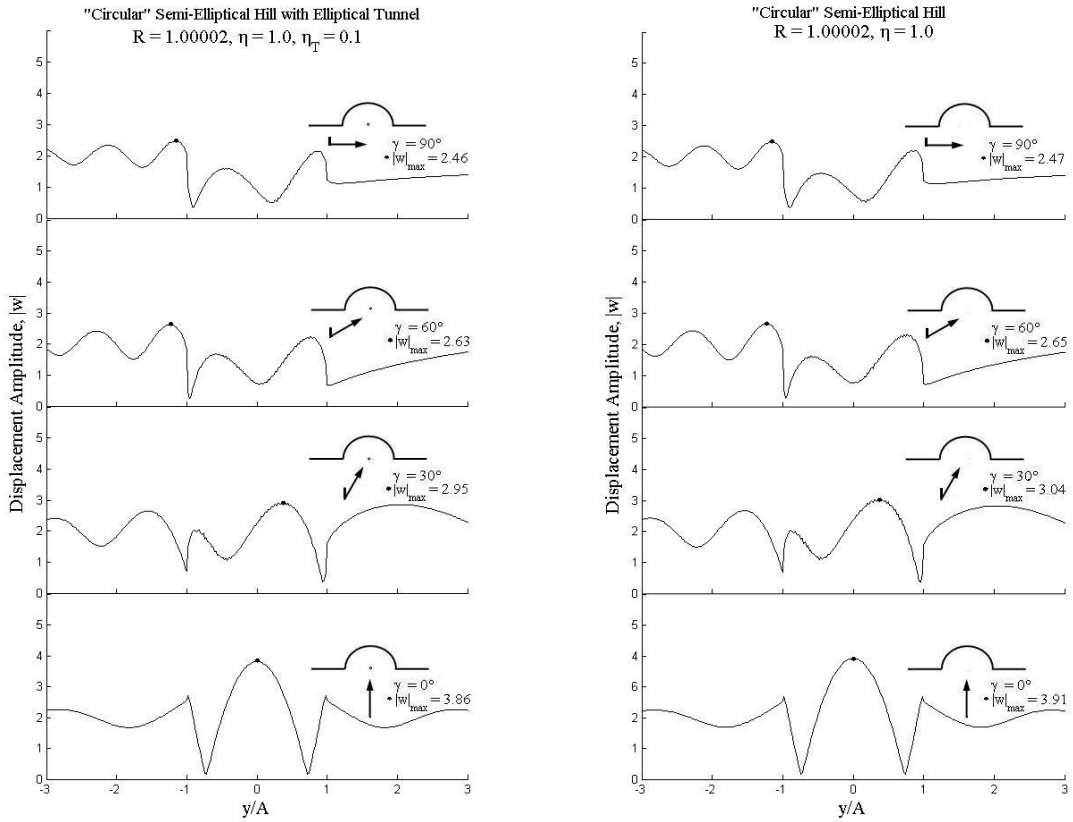


(a) "Circular" Semi-Elliptical Hill with an elliptical tunnel $\eta_T = 0.1$

(b) "Circular" Semi-Elliptical Hill

The prior Figure 6.2 demonstrates the resemblance for both semi-elliptical hills with and without an elliptical tunnel when $R = 1.00002$ at $\eta = 1$ and $\eta_T = 0.1$ for the tunnel. We found out that the derived results are remarkably in harmonic not only to the reference, semi-circular, but also to results shown in Figure 5.2a; less than 3% difference for the maximum values.

Figure 6.3: Displacement Amplitudes for $R = 1.00002$ with Tunnel $T = 0.2A$

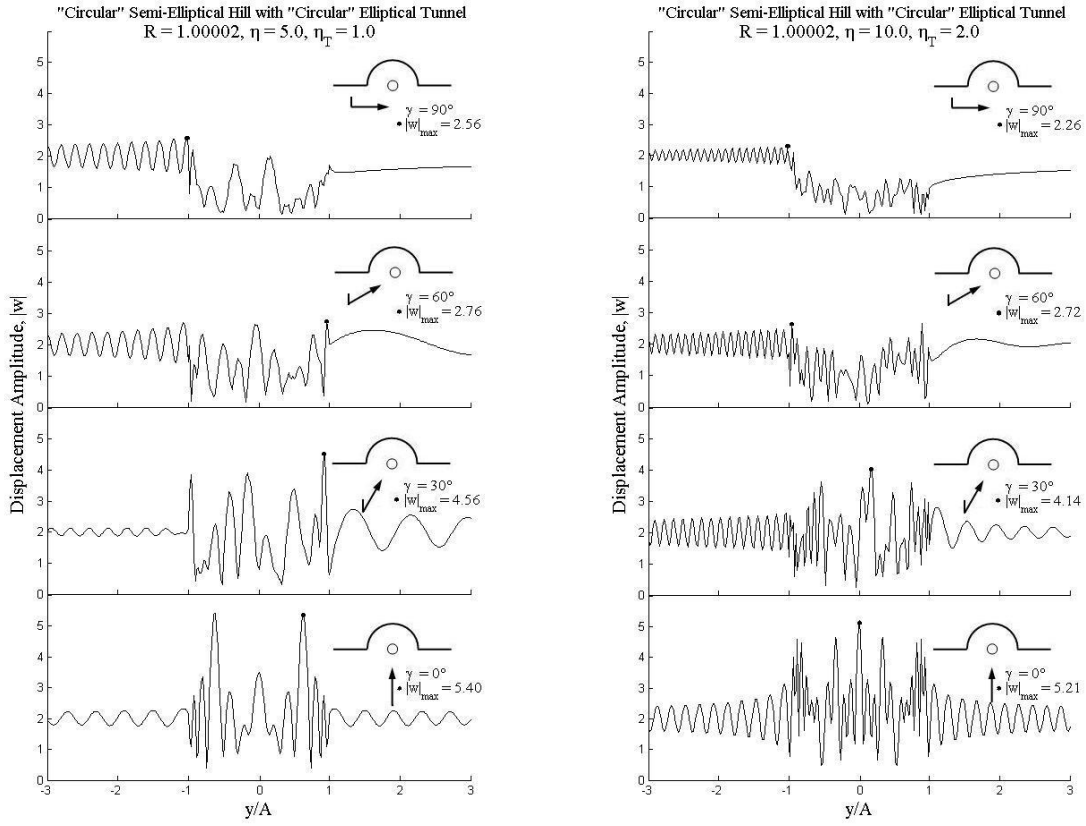


(a) $\eta = 5$ (b) $\eta = 10$

Figures 6.3 through 6.5 are the plots of surface displacement for “circular” semi-elliptical hill with “circular” elliptical tunnel $T = 0.2A$, $0.5A$ and $0.8A$ respectively; on each plot there are 2 subplots for $\eta = 5$ and 10 at four incidence $\gamma = 0°$, 30°, 60° and 90°. The formulation developed in this chapter gives exceptionally consistent results in comparison to Figures 5.7, 5.8 and 5.9.

Figure 6.4: Displacement Amplitudes for $R = 1.00002$ with Tunnel $T = 0.5A$

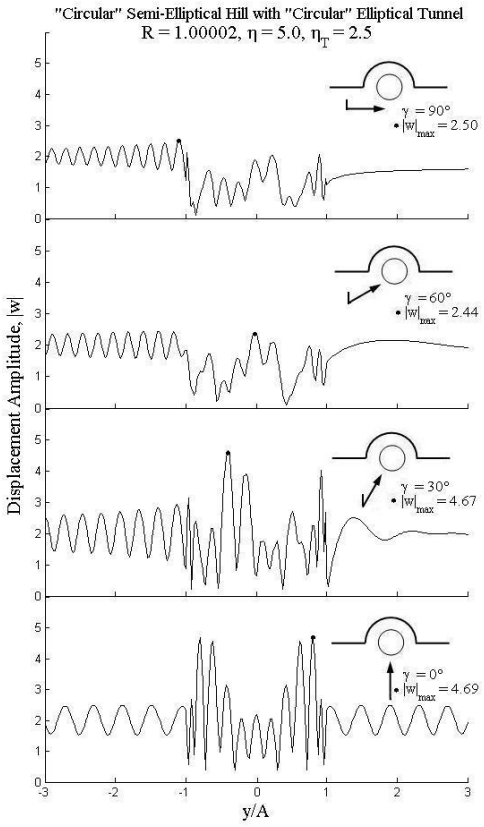


(a) $\eta = 5$

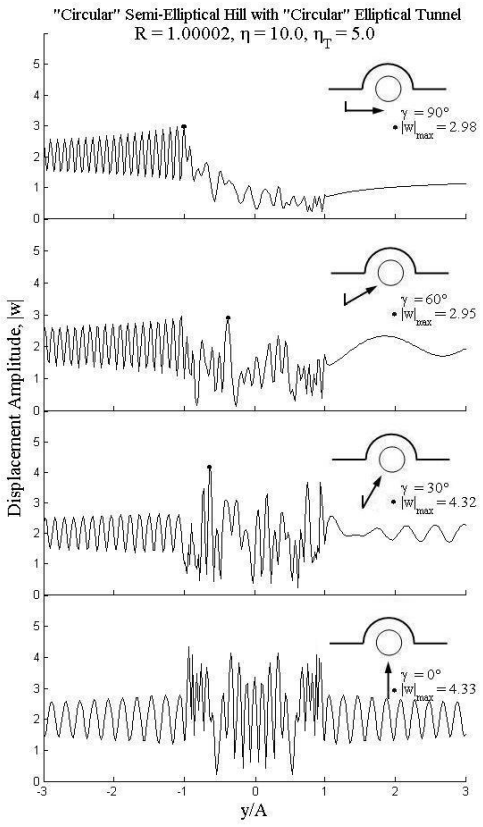


(b) $\eta = 10$

Figure 6.5: Displacement Amplitudes for $R = 1.00002$ with Tunnel $T = 0.8A$

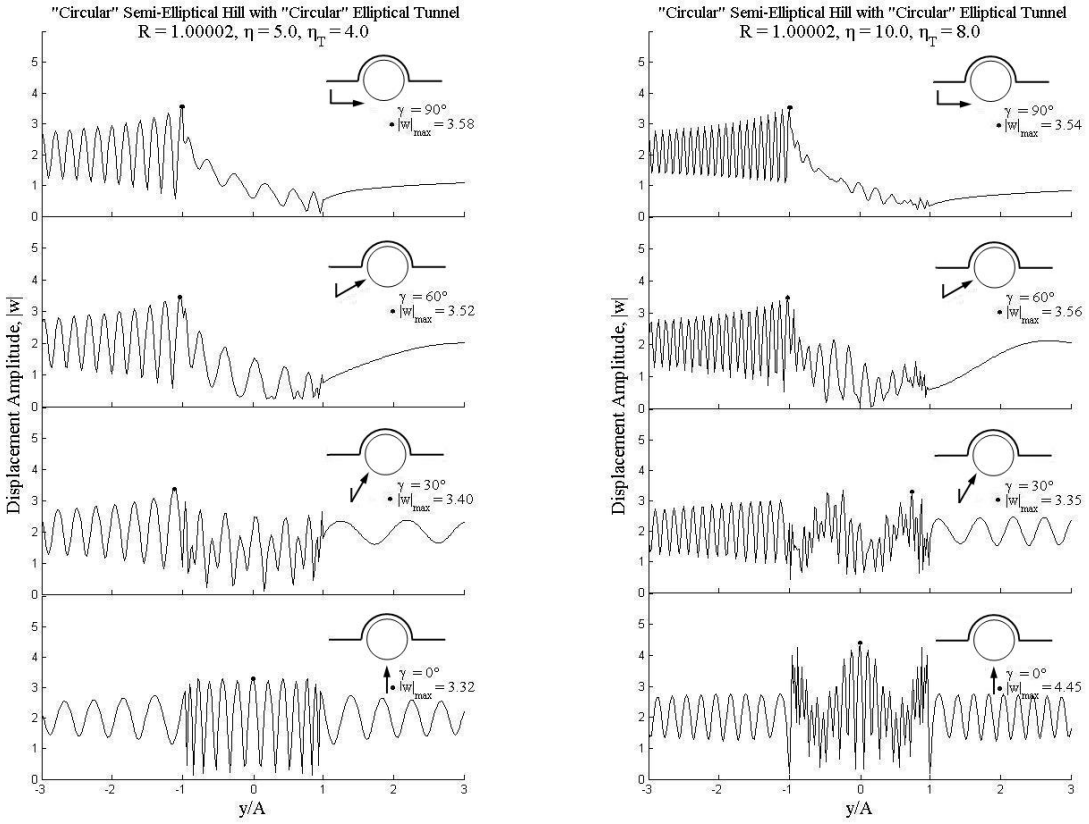


(a) $\eta = 5$ (b) $\eta = 10$

**Effects of Tunnel, and Incident Angle to Semi-Elliptical Hill:**

Figures 6.6 to 6.11 illustrate amplitudes of surface displacements at four prescribed incidences versus the distance *y/A* on and around the hill with the dimensionless frequency $\eta = 5$ and 10 for the semi-elliptical hill $R = 1.2$, 1.4 and 1.6 with an elliptical tunnel $T = 0.5A$; their corresponding plots of surface displacement for the semi-elliptical hill without a tunnel are shown on their right-hand side. It can be seen that the presence of the tunnel significantly distorts the

amplitude of ground motion in comparison to the reference, semi-elliptical hill without tunnel. In contrast to semi-elliptical hill which their locations of maximum surface displacement may located close to the right-edge of the hill, the tunnel causes the reflection and makes the location of maximum amplitude of surface displacement always in the left half or front of the hill. Please note that for vertical incidence the response is symmetric; consequently there are corresponding points of maximum amplitude on both sides of the hill.

Figure 6.6: Displacement Amplitude for $R = 1.2$ at $\eta = 5$

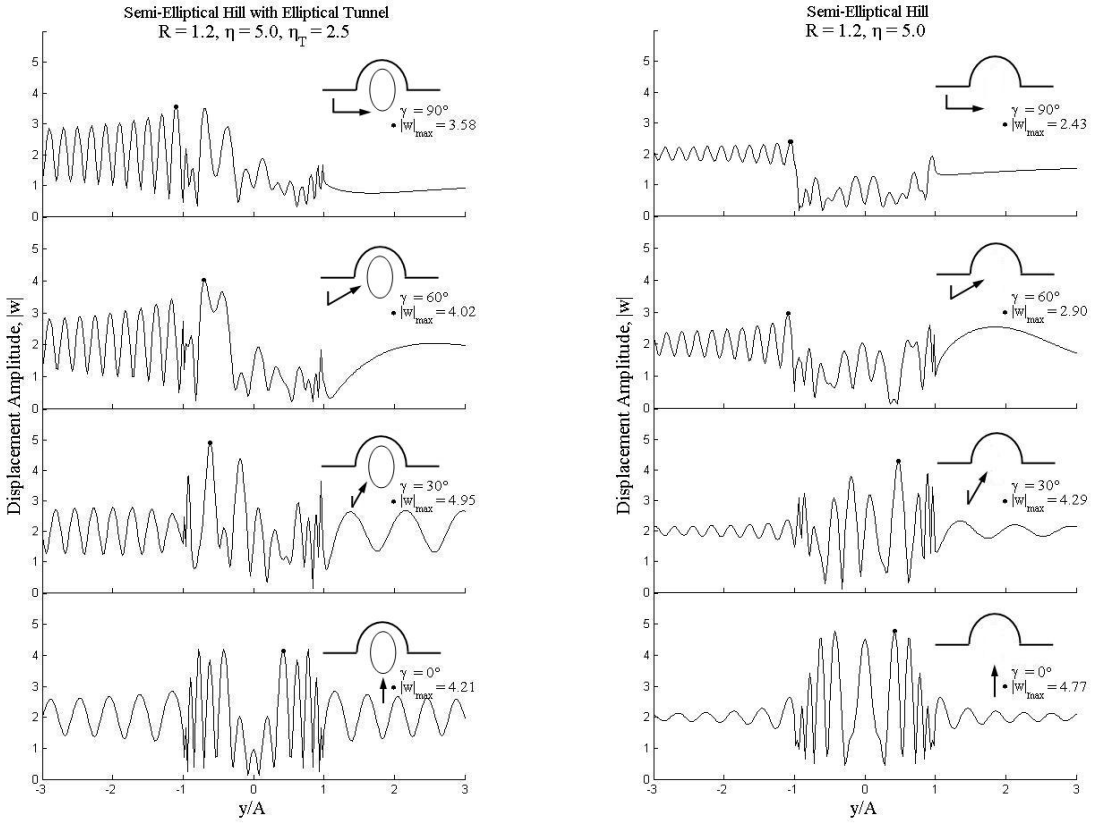


(a) with Tunnel; $T = 0.5A$ (b) without Tunnel

Generally when the angle of incidence is nearly parallel to the flat surface tunnels turn to be barricades blocking the coming wave passages and creating shadow zone on the right-side of the hill; amplitude of ground displacement is always less than one. Furthermore the strong oscillation is observed on the left-side of the hill; while in the case of semi-elliptical hill this amplitude of ground motion is always in the range of 2.5 or less, the existence of tunnels greatly affects the displacement in the front of the hill and results in the amplitude greater than 3.

Figure 6.7: Displacement Amplitude for $R = 1.2$ at $\eta = 10$

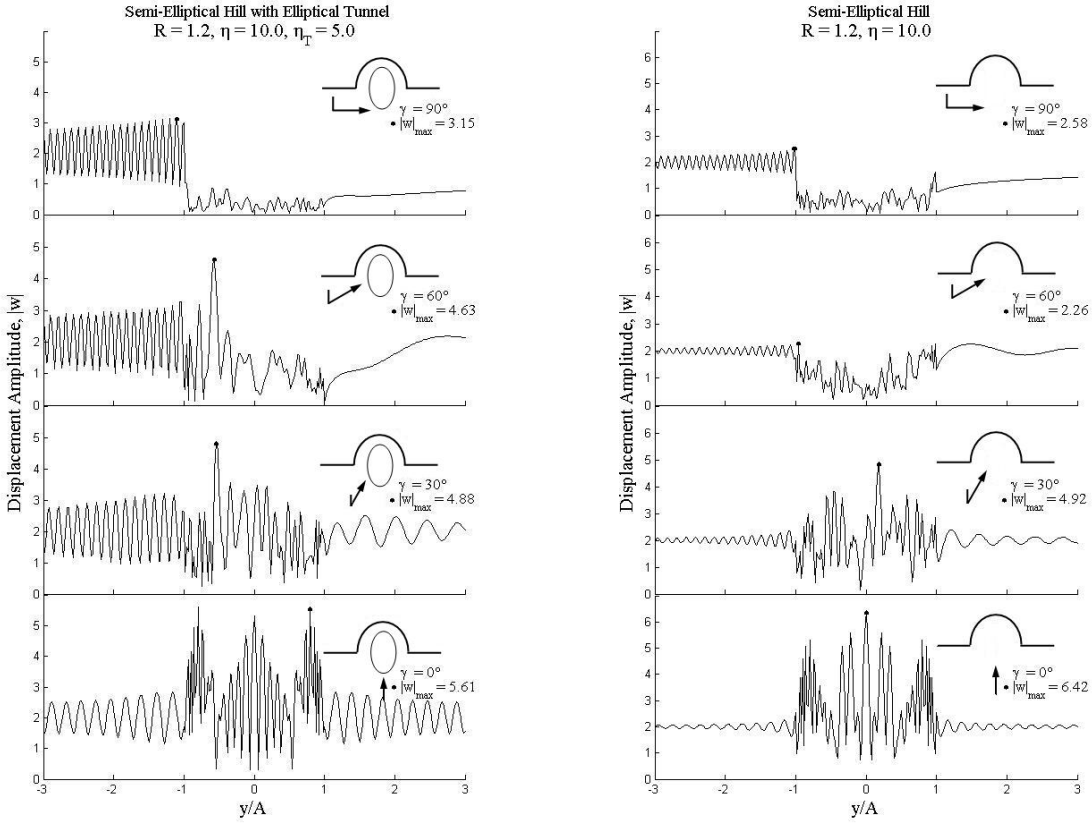


(a) with Tunnel; $T = 0.5A$ (b) without Tunnel

Figure 6.8: Displacement Amplitude for $R = 1.4$ at $\eta = 5$

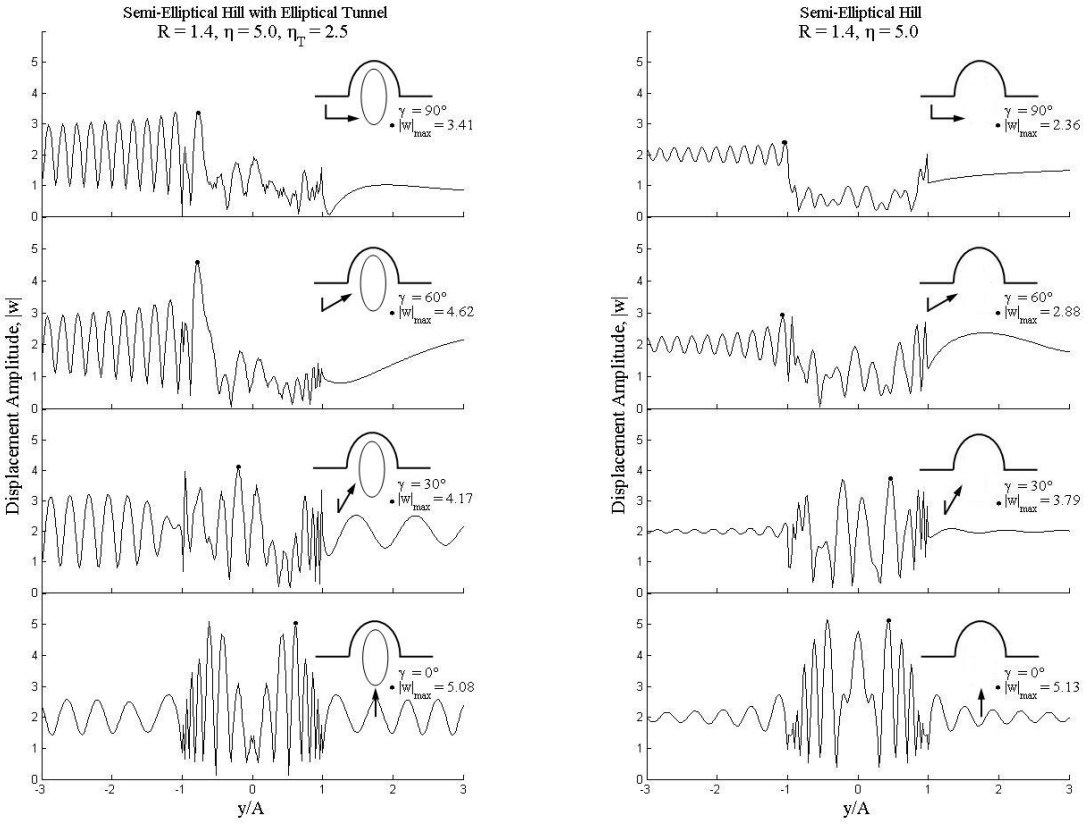


(a) with Tunnel; $T = 0.5A$ (b) without Tunnel

On another hand tunnels become less efficient obstacles when the angle of incidence is nearly vertical. Even though a location of maximum displacement amplitude is different from its corresponding reference in the case of inexistence of a tunnel, visibly a maximum amplitude value of ground displacement is insignificant disturbed by tunnel; the presence of a tunnel amplifies maximum displacement by 30%-70% from corresponding value of reference for the horizontal incidence, while de-amplifies maximum displacement in the range of

1%-15% for the vertical incidence. It can be said that the hinder efficiency of an elliptical tunnel depends on the direction of wave passage; the tunnel becomes better obstruction when the incident wave is perpendicular to its major axis. Moreover the surface displacements on both sides of the hill are more fluctuated than the reference.

Figure 6.9: Displacement Amplitude for $R = 1.4$ at $\eta = 10$

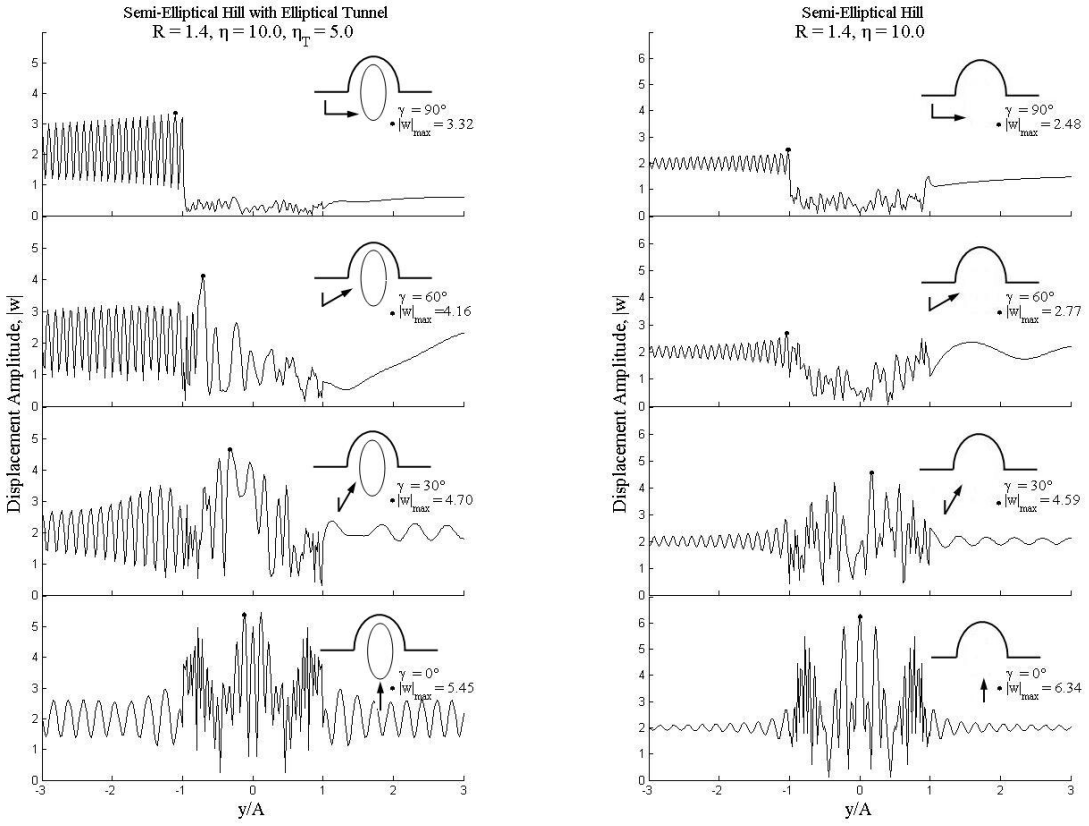


(a) with Tunnel; $T = 0.5A$ (b) without Tunnel

Figure 6.10: Displacement Amplitude for $R = 1.6$ at $\eta = 5$

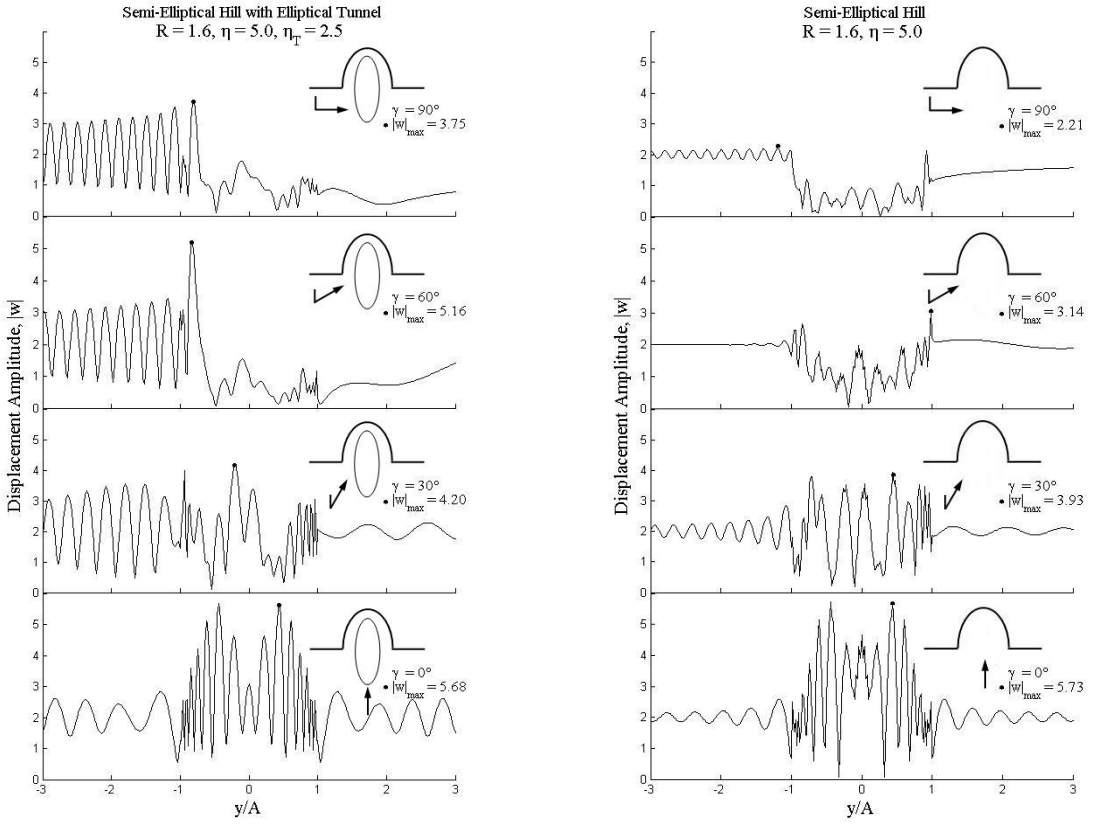


(a) with Tunnel; $T = 0.5A$ (b) without Tunnel

To study the influence of tunnel-size, we consider only $R = 1.6$ with three sizes of tunnel, $T = 0.2A$, $0.5A$ and $0.8A$. Due to the formulation of the problem, we may see this as the width effect; the height of tunnel is very comparable. After evaluating Figures 6.12 and 6.13 $T = 0.2A$ and $0.8A$ respectively against Figures 6.10 and 6.11, it may be said that the high oscillation of wave passage is inconsequent to the size of tunnel for nearly grazing angles; furthermore the maximum values of surface displacement are different less than 12 percents. In

addition the shadow zone on the left-side of the hill seems independent to the change of width at least in the distance of interest, $1 \leq y/A \leq 3$; maximum surface displacements are less than one at all times.

Figure 6.11: Displacement Amplitude for $R = 1.6$ at $\eta = 10$

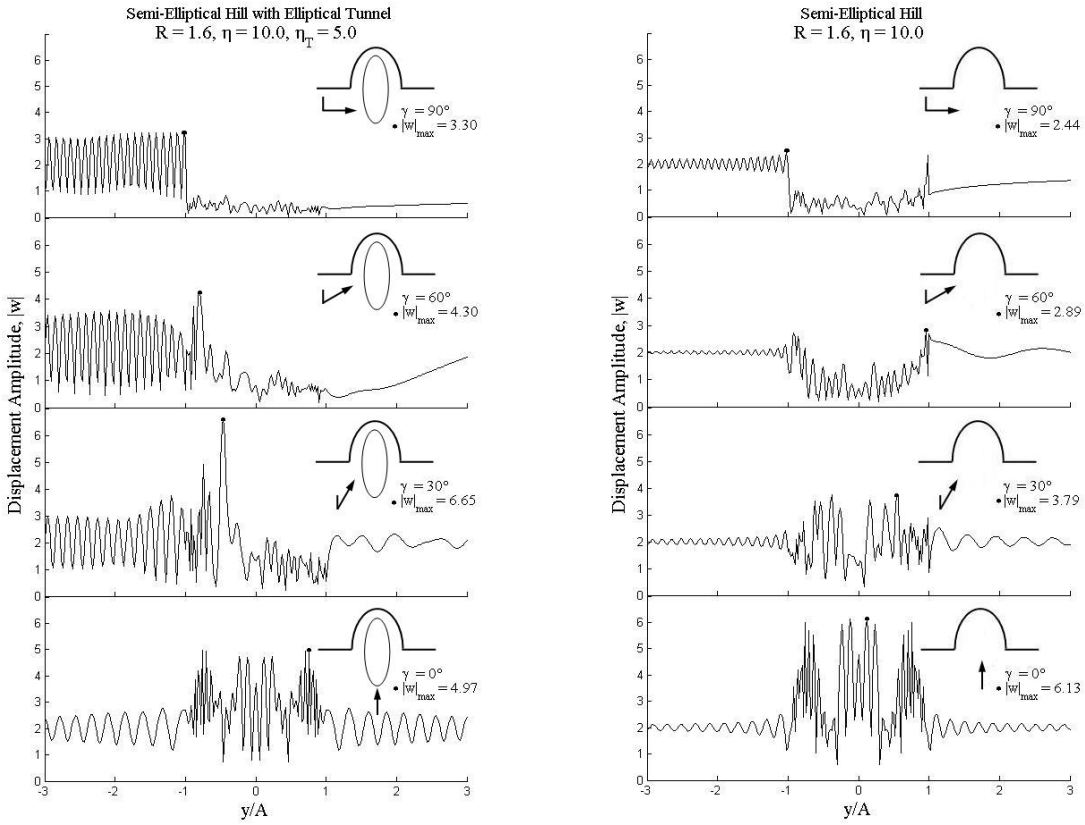


(a) with Tunnel; $T = 0.5A$ (b) without Tunnel

Figure 6.12: Displacement Amplitude for $R = 1.6$ with Tunnel $T = 0.2A$

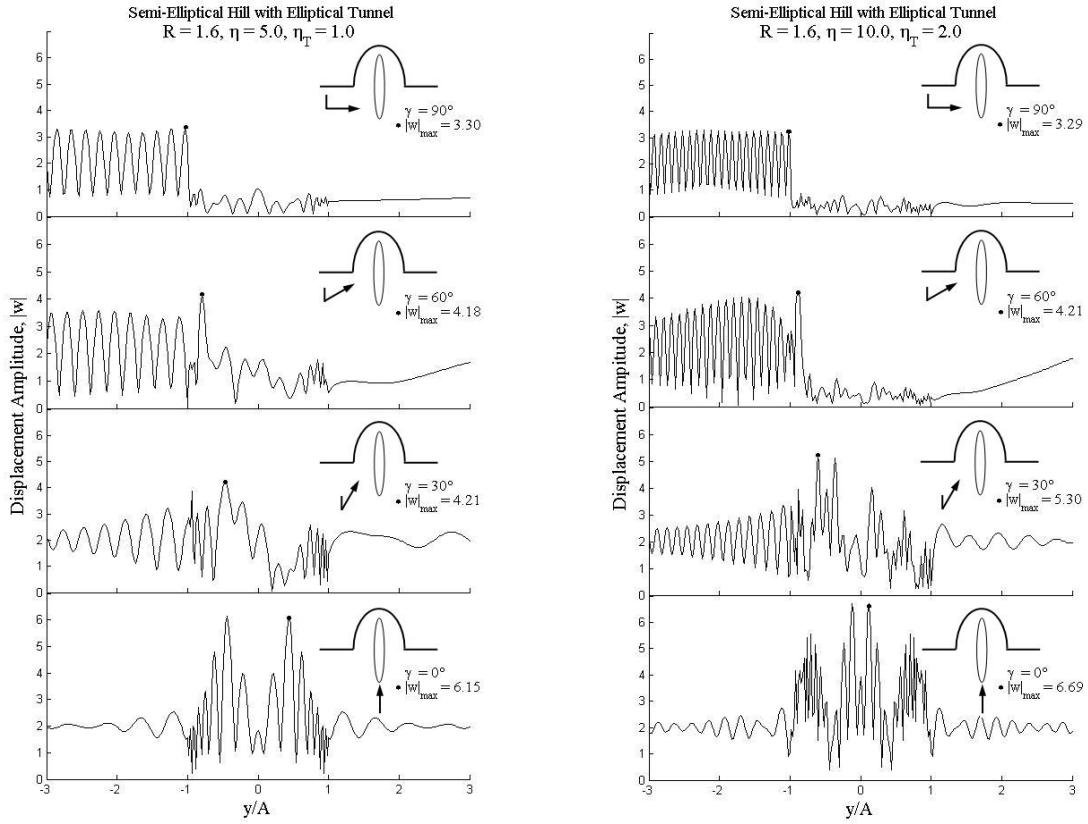


(a) $\eta = 5$ (b) $\eta = 10$

Contrastingly the size of tunnel, or in this case its width, does really matter when the incidence wave is in vertical direction. The maximum values of surface displacement become smaller when the width of tunnel gets larger. In addition we also found that the wave length plays important role in the size effect since the maximum value of displacement is greater affected by the increasing width for $\eta = 5$ than $\eta = 10$.

Figure 6.13: Displacement Amplitude for $R = 1.6$ with Tunnel $T = 0.8A$

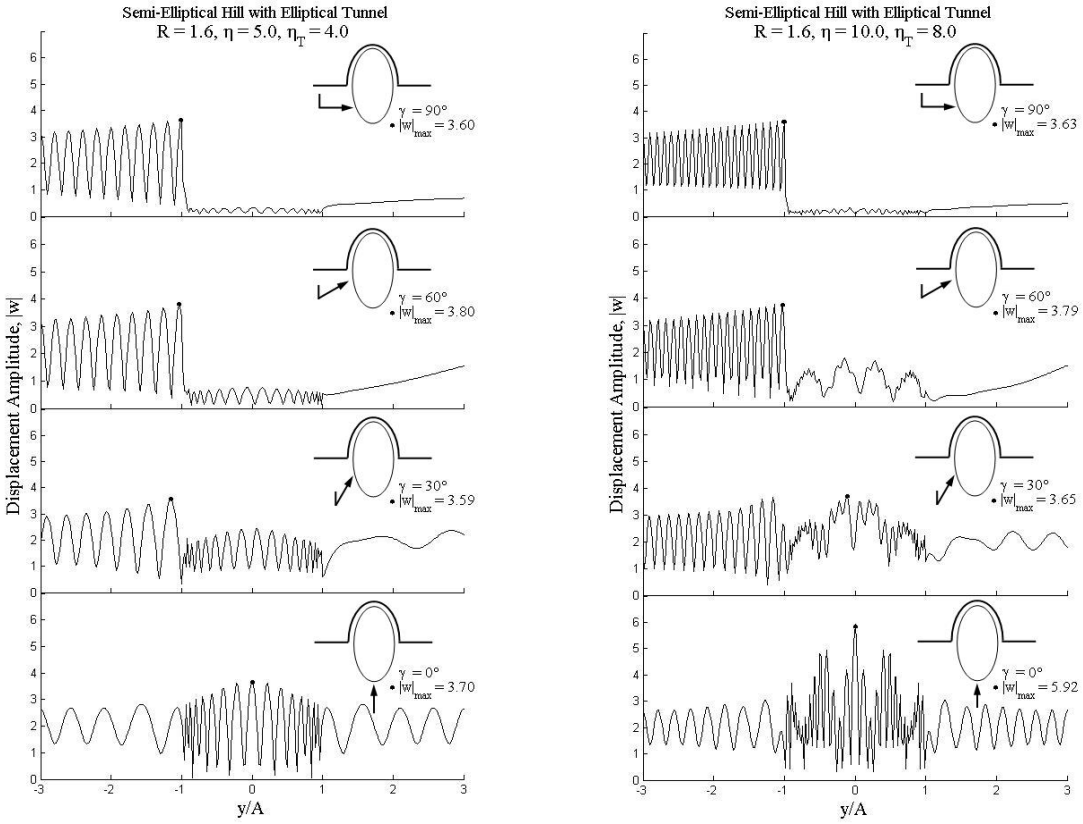


(a) $\eta = 5$ (b) $\eta = 10$

Figures 6.14 through 6.49 show three-dimensional plots of surface displacements for $R = 1.2$, 1.4 and 1.6, equivalent to the height-to-width ratios of 0.6, 0.7 and 0.8 respectively; three values of $T$ are assigned. Each figure illustrates the plots at four incident angles, $\gamma = 0°$, 30°, 60° and 90°, versus the distance *y/A* on and around the hill and the dimensionless frequency $\eta$ in the range of 0.5 to 10; the amplitudes in the range of *y/A* in $[-1,1]$ are those on the elliptical surface of the hill.

Figure 6.14: Displacement Amplitude for $R = 1.2$, $T = 0.2A$ when $\gamma = 0°$

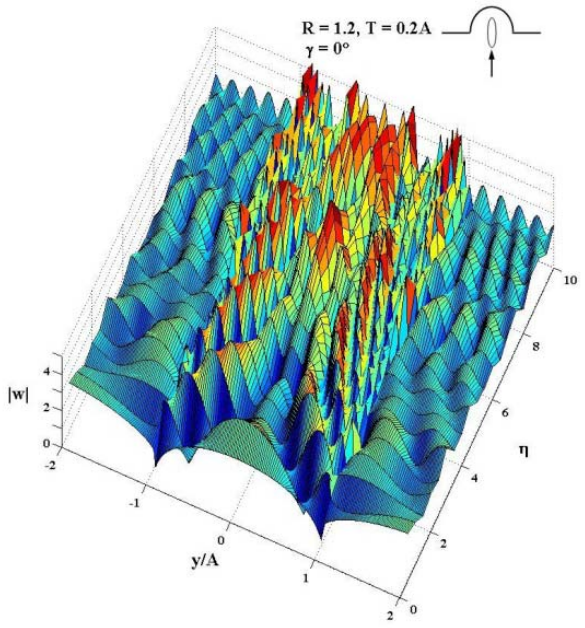


Figure 6.15: Displacement Amplitude for $R = 1.2$, $T = 0.2A$ when $\gamma = 30°$

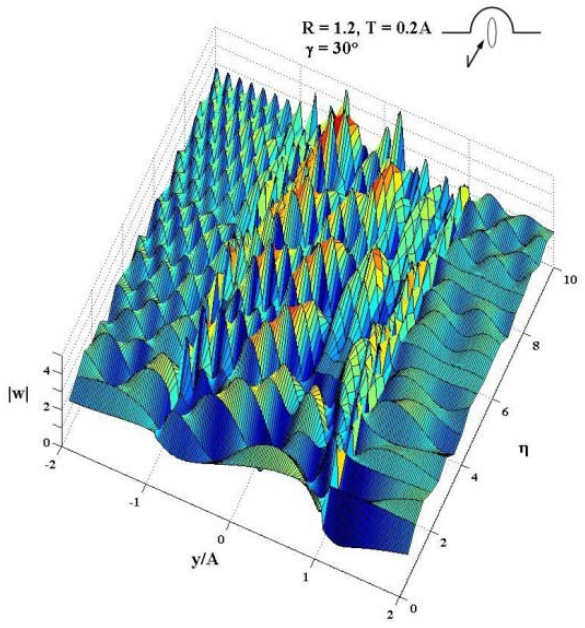

Figure 6.16: Displacement Amplitude for $R = 1.2$, $T = 0.2A$ when $\gamma = 60°$

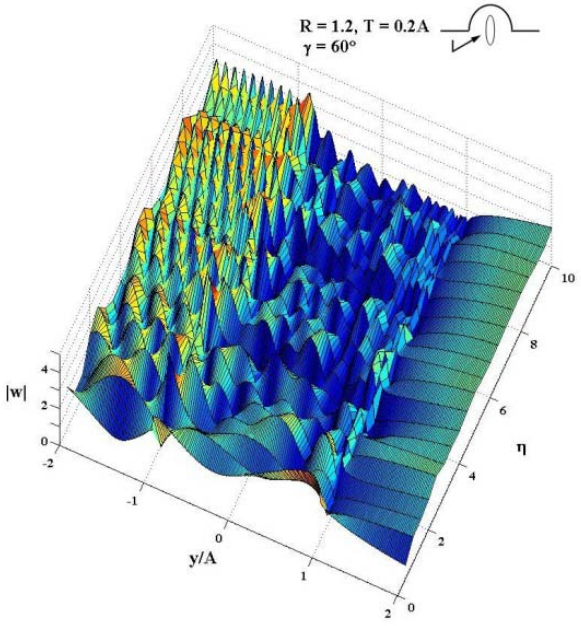


Figure 6.17: Displacement Amplitude for $R = 1.2$, $T = 0.2A$ when $\gamma = 90°$

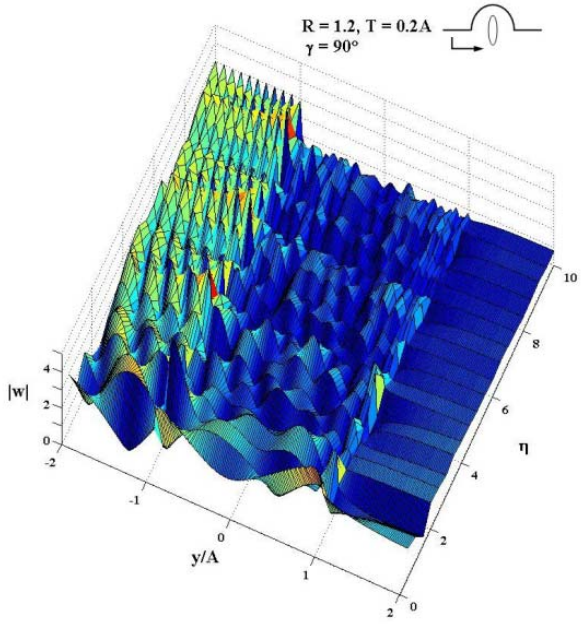

Figure 6.18: Displacement Amplitude for $R = 1.2$, $T = 0.5A$ when $\gamma = 0°$

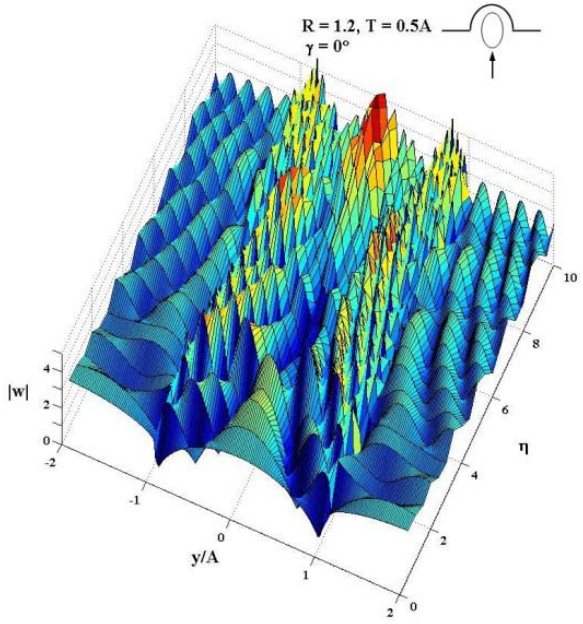


Figure 6.19: Displacement Amplitude for $R = 1.2$, $T = 0.5A$ when $\gamma = 30°$

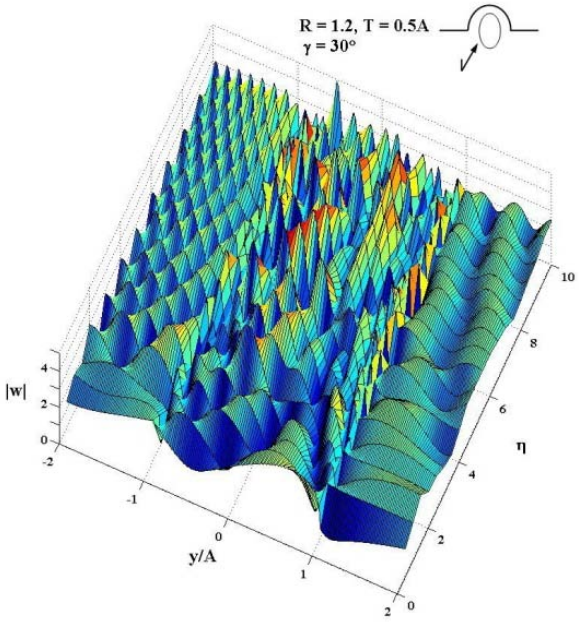

Figure 6.20: Displacement Amplitude for $R = 1.2$, $T = 0.5A$ when $\gamma = 60°$

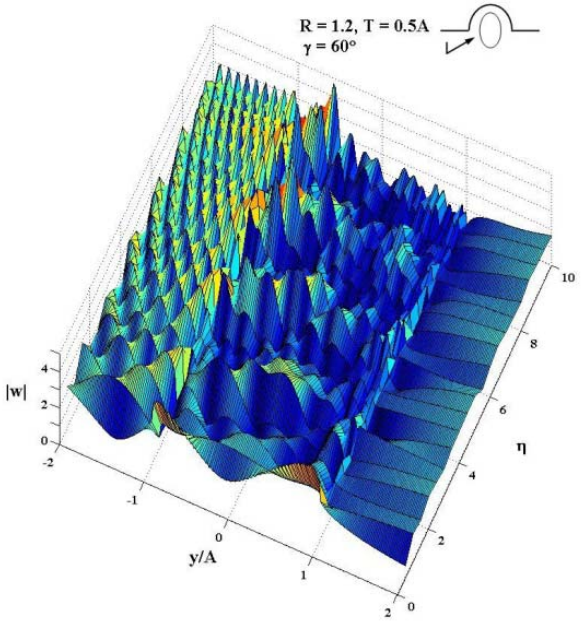


Figure 6.21: Displacement Amplitude for $R = 1.2$, $T = 0.5A$ when $\gamma = 90°$

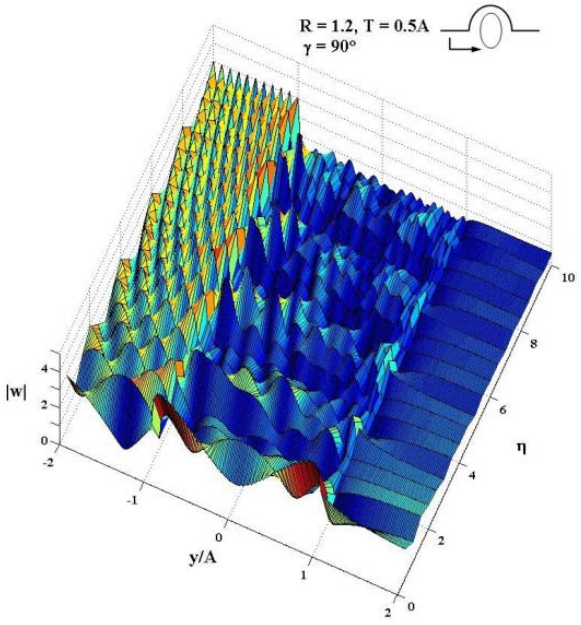

Figure 6.22: Displacement Amplitude for $R = 1.2$, $T = 0.8A$ when $\gamma = 0°$

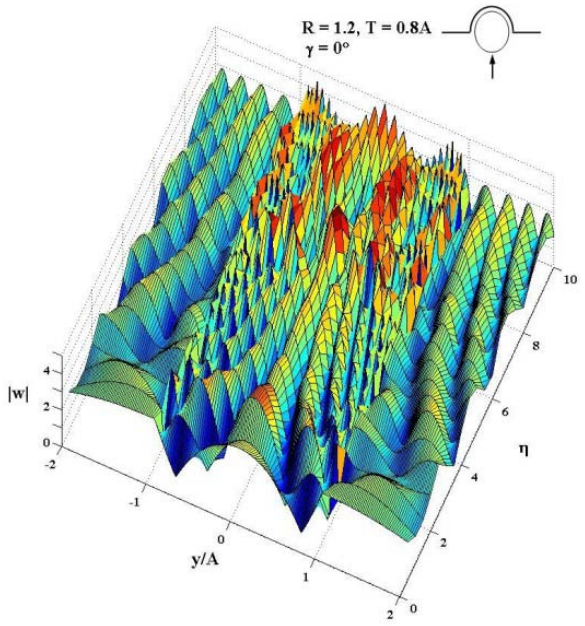


Figure 6.23: Displacement Amplitude for $R = 1.2$, $T = 0.8A$ when $\gamma = 30°$

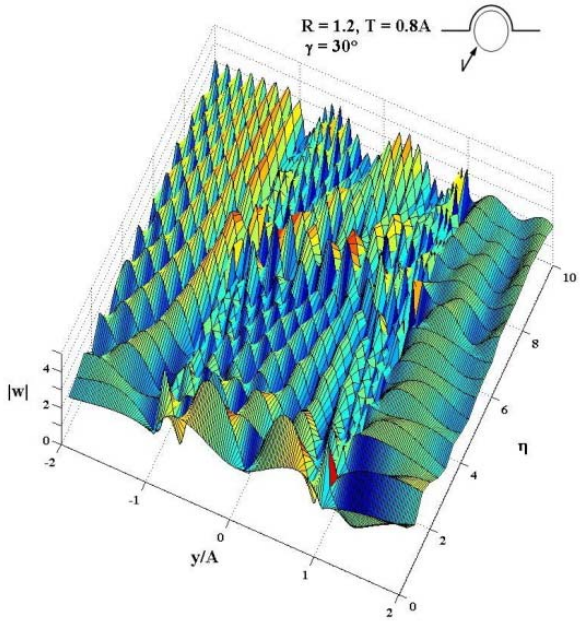

Figure 6.24: Displacement Amplitude for $R = 1.2$, $T = 0.8A$ when $\gamma = 60°$

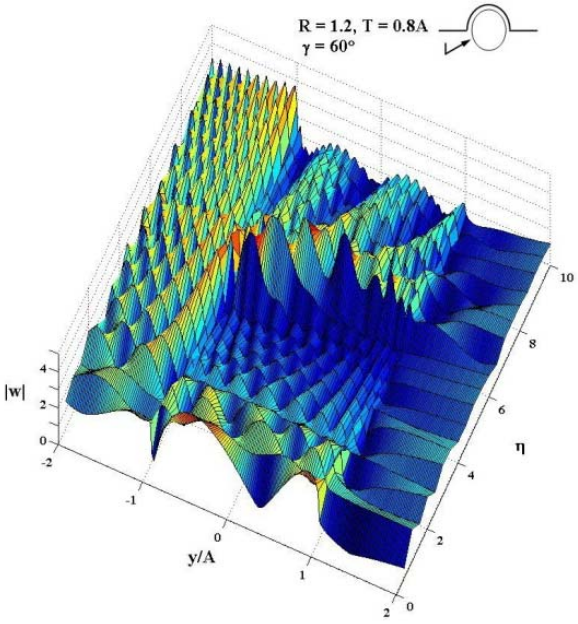


Figure 6.25: Displacement Amplitude for $R = 1.2$, $T = 0.8A$ when $\gamma = 90°$

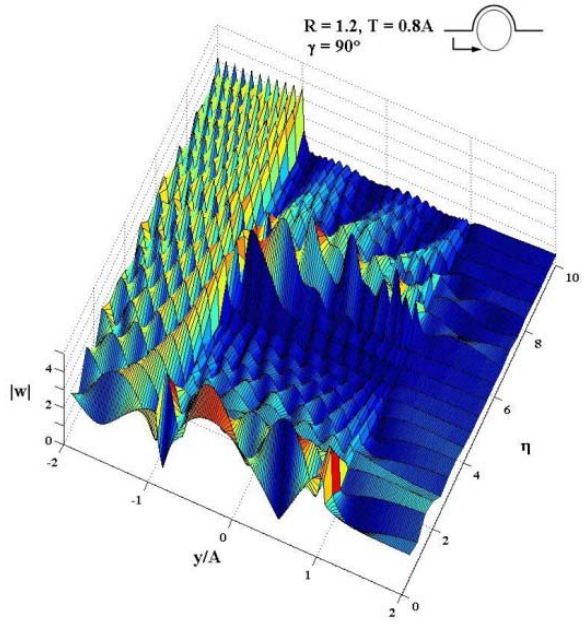

Figure 6.26: Displacement Amplitude for $R = 1.4$, $T = 0.2A$ when $\gamma = 0°$

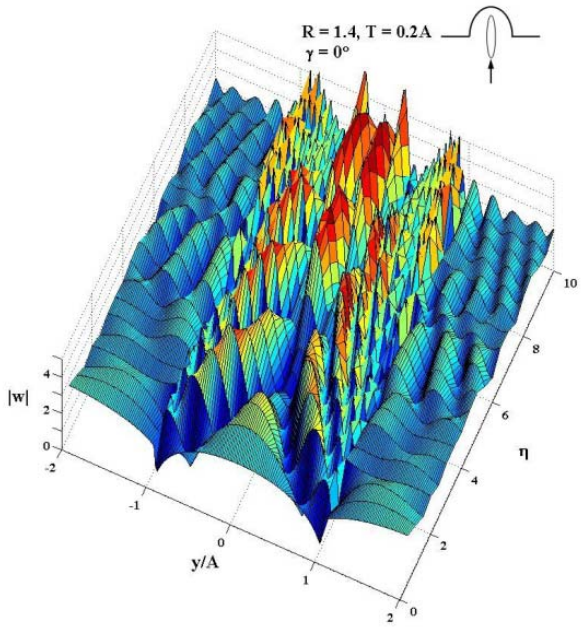


Figure 6.27: Displacement Amplitude for $R = 1.4$, $T = 0.2A$ when $\gamma = 30°$

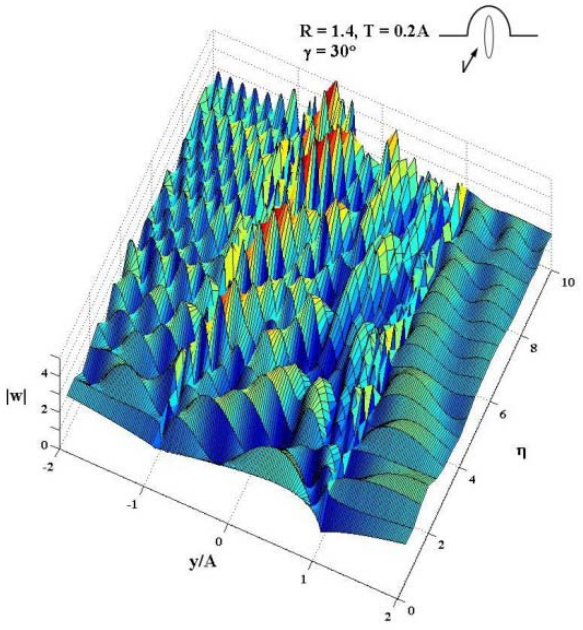

Figure 6.28: Displacement Amplitude for $R = 1.4$, $T = 0.2A$ when $\gamma = 60°$

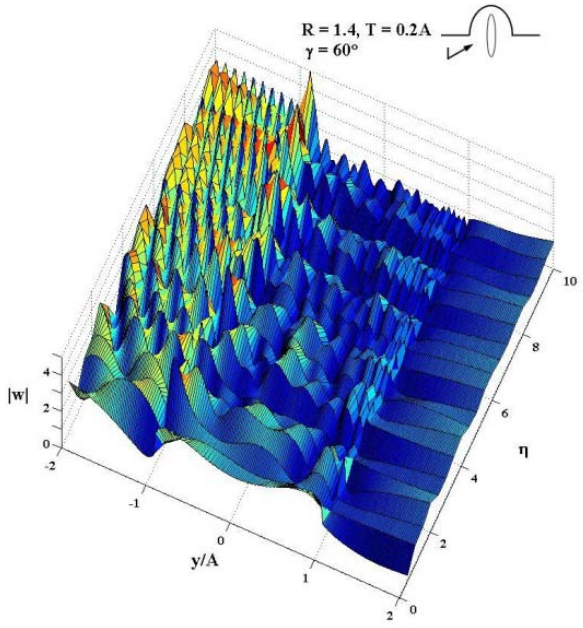


Figure 6.29: Displacement Amplitude for $R = 1.4$, $T = 0.2A$ when $\gamma = 90°$

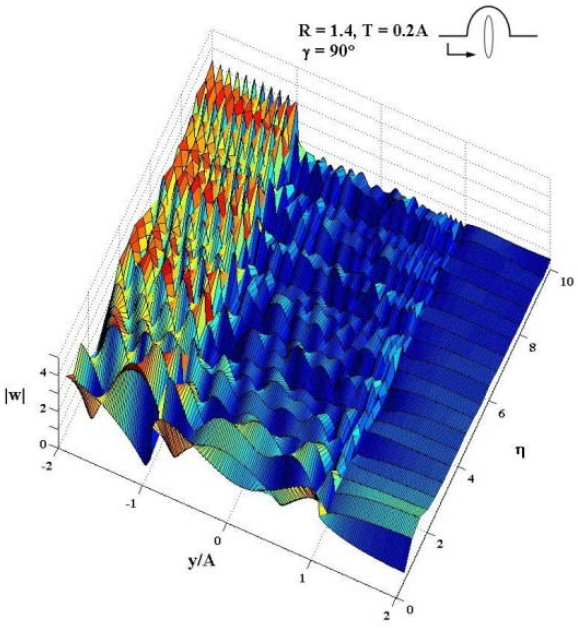

Figure 6.30: Displacement Amplitude for $R = 1.4$, $T = 0.5A$ when $\gamma = 0°$

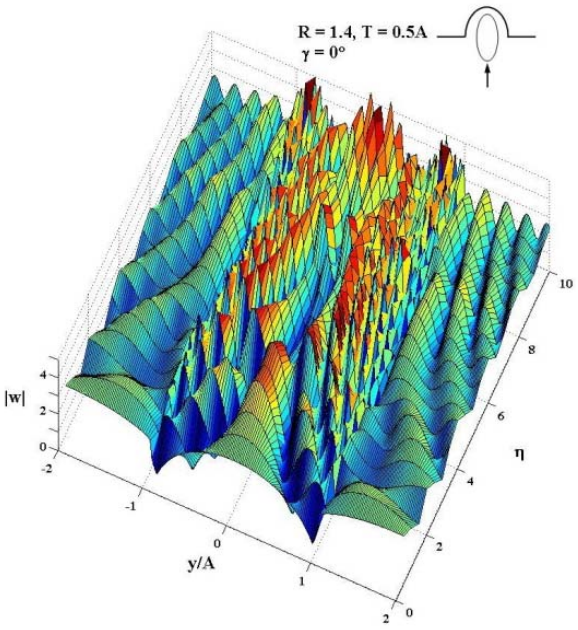


Figure 6.31: Displacement Amplitude for $R = 1.4$, $T = 0.5A$ when $\gamma = 30°$

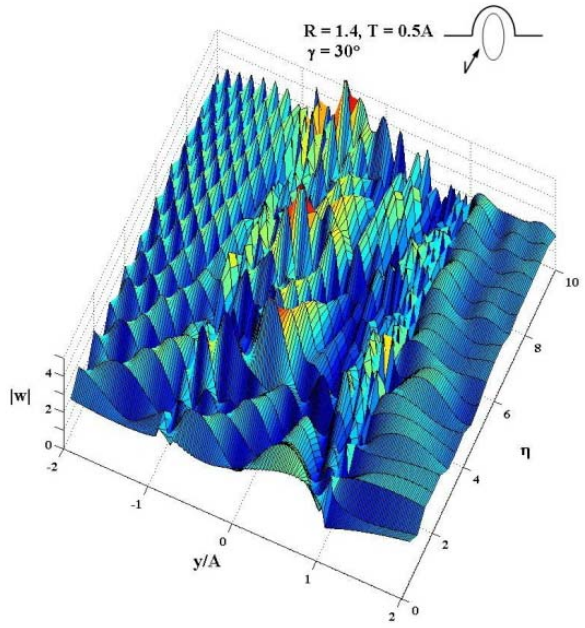

Figure 6.32: Displacement Amplitude for $R = 1.4$, $T = 0.5A$ when $\gamma = 60°$

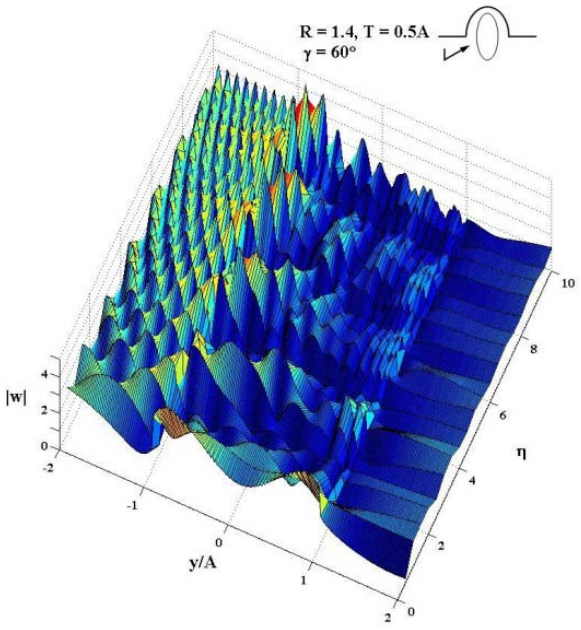


Figure 6.33: Displacement Amplitude for $R = 1.4$, $T = 0.5A$ when $\gamma = 90°$

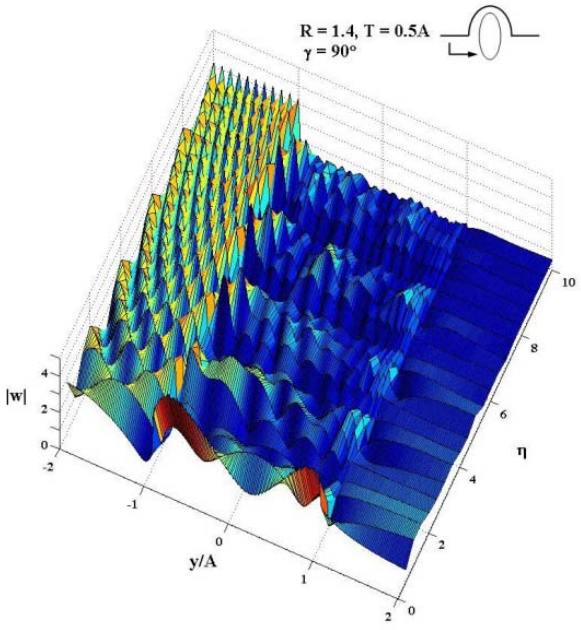

Figure 6.34: Displacement Amplitude for $R = 1.4$, $T = 0.8A$ when $\gamma = 0°$

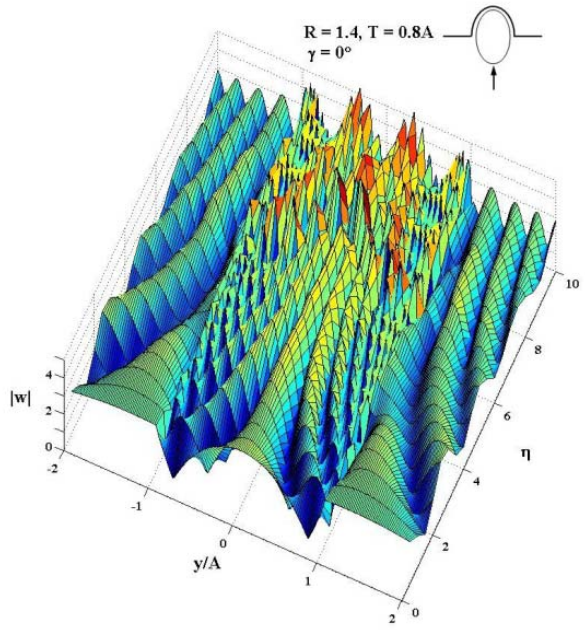


Figure 6.35: Displacement Amplitude for $R = 1.4$, $T = 0.8A$ when $\gamma = 30°$

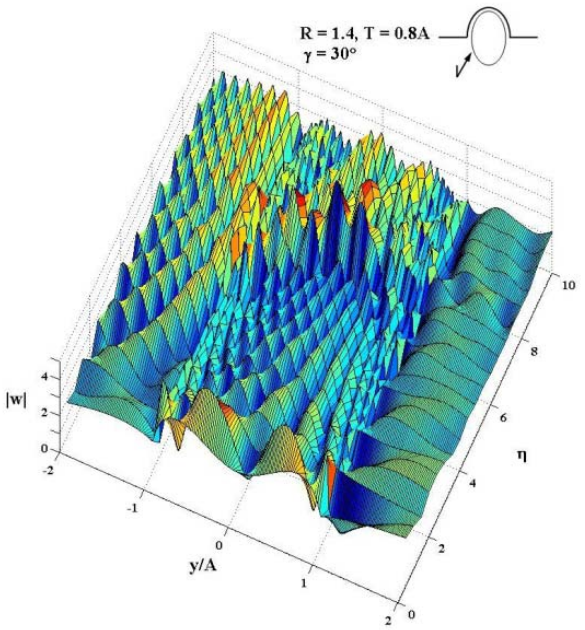

Figure 6.36: Displacement Amplitude for $R = 1.4$, $T = 0.8A$ when $\gamma = 60°$

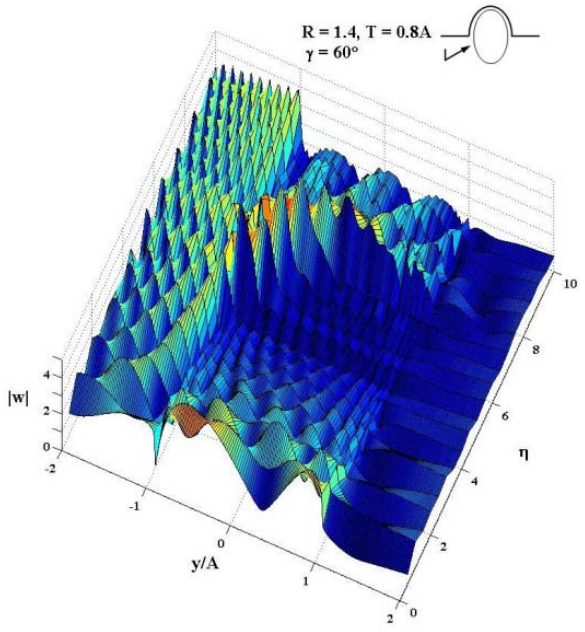


Figure 6.37: Displacement Amplitude for $R = 1.4$, $T = 0.8A$ when $\gamma = 90°$

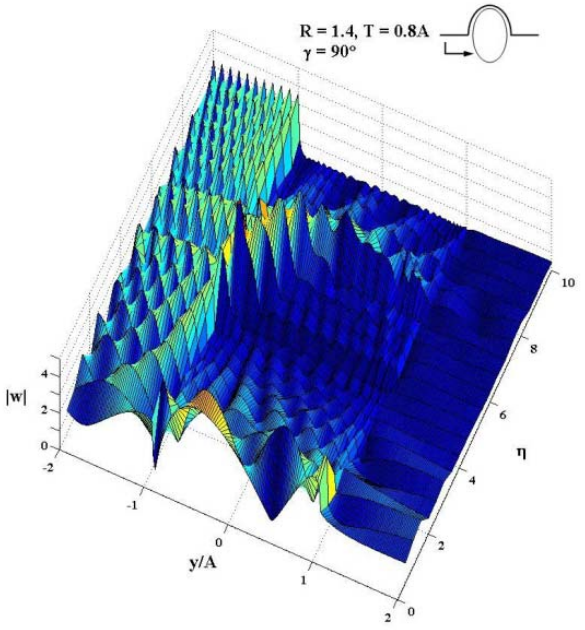

Figure 6.38: Displacement Amplitude for $R = 1.6, T = 0.2A$ when $\gamma = 0°$

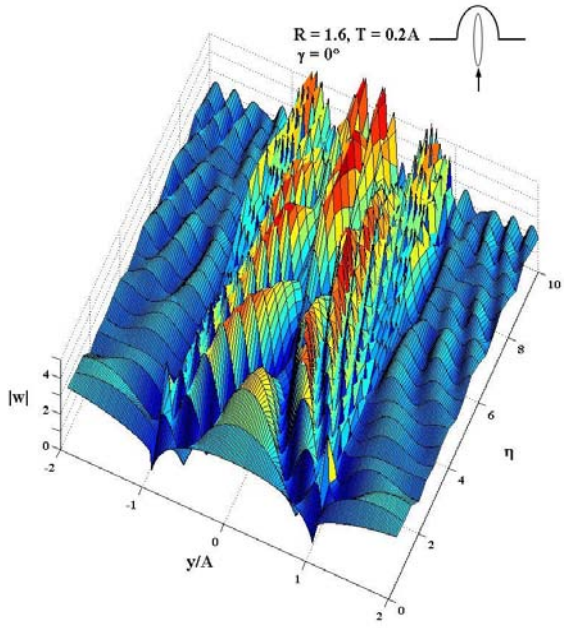


Figure 6.39: Displacement Amplitude for $R = 1.6, T = 0.2A$ when $\gamma = 30°$

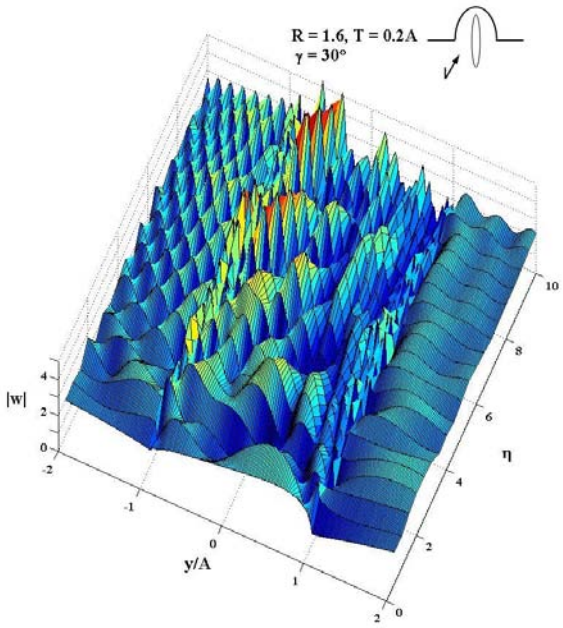

Figure 6.40: Displacement Amplitude for $R = 1.6$, $T = 0.2A$ when $\gamma = 60°$

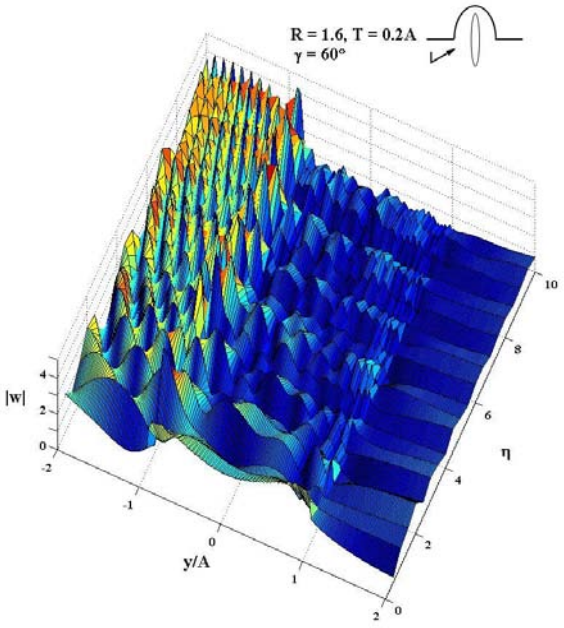


Figure 6.41: Displacement Amplitude for $R = 1.6$, $T = 0.2A$ when $\gamma = 90°$

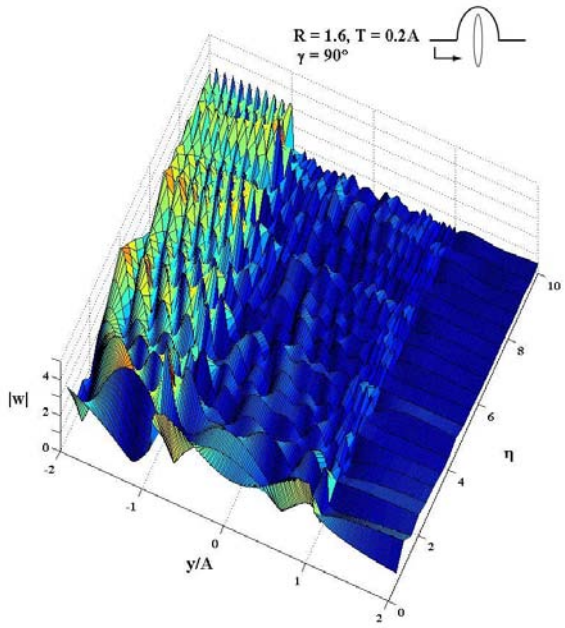

Figure 6.42: Displacement Amplitude for $R = 1.6$, $T = 0.5A$ when $\gamma = 0°$

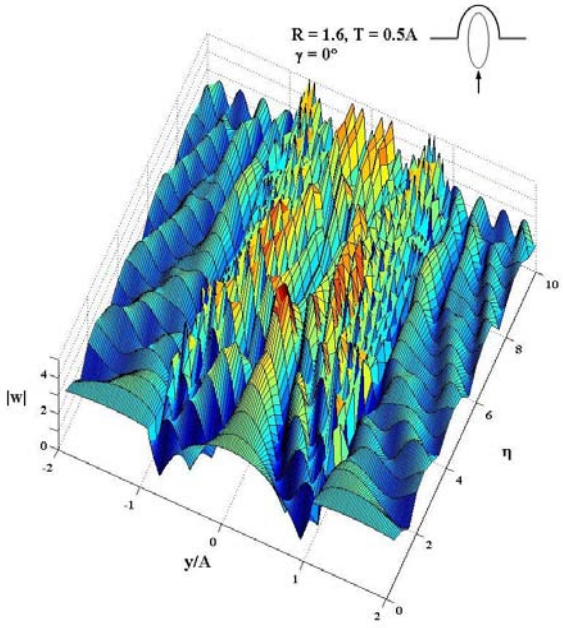


Figure 6.43: Displacement Amplitude for $R = 1.6$, $T = 0.5A$ when $\gamma = 30°$

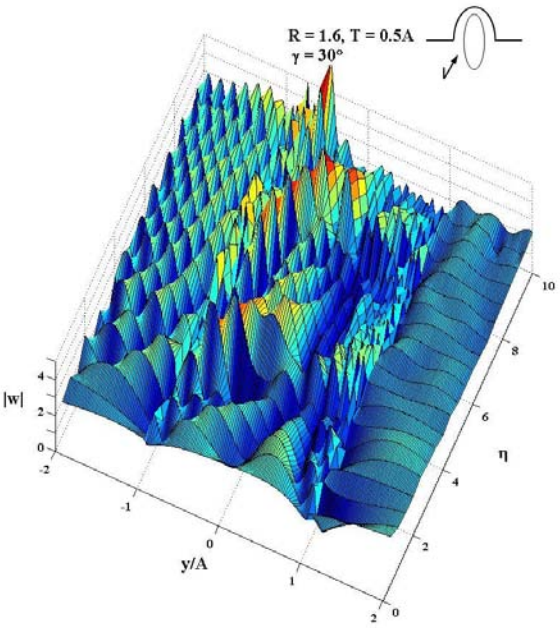

Figure 6.44: Displacement Amplitude for $R = 1.6$, $T = 0.5A$ when $\gamma = 60°$

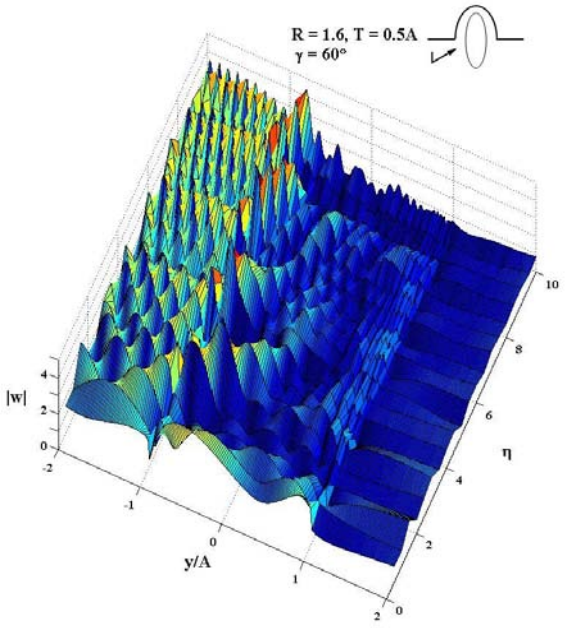


Figure 6.45: Displacement Amplitude for $R = 1.6$, $T = 0.5A$ when $\gamma = 90°$

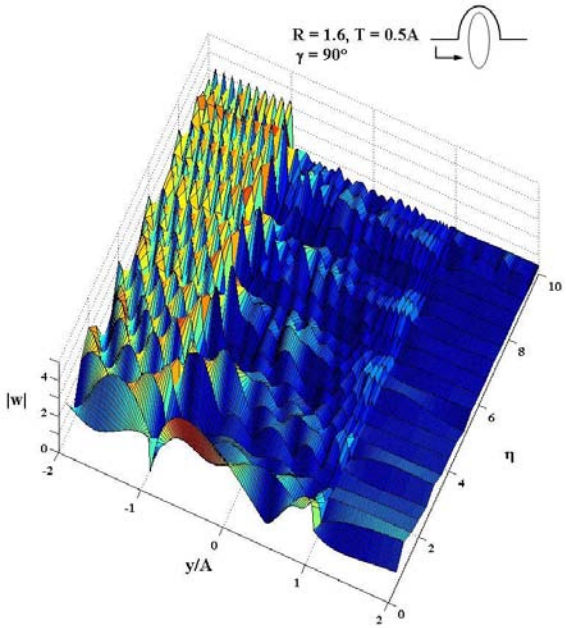

Figure 6.46: Displacement Amplitude for $R = 1.6$, $T = 0.8A$ when $\gamma = 0°$

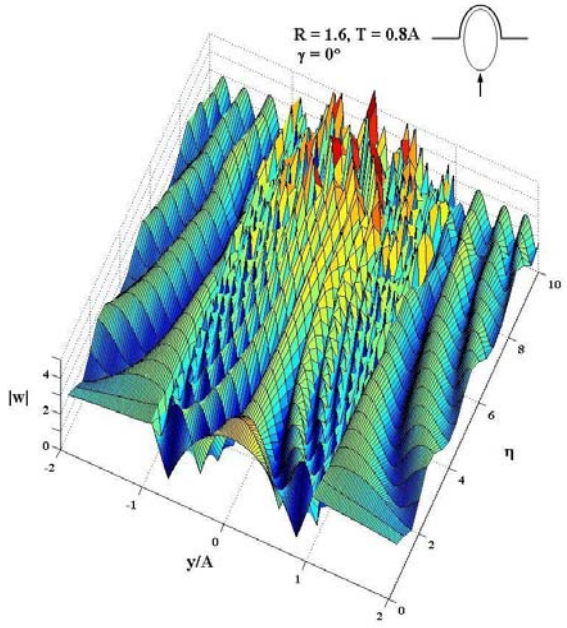


Figure 6.47: Displacement Amplitude for $R = 1.6$, $T = 0.8A$ when $\gamma = 30°$

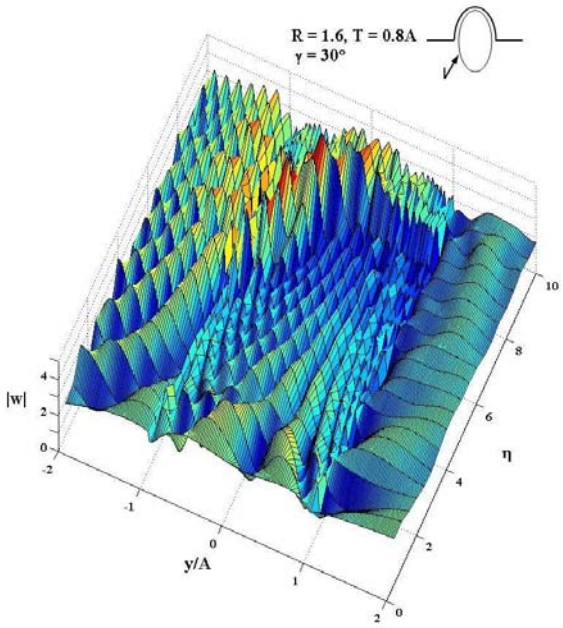

Figure 6.48: Displacement Amplitude for $R = 1.6$, $T = 0.8A$ when $\gamma = 60°$

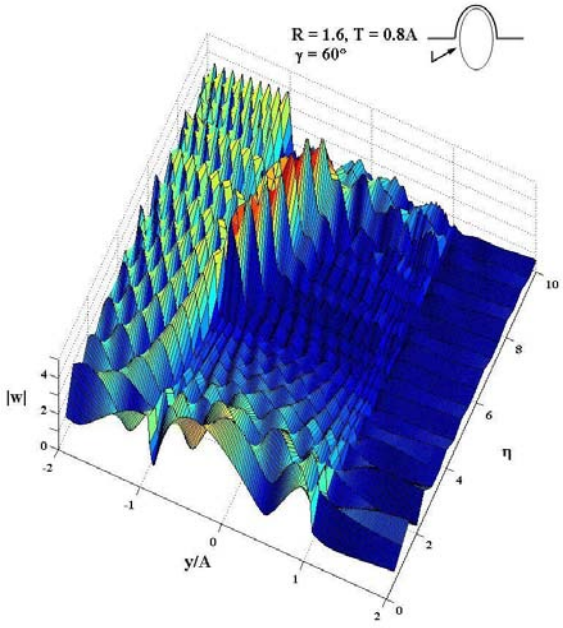


Figure 6.49: Displacement Amplitude for $R = 1.6$, $T = 0.8A$ when $\gamma = 90°$

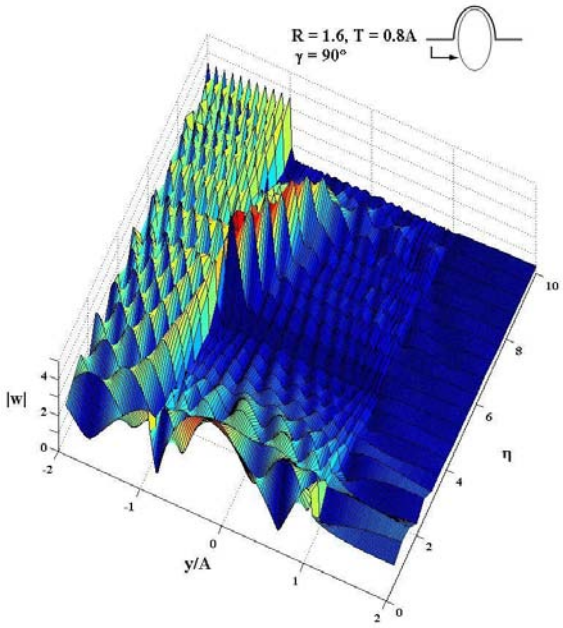

Considering all three-dimensional plots, wave pattern of surface displacement becomes visibly more intricate when the incident waves become shorter. In addition for the tunnel $T = 0.8A$ with nearly grazing angles, we observed quite interesting behavior. The surface displacement of points on a hill, which seems to be smaller while the dimensionless frequency $\eta$ gets larger, suddenly jumps at $\eta$ equal to 5 and again diminishes gradually as $\eta$ becomes bigger.

# CHAPTER 7: SCATTERING OF PLANE (SH) WAVES BY A SHALLOW SEMI-ELLIPTICAL HILL WITH A SEMI-ELLIPTICAL TUNNEL

In this chapter, an analytic solution to the boundary-valued problem of the two-dimensional scattering of anti-plane (SH) waves by a shallow semi-elliptical hill with a semi-elliptical tunnel is presented. Scattering effects due to the existence of semi-elliptical tunnel in the hill are studied and compared with the results of Chapter 5, the scattering effects due to the shallow semi-elliptical hill with an elliptical tunnel.

## 7.1 The Shallow Semi-Elliptical Hill with a Semi-Elliptical Tunnel Model

The cross-section of two-dimensional model is shown in Figure 7.1. Similar configuration, material properties, and coordinate systems to what we have in Chapters 3 and 5 are employed here, but with the presence of a semi-elliptical tunnel; A, B and $a$ are expressed as in Chapter 3, while T is again the half-width of the tunnel. Due to the configuration of a semi-elliptical tunnel, the model consists of the three regions. Similar to sections 3.1 and 5.1, the exterior region *D* consists of and extends over the same domain and boundaries, where the ring region $\Omega$ has the outer boundaries $L$ and $\overline{L}$ and the inner boundaries $M$ and $\overline{M}$. The last region $\Pi$ is semi-elliptical and bounded by boundaries $\overline{M}$ and $\overline{\Gamma}$.

Figure 7.1: Shallow Semi-Elliptical Hill with a Semi-Elliptical Tunnel Model

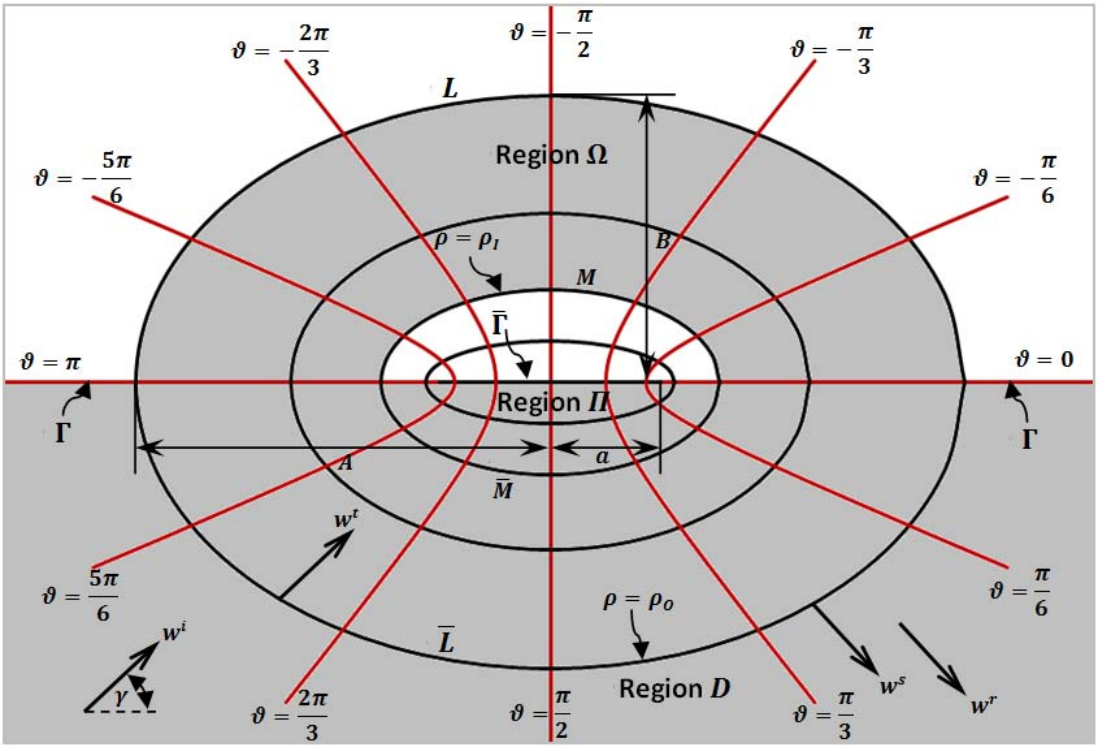


## 7.2 Series Expansion of Wave Functions

**Incident and Reflected Waves:**

The excitation $w^i$ consists of infinite trains of plane SH waves and travelling in the direction $\gamma$ to positive x axis. In the free field without the existence of the hill and tunnel, the incident waves strike the flat surface $\Gamma$ and create the reflected plane waves $w^r$; their interference yields the free field waves which can be expressed in elliptical coordinate as Equation (3.3).

**Scattered and Transmitted Waves:**

The scattered waves $w^s$ in the exterior region *D* and the transmitted waves $w_\Omega^t$ the ring region $\Omega$ are given by Equations (3.4) and (5.1) respectively. In addition the new transmitted waves in the semi-elliptical region $\Pi$ may take the same form as Wong and Trifunac (1974**a**) used in their valley model.

$$w_\Pi^t = \sum_{n=0}^{\infty} F_n Mc_n^{(1)}(\rho, q) ce_n(\vartheta, q) \qquad (7.1)$$

where $F_n$, in addition to $A_n$, $B_n$, $C_n$, $D_n$, and $E_n$, in Equations (3.4) and (5.1), is unknown coefficient to be calculated. The transmitted waves in the semi-elliptical region $\Pi$ have $Mc_n^{(1)}(\cdot)$ as radial wave functions since their asymptotic behaviors are Bessel functions of the first kind, representing standing waves in the semi-elliptical region $\Omega$ (Pao and Mow, 1973). Furthermore only $ce_n(\cdot)$ forms a complete orthogonal set of angular domain, $0 \leq \vartheta \leq \pi$. It is noteworthy that the transmitted waves $w_\Pi^t$, Equation (7.1), in the semi-elliptical region $\Pi$ automatically satisfies the traction free on the flat surface $\overline{\Gamma}$.

**Solution of the Problem using Angular Half-range Expansion**

The wave functions $w = w^{ff} + w^s$ in the exterior region *D*, $w_\Omega^t$ in the elliptical region $\Omega$ and $w_\Pi^t$ in the semi-elliptical region $\Pi$ must satisfy the Helmholtz equation, Equation (2.8), and the additional boundary conditions, beside those in Chapter 3; the traction-free boundary condition at the surface of the elliptical

tunnel $(\rho = \rho_I, \pi \le \vartheta \le 0)$ and the continuity of displacement and radial stress at the interface $\overline{M}$.

$$\tau_{\rho z}\big|_{\rho=\rho_I} = \frac{\mu}{aJ}\frac{\partial w^t}{\partial \rho}\Big|_{\rho=\rho_I} = 0; \pi \le \vartheta \le 0 \tag{7.2}$$

$$\begin{aligned} w_\Omega^t|_{\rho=\rho_\mathrm{I}} &= w_\Pi^t|_{\rho=\rho_\mathrm{I}} \\ \tau_{\rho z}\big|_{\rho=\rho_\mathrm{I}} &= \frac{\mu}{aJ}\frac{\partial w_\Omega^t}{\partial \rho}\Big|_{\rho=\rho_\mathrm{I}} = \frac{\mu}{aJ}\frac{\partial w_\Pi^t}{\partial \rho}\Big|_{\rho=\rho_\mathrm{I}} \quad ; 0 \le \vartheta \le \pi \end{aligned} \tag{7.3}$$

Here same difficulty comes up since, along the circumferences $\rho = \rho_\mathrm{O}$ and $\rho = \rho_\mathrm{I}$, the transmitted waves $w_\Omega^t$ expressing the displacement motion in the full elliptical region once more must satisfy two disjoint sets of boundary conditions; for example Equations (7.2) and (7.3).

Hence we must utilize the orthogonality of angular Mathieu functions in the half-range. Without any intricacy, the transmitted waves $w_\Omega^t$ and their radial stresses may be expressed as follows

$$\begin{aligned} w_\Omega^t = {} & \sum_{n=0}^{\infty}\Big[B_n Mc_n^{(3)}(\rho,q) \mp \sum_{m=1}^{\infty}\mathfrak{C}_{mn}C_m Ms_m^{(3)}(\rho,q)\Big]ce_n(\vartheta,q) \\ & + \sum_{n=0}^{\infty}\Big[D_n Mc_n^{(4)}(\rho,q) \mp \sum_{m=1}^{\infty}\mathfrak{C}_{mn}E_m Ms_m^{(4)}(\rho,q)\Big]ce_n(\vartheta,q) \end{aligned} \tag{7.4}$$

$$\begin{aligned} \tau_{\rho z}^{\Omega} = {} & \sum_{n=0}^{\infty}\Big[B_n Mc_n^{(3)\prime}(\rho,q) \mp \sum_{m=1}^{\infty}\mathfrak{C}_{mn}C_m Ms_m^{(3)\prime}(\rho,q)\Big]ce_n(\vartheta,q) \\ & + \sum_{n=0}^{\infty}\Big[D_n Mc_n^{(4)\prime}(\rho,q) \mp \sum_{m=1}^{\infty}\mathfrak{C}_{mn}E_m Ms_m^{(4)\prime}(\rho,q)\Big]ce_n(\vartheta,q) \end{aligned} \tag{7.5}$$

Again, –ve above and +ve below are assigned for $-\pi \le \vartheta \le 0$ and $0 \le \vartheta \le \pi$ respectively, and $\mathfrak{C}_{mn}$ is given by Equation (2.29). Then all displacement and stress functions are convenient to be applied since they are in the form of elliptical cosine series.

Applying all boundary conditions along both circumferences of the elliptical ring region $\Omega$, we establish six sets of infinite equations for the six sets of unknowns; $A_n$ through $F_n$.

$$\left\{\begin{matrix} B_n Mc_n^{(3)\prime}(\rho_O,q) - \sum_{m=1}^{\infty} \mathbb{C}_{mn} C_m Ms_m^{(3)\prime}(\rho_O,q) \\ +D_n Mc_n^{(4)\prime}(\rho_O,q) - \sum_{m=1}^{\infty} \mathbb{C}_{mn} E_m Ms_m^{(4)\prime}(\rho_O,q) \end{matrix}\right\} = 0 \tag{7.6}$$

$$\left\{\begin{matrix} B_n Mc_n^{(3)}(\rho_O,q) + \sum_{m=1}^{\infty} \mathbb{C}_{mn} C_m Ms_m^{(3)}(\rho_O,q) \\ +D_n Mc_n^{(4)}(\rho_O,q) + \sum_{m=1}^{\infty} \mathbb{C}_{mn} E_m Ms_m^{(4)}(\rho_O,q) \end{matrix}\right\} = \left\{\begin{matrix} 4w_0 i^n Mc_n^{(1)}(\rho_O,q) ce_n(\gamma,q) \\ +A_n Mc_n^{(3)}(\rho_O,q) \end{matrix}\right\} \tag{7.7}$$

$$\left\{\begin{matrix} B_n Mc_n^{(3)\prime}(\rho_O,q) + \sum_{m=1}^{\infty} \mathbb{C}_{mn} C_m Ms_m^{(3)\prime}(\rho_O,q) \\ +D_n Mc_n^{(4)\prime}(\rho_O,q) + \sum_{m=1}^{\infty} \mathbb{C}_{mn} E_m Ms_m^{(4)\prime}(\rho_O,q) \end{matrix}\right\} = \left\{\begin{matrix} 4w_0 i^n Mc_n^{(1)\prime}(\rho_O,q) ce_n(\gamma,q) \\ +A_n Mc_n^{(3)\prime}(\rho_O,q) \end{matrix}\right\} \tag{7.8}$$

$$\left\{\begin{matrix} B_n Mc_n^{(3)\prime}(\rho_I,q) - \sum_{m=1}^{\infty} \mathbb{C}_{mn} C_m Ms_m^{(3)\prime}(\rho_I,q) \\ +D_n Mc_n^{(4)\prime}(\rho_I,q) - \sum_{m=1}^{\infty} \mathbb{C}_{mn} E_m Ms_m^{(4)\prime}(\rho_I,q) \end{matrix}\right\} = 0 \tag{7.9}$$

$$\left\{\begin{matrix} B_n Mc_n^{(3)}(\rho_I,q) + \sum_{m=1}^{\infty} \mathbb{C}_{mn} C_m Ms_m^{(3)}(\rho_I,q) \\ +D_n Mc_n^{(4)}(\rho_I,q) + \sum_{m=1}^{\infty} \mathbb{C}_{mn} E_m Ms_m^{(4)}(\rho_I,q) \end{matrix}\right\} = F_n Mc_n^{(1)}(\rho_I,q) \tag{7.10}$$

$$\left\{\begin{matrix} B_n Mc_n^{(3)\prime}(\rho_I,q) + \sum_{m=1}^{\infty} \mathbb{C}_{mn} C_m Ms_m^{(3)\prime}(\rho_I,q) \\ +D_n Mc_n^{(4)\prime}(\rho_I,q) + \sum_{m=1}^{\infty} \mathbb{C}_{mn} E_m Ms_m^{(4)\prime}(\rho_I,q) \end{matrix}\right\} = F_n Mc_n^{(1)\prime}(\rho_I,q) \tag{7.11}$$

The system of Equations (7.6) through (7.11) can be solved numerically by matrix truncation. Due to the ill-condition of the matrix, the above system is solved by using subroutine LAPACK and the SVD, Singular Matrix Decomposition, provided by MATLAB. However the number of terms must be large enough to satisfy the required accuracy; in this case we test the accuracy of the sum by comparing the series n-term with (n+1)-terms and check if the maximum displacements at the same point are within 1%-difference.

## 7.3 Results and Analysis

Amplitudes of ground motions are analyzed. Similar to previous chapters we assume the excitation with amplitude 1, and present the results in term of the dimensionless parameters $\eta$, *R* and $\eta_T$ which are defined by Equations (3.16), (3.18) and (5.9). Furthermore to investigate the scattering effect due to the presence of a semi-elliptical tunnel, again for each aspect ratio *R* its minimum value of $T$ is equal to the focal length $a$ which is governed by Equation (3.17). Since we limit $T$ to $0.8A$, 0.6 is the minimum aspect ratio $R$ in this chapter; the minimum ratio $T/A$ of the aspect ratio $R = 0.6$, 0.8 and 0.999 in Table 3.1 are applicable.

**Comparison with the Solutions of "Circular" Semi-Elliptical Hill:**

When a tunnel is really small in comparison to the hill, ground surface displacements obtained from the above equations must be in agreement with those of semi-elliptical hill without tunnel. Comparison-wise this is only applicable to *R* = 0.9999 since we could make the tunnel so small without becoming a slit-like. The following Figure (7.2) shows the similarity for both semi-elliptical hills with and without a semi-elliptical tunnel when semi-elliptical tends to semi-circular $(R = 0.9999)$ at $\eta = 1$; $\eta_T = 0.1$ is assigned for the case of tunnel. In general their trends are in harmony with 2% difference at large for the maximum values, except at incident angle 60°.

Figure 7.2: Displacement Amplitudes of Ground Motion at $\eta = 1$

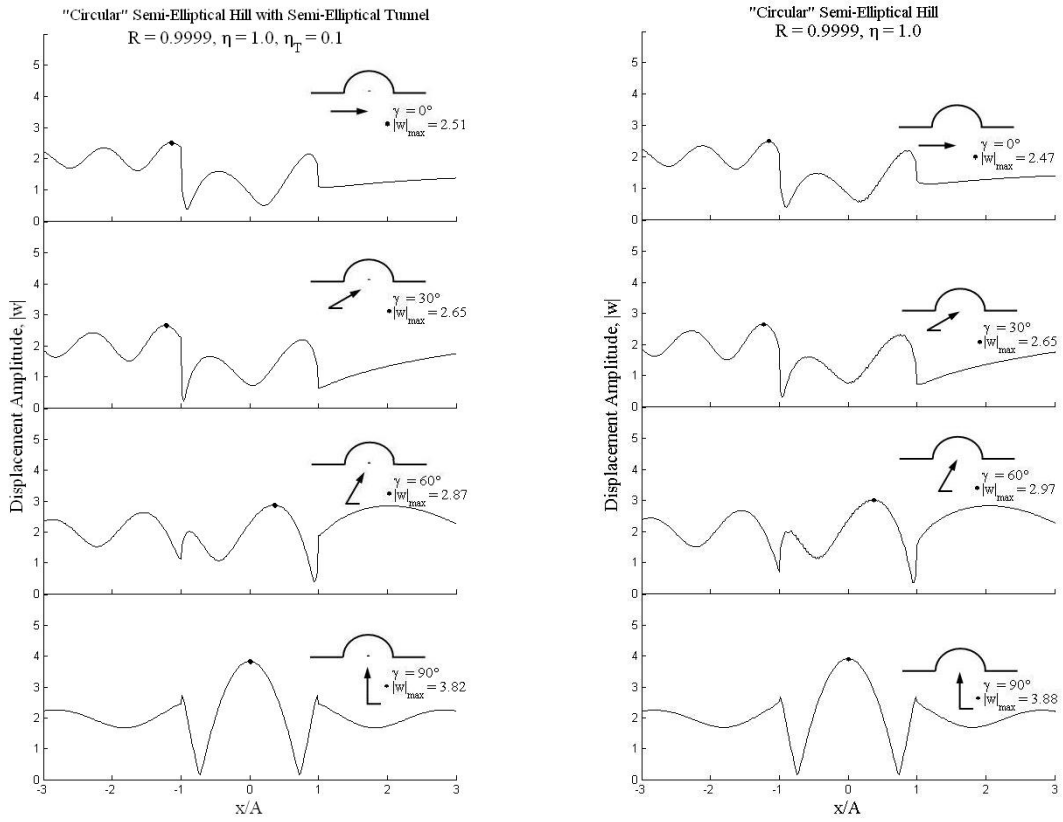


(a) "Circular " Semi-Elliptical Hill with a semi-elliptical tunnel $\eta_T = 0.1$

(b) Semi-Circular Hill

**Effects of Tunnel, and Incident Angle to Semi-Elliptical Hill:**

To study the effect of the existence of an elliptical tunnel, we consider only three aspect ratios $R$; 0.6, 0.8 and 0.9999. Furthermore we consider the effect of incident angle by assuming four different incident angles of $\gamma = 0°$, 30°, 60° and 90° for each case of study.

Figure 7.3: Displacement Amplitude for $R = 0.6$ and $T = 0.8A$ at $\eta = 5$

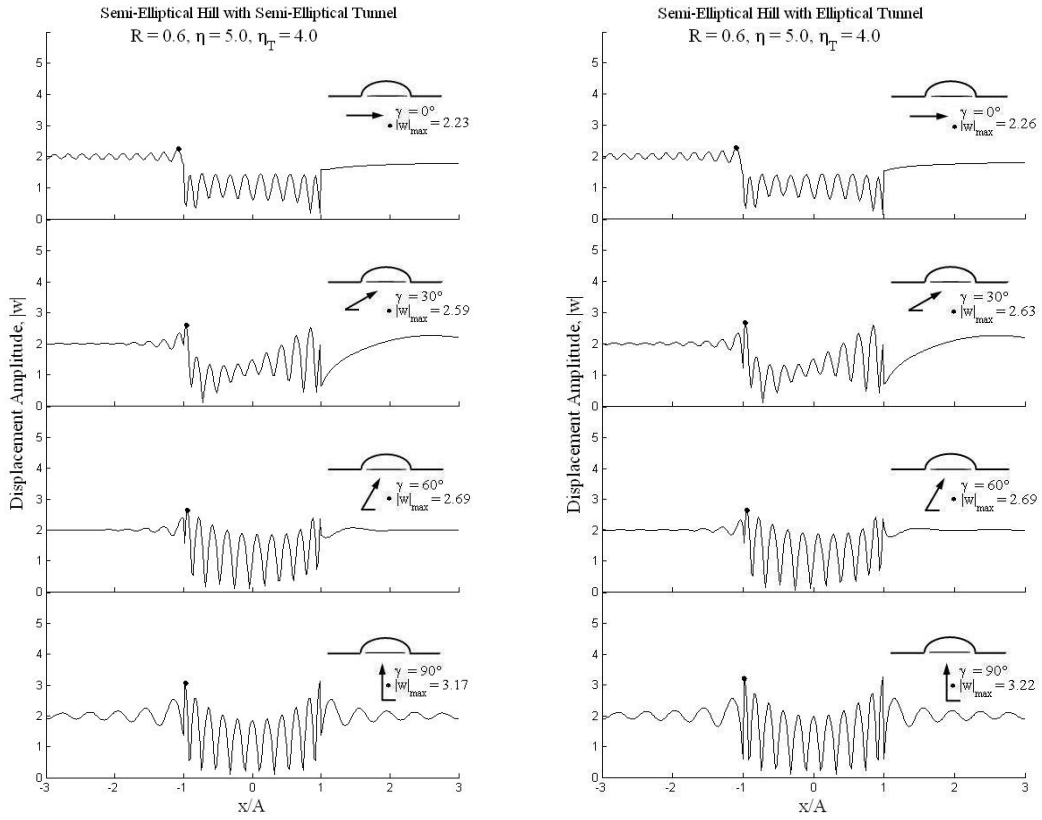


(a) Semi-Elliptical Tunnel (b) Elliptical Tunnel

Figures 7.3 and 7.4 show amplitudes of surface displacements at four prescribed incidences with the dimensionless frequency $\eta = 5$ and 10 for the semi-elliptical hill $R = 0.6$ with semi-elliptical and elliptical tunnels $T = 0.8A$. We found out that our solutions derived in this Chapter are reliable. Even though at particular angle the maximum value may be about 4% difference, but their overall patterns are almost indistinguishable since both tunnels are slit-like.

Figure 7.4: Displacement Amplitude for $R = 0.6$ and $T = 0.8A$ at $\eta = 10$

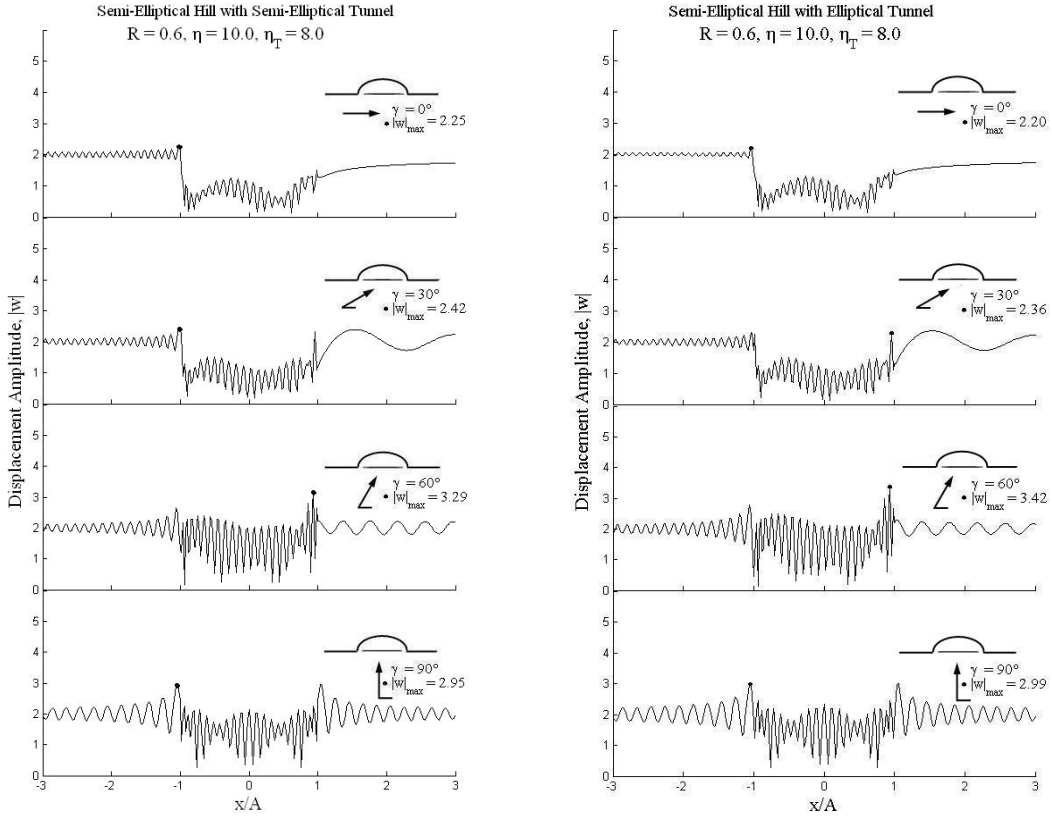


(a) Semi-Elliptical Tunnel (b) Elliptical Tunnel

The presence of the semi-elliptical tunnel influences the wave patterns and especially the maximum value of ground surface motion and its location. Considering Figure 7.5 and 7.6 together with Figures 5.5 through 5.7, we found that for nearly grazing angle, the maximum values of ground surface motion in the case of semi-elliptical tunnel are comparable or higher than of elliptical one; In contrast to the elliptical tunnel the locations of the maximum value are always located on the hill, not on the front of the hill. The similar shielding effect to the

full-elliptical tunnel has been detected here too for semi-elliptical tunnel, but less effective. Moreover we also observed abrupt jumps of the displacement amplitudes at the right edge of the hill $(x/A = 1)$, which we have rarely seen while investigating the effect of elliptical tunnel. Besides the existence of semi-elliptical tunnel create more shielding effect which results in the smaller value of the maximum displacements while the incidence waves approach the hill in vertical directions.

Figure 7.5: Displacement Amplitude for $R = 0.8$ with Tunnel; $T = 0.8A$

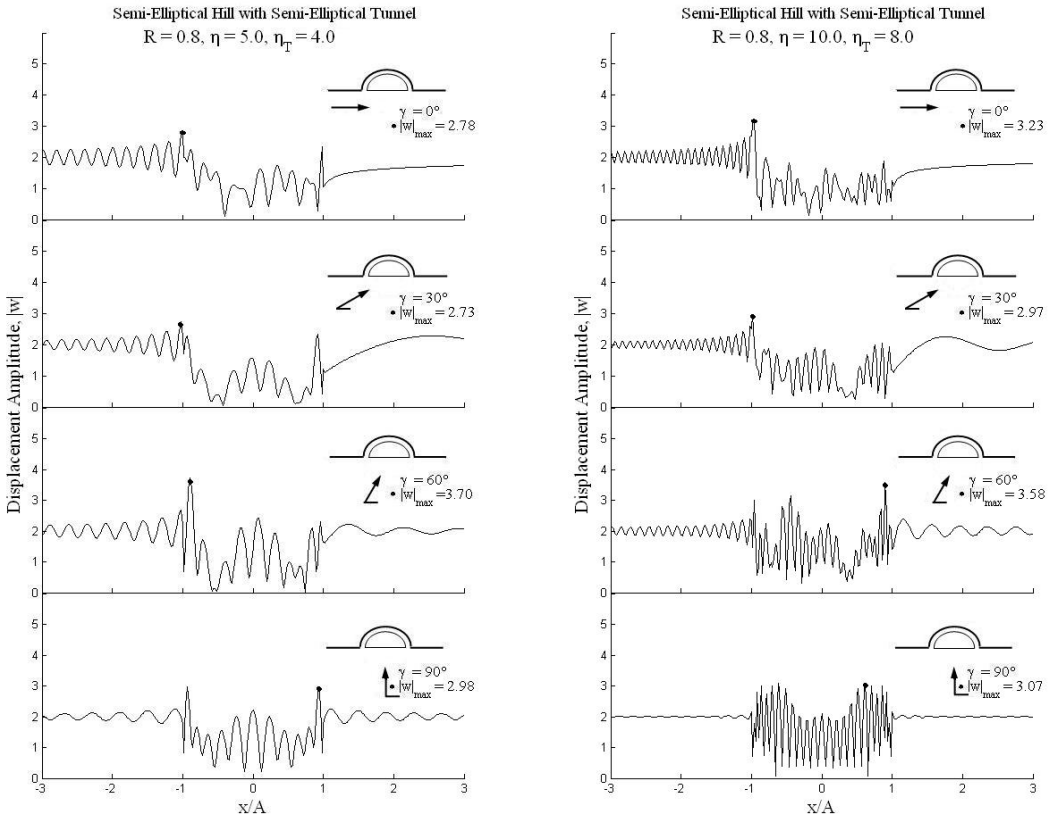


(a) $\eta = 5$ (b) $\eta = 10$

Figure 7.6: Displacement Amplitude for $R = 0.9999$ with Tunnel $T = 0.8A$

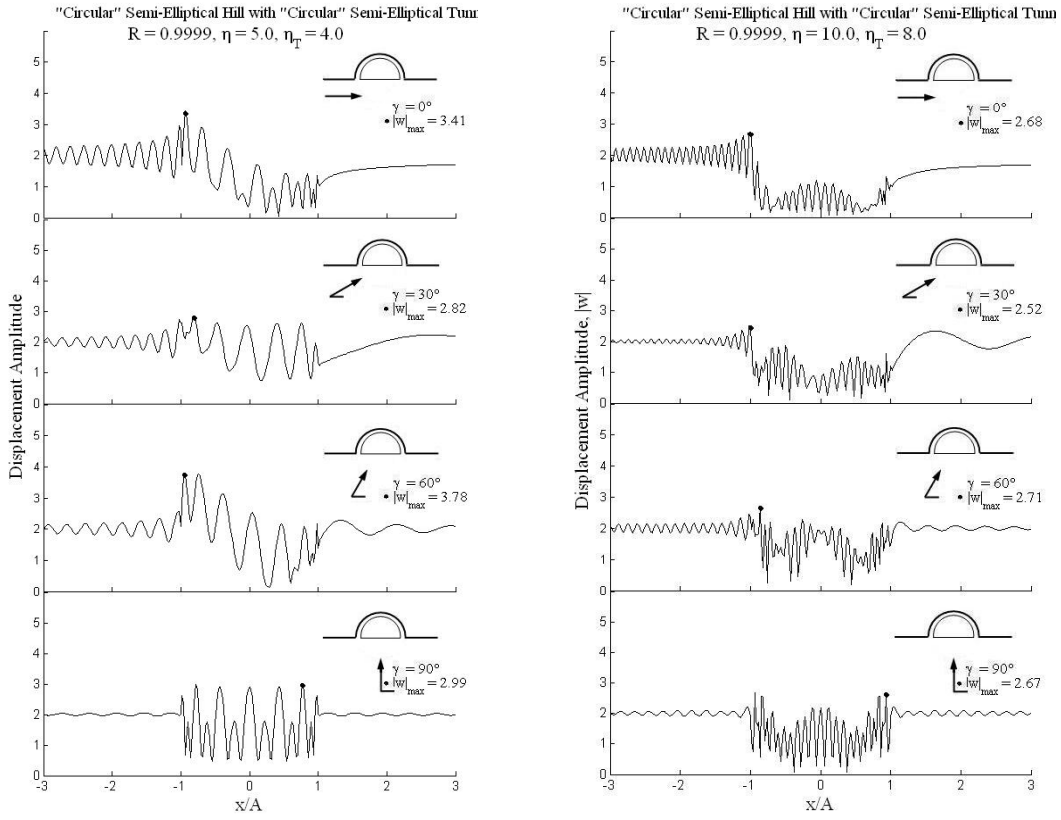


(a) $\eta = 5$ (b) $\eta = 10$

To study the influence of tunnel-size, again we consider only “circular” semi-elliptical hill with a “circular” semi-elliptical tunnel. After evaluating Figures 7.7 and 7.8 of “semi-circular” tunnels $T = 0.2A$ and $0.5A$ against the above figure, it may be said that for nearly horizontal angle standing waves on the left-side seems bigger as the tunnel is getting larger. Nevertheless the shielding effect seems irrelevant to the size of the tunnel; the displacements on the right-handed of the hill are approximately greater than unity.

Similar to the full-elliptical tunnel, for vertical angle of incidence the maximum value of surface displacement is noticeably less when the elliptical obstacle gets bigger. Furthermore it can confirm that the semi-elliptical tunnels are more effective in shielding the vertical incident waves than the elliptical ones. Besides that, the fluctuation of surface displacements on both sides of the hill, which have been noticed with the existence of elliptical tunnels, is insignificant in this case of semi-elliptical tunnel.

Figure 7.7: Displacement Amplitude for $R = 0.9999$ with Tunnel $T = 0.2A$

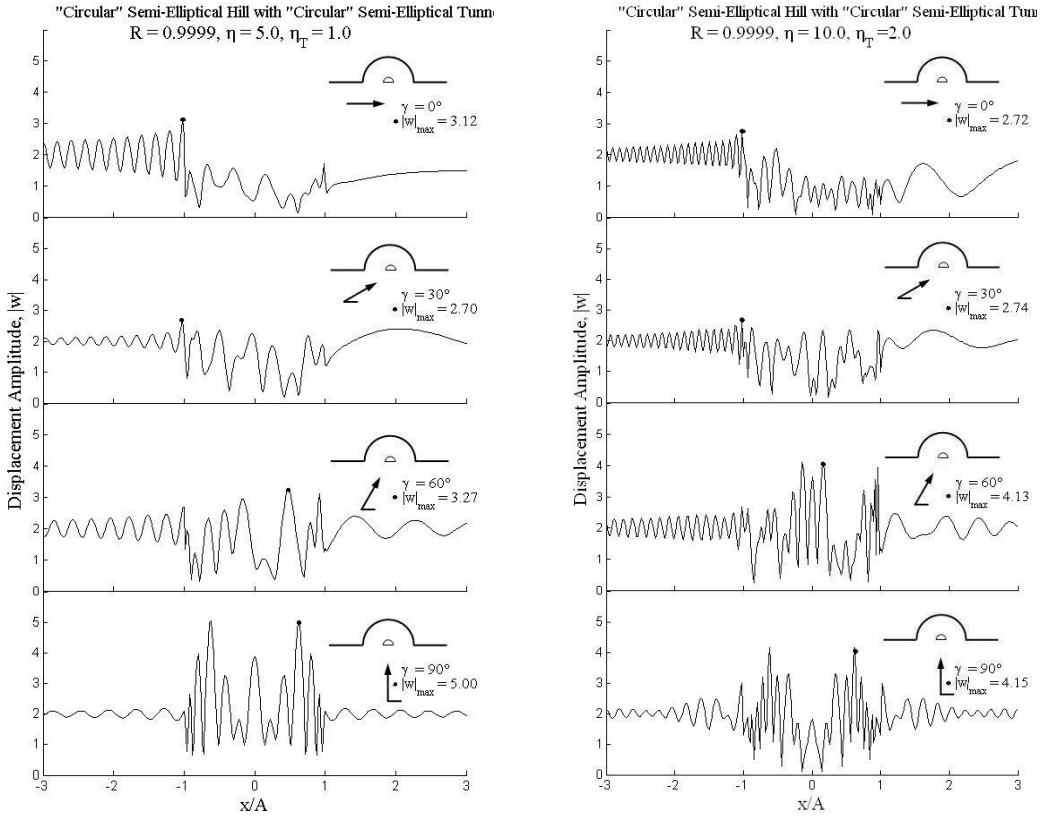


(a) $\eta = 5$ (b) $\eta = 10$

Figure 7.8: Displacement Amplitude for $R = 0.9999$ with Tunnel $T = 0.5A$

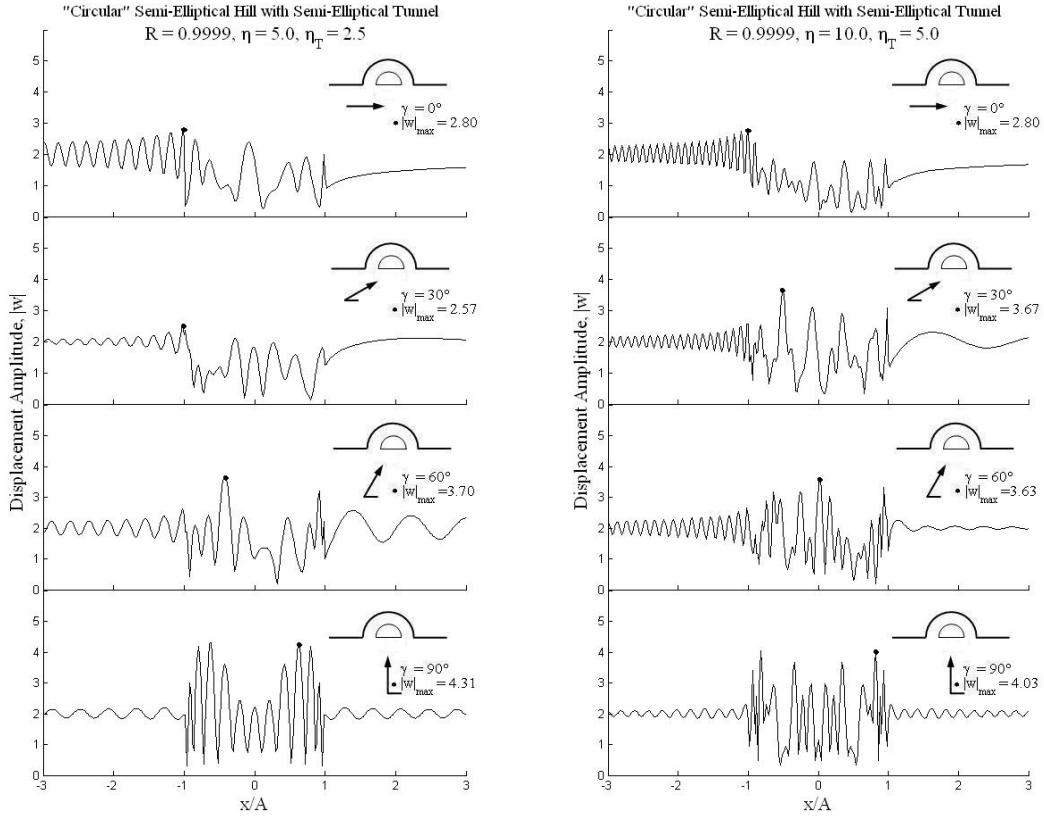


(a) $\eta = 5$ (b) $\eta = 10$

Figures 7.9 through 7.28 show three-dimensional plots of surface displacements for $R = 0.6$, 0.8, and 0.9999, equivalent to the height-to-width ratios of 0.3, 0.4, and 0.4999 respectively; the values of $T$ for particular $R$ are as at the beginning of this section. Each figure illustrates the plots at four incident angles, $\gamma = 0°$, 30°, 60° and 90°, versus the distance *x/A* on and around the hill and the dimensionless frequency $\eta$ in the range of 0.5 to 10; the amplitudes in the range of *x/A* in $[-1,1]$ are those on the elliptical surface of the hill.

Figure 7.9: Displacement Amplitude for $R = 0.6$, $T = 0.8A$ when $\gamma = 0°$

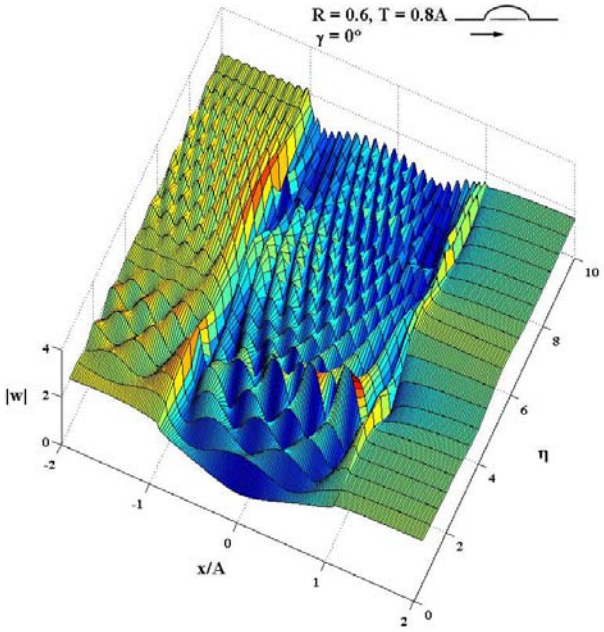


Figure 7.10: Displacement Amplitude for $R = 0.6$, $T = 0.8A$ when $\gamma = 30°$

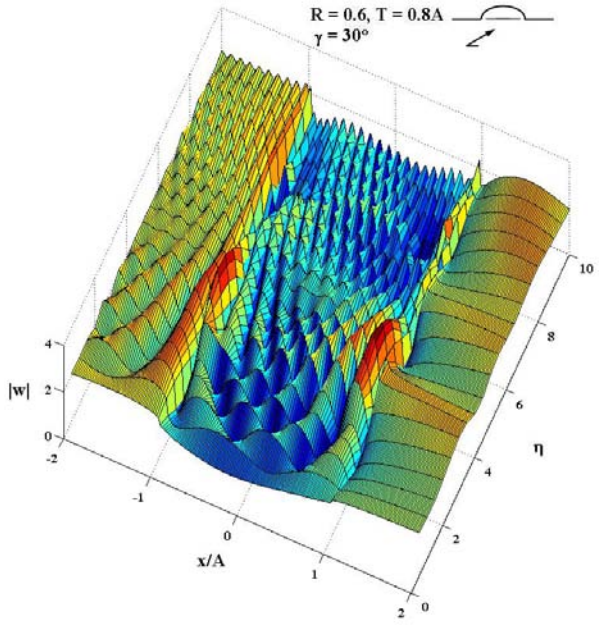

Figure 7.11: Displacement Amplitude for $R = 0.6$, $T = 0.8A$ when $\gamma = 60°$

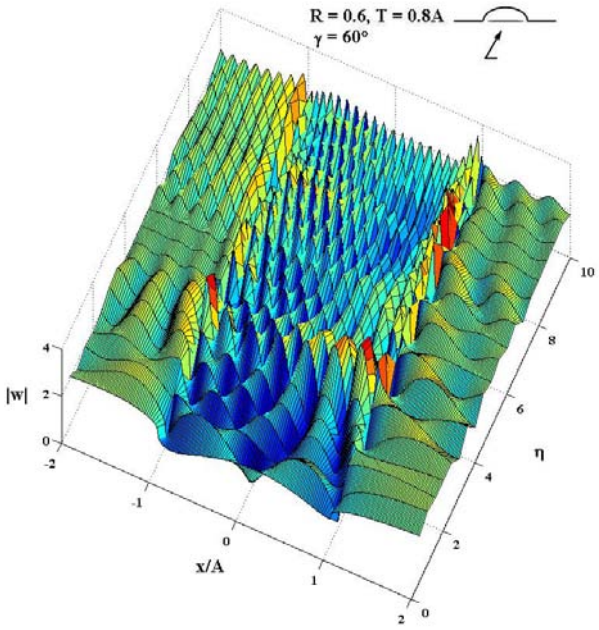


Figure 7.12: Displacement Amplitude for $R = 0.6$, $T = 0.8A$ when $\gamma = 90°$

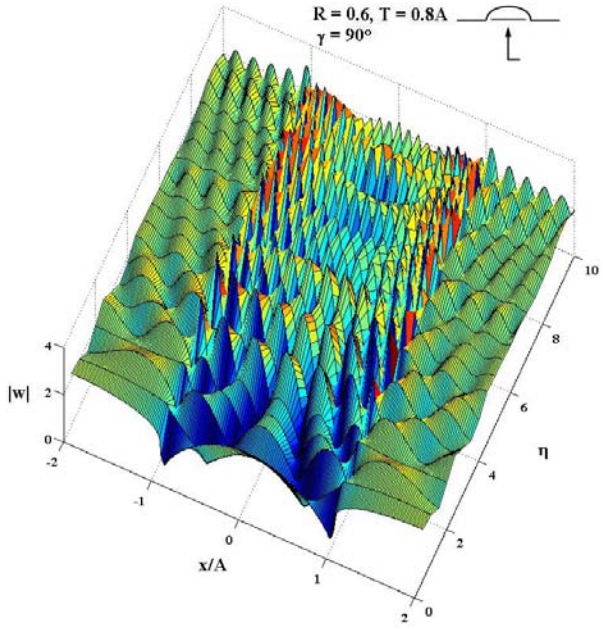

Figure 7.13: Displacement Amplitude for $R = 0.8$, $T = 0.8A$ when $\gamma = 0°$

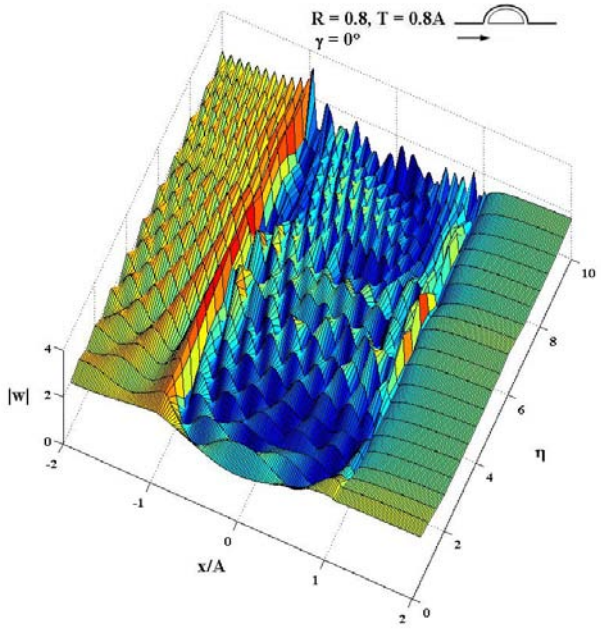


Figure 7.14: Displacement Amplitude for $R = 0.8$, $T = 0.8A$ when $\gamma = 30°$

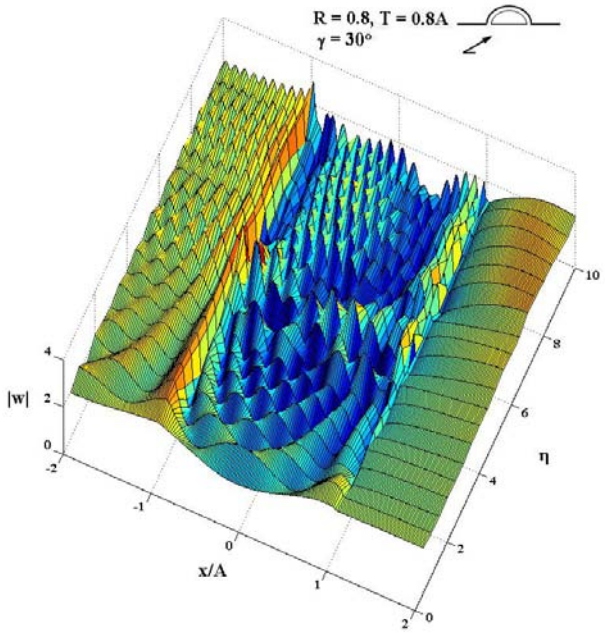

Figure 7.15: Displacement Amplitude for $R = 0.8$, $T = 0.8A$ when $\gamma = 60°$

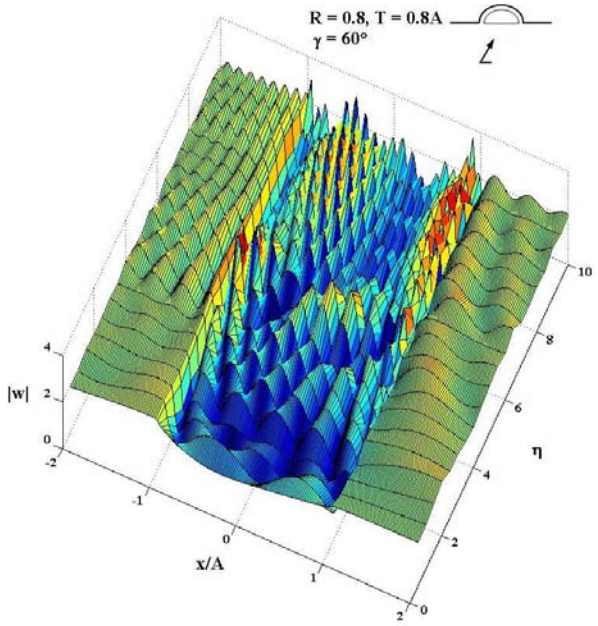


Figure 7.16: Displacement Amplitude for $R = 0.8$, $T = 0.8A$ when $\gamma = 90°$

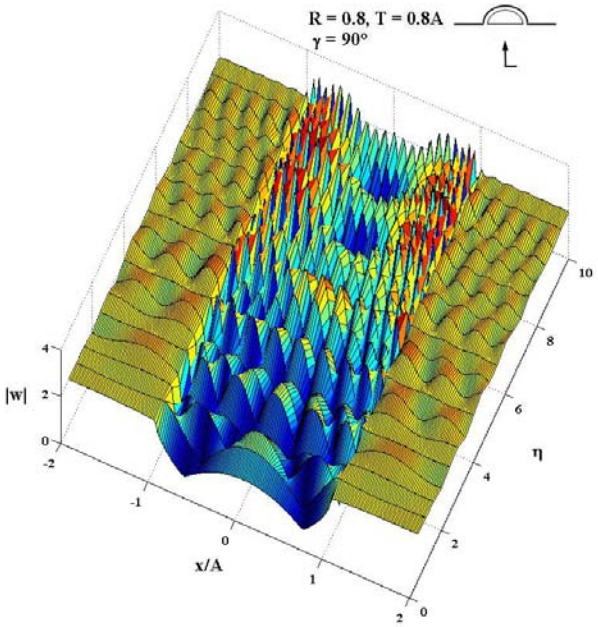

Figure 7.17: Displacement Amplitude for $R = 0.9999$, $T = 0.2A$ when $\gamma = 0°$

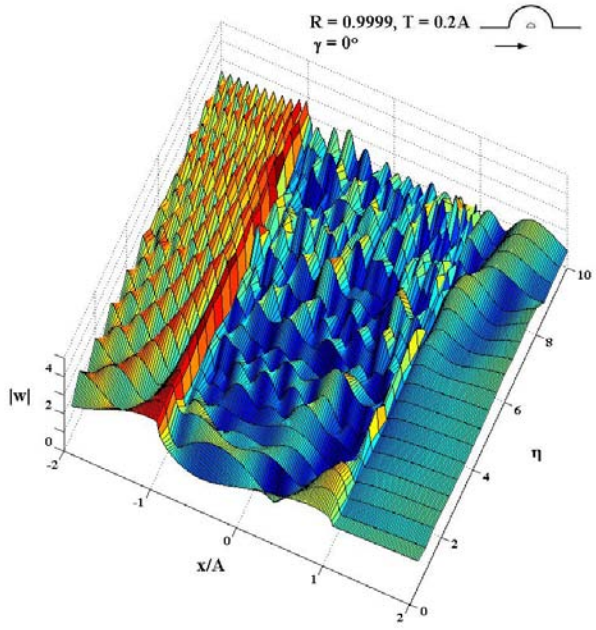


Figure 7.18: Displacement Amplitude for $R = 0.9999$, $T = 0.2A$ when $\gamma = 30°$

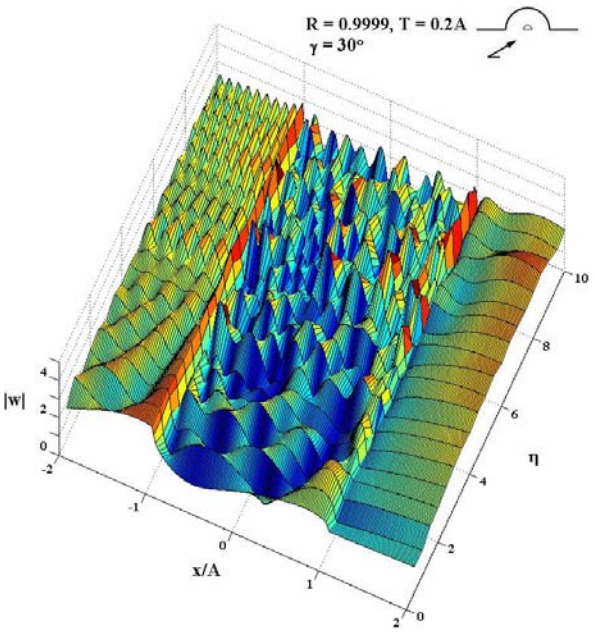

Figure 7.19: Displacement Amplitude for $R = 0.9999$, $T = 0.2A$ when $\gamma = 60°$

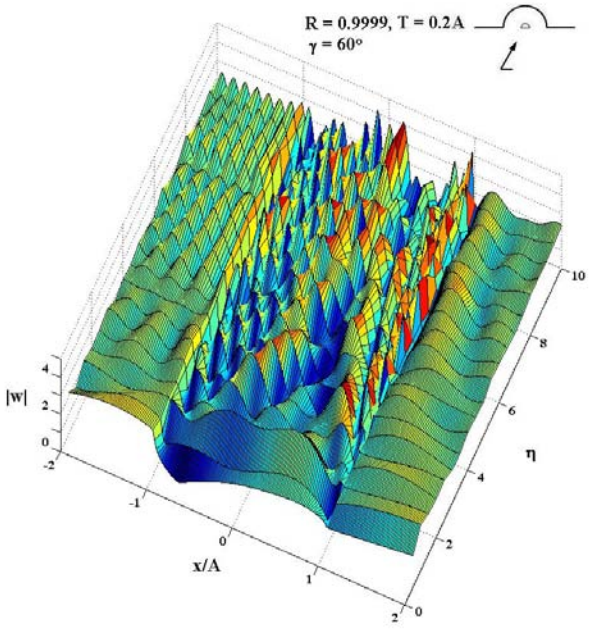


Figure 7.20: Displacement Amplitude for $R = 0.9999$, $T = 0.2A$ when $\gamma = 90°$

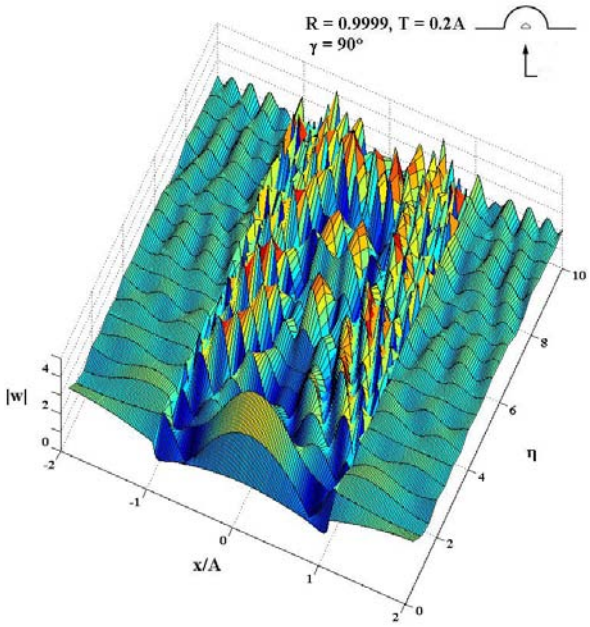

Figure 7.21: Displacement Amplitude for $R = 0.9999$, $T = 0.5A$ when $\gamma = 0°$

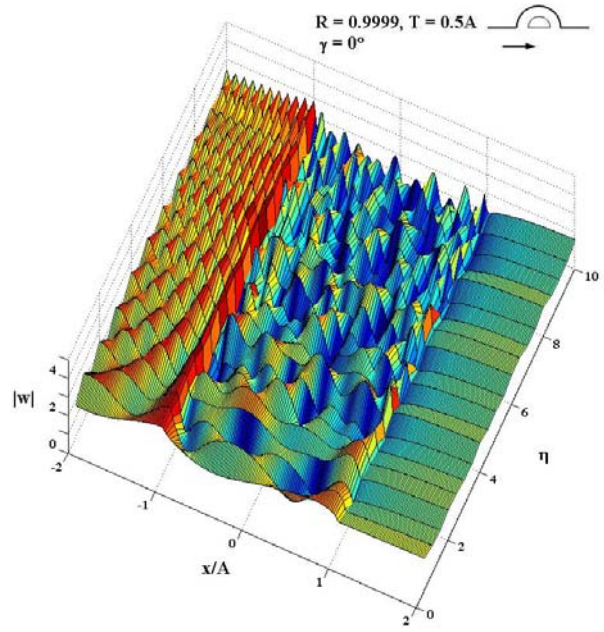


Figure 7.22: Displacement Amplitude for $R = 0.9999$, $T = 0.5A$ when $\gamma = 30°$

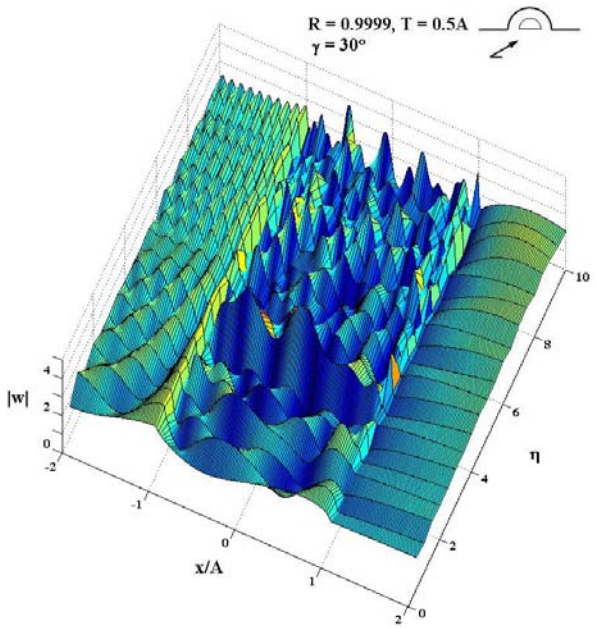

Figure 7.23: Displacement Amplitude for $R = 0.9999$, $T = 0.5A$ when $\gamma = 60°$

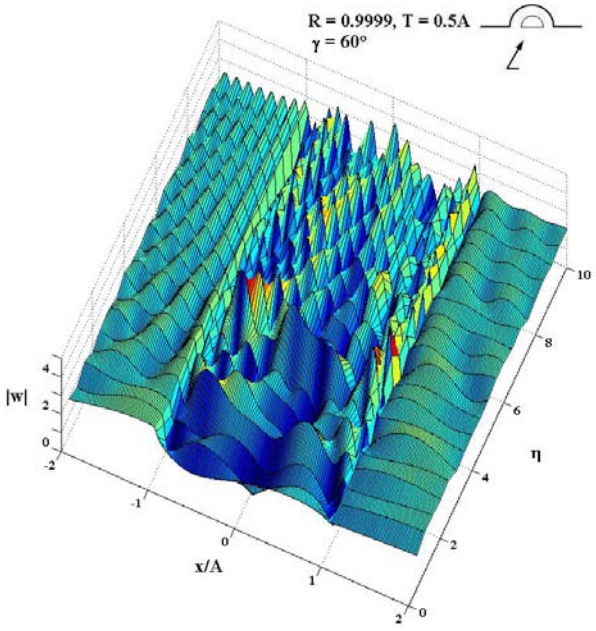


Figure 7.24: Displacement Amplitude for $R = 0.9999$, $T = 0.5A$ when $\gamma = 90°$

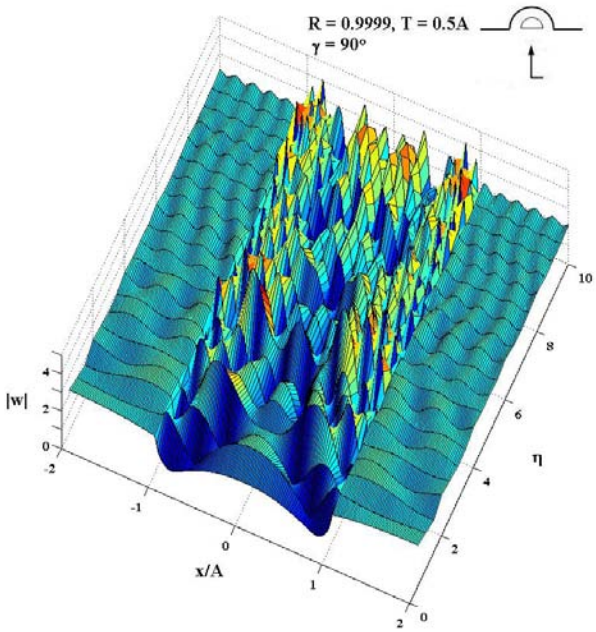

Figure 7.25: Displacement Amplitude for $R = 0.9999$, $T = 0.8A$ when $\gamma = 0°$

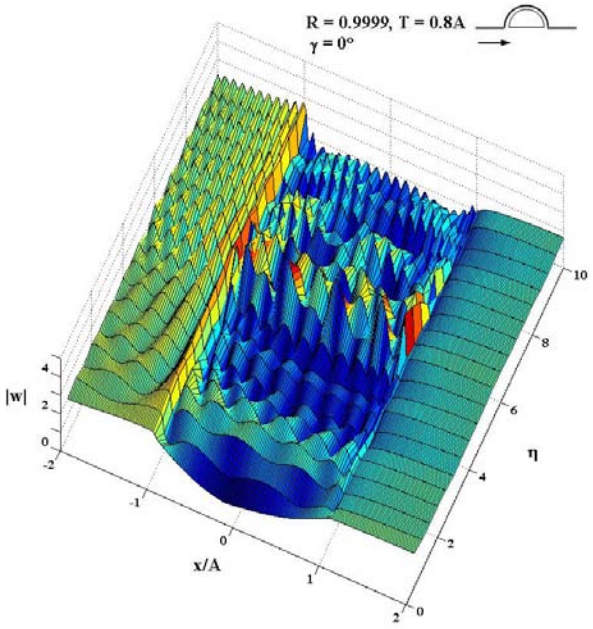


Figure 7.26: Displacement Amplitude for $R = 0.9999$, $T = 0.8A$ when $\gamma = 30°$

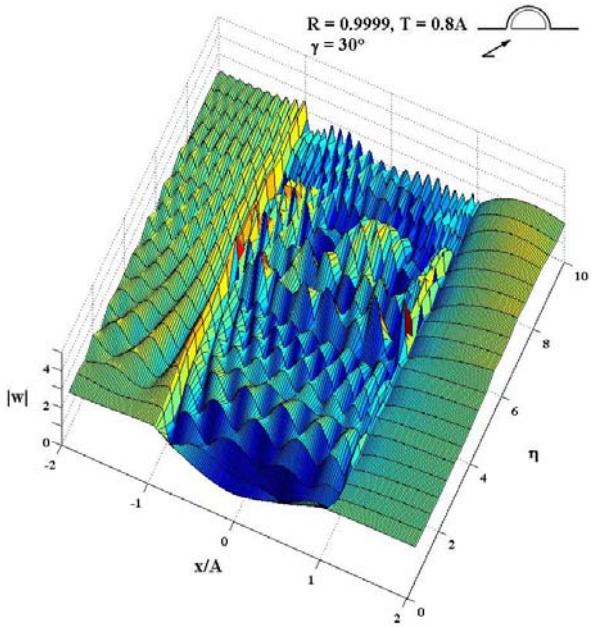

Figure 7.27: Displacement Amplitude for $R = 0.9999$, $T = 0.8A$ when $\gamma = 60°$

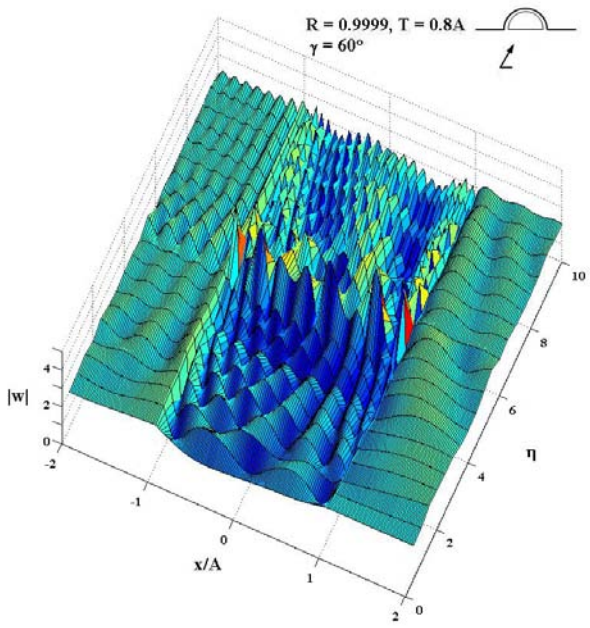


Figure 7.28: Displacement Amplitude for $R = 0.9999$, $T = 0.8A$ when $\gamma = 90°$

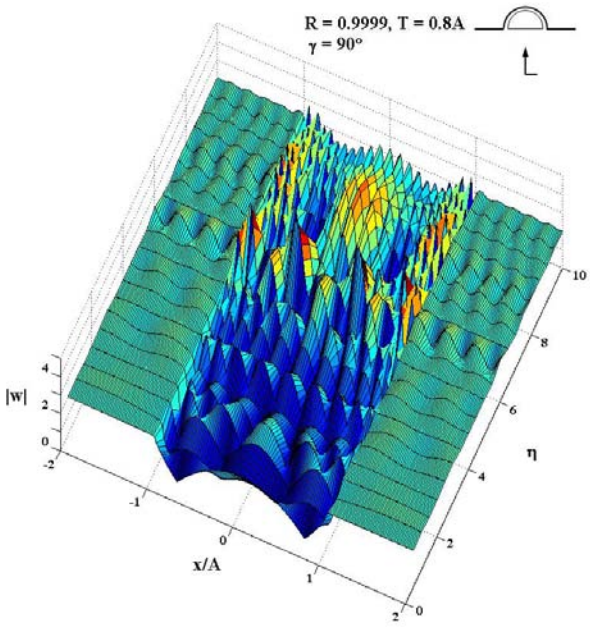

Obviously, Figures 7.9 through 7.12 back up what we have mentioned earlier about the validity of the equation we developed in this Chapter 7; they are almost identical to plots in Chapter 5. In addition Figures 7.9 through 7.28 again could validate what we have seen earlier about the shape, size effects of tunnels and their shielding efficiency. Once more pattern of all surface displacement turn out to be increasingly more complicated when the incident waves become shorter.

# CHAPTER 8: SCATTERING OF PLANE (SH) WAVES BY A DEEP SEMI-ELLIPTICAL HILL WITH A SEMI-ELLIPTICAL TUNNEL

The wave expansion method together with half-range expansion of elliptical cosine and elliptical sine is applied to study the response of the two-dimensional deep semi-elliptical hill with a semi-elliptical tunnel. The solution as a function of incidence angle and wave frequency is presented. In addition scattering effects due to the presence of semi-elliptical tunnel in the hill are examined and compared to the scattering effects due to the existence of a full-elliptical tunnel.

## 8.1 The Deep Semi-Elliptical Hill with a Semi-Elliptical Tunnel Model

The two-dimensional model of a deep semi-elliptical hill with a semi-elliptical tunnel is shown in Figure 8.1; similar configuration, material properties, and coordinate systems to Chapters 4 and 6 are utilized. Parameters A, B and $a$ are expressed as in Chapter 4, while T is again the half-width of the tunnel. Due to the existence of semi-concentric tunnel, the model consists of the three regions. Similar to sections 4.1 and 6.1, the exterior region *D* extends over the same domain and have the same boundaries, where the ring region $\Omega$ has the outer boundaries $L$ and $\overline{L}$ and the inner boundaries $M$ and $\overline{M}$. The last region $\Pi$ is semi-elliptical and bounded by boundaries $\overline{M}$ and $\overline{\Gamma}$.

Figure 8.1: Deep Semi-Elliptical Hill with a Semi-Elliptical Tunnel Model

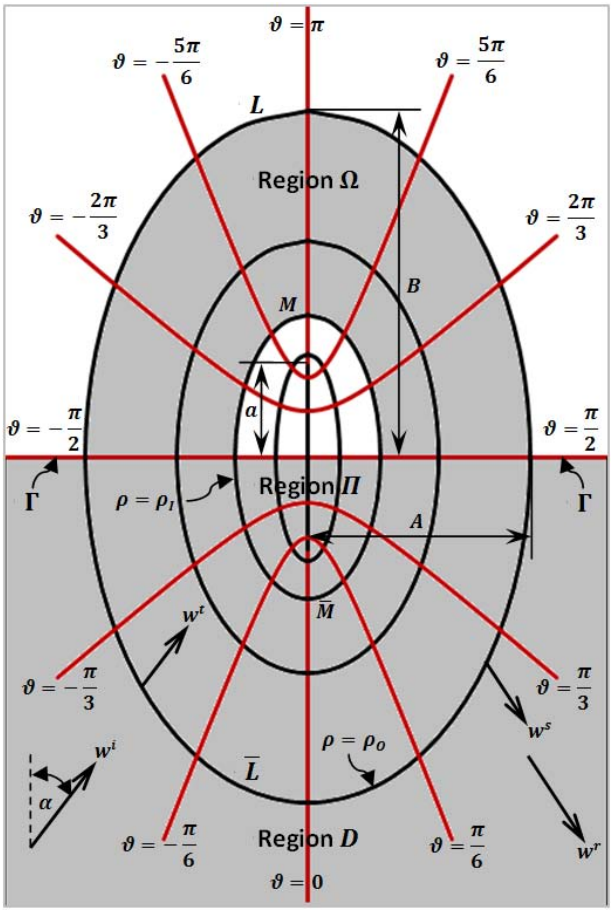


## 8.2 Series Expansion of Wave Functions

**Incident and Reflected Waves:**

The excitation $w^i$ consists of infinite trains of plane SH waves and travelling in the direction $\pi - \gamma$ to positive x axis. Without hill and tunnel, the incident waves strike the flat surface and yield the reflected plane waves $w^r$ in the free field; their summation called the free field waves can be expressed in elliptical coordinate as Equation (4.1).

**Scattered and Transmitted Waves:**

The scattered waves $w^s$ in the exterior region *D* and the transmitted waves $w_\Omega^t$ the ring region $\Omega$ are given by Equations (4.2) and (5.1) respectively. In addition the new transmitted waves in the semi-elliptical region $\Pi$ may take the same form as Wong and Trifunac (1974**a**) used in their valley model.

$$w_\Pi^t = \sum_{n=0}^{\infty} F_{2n} Mc_{2n}^{(1)}(\rho, q) ce_{2n}(\vartheta, q) + \sum_{n=0}^{\infty} F_{2n+1} Ms_{2n+1}^{(1)}(\rho, q) se_{2n+1}(\vartheta, q) \qquad (8.1)$$

where $F_n$, in addition to unknowns $A_n$, $B_n$, $C_n$, $D_n$, and $E_n$, in Equations (4.2) and (5.1), is another unknown coefficient to be determined. The transmitted waves in the semi-elliptical region $\Pi$ have $Mc_{2n}^{(1)}(\cdot)$ and $Ms_{2n+1}^{(1)}(\cdot)$ as radial wave functions since their asymptotic behaviors are Bessel functions of the first kind, representing standing waves in the semi-elliptical region $\Omega$ (Pao and Mow, 1973). Furthermore $ce_{2n}(\cdot)$ and $se_{2n+1}(\cdot)$ form a complete orthogonal set of angular domain in the half-range $[-\pi/2, \pi/2]$ (and similarly in $[\pi/2, -\pi/2]$). It is noteworthy that the transmitted waves $w_\Pi^t$, Equation (8.1), in the semi-elliptical region $\Pi$ automatically satisfies the traction free on the flat surface $\overline{\Gamma}$.

**Solution of the Problem using Angular Half-range Expansion**

The wave functions $w = w^{ff} + w^s$ in the exterior region *D*, $w_\Omega^t$ in the elliptical region $\Omega$ and $w_\Pi^t$ in the semi-elliptical region $\Pi$ must satisfy the Helmholtz equation, Equation (2.8), and the additional boundary conditions, beside those in

Chapter 4; the traction-free boundary condition at the surface of the elliptical tunnel $(\rho = \rho_I, \pi \le \vartheta \le 0)$ and the continuity of displacement and radial stress at the interface $\overline{M}$.

$$\tau_{\rho z}\big|_{\rho=\rho_I} = \frac{\mu}{aJ}\frac{\partial w^t}{\partial \rho}\Big|_{\rho=\rho_I} = 0;\ -\frac{\pi}{2} \le \vartheta \le \frac{\pi}{2} \tag{8.2}$$

$$\begin{aligned} w^t_{\Omega}\big|_{\rho=\rho_{\mathrm{I}}} &= w^t_{\Pi}\big|_{\rho=\rho_{\mathrm{I}}} \\ \tau_{\rho z}\big|_{\rho=\rho_{\mathrm{I}}} &= \frac{\mu}{aJ}\frac{\partial w^t_{\Omega}}{\partial \rho}\Big|_{\rho=\rho_{\mathrm{I}}} = \frac{\mu}{aJ}\frac{\partial w^t_{\Pi}}{\partial \rho}\Big|_{\rho=\rho_{\mathrm{I}}} ;\ \frac{\pi}{2} \le \vartheta \le -\frac{\pi}{2} \end{aligned} \tag{8.3}$$

Mathematically the transmitted waves $w^t_{\Omega}$ expressing the displacement motion in the full elliptical region must satisfy two disjoint sets along the circumferences $\rho = \rho_{\mathrm{O}}$ and $\rho = \rho_{\mathrm{I}}$. Hence we must utilize the orthogonality of angular Mathieu functions in the half-range we developed in Chapter 4; then the transmitted waves $w^t_{\Omega}$ and their radial stresses may be expressed as follows

$$\begin{aligned} w^t = &\sum_{n=0}^{\infty}\Big[Mc^{(3)}_{2n}(\rho,q)B_{2n} \mp \sum_{m=0}^{\infty}\mathfrak{M}_{mn}Mc^{(3)}_{2m+1}(\rho,q)B_{2m+1}\Big]ce_{2n}(\vartheta,q) \\ &+\sum_{n=0}^{\infty}\Big[Ms^{(3)}_{2n+1}(\rho,q)C_{2n+1} \mp \sum_{m=0}^{\infty}\mathfrak{N}_{mn}Ms^{(3)}_{2m+2}(\rho,q)C_{2m+2}\Big]se_{2n+1}(\vartheta,q) \\ &+\sum_{n=0}^{\infty}\Big[Mc^{(4)}_{2n}(\rho,q)D_{2n} \mp \sum_{m=0}^{\infty}\mathfrak{M}_{mn}Mc^{(4)}_{2m+1}(\rho,q)D_{2m+1}\Big]ce_{2n}(\vartheta,q) \\ &+\sum_{n=0}^{\infty}\Big[Ms^{(4)}_{2n+1}(\rho,q)E_{2n+1} \mp \sum_{m=0}^{\infty}\mathfrak{N}_{mn}Ms^{(4)}_{2m+2}(\rho,q)E_{2m+2}\Big]se_{2n+1}(\vartheta,q) \end{aligned} \tag{8.4}$$

$$\begin{aligned} \tau_{\rho z} = &\frac{\mu}{aJ}\sum_{n=0}^{\infty}\Big[Mc^{(3)\prime}_{2n}(\rho,q)B_{2n} \mp \sum_{m=0}^{\infty}\mathfrak{M}_{mn}Mc^{(3)\prime}_{2m+1}(\rho,q)B_{2m+1}\Big]ce_{2n}(\vartheta,q) \\ &+\frac{\mu}{aJ}\sum_{n=0}^{\infty}\Big[Ms^{(3)\prime}_{2n+1}(\rho,q)C_{2n+1} \mp \sum_{m=0}^{\infty}\mathfrak{N}_{mn}Ms^{(3)\prime}_{2m+2}(\rho,q)C_{2m+2}\Big]se_{2n+1}(\vartheta,q) \\ &+\frac{\mu}{aJ}\sum_{n=0}^{\infty}\Big[Mc^{(4)\prime}_{2n}(\rho,q)D_{2n} \mp \sum_{m=0}^{\infty}\mathfrak{M}_{mn}Mc^{(4)\prime}_{2m+1}(\rho,q)D_{2m+1}\Big]ce_{2n}(\vartheta,q) \\ &+\frac{\mu}{aJ}\sum_{n=0}^{\infty}\Big[Ms^{(4)\prime}_{2n+1}(\rho,q)E_{2n+1} \mp \sum_{m=0}^{\infty}\mathfrak{N}_{mn}Ms^{(4)\prime}_{2m+2}(\rho,q)E_{2m+2}\Big]se_{2n+1}(\vartheta,q) \end{aligned} \tag{8.5}$$

where –ve above and +ve below are assigned for $\pi/2 \le \vartheta \le -\pi/2$ and $-\pi/2 \le \vartheta \le \pi/2$; $\mathfrak{M}_{mn}$ and $\mathfrak{N}_{mn}$ are given by Equations (2.35) and (2.38). Then all

displacement and stress functions are convenient to be applied since they are in the forms of elliptical cosine series with order 2n and of elliptical sine series with order 2n+1. Applying all boundary conditions along both circumferences of the elliptical ring region $\Omega$, we establish two groups of six infinite-equation sets.

The first set is:

$$\begin{Bmatrix} B_{2n}Mc_{2n}^{(3)\prime}(\rho_O,q)-\sum_{m=0}^{\infty}\mathfrak{M}_{mn}B_{2m+1}\,Mc_{2m+1}^{(3)\prime}(\rho_O,q) \\ +D_{2n}Mc_{2n}^{(4)\prime}(\rho_O,q)-\sum_{m=0}^{\infty}\mathfrak{M}_{mn}D_{2m+1}\,Mc_{2m+1}^{(4)\prime}(\rho_O,q) \end{Bmatrix}=0 \tag{8.6}$$

$$\begin{Bmatrix} B_{2n}Mc_{2n}^{(3)}(\rho_O,q)+\sum_{m=0}^{\infty}\mathfrak{M}_{mn}B_{2m+1}\,Mc_{2m+1}^{(3)}(\rho_O,q) \\ +D_{2n}Mc_{2n}^{(4)}(\rho_O,q)+\sum_{m=0}^{\infty}\mathfrak{M}_{mn}D_{2m+1}\,Mc_{2m+1}^{(4)}(\rho_O,q) \end{Bmatrix}=\begin{Bmatrix} 4w_0(-1)^n Mc_{2n}^{(1)}(\rho_O,q)ce_{2n}(\gamma,q) \\ +A_{2n}Mc_{2n}^{(3)}(\rho_O,q) \end{Bmatrix} \tag{8.7}$$

$$\begin{Bmatrix} B_{2n}Mc_{2n}^{(3)\prime}(\rho_O,q)+\sum_{m=0}^{\infty}\mathfrak{M}_{mn}B_{2m+1}\,Mc_{2m+1}^{(3)\prime}(\rho_O,q) \\ +D_{2n}Mc_{2n}^{(4)\prime}(\rho_O,q)+\sum_{m=0}^{\infty}\mathfrak{M}_{mn}D_{2m+1}\,Mc_{2m+1}^{(4)\prime}(\rho_O,q) \end{Bmatrix}=\begin{Bmatrix} 4w_0(-1)^n Mc_{2n}^{(1)\prime}(\rho_O,q)ce_{2n}(\gamma,q) \\ +A_{2n}Mc_{2n}^{(3)\prime}(\rho_O,q) \end{Bmatrix} \tag{8.8}$$

$$\begin{Bmatrix} B_{2n}Mc_{2n}^{(3)\prime}(\rho_I,q)-\sum_{m=0}^{\infty}\mathfrak{M}_{mn}B_{2m+1}\,Mc_{2m+1}^{(3)\prime}(\rho_I,q) \\ +D_{2n}Mc_{2n}^{(4)\prime}(\rho_I,q)-\sum_{m=0}^{\infty}\mathfrak{M}_{mn}D_{2m+1}\,Mc_{2m+1}^{(4)\prime}(\rho_I,q) \end{Bmatrix}=0 \tag{8.9}$$

$$\begin{Bmatrix} B_{2n}Mc_{2n}^{(3)}(\rho_I,q)+\sum_{m=0}^{\infty}\mathfrak{M}_{mn}B_{2m+1}\,Mc_{2m+1}^{(3)}(\rho_I,q) \\ +D_{2n}Mc_{2n}^{(4)}(\rho_I,q)+\sum_{m=0}^{\infty}\mathfrak{M}_{mn}D_{2m+1}\,Mc_{2m+1}^{(4)}(\rho_I,q) \end{Bmatrix}=F_{2n}Mc_{2n}^{(1)}(\rho_I,q) \tag{8.10}$$

$$\begin{Bmatrix} B_{2n}Mc_{2n}^{(3)\prime}(\rho_I,q)+\sum_{m=0}^{\infty}\mathfrak{M}_{mn}B_{2m+1}\,Mc_{2m+1}^{(3)\prime}(\rho_I,q) \\ +D_{2n}Mc_{2n}^{(4)\prime}(\rho_I,q)+\sum_{m=0}^{\infty}\mathfrak{M}_{mn}D_{2m+1}\,Mc_{2m+1}^{(4)\prime}(\rho_I,q) \end{Bmatrix}=F_{2n}Mc_{2n}^{(1)\prime}(\rho_I,q) \tag{8.11}$$

In addition the latter set is:

$$\begin{Bmatrix} C_{2n+1}Ms_{2n+1}^{(3)\prime}(\rho_O,q)-\sum_{m=0}^{\infty}\mathfrak{N}_{mn}C_{2m+2}Ms_{2m+2}^{(3)\prime}(\rho_O,q) \\ +E_{2n+1}Ms_{2n+1}^{(4)\prime}(\rho_O,q)-\sum_{m=0}^{\infty}\mathfrak{N}_{mn}E_{2m+2}\,Ms_{2m+2}^{(4)\prime}(\rho_O,q) \end{Bmatrix}=0 \tag{8.12}$$

$$\begin{Bmatrix} C_{2n+1}Ms_{2n+1}^{(3)}(\rho_O,q)+\sum_{m=0}^{\infty}\mathfrak{N}_{mn}C_{2m+2}Ms_{2m+2}^{(3)}(\rho_O,q) \\ +E_{2n+1}Ms_{2n+1}^{(4)}(\rho_O,q)+\sum_{m=0}^{\infty}\mathfrak{N}_{mn}E_{2m+2}\,Ms_{2m+2}^{(4)}(\rho_O,q) \end{Bmatrix}=\begin{Bmatrix} 4w_0\mathrm{i}(-1)^n Ms_{2n}^{(1)}(\rho_O,q)se_{2n}(\gamma,q) \\ +A_{2n+1}Ms_{2n+1}^{(3)}(\rho_O,q) \end{Bmatrix} \tag{8.13}$$

$$\begin{Bmatrix} C_{2n+1}Ms_{2n+1}^{(3)\prime}(\rho_O,q)+\sum_{m=0}^{\infty}\mathfrak{N}_{mn}C_{2m+2}Ms_{2m+2}^{(3)\prime}(\rho_O,q) \\ +E_{2n+1}Ms_{2n+1}^{(4)\prime}(\rho_O,q)+\sum_{m=0}^{\infty}\mathfrak{N}_{mn}E_{2m+2}\,Ms_{2m+2}^{(4)\prime}(\rho_O,q) \end{Bmatrix}=\begin{Bmatrix} 4w_0\mathrm{i}(-1)^n Ms_{2n}^{(1)}(\rho_O,q)se_{2n}(\gamma,q) \\ +A_{2n+1}Ms_{2n+1}^{(3)\prime}(\rho_O,q) \end{Bmatrix} \tag{8.14}$$

$$\begin{Bmatrix} C_{2n+1}Ms_{2n+1}^{(3)\prime}(\rho_I,q) - \sum_{m=0}^{\infty}\Re_{mn}C_{2m+2}Ms_{2m+2}^{(3)\prime}(\rho_I,q) \\ +E_{2n+1}Ms_{2n+1}^{(4)\prime}(\rho_I,q) - \sum_{m=0}^{\infty}\Re_{mn}E_{2m+2}\,Ms_{2m+2}^{(4)\prime}(\rho_I,q) \end{Bmatrix} = 0 \tag{8.15}$$

$$\begin{Bmatrix} C_{2n+1}Ms_{2n+1}^{(3)}(\rho_I,q) + \sum_{m=0}^{\infty}\Re_{mn}C_{2m+2}Ms_{2m+2}^{(3)}(\rho_I,q) \\ +E_{2n+1}Ms_{2n+1}^{(4)}(\rho_I,q) + \sum_{m=0}^{\infty}\Re_{mn}E_{2m+2}\,Ms_{2m+2}^{(4)}(\rho_I,q) \end{Bmatrix} = F_{2n+1}Ms_{2n+1}^{(1)}(\rho_I,q) \tag{8.16}$$

$$\begin{Bmatrix} C_{2n+1}Ms_{2n+1}^{(3)\prime}(\rho_I,q) + \sum_{m=0}^{\infty}\Re_{mn}C_{2m+2}Ms_{2m+2}^{(3)\prime}(\rho_I,q) \\ +E_{2n+1}Ms_{2n+1}^{(4)\prime}(\rho_I,q) + \sum_{m=0}^{\infty}\Re_{mn}E_{2m+2}\,Ms_{2m+2}^{(4)\prime}(\rho_I,q) \end{Bmatrix} = F_{2n+1}Ms_{2n+1}^{(1)\prime}(\rho_I,q) \tag{8.17}$$

Equations (8.6) through (8.11) and Equations (8.12) through (8.17) form infinite linear equations which could be solved numerically by matrix truncation. Again the above systems are solved by using subroutine LAPACK and the SVD provided by MATLAB. Moreover the same scheme as usage in previous chapters is implemented here to test accuracy.

## 8.3 Results and Analysis

The amplitudes of ground surface displacements given by the proposed solutions are evaluated for the different values of the dimensionless parameters $\eta$, $R$ and $\eta_T$ which are again given by Equations (3.16), (4.10) and (5.9); values of $R$ are limited to 1.00002, 1.2, 1.4, and 1.6. For each value of $R$ we limit values of $T$ to $0.2A$, $0.5A$ and $0.8A$. Furthermore the amplitude of incidence is assumed to unity.

**Comparison with the Solutions of Shallow "Circular" Semi-Elliptical Hill:**

Figures 8.2 through 8.4 show the plots of surface displacement for "almost-circular" semi-elliptical hill with "almost-circular" semi-elliptical tunnel $T = 0.2A$, $0.5A$ and $0.8A$ respectively; on each plot there are 2 subplots for $\eta = 5$ and $10$ at four incidence $\gamma =$ 0°, 30°, 60° and 90°. These plots are substantially in agreement with plots of shallow case, Figures 7.6 through 7.8; this authenticates the formulation we develop in this chapter.

Figure 8.2: Displacement Amplitudes for $R = 1.00002$ with Tunnel $T = 0.2A$

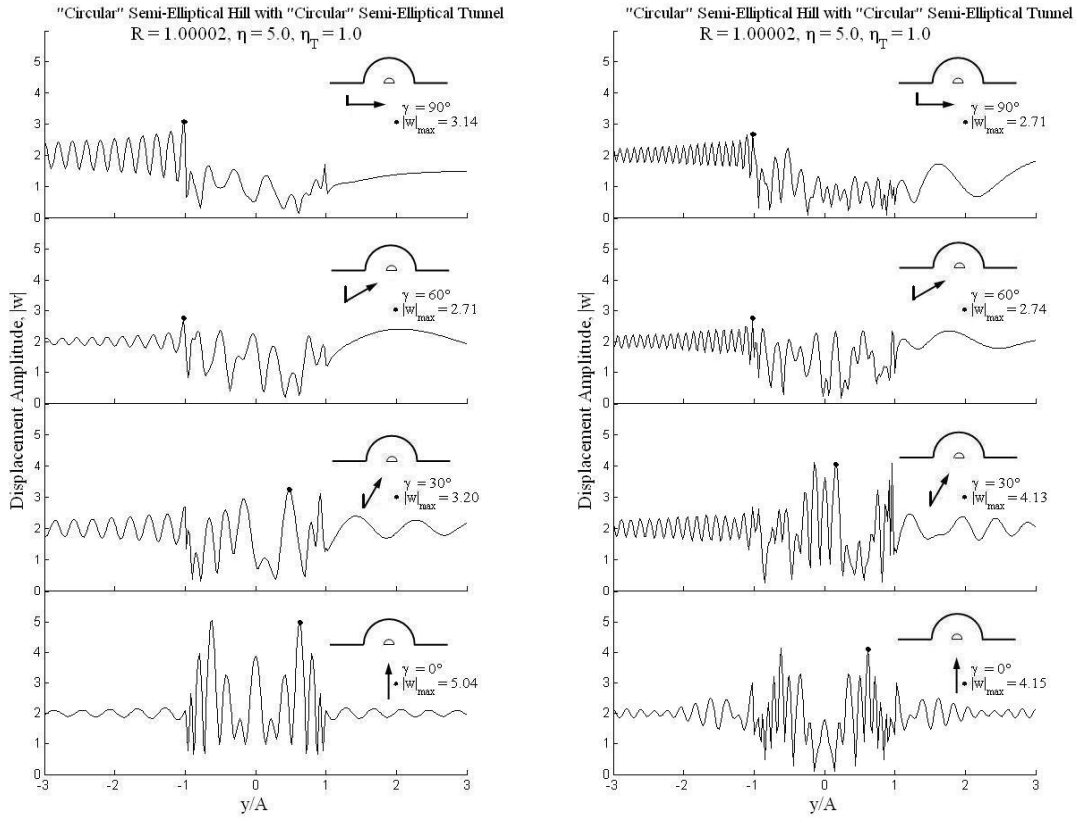


(a) $\eta = 5$ (b) $\eta = 10$

Figure 8.3: Displacement Amplitudes for $R = 1.00002$ with Tunnel $T = 0.5A$

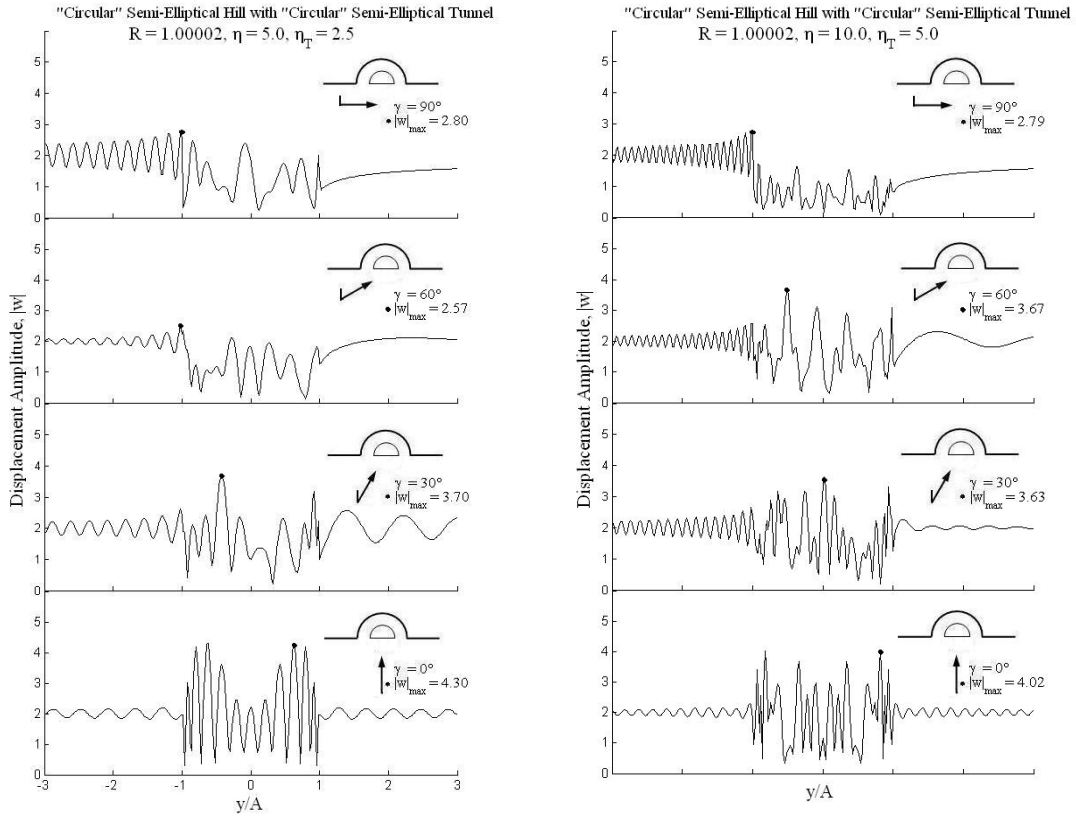


(a) $\eta = 5$ (b) $\eta = 10$

**Effects of Tunnel, and Incident Angle to Semi-Elliptical Hill:**

Figures 8.5 to 8.7 illustrate surface displacements at four prescribed incidences versus the distance *y/A* on and around the hill with the dimensionless frequency $\eta = 5$ and 10 for the semi-elliptical hill $R = 1.2$, 1.4 and 1.6 with semi-elliptical tunnels $T = 0.5A$. In general the locations of the maximum value are always on the hill which is similar to the shallow case.

Figure 8.4: Displacement Amplitudes for $R = 1.00002$ with Tunnel $T = 0.8A$

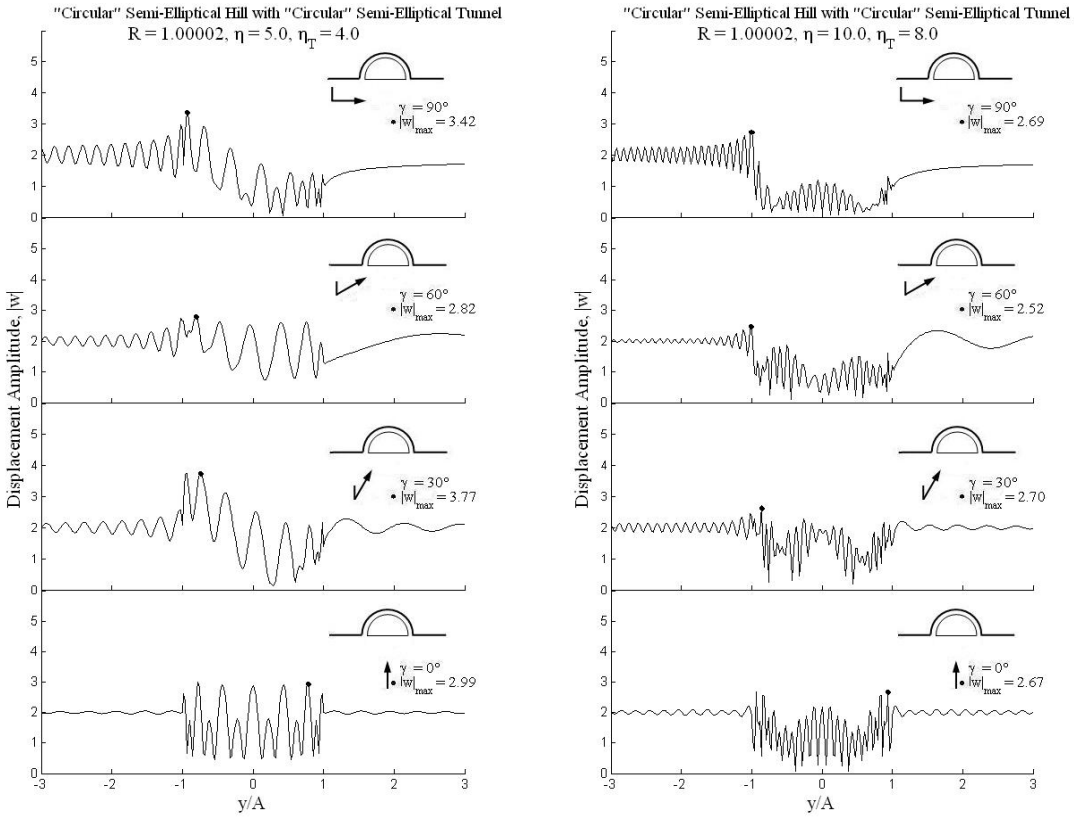


(a) $\eta = 5$ (b) $\eta = 10$

In comparison to Figures 6.6 through 6.11, semi-elliptical tunnels disfigure patterns of ground motion in different way. When incidence waves are in horizontal direction, they are able to slip underneath semi-tunnels. Hence the presence of semi-elliptical tunnels yields less shielding effect or weaker shadow zone on the right end of the hill than the existence of full elliptical tunnel. The amplitudes of ground displacement are always greater than unity for all points located along the free surface on the right end of the hill.

Figure 8.5: Displacement Amplitudes for $R = 1.2$ with Tunnel $T = 0.5A$

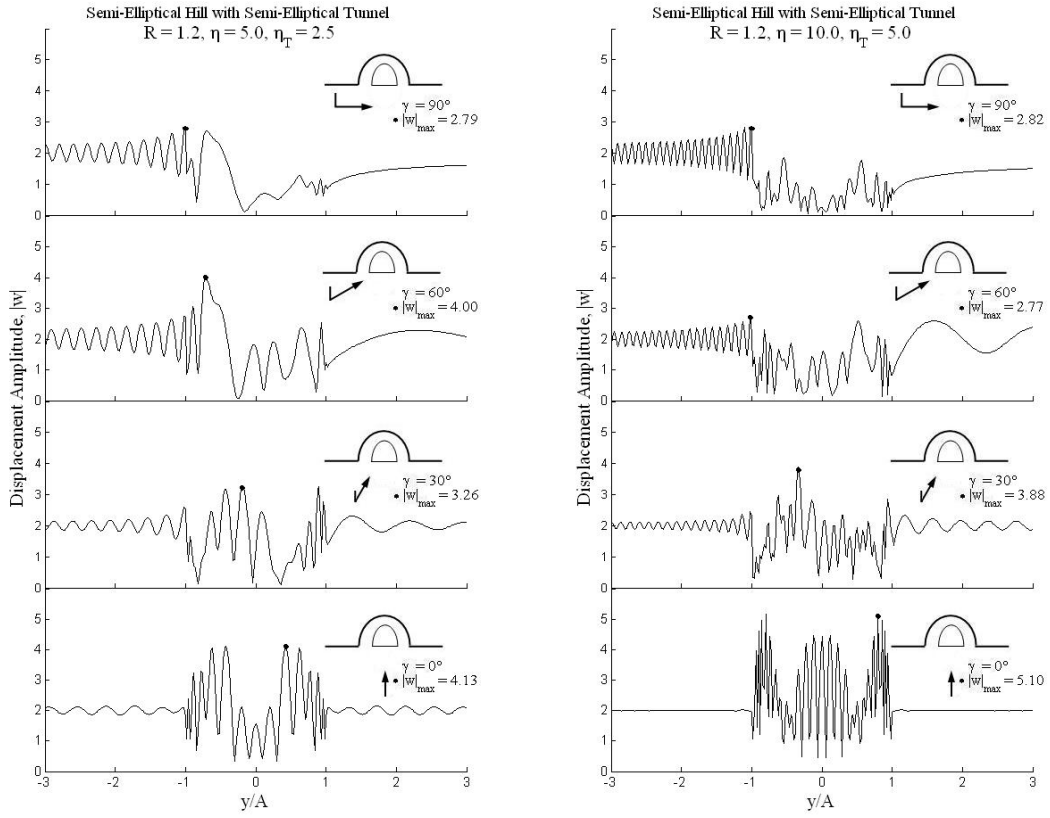


(a) $\eta = 5$ (b) $\eta = 10$

There is interesting point to be mentioned. At 30° angle of incidence, we found out that the maximum amplitude of surface displacement always on the right-half of the hill which is similar to the case of full-elliptical tunnel. Moreover when the dimensionless parameter $\eta$ equals to 5, the presence of semi-elliptical tunnel yields the same effect as of full-elliptical tunnel; the discrepancy of their maximum amplitudes of surface displacement is within 5%, except $R = 1.6$.

Figure 8.6: Displacement Amplitudes for $R = 1.4$ with Tunnel $T = 0.5A$

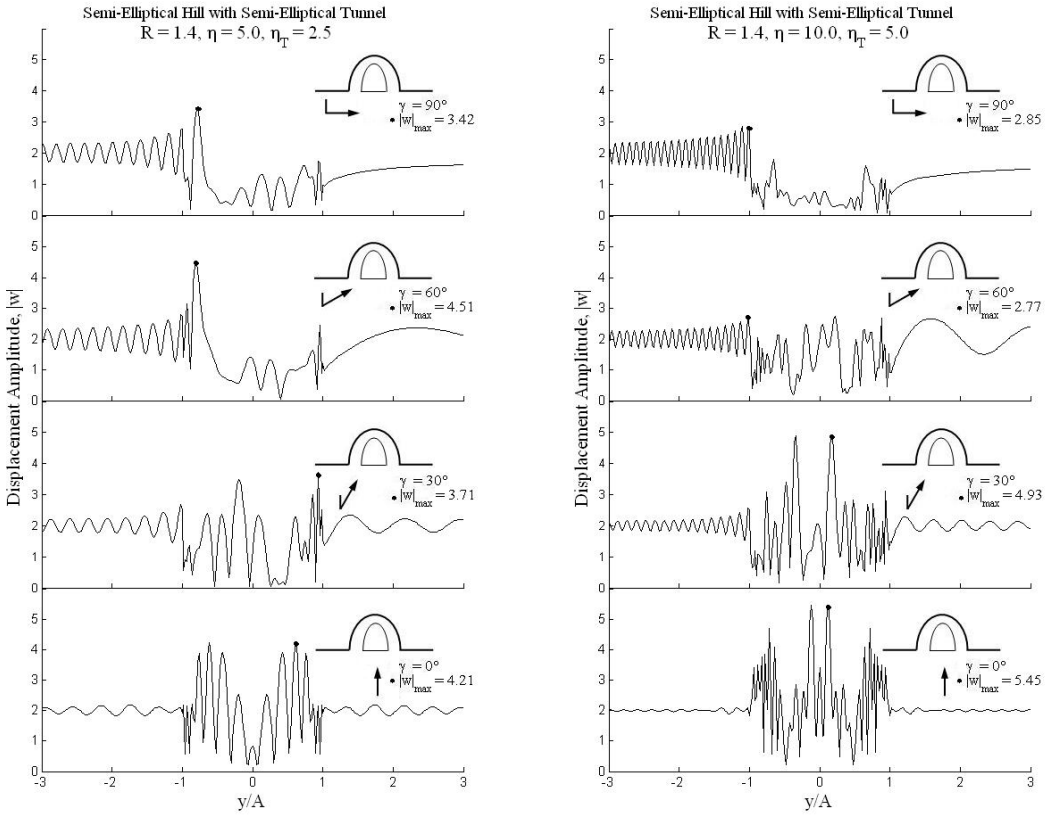


(a) $\eta = 5$ (b) $\eta = 10$

When the incident waves are nearly vertical for dimensionless parameters $\eta = 5$, we noticed the stronger shielding effect due to semi-elliptical tunnels than to full-elliptical ones, like to the shallow case. In addition we can confirm that the there is no major fluctuation of surface displacements on both sides of the hill, which have been noticed with the existence of full-elliptical tunnels. These previous trends could be monitored for dimensionless parameters $\eta = 10$, except again $R = 1.6$.

Figure 8.7: Displacement Amplitudes for $R = 1.6$ with Tunnel $T = 0.5A$

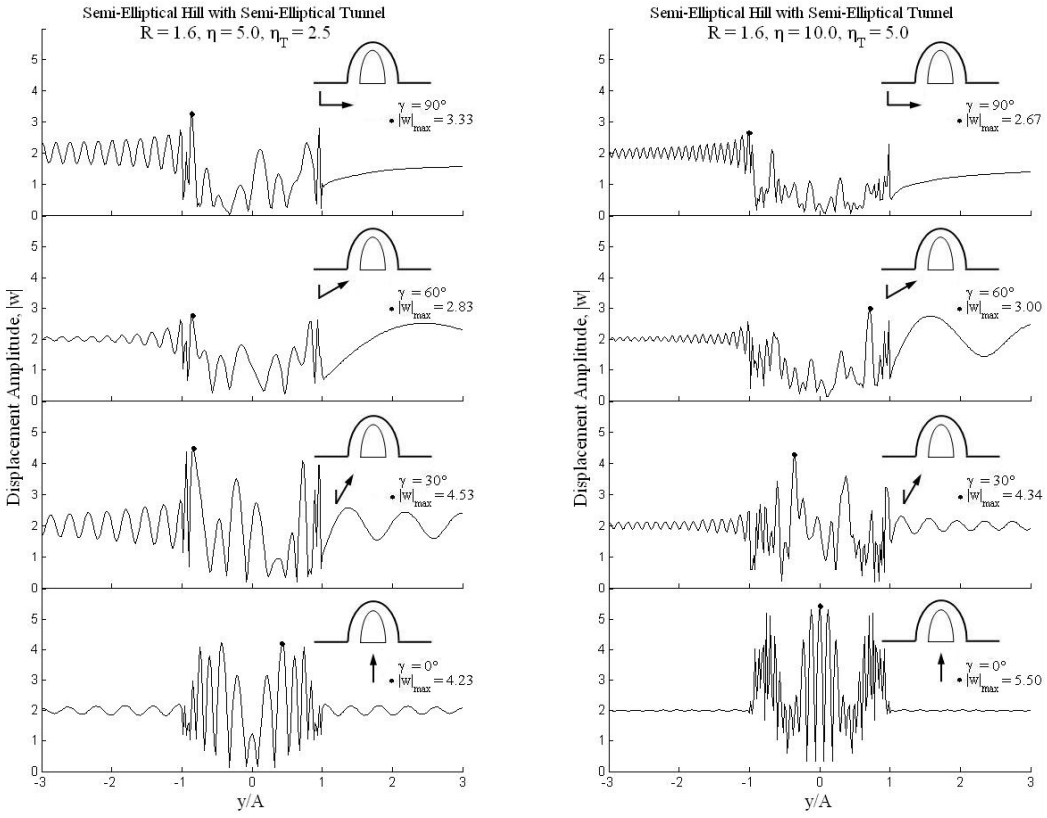


(a) $\eta = 5$ (b) $\eta = 10$

To study the influence of tunnel-size, we consider only $R = 1.6$ with three sizes of tunnel, $T = 0.2A$, $0.5A$ and $0.8A$. Due to the formulation of the deep case, this may be seen as the width effect since the height of tunnel is very comparable. After evaluating Figures 8.8 and 8.9, $T = 0.2A$ and $0.8A$ respectively, together with Figure 8.7, it may be said that semi-tunnels yield identical effects when the angle of incidence is nearly horizontal. The maximum values of surface displacement are inconsiderably relevant to the size of tunnel since their

differences are less than 10 percents. In addition maximum surface displacements are in vicinity of one at all times. On another hand size of tunnel is of importance when the angle of incidence is nearly vertical. As expected, the wider tunnel provides the stronger shielding effect. The presence of tunnel with $T = 0.8A$ de-amplifies maximum displacement by 20%-50% from corresponding values with $T = 0.2A$. Again this confirms the hinder efficiency depends on the direction of wave passage.

Figure 8.8: Displacement Amplitudes for $R = 1.6$ with Tunnel $T = 0.2A$

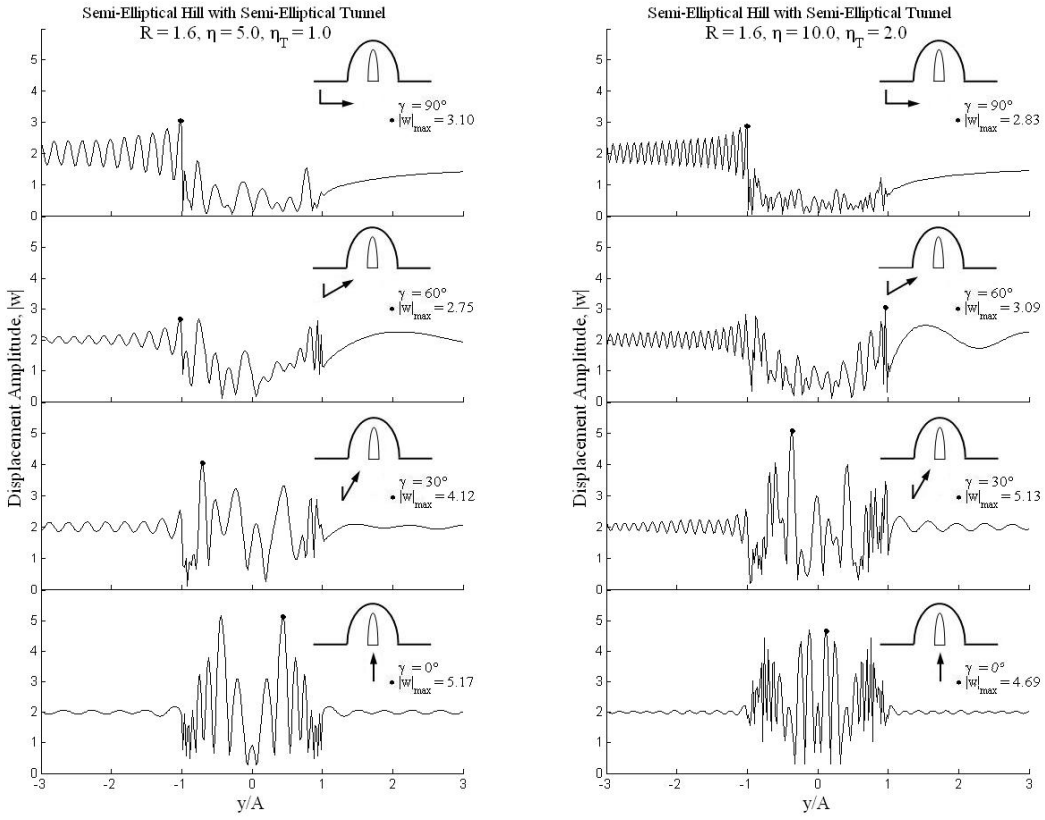


(a) $\eta = 5$ (b) $\eta = 10$

Figure 8.9: Displacement Amplitudes for $R = 1.6$ with Tunnel $T = 0.8A$

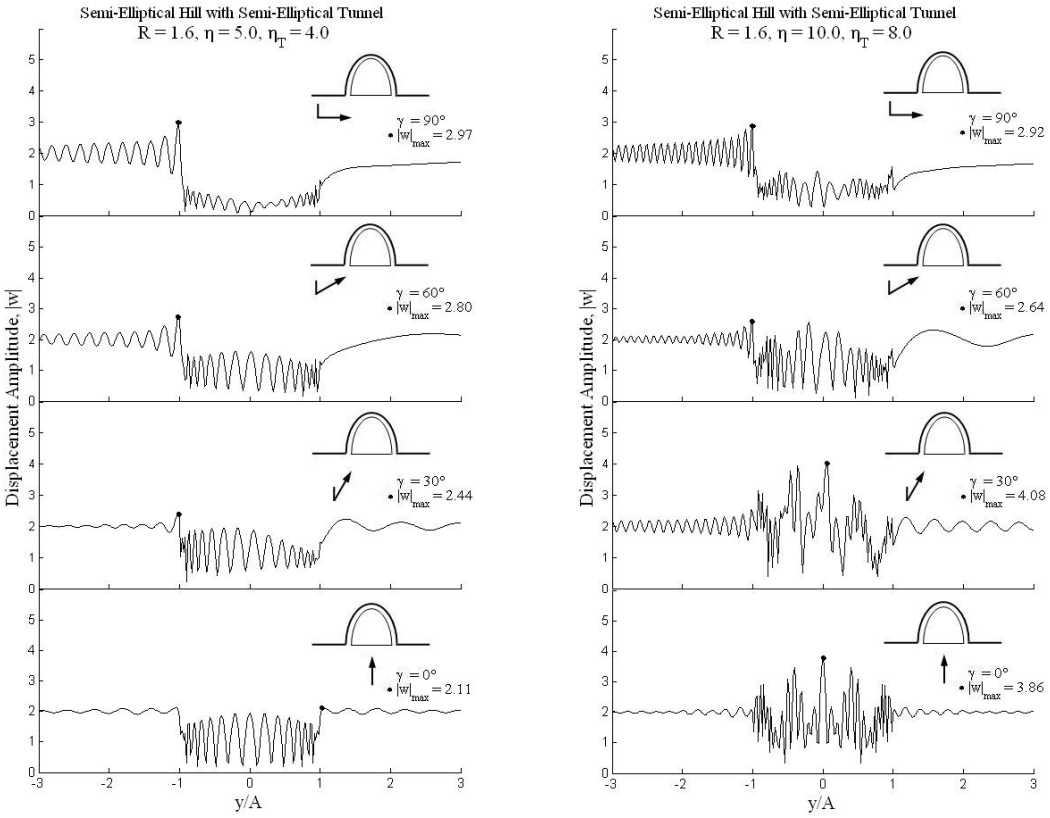


(a) $\eta = 5$ (b) $\eta = 10$

Figures 8.10 through 8.45 show three-dimensional plots of surface displacements for $R = 1.2$, 1.4, and 1.6, equivalent to the height-to-width ratios of 0.6, 0.7, and 0.8 respectively; the values of $T$ for particular $R$ are as at the beginning of this section. Each figure illustrates the plots at four incident angles, $\gamma = 0°$, 30°, 60° and 90°, versus the distance *y/A* on and around the hill and the dimensionless frequency $\eta$ in the range of 0.5 to 10; the amplitudes in the range of *y/A* in $[-1,1]$ are those on the elliptical surface of the hill.

Figure 8.10: Displacement Amplitude for $R = 1.2$, $T = 0.2A$ when $\gamma = 0°$

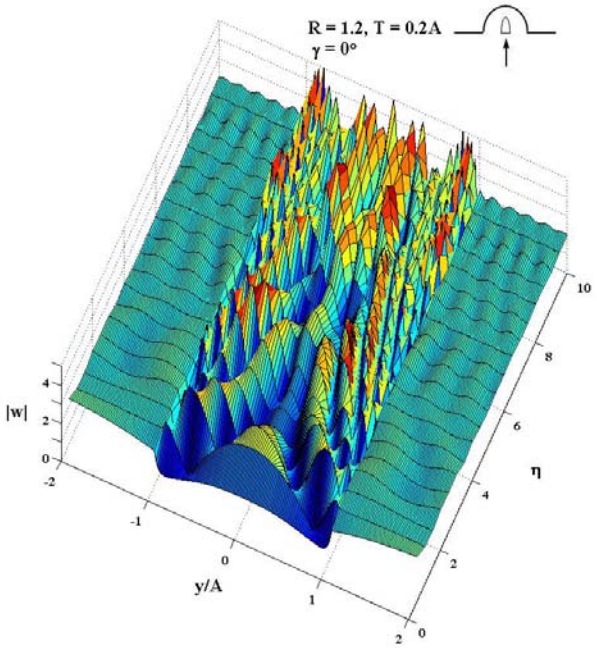


Figure 8.11: Displacement Amplitude for $R = 1.2$, $T = 0.2A$ when $\gamma = 30°$

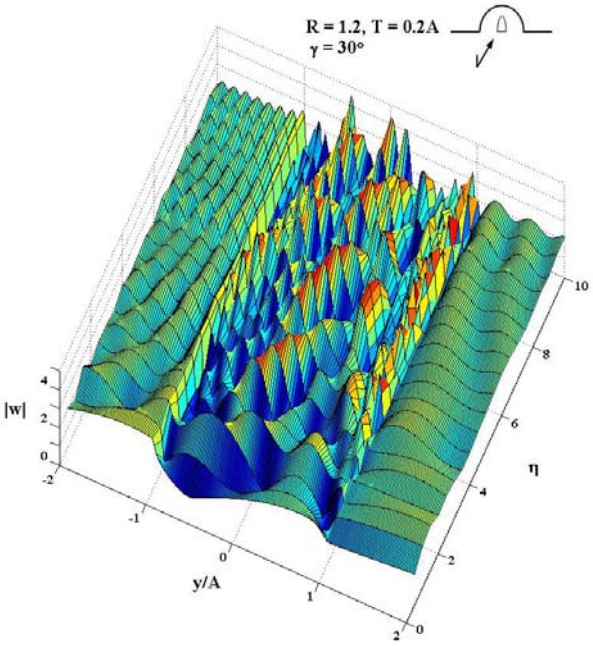

Figure 8.12: Displacement Amplitude for $R = 1.2$, $T = 0.2A$ when $\gamma = 60°$

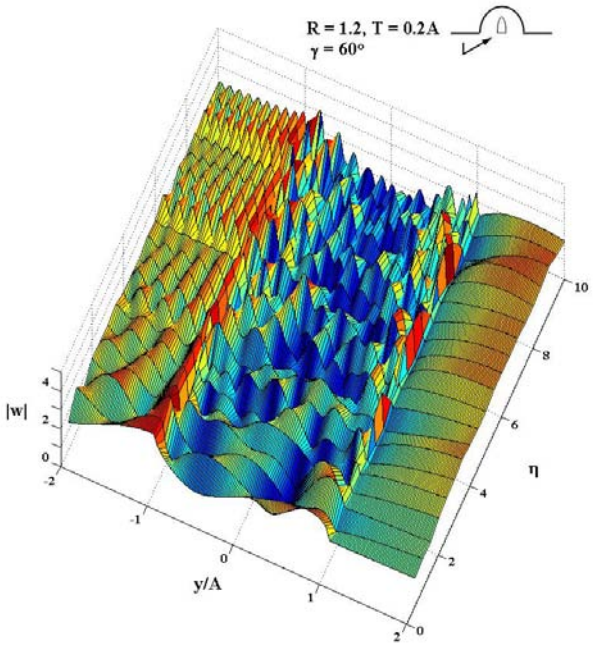


Figure 8.13: Displacement Amplitude for $R = 1.2$, $T = 0.2A$ when $\gamma = 90°$

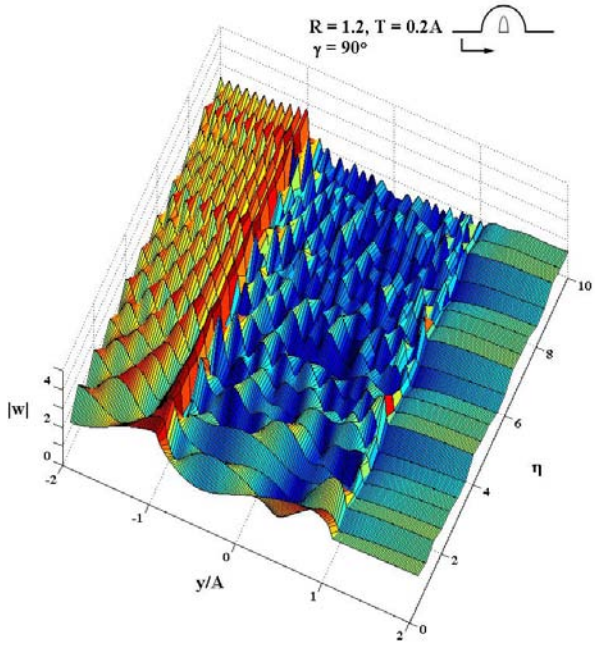

Figure 8.14: Displacement Amplitude for $R = 1.2$, $T = 0.5A$ when $\gamma = 0°$

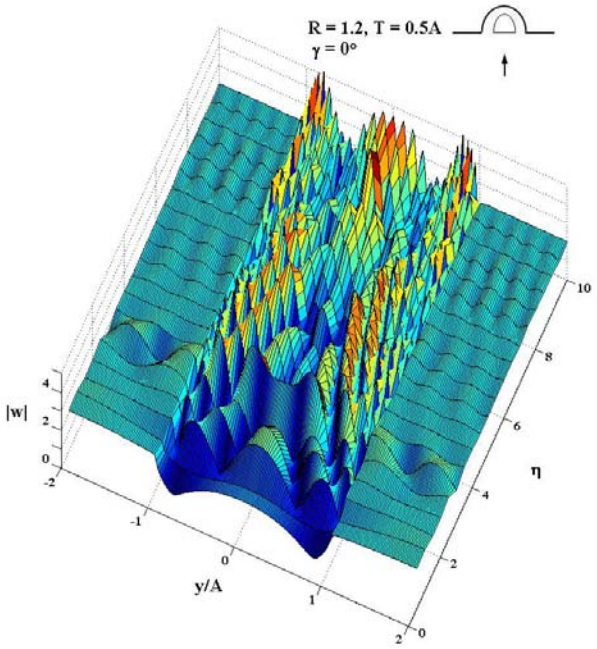


Figure 8.15: Displacement Amplitude for $R = 1.2$, $T = 0.5A$ when $\gamma = 30°$

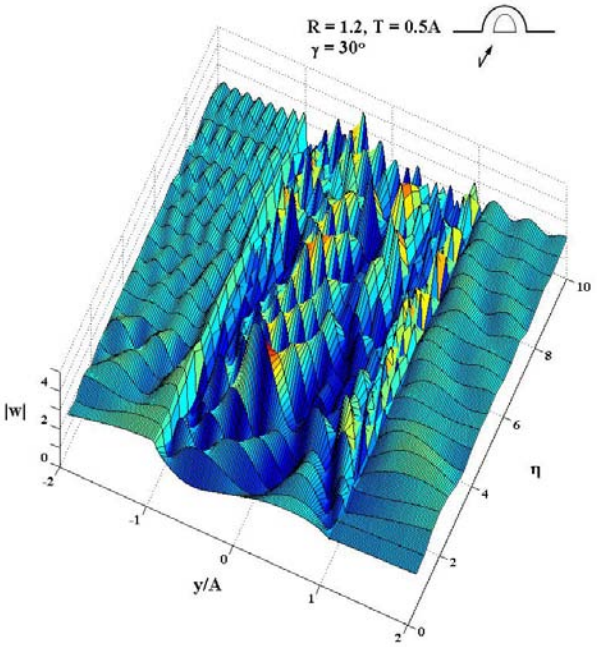

Figure 8.16: Displacement Amplitude for $R = 1.2$, $T = 0.5A$ when $\gamma = 60°$

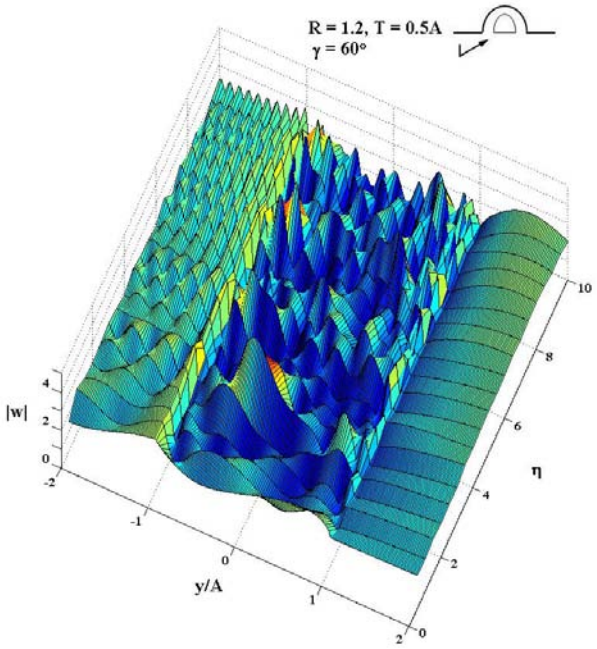


Figure 8.17: Displacement Amplitude for $R = 1.2$, $T = 0.5A$ when $\gamma = 90°$

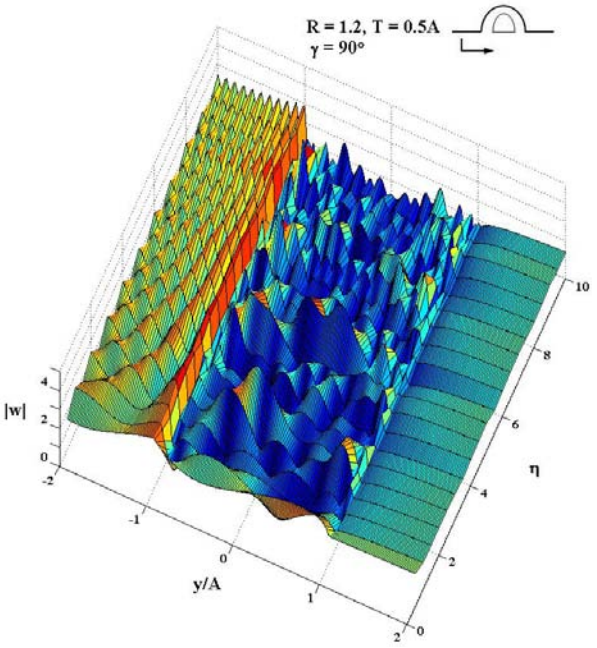

Figure 8.18: Displacement Amplitude for $R = 1.2$, $T = 0.8A$ when $\gamma = 0°$

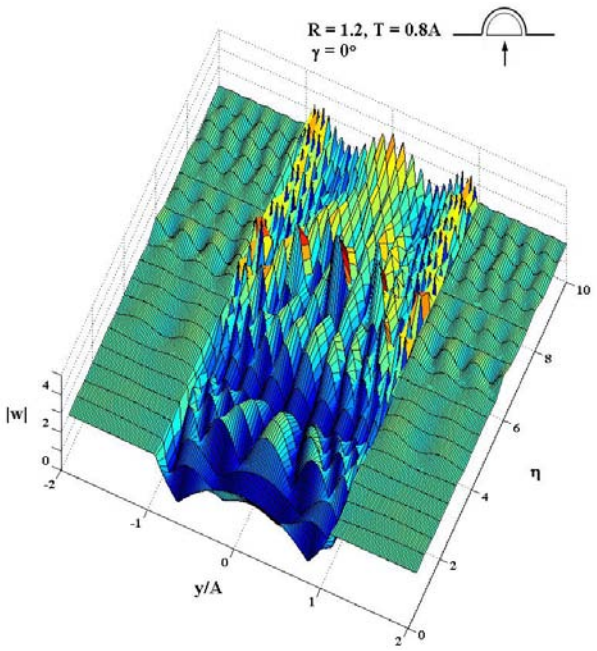


Figure 8.19: Displacement Amplitude for $R = 1.2$, $T = 0.8A$ when $\gamma = 30°$

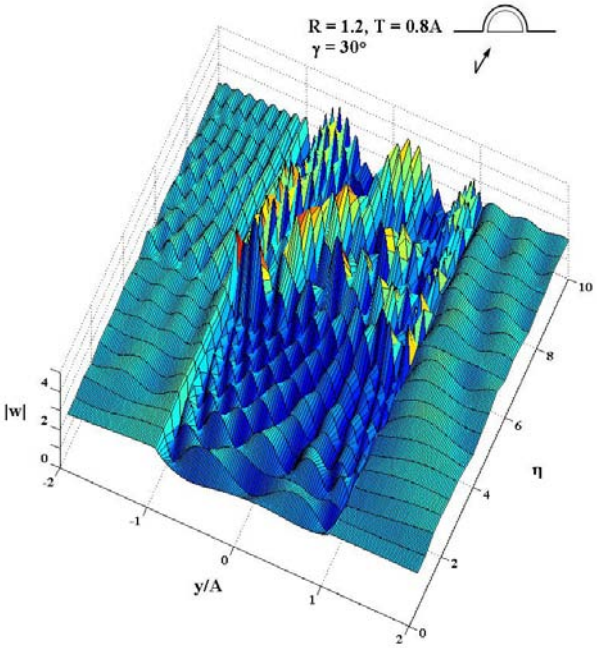

Figure 8.20: Displacement Amplitude for $R = 1.2$, $T = 0.8A$ when $\gamma = 60°$

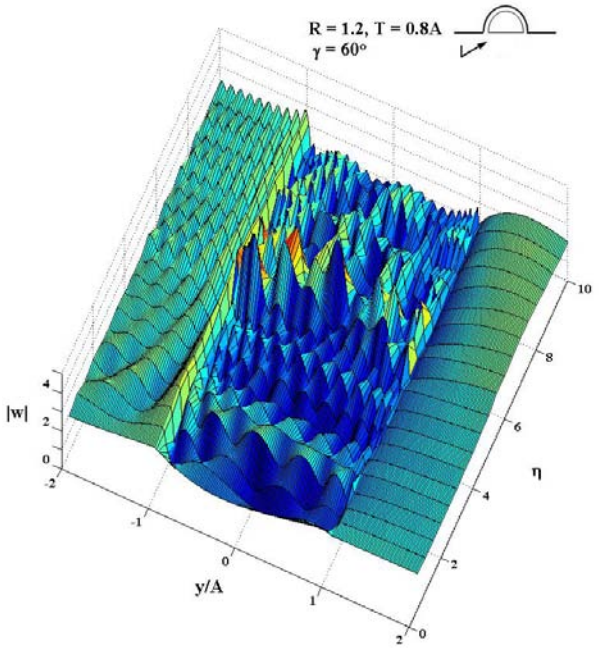


Figure 8.21: Displacement Amplitude for $R = 1.2$, $T = 0.8A$ when $\gamma = 90°$

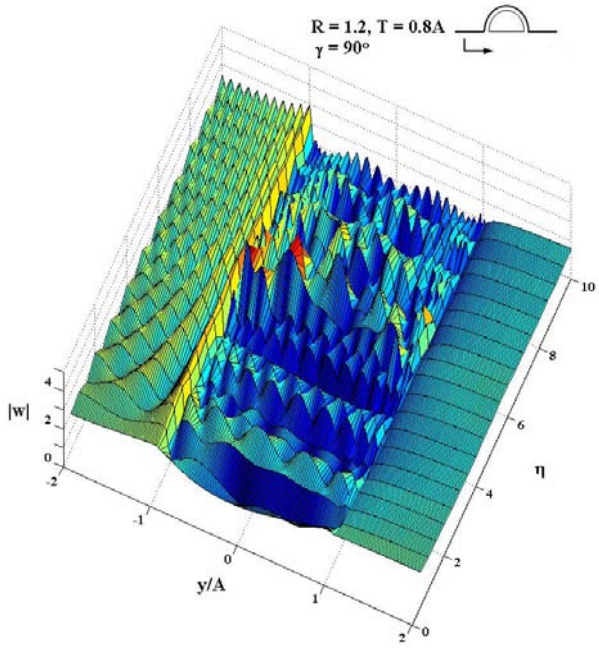

Figure 8.22: Displacement Amplitude for $R = 1.4$, $T = 0.2A$ when $\gamma = 0°$

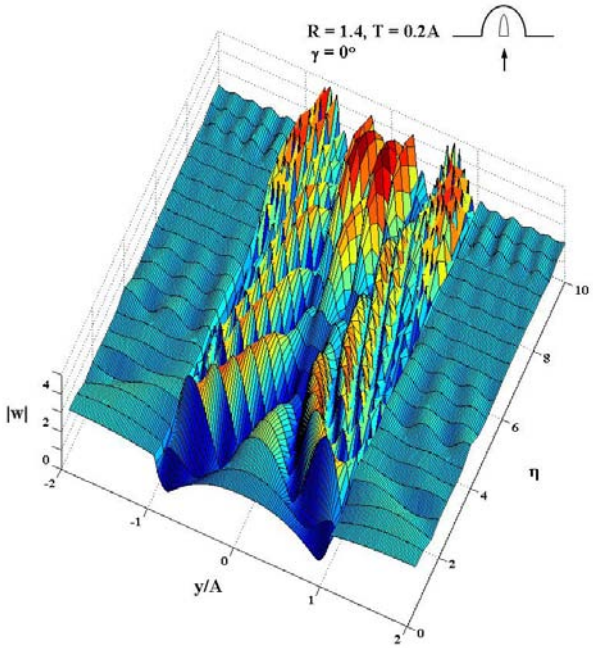


Figure 8.23: Displacement Amplitude for $R = 1.4$, $T = 0.2A$ when $\gamma = 30°$

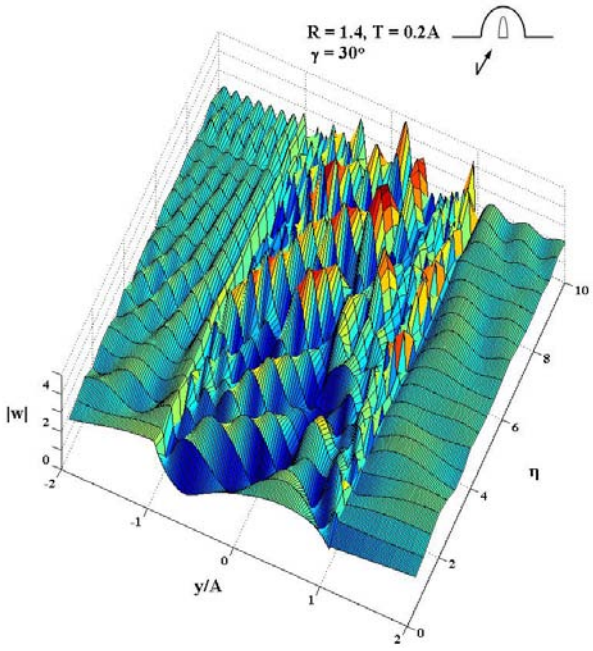

Figure 8.24: Displacement Amplitude for $R = 1.4$, $T = 0.2A$ when $\gamma = 60°$

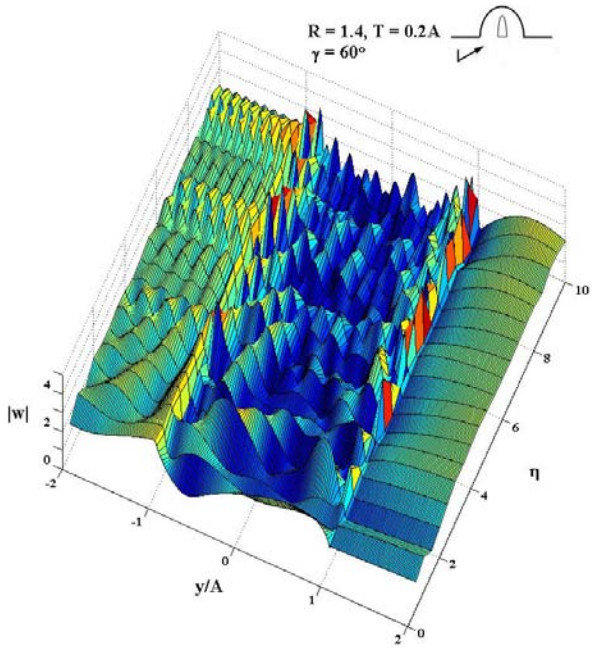


Figure 8.25: Displacement Amplitude for $R = 1.4$, $T = 0.2A$ when $\gamma = 90°$

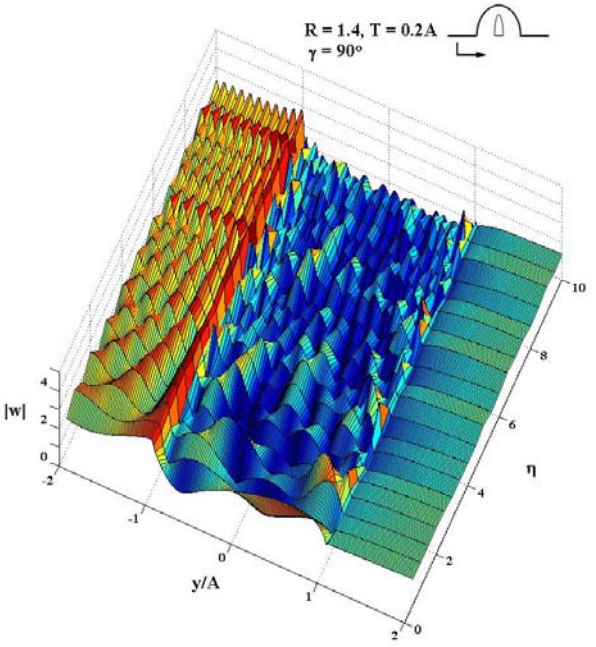

Figure 8.26: Displacement Amplitude for $R = 1.4$, $T = 0.5A$ when $\gamma = 0°$

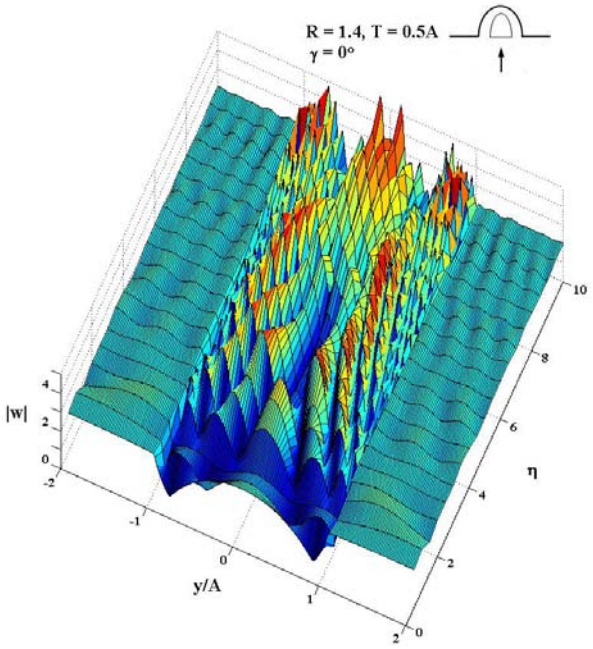


Figure 8.27: Displacement Amplitude for $R = 1.4$, $T = 0.5A$ when $\gamma = 30°$

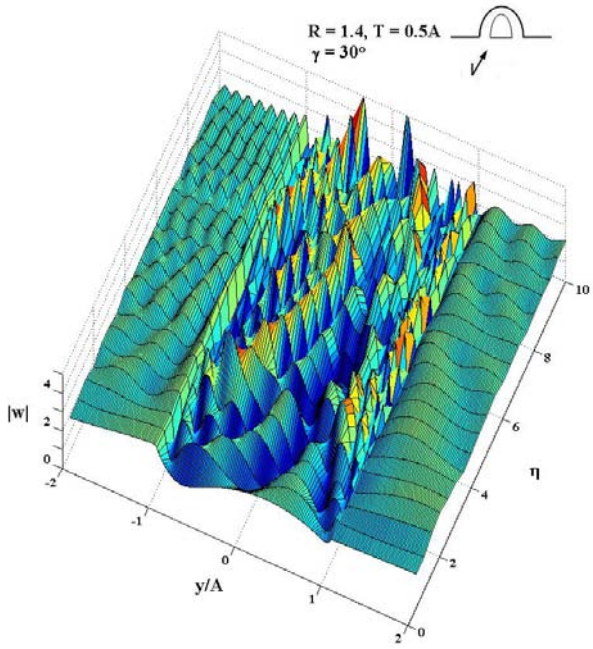

Figure 8.28: Displacement Amplitude for $R = 1.4$, $T = 0.5A$ when $\gamma = 60°$

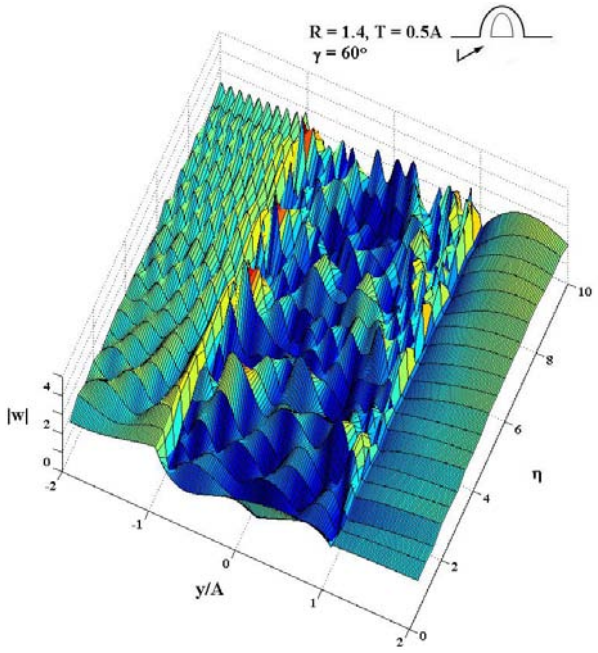


Figure 8.29: Displacement Amplitude for $R = 1.4$, $T = 0.5A$ when $\gamma = 90°$

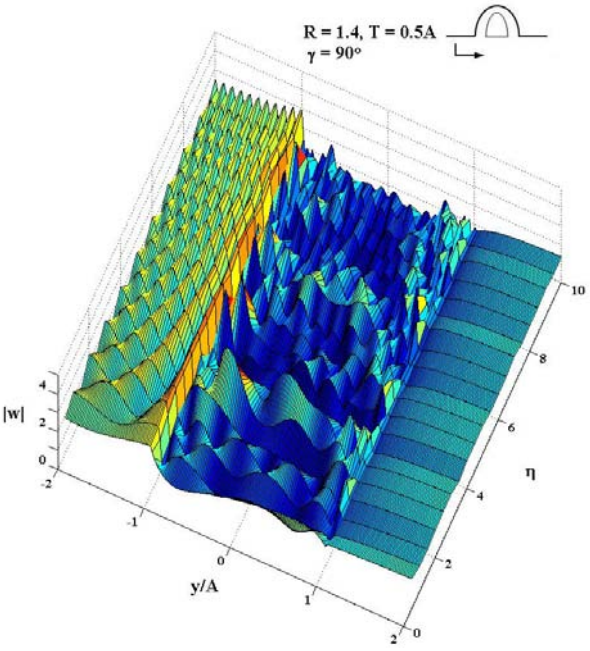

Figure 8.30: Displacement Amplitude for $R = 1.4$, $T = 0.8A$ when $\gamma = 0°$

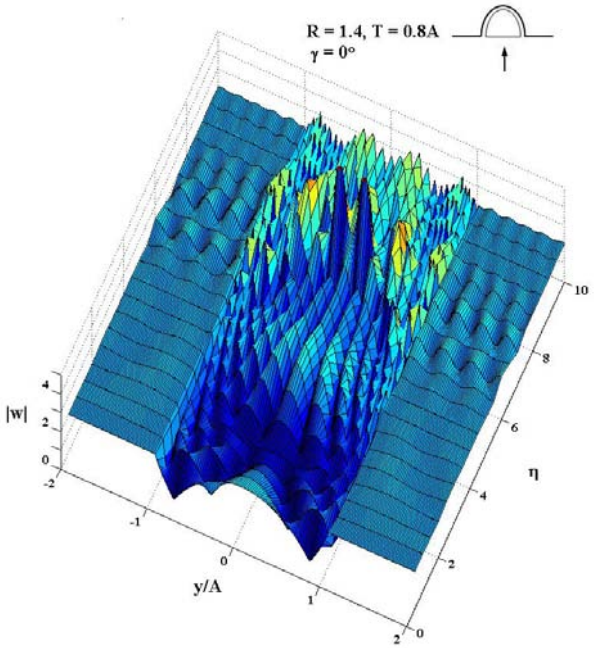


Figure 8.31: Displacement Amplitude for $R = 1.4$, $T = 0.8A$ when $\gamma = 30°$

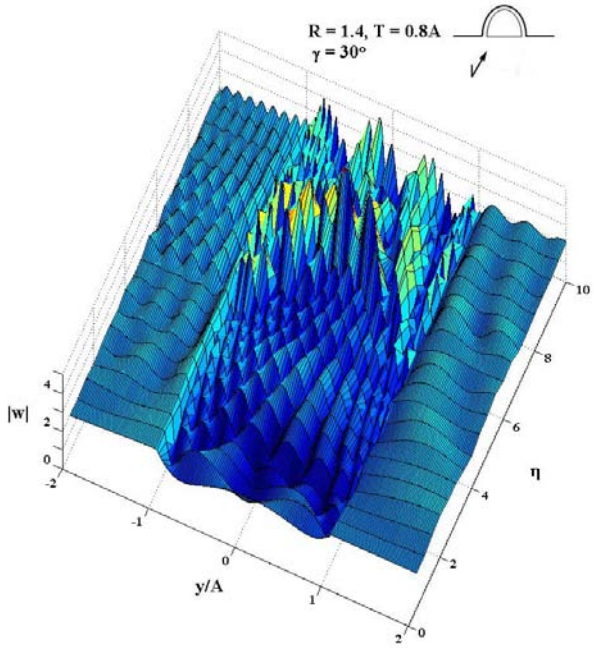

Figure 8.32: Displacement Amplitude for $R = 1.4$, $T = 0.8A$ when $\gamma = 60°$

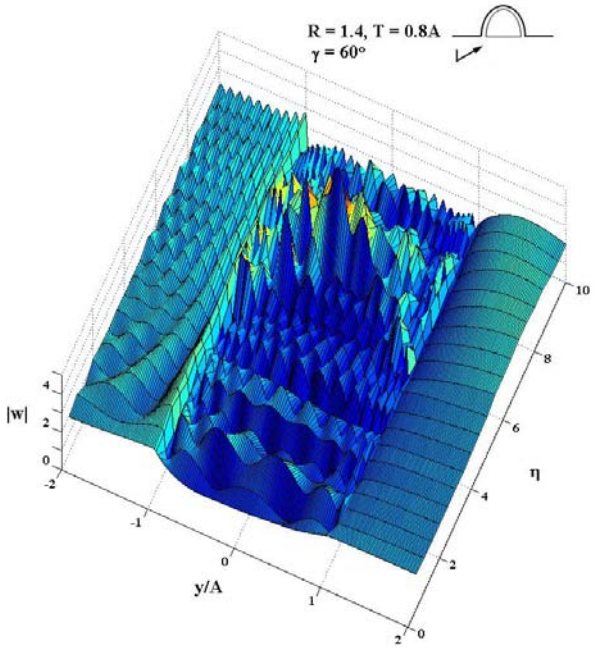


Figure 8.33: Displacement Amplitude for $R = 1.4$, $T = 0.8A$ when $\gamma = 90°$

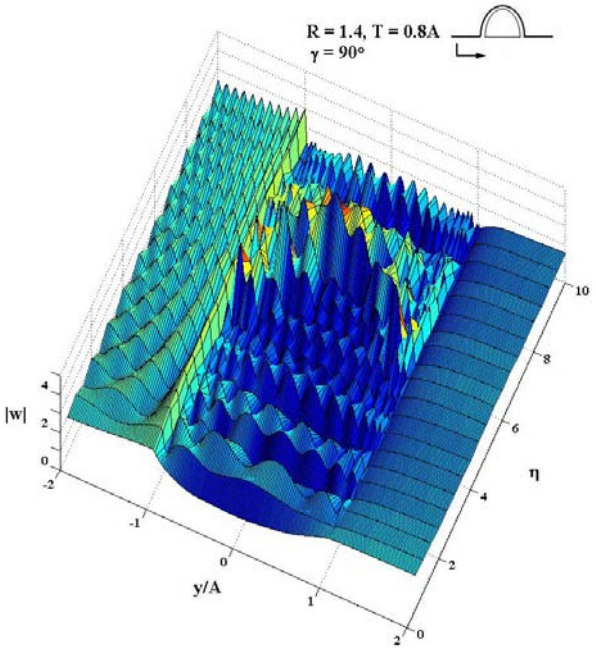

Figure 8.34: Displacement Amplitude for $R = 1.6$, $T = 0.2A$ when $\gamma = 0°$

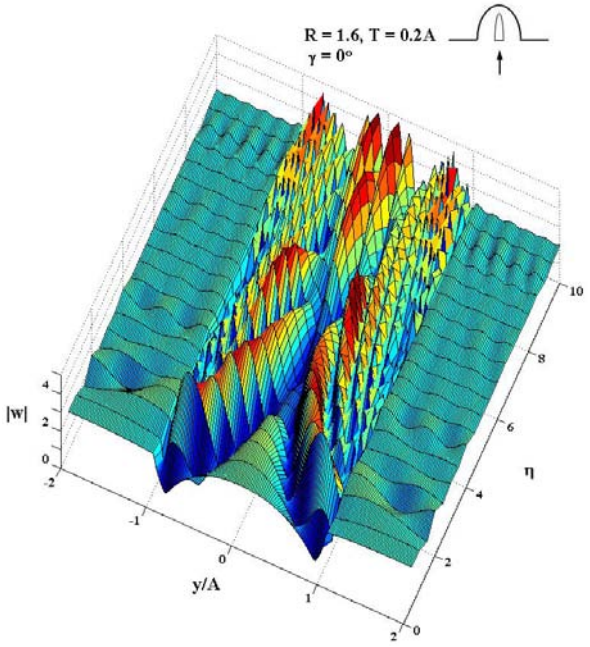


Figure 8.35: Displacement Amplitude for $R = 1.6$, $T = 0.2A$ when $\gamma = 30°$

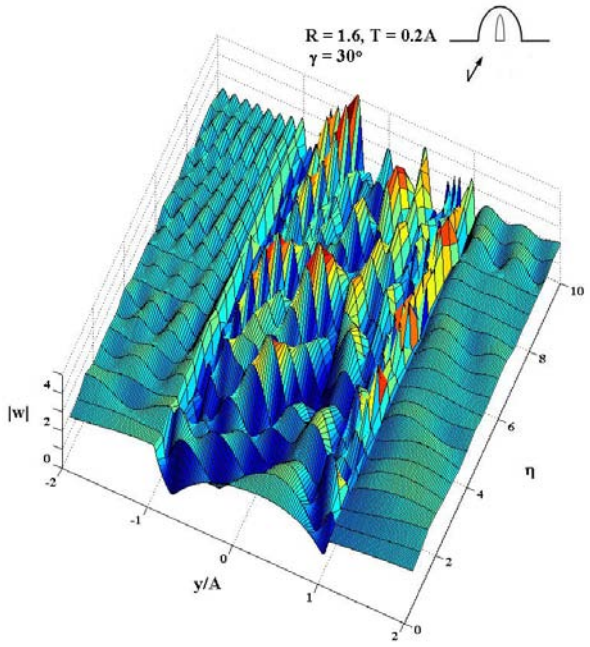

Figure 8.36: Displacement Amplitude for $R = 1.6$, $T = 0.2A$ when $\gamma = 60°$

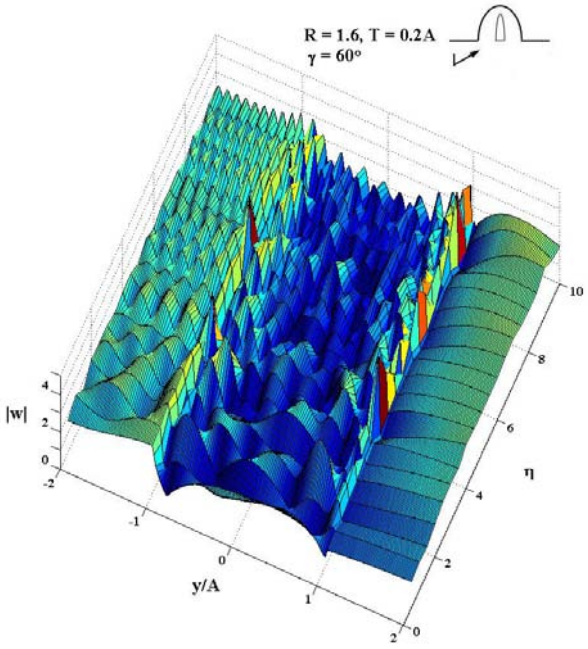


Figure 8.37: Displacement Amplitude for $R = 1.6$, $T = 0.2A$ when $\gamma = 90°$

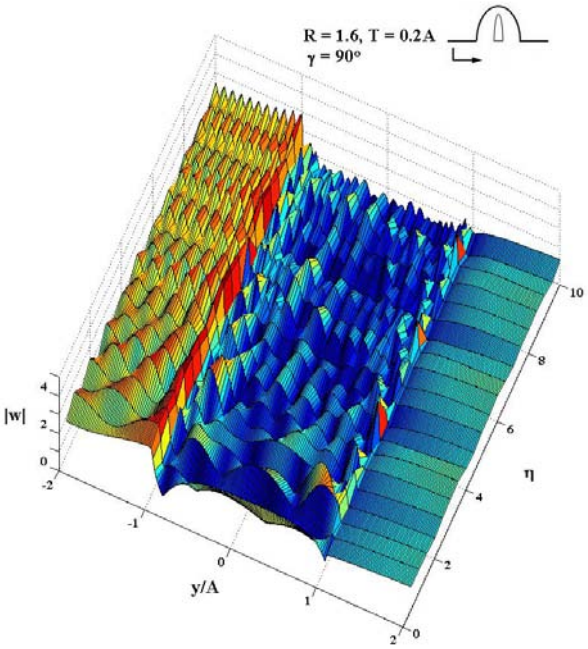

Figure 8.38: Displacement Amplitude for $R = 1.6$, $T = 0.5A$ when $\gamma = 0°$

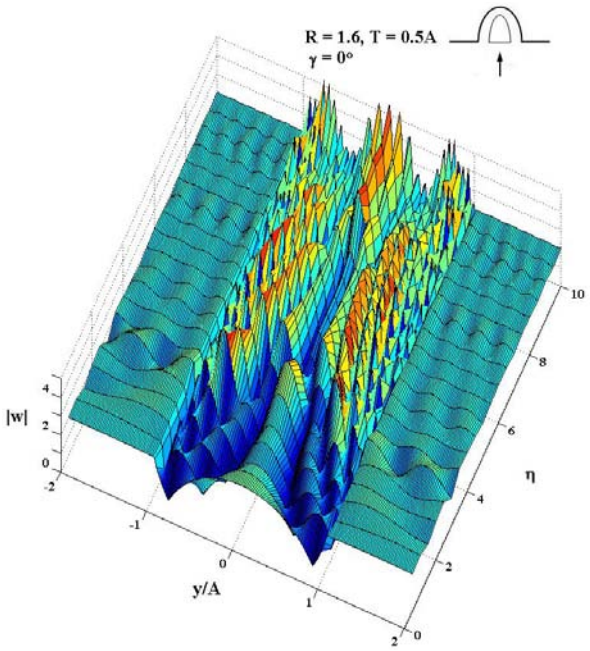


Figure 8.39: Displacement Amplitude for $R = 1.6$, $T = 0.5A$ when $\gamma = 30°$

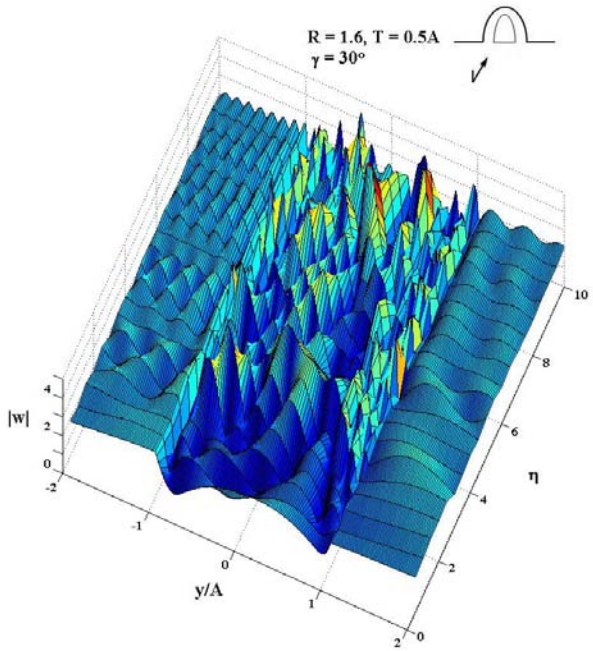

Figure 8.40: Displacement Amplitude for $R = 1.6$, $T = 0.5A$ when $\gamma = 60°$

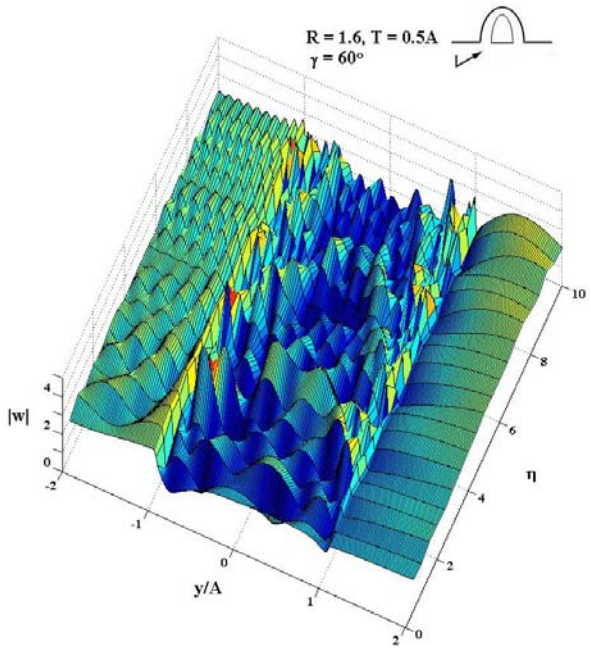


Figure 8.41: Displacement Amplitude for $R = 1.6$, $T = 0.5A$ when $\gamma = 90°$

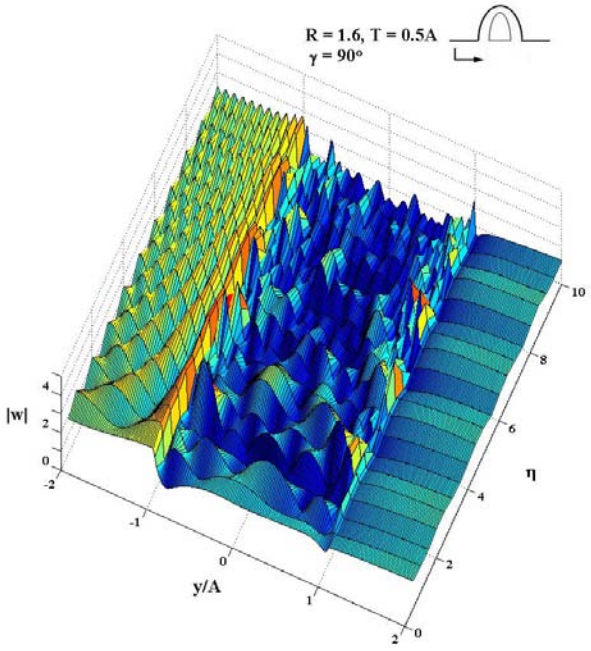

Figure 8.42: Displacement Amplitude for $R = 1.6$, $T = 0.8A$ when $\gamma = 0°$

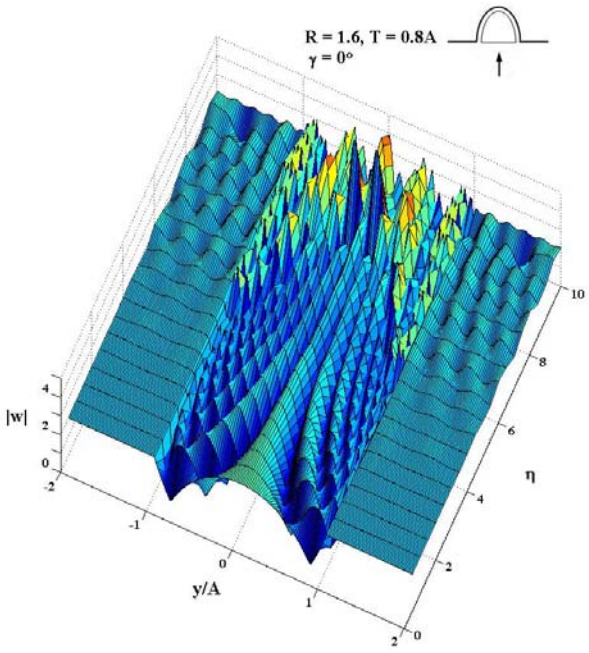


Figure 8.43: Displacement Amplitude for $R = 1.6$, $T = 0.8A$ when $\gamma = 30°$

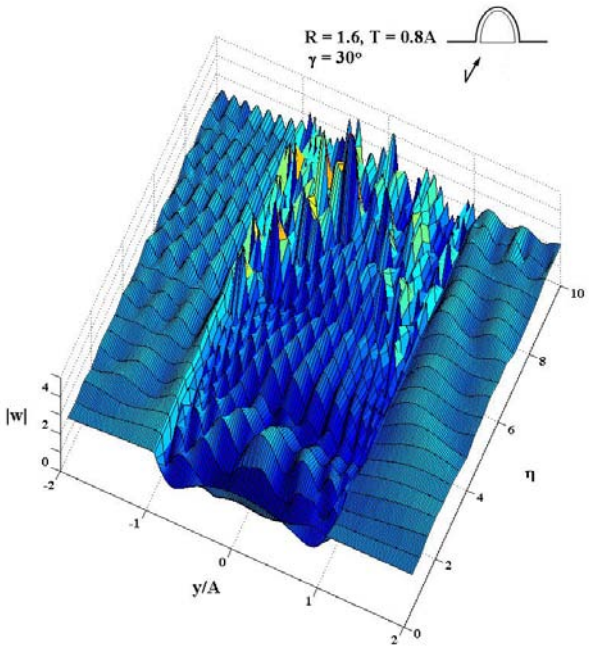

Figure 8.44: Displacement Amplitude for $R = 1.6$, $T = 0.8A$ when $\gamma = 60°$

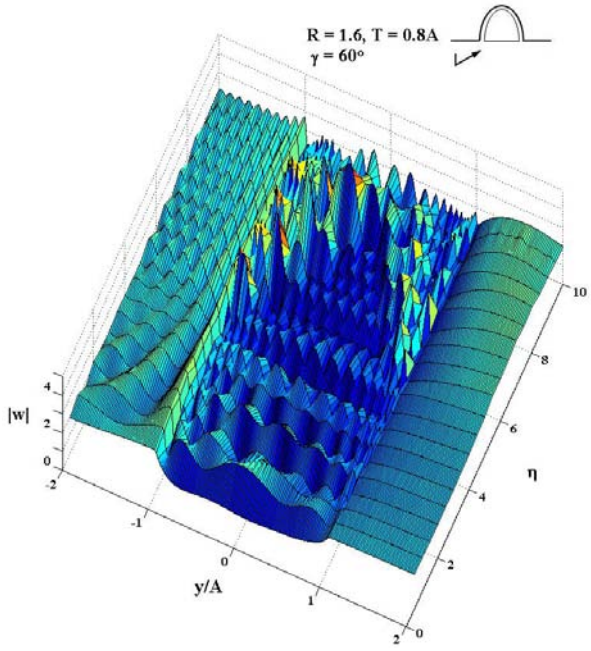


Figure 8.45: Displacement Amplitude for $R = 1.6$, $T = 0.8A$ when $\gamma = 90°$

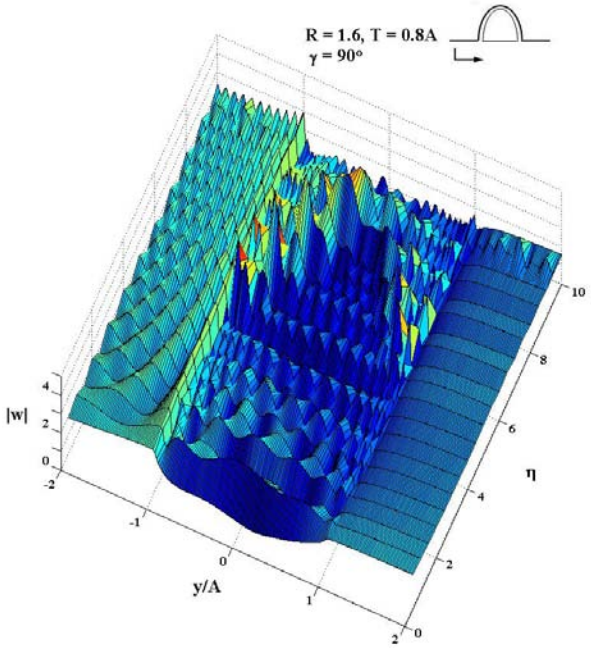

After observing previous three-dimensional plots, we found out the identical characteristics to results shown in previous chapters. Surface displacements are getting more complex as the incident waves become shorter. Moreover considering the semi-elliptical tunnel $T = 0.8A$ with nearly grazing angles, again similar behaviors to the full-elliptical tunnel are monitored; the surface displacement of points on a hill, which seems to be smaller while the dimensionless frequency $\eta$ gets larger, rapidly rises at $\eta$ equal to 5 and again lessens continuously as $\eta$ becomes larger.

# CHAPTER 9:SUMMARY

Various two-dimensional hill models subjected to incident plane SH wave have been investigated so far within the framework of linear elasto-dynamic theory. Solutions are based on the analytical approach called the method of wave function expansions. As geometric boundaries are either linear or elliptical, wave function expansion in form of Mathieu functions provides mathematical simplicity to be implemented and meet the requirements of analytical expression for free or continuity boundary conditions. Moreover similar wave functions were reappeared in several models such as the scattered and transmitted waves.

In contrast to canyon and valley models (Wong and Trifunac, 1974**a;b**) conventional approach suggested by Pao and Mow (1973) is not able to solve for unknowns arisen during mathematical implementation of the hill model since it involves the consideration of a mixed boundary conditions; the traction-free boundary condition at the surface of the elliptical hill and the continuity of displacement and stress at the semi-elliptical interface. However by the utilization of the angular half-range expansion technique, all correspondent displacement and stress functions are in the proper form and boundary conditions are convenient to apply by utilizing the orthogonality of angular Mathieu functions; implementation of shallow semi-elliptical hill requires the half-range expansion of elliptical sine as a series of elliptical cosine, whereas of deep semi-elliptical hill

engages the half-range expansion of Odd elliptical cosine as a series of Even elliptical cosine and the half-range expansion of Even elliptical sine as a series of Odd elliptical sine.

The existence of a hill results in complex pattern of surface displacement which becomes progressively more complicated as an semi-elliptical hill gets steeper. Moreover for nearly grazing angle ($\gamma = 0°$ and $30°$) the hill acts like a barrier shielding the propagating waves coming from the left, resulting in a standing wave pattern in the front of the hill and the focusing of the amplitude at the right edge of the hill, $x/A = 1$ or $y/A = 1$. While possibly maximum amplitudes of surface displacement for the horizontal angles of incidence are about 4, the maximum amplitudes of 5 or larger are perhaps monitored for vertical incidence.

The presence of the concentric tunnels has significant effect on the amplitude of ground motion. In general the presence of the tunnels lessens maximum values of ground displacement. The shielding effect of tunnel becomes much stronger and the standing waves on the left-side become more prominent as the tunnel is getting larger; amplitudes of ground motion in the neighborhood of unity or less may be monitored without the abrupt jump at the right edge when the incoming waves is nearly horizontal. Normally the presence of a concentric tunnel amplifies maximum displacement by 30%-70% from corresponding value of reference (inexistence of a tunnel) for the horizontal incidence, while de-amplifies

maximum displacement in the range of 1%-15% for the vertical incidence. It could be said that the hinder efficiency of an elliptical tunnel depends on the direction of wave passage; the tunnel becomes better obstruction when the incident wave is perpendicular to its major axis.

The interference of the semi-elliptical tunnel on ground surface motion is different from of full-elliptical one. For nearly grazing angle, incident waves are able to slip underneath semi-tunnels. The weaker standing wave on the left side and weaker shadow zone on the right end of the hill are observed; the associated high jumps of the displacement amplitude at the right edge of the hill are also detected. However there is interesting point to be mentioned. At 30° angle of incidence with the dimensionless parameter $\eta$ equals to 5, the presence of semi-elliptical tunnel yields the same effect as of full-elliptical tunnel; the discrepancy of their maximum amplitudes of surface displacement is within 5%, except $R = 1.6$. When the incident waves are nearly vertical, we noticed the stronger shielding effect due to semi-elliptical tunnels than to full-elliptical ones. Furthermore bigger tunnel provides the stronger shielding effect. The presence of tunnel with $T = 0.8A$ de-amplifies maximum displacement by 20%-50% from corresponding values with $T = 0.2A$.

Even though in the frame work of this study we dealt with only incident plane SH wave, the mathematical techniques may be successfully applied to various

incident P- or SV-wave. Normally P or SV-waves, which are coupling by their nature when reflected or refracted at free surface or interface between two different mediums, involve more complex boundary conditions.

# BLIBIOGRAPHY

Abramowitz, M., and Stegun, I.A. (1972). *Handbook of mathematical functions, with formulas, graphs, and mathematical tables*, Dover Publications, Inc., New York.

Achenbach, J.D. (1999). *Wave Propagation in Elastic Solids*, North-Holland, New York.

Alcock, E.D. (1969). *The Influence of Geologic Environment on Seismic Response,* Bulletin of the Seismological Society of America, 59(1), 245-268.

Bisward, N.N., and Knopoff, L. (1970). *Exact Earth-Flattening Calculation for Love Waves*, Bulletin of the Seismological Society of America, 60(4), 1123-1137.

Borcherdt, R.D. (1970). *Effects of local geology on ground motion near San Francisco Bay*, Bulletin of the Seismological Society of America, 60(1), 29-61.

Cao, H., and Lee, V.W. (1989). *Scattering of Plane SH Waves by Circular Cylindrical Canyons with Variable Depth-to-Width Ratio*, European Journal of Earthquake Engineering, III(2), 29-37.

Cao, H., and Lee, V.W. (1990). *Scattering and Diffraction of Plane P Waves by Circular Cylindrical Canyons with Variable Depth-to-Width Ratio*, International Journal of Soil Dynamics and Earthquake Engineering, 9(3), 141-150.

Clayton, R., and Engquist, B. (1977). *Absorbing Boundary Conditions for Acoustic and Elastic Wave Equations*, Bulletin of the Seismological Society of America, 67(6), 1529-1540.

Cohen, M., and Jennings, P.C. (1983). *Silent Boundary method for Transient Analysis*, *in Computational Methods for Transient Analysis*, North Holland, Amsterdam, 301-357.

Emerman, S. H., and Stephen, R.A. (1983). *Comment on "Absorbing Boundary Conditions for Acoustic and Elastic Wave Equation," by R. Clayton and B. Engquist*, Bulletin of the Seismological Society of America, 73(2), 661-665.

Ewing, W.M., Jardetzky, W. S., and Press, F. (1957). *Elastic Waves in Layered Media*, McGraw-Hill Book Company, Inc.

Fu, L., and Bouchon, M. (2004). *Discrete Wavenumber Solutions to Numerical Wave Propagation in Piecewise Heterogeneous Media-I. Theory of Teo-Dimensional SH Case*, Geophysical Journal International, 157(2), 481-498.

Fuyuki, M., and Matsumoto, Y. (1980). Finite Difference Analysis of Rayleigh Wave Scattering at a Trench, Bulletin of the Seismological Society of America, 70(6), 2051-2069.

Gilbert, F., and Knopoff., K. (1960). *Seismic Scattering from Topographic Irregularities,* Journal of Geophysical Research, 65(10), 3437–3444.

Graff, K.F. (1975). *Wave Motion in Elastic Solids*, Oxford University Press, Dover Publications, Inc., New York, New York.

Griffiths, D.W., and Bollinger, G.A. (1979). *The Effect of the Appalachian Mountain Topography on Seismic Waves*, Bulletin of the Seismological Society of America, 69(4), 1081-1105.

Gutenberg, B. (1957). *Effect of Ground on Earthquake Motion*, Bulletin of the Seismological Society of America, 47(3), 221-250.

Hayir, A., Todorovska, and M.I., Trifunac, M.D. (2001). *Antiplane Response of a Dike with Flexible Soil-Structure Interface to Incident SH Waves*, Soil Dynamics and Earthquake Engineering, 21(7), 603-613.

Hill, D.P. (1972). *An Earth-Flattening Transformation for Wave from Point Source*, Bulletin of the Seismological Society of America, 62(5), 1195-1210.

Hudson, D.E. (1972). *Local Distribution of Strong Earthquake Ground Motion*, Bulletin of the Seismological Society of America, 62(6), 1765-1786.

Jian-wen, L., Lin-jun, Y., and Lee, V.W. (2001). *Scattering of Plane P Waves by Circular-Arc Layered Alluvial Valleys: an Analytical Solution*, ACTA Seismologica Sinica, 14(2), 176-195.

Jian-wen, L., Hao, L., and Lee, V.W. (2004). *Scattering of Plane SH Waves by a Circular-Arc Hill with a Circular Tunnel*, ACTA Seismologica Sinica, 17(5), 549-563.

Kanai, K. (1950). *The Effect of Solid Viscosity of Surface Layer on the Earthquake Movement*, Earthquake Research Institute, Vol. XXVIII, 31-35.

Kanai, K., and Yoshizawa, S. (1953). *Relation between the Amplitude of Earthquake Motions and the Nature of Surface Layer. III.,* Earthquake Research Institute, Vol. XXXI, 275-279.

Kanai, K. and Suzuki, T. (1953). *Relation between the Property of Building Vibration and the Nature of Ground (Observation of Earthquake Motion at Actual Buildings.),* Earthquake Research Institute, Vol. XXXI, 305-316.

Kanai, K., Suzuki, T., and Yoshizawa, S. (1955). *Relation between the Property of Building Vibration and the Nature of Ground (Observation of Earthquake Motion at Actual Buildings.),* Earthquake Research Institute, Vol. XXXIV, 61-86.

Kanai, K., Tanaka, T., and Yoshizawa, S. (1958). *Comparative Studies of Earthquake Motions on the Ground and Underground (Multiple Reflection Problem),* Bulletin of the Earthquake Research Institute, Vol. 37, 53-87.

Kawase, H. (1988). *Time-Domain Response of a Semi-Circular Canyon for Incident SV, P, and Rayleigh Waves Calculated by the Discrete Wavenumber Boundary Element Method*, Bulletin of the Seismological Society of America, 78(4), 1415-1437.

Kreyszig, E., (1983). *Advanced Engineering Mathematics*, 5th Edition, Wiley, New York.

Lebedev, L.P., and Cloud, M.J. (2003). *Tenser Analysis*, World Scientific Publishing Co. Pte. Ltd., Singapore.

Lee, V.W., and Cao, H. (1989). *Diffraction of SV Waves by Circular Cylindrical Canyons of Various Depths*, Journal of Engineering Mechanics, ASCE, 115(9), 2035-2056.

Lee, V.W., Luo, H., and Liang, J.W. (2004). *Diffraction of Anti-Plane SH Waves by a Semi-Circular Cylindrical Hill with an Inside Semi-Circular Concentric Tunnel*, Earthquake Engineering and Engineering Vibration, 3(2), 249-262.

Lee, V.W., Luo, H., and Liang, J.W. (2006). *Anti-Plane (SH) Waves Diffraction by a Semi-Circular Cylindrical Hill Revisited: An Improved Accurate Wave Series Analytic Solution*, Journal of Engineering Mechanics, ASCE, 132(10), 1106-1114.

McLachlan, N.W. (1947). *Theory and Application of Mathieu Functions*, Oxford University Press, England.

Meixner, J., and Schäfke, F.W. (1954). *Mathieusche Funktionen und Sphäroidfunktionen*, Springer-Verlag, Berlin.

Milne, J. (1880). *The Earthquake in Japan of February 22nd, 1880*, Transactions of the Seismological Society of Japan Vol. I Part II, 1-116.

Moeen-Vaziri, N., Trifunac, M.D. (1981). *A Note on the Vibrations of a Semi-Circular Canal Excited by Plane SH-Wave*, Bull. ISET, 18(2), 88-100.

Moeen-Vaziri, N., Trifunac, M.D. (1985). *Scattering of Plane SH-Waves by Cylindrical Canals of Arbitrary Shape*, Soil Dynamics and Earthquake Engineering, 4(1), 18-23.

Moeen-Vaziri, N., Trifunac, M.D. (1988**a**). *Scattering and Diffraction of Plane SH-Waves by Two-Dimensional Inhomogeneities: Part I*, Dynamics and Earthquake Engineering, 7(4), 179-188.

Moeen-Vaziri, N., Trifunac, M.D. (1988**b**). *Scattering and Diffraction of Plane P and SV Waves by Two-Dimensional Inhomogeneities: Part II*, Dynamics and Earthquake Engineering, 7(4), 189-200.

Morse, M.P., and Feshbach, H. (1953). *Methods of Theorethical Physics: Part I and II***,** McGraw-Hill, New York.

Mostaghel, N., and Nowroozi, A.A. (1975). *Earthquake Response of hills***,** Bulletin of the Seismological Society of America, 65(6), 1733 - 1742.

Pao, Y.-H, and Mow, C.C. (1973). *Diffraction of Elastic Waves and Dynamics Stress Concentrations.* Crane, Russak & Company Inc., New York, N.Y.

Qiu, F.-Q, and Liu, D.-K. (1993). *Antiplane Response of Isosceles Triangular Hill to Incident SH Waves*, Earthquake Engineering and Engineering Vibration, 4(1), 37-46.

Sánchez-Sesma, F.J. (1985). *Diffraction of Elastic SH Waves by Wedges*, *Bulletin of the Seismological Society of America,* 75(5), 1435-1446.

Sánchez-Sesma, F.J., Herrera, I., and Avilés (1982). *A Boundary Method for Elastic Wave Diffraction: Application to Scattering of SH-Waves by Surface Irregularities*, *Bulletin of the Seismological Society of America,* 72(2), 473-490.

Todorovska, M.I., and Lee, V.W. (1990). *A Note on Response of Shallow Circular Valleys to Rayleigh Waves: Analytical Approach*, Earthquake Engineering and Engineering Vibration, 10(1), 21-34.

Todorovska, M.I., and Lee, V.W. (1991**a**). *A Note on Scattering of Rayleigh Waves by Shallow Circular Canyons: Analytical Approach*, Bull. Ind. Soc. Earth. Tech., 28(2), 1-26.

Todorovska, M.I., and Lee, V.W. (1991**b**). *Surface Motion of Shallow Circular Alluvial Valleys for Incident Plane SH Waves - Analytical Solution*, International Journal of Soil Dynamics and Earthquake Engineering, 10(4), 192-200.

Todorovska, M.I., Hayir, A., and Trifunac, M.D. (2001). *Antiplane Response of A Dike on Flexible Embedded Foundation to Incident SH-waves*, Soil Dynamics and Earthquake Engineering, 21(7), 593-601.

Trifunac, M.D. (1971). *Surface Motion of a Semi-Cylindrical Alluvial Valley for Incident Plane SH Wave*. Bulletin of Seismological and Society of America, 61(6), 1755-1770.

Trifunac, M.D. (1973). *Scattering of Plane SH Wave by a Semi-Cylindrical Canyon*. Earthquake Engineering and Structural Dynamics, 1(3), 267-281.

Tsai, N. C. (1969). *Influence of Local Geology on Earthquake Ground Motion,* Ph.D. degree Dissertation, California Institute of Technology, Pasadena.

Watson, G.N. (2006). *A Treatise on the Theory of Bessel Functions*, 2nd Edition, Cambridge University Press, New York.

Wolf, J. P., and Song, S. (1996). Finite *Element Modeling of Unbounded Media*, John Wiley&Sons Ltd., Chichester.

Wong, H.L., and Trifunac, M.D. (1974**a**). *Surface Motion of a Semi-Elliptical Alluvial Valley for Incident Plane SH Waves*, Bulletin of the Seismological Society of America, 64(5), 1389-1408.

Wong, H.L., and Trifunac, M.D. (1974**b**). *Scattering of Plane SH Waves by a Semi-Elliptical Canyon*, Earthquake Engineering and Structural Dynamics, 3(2), 157-169.

Yuan, X., and Men, F.L. (1992). *Scattering of Plane SH Waves by a Semi-Cylindrical Hill*, Earthquake Engineering and Structural Dynamics, 21(12), 1091-1098.

Yuan, X., and Liao, Z.P. (1994). *Scattering of Plane SH Waves by a Cylindrical Canyon of Circular-Arc Cross-Section*, Soil Dynamics and Earthquake Engineering, 13(6), 407-412.

Yuan, X., and Liao, Z.P. (1996). *Surface Motion of a Cylindrical Hill of Circular-Arc Cross-Section for Incident Plane SH Waves*, Soil Dynamics and Earthquake Engineering, 15(3), 189-199.

Zienkiewicz, O. C. and Taylor, R. L. (2000). *The Finite Element Method Volume.1*, 5th Ed., Butterworth-Heinemann, Oxford

# APPENDIX A: GREEN'S FUNCTIONS

Green's function is very useful mathematics which helps us to expand the line source and plane waves into a series of functions. Green's function is the solution of the inhomogeneous Helmholtz equation with a unit point source at $\mathrm{r}'$.

$$\nabla^2 G(r;\mathrm{r}') + k^2 G(r;\mathrm{r}') = -4\pi\delta(r-\mathrm{r}') \tag{A.1}$$

For any orthogonal curvilinear coordinate system Green's function can be expressed as follows (Morse and Feshbach, 1953)

$$G(\tilde{r};\tilde{r}') = -4\pi\left(\frac{h_1}{h_2 h_3}\right)\rho(\xi_2',\xi_3')\sum_n \bar{W}_n(\xi_2',\xi_3')\,W_n(\xi_2\ ,\xi_3\ ) \cdot\frac{1}{\Delta(y_{1n},y_{2n})}\begin{cases} y_{1n}(\xi_1\ )y_{2n}(\xi_1'); & \xi_1\ \le \xi_1' \\ y_{1n}(\xi_1')y_{2n}(\xi_1\ ); & \xi_1' < \xi_1 \end{cases} \tag{A.2}$$

where $h_i$ is a scale factor, $\Delta(y_{1n},y_{2n})$ is the Wronskian of solutions $y_{1n}$ and $y_{2n}$ to homogeneous Helmholtz equation, $\sigma$ is a weight function, and $W_n$ is a complete set of Eigen functions satisfying orthonormal condition

$$\iint \bar{W}_m(\xi_2\ ,\xi_3\ )W_n(\xi_2\ ,\xi_3\ )\sigma(\xi_2\ ,\xi_3\ )d\xi_2 d\xi_3 = \delta_{mn} \tag{A.3}$$

In circular cylindrical coordinate system (see Figure A.1), the source is located at $(r',\theta')$ while the observation point is located at $(r,\theta)$. Then we have $\xi_1 = r$, $\xi_2 = \theta$, $\xi_3 = z$, $h_1 = h_3 = 1$, and $h_2 = r$. In addition without further proof we can define the complete set of Eigenfunctions as $e^{in\theta}/\sqrt{2\pi}$ with $\sigma = 1$. The solutions to homogeneous Helmholtz may be ones of Bessel or Hankel functions; the boundary conditions determine which functions are to be employed. Since at

$r = 0$ function must be finite, and at $r' = 0$ function must be singular due to the diverging behavior of source, $y_{1n} = J_n(kr)$ and $y_{2n} = H_n^{(1)}(kr)$. Hence Equation (A.3) becomes

$$G(r;\mathrm{r}') = \left(\frac{-2}{r}\right)\sum_n (cos\, n\theta' - isin\, n\theta')\,(cos\, n\theta + isin\, n\theta) \cdot \frac{1}{\Delta(y_{1n},y_{2n})}\begin{cases} J_n(kr)\, H_n^{(1)}(kr')\,;\ r \le r' \\ J_n(kr')H_n^{(1)}(kr)\ ;\ r' < r \end{cases} \tag{A.4}$$

Since the Wronskian must also be satisfied for each term of asymptotic series. By utilizing the asymptotic behavior of Bessel function and Hankel function of the first kind (Watson, 1995)

$$\begin{aligned} \lim_{r\to\infty} J_n\,(kr) &= \sqrt{\frac{2}{\pi kr}}\, cos\left(kr - \frac{\pi}{4} - \frac{n\pi}{2}\right) \\ \lim_{r\to\infty} H_n^{(1)}(kr) &= \sqrt{\frac{2}{\pi kr}}\, exp\left(kr - \frac{\pi}{4} - \frac{n\pi}{2}\right) \end{aligned} \tag{A.5}$$

the Wronskian asymptotically becomes $2i/\pi r$. Green's function becomes

$$G(r;\mathrm{r}') = \pi i \sum_n e^{in(\theta-\theta')}\begin{cases} J_n(kr)\, H_n^{(1)}(kr')\,;\ r \le r' \\ J_n(kr')H_n^{(1)}(kr)\ ;\ r' < r \end{cases} \tag{A.6}$$

Next Green's function may be expressed as follows

$$G(r;\mathrm{r}') = \pi i H_0^{(1)}(kR) \tag{A.7}$$

where $r, r'$ and $R$ are shown below in the following figure.

Comparing Equations (A.6) with (A.7), an expansion of Hankel function of the first kind with zero order becomes

$$H_0^{(1)}(kR) = \sum_n e^{in(\theta-\theta')}\begin{cases} J_n(kr)\, H_n^{(1)}(kr')\,;\ r \le r' \\ J_n(kr')H_n^{(1)}(kr)\ ;\ r' < r \end{cases} \tag{A.8}$$

Figure A.1: Line Source in x-y Plane

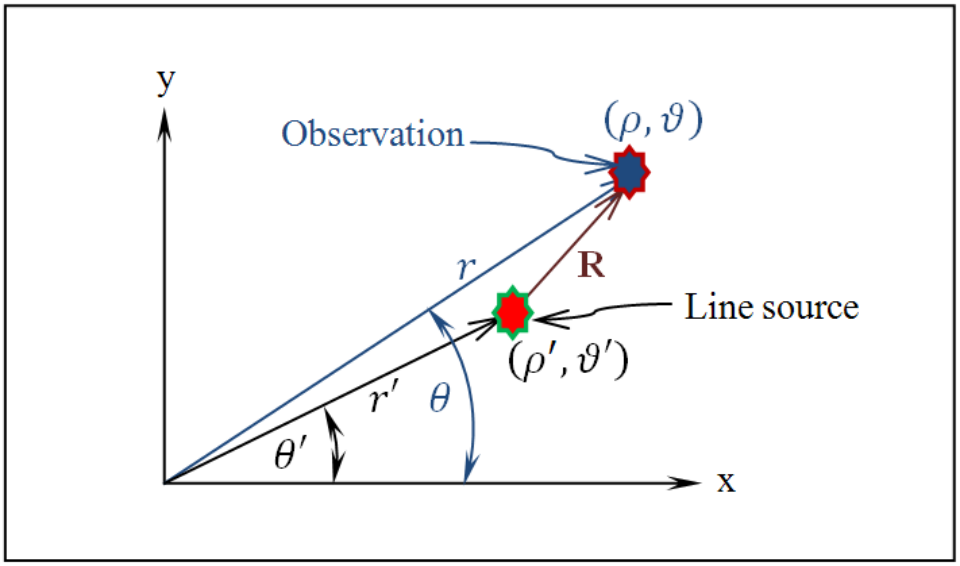


Equation (A.8) can verify easily as we let $r' \to 0$; only Bessel function of order zero in the series exists and equals unity. In addition this equation can be considered as one form of Graf's addition formula. (Graff, 1975)

In elliptical cylindrical coordinate system (see Figures 2.1 and A.1), the source is located at $(\rho', \vartheta')$ while the observation point is located at $(\rho, \vartheta)$. Next we have $\xi_1 = \rho$, $\xi_2 = \vartheta$, $\xi_3 = z$, $h_1 = h_2 = a\sqrt{sinh^2\rho + sin^2\vartheta}$, and $h_3 = 1$. The appropriate Eigenfunctions that we can utilize in this case must be in the form of $ce_n(\vartheta, q)$ and $se_n(\vartheta, q)$. However Equation (A.3) must be satisfied in order to implement Equation (A.2). Then the normalized factor for those Mathieu functions become $\pi$ as Equation (2.13). Later the complete set of Eigenfunctions is $\{ce_n(\vartheta, q)/\sqrt{\pi},\ se_n(\vartheta, q)/\sqrt{\pi}\}$.

Analogically to circular case, we can take

$$y_{1n} = \begin{cases} Mc_n^{(1)}(\rho, q) \\ Ms_n^{(1)}(\rho, q) \end{cases}$$
$$y_{2n} = \begin{cases} Mc_n^{(3)}(\rho, q) \\ Ms_n^{(3)}(\rho, q) \end{cases} \tag{A.9}$$

Similar to previous section, the Wronskian must also be satisfied for each term of asymptotic series. By utilizing the asymptotic behavior of Modified Mathiue functions (Mow and Pao, 1971; Mechel, 1997) as follows

$$\lim_{\rho\to\infty} Mc_n^{(1)}(\rho, q) = \sqrt{\frac{2}{\pi a \cosh\rho}} cos\left(a\cosh\rho - \frac{\pi}{4} - \frac{n\pi}{2}\right)$$
$$\lim_{\rho\to\infty} Ms_n^{(1)}(\rho, q) = (-1)^n \sqrt{\frac{2}{\pi a \cosh\rho}} cos\left(a\cosh\rho - \frac{\pi}{4} + \frac{n\pi}{2}\right)$$
$$\lim_{\rho\to\infty} Mc_n^{(3)}(\rho, q) = \sqrt{\frac{2}{\pi a \cosh\rho}} e^{i\left(a\cosh\rho - \frac{\pi}{4} - \frac{n\pi}{2}\right)} \tag{A.10}$$
$$\lim_{\rho\to\infty} Ms_n^{(3)}(\rho, q) = (-1)^n \sqrt{\frac{2}{\pi a \cosh\rho}} e^{i\left(a\cosh\rho - \frac{\pi}{4} + \frac{n\pi}{2}\right)}$$

the Wronskian asymptotically becomes $2i/\pi$. Hence Green's function becomes

$$G(r; \mathrm{r}') = 2\pi i \left\{ \sum_{n=0}^{\infty} ce_n(\vartheta', q) ce_n(\vartheta, q) \begin{cases} Mc_n^{(1)}(\rho, q) Mc_n^{(3)}(\rho', q)\ ;\ \rho \le \rho' \\ Mc_n^{(1)}(\rho', q) Mc_n^{(3)}(\rho, q)\ ;\ \rho' < \rho \end{cases} \right.$$
$$\left. + \sum_{n=1}^{\infty} se_n(\vartheta', q) se_n(\eta, q) \begin{cases} Ms_n^{(1)}(\rho, q) Ms_n^{(3)}(\rho', q)\ ;\ \rho \le \rho' \\ Ms_n^{(1)}(\rho', q) Ms_n^{(3)}(\rho, q)\ ;\ \rho' < \rho \end{cases} \right\} \tag{A.11}$$

Later we can transform the line source function into elliptical cylindrical coordinate as follows

$$H_0^{(1)}(kR) = 2 \left\{ \sum_{n=0}^{\infty} ce_n(\vartheta', q) ce_n(\vartheta, q) \begin{cases} Mc_n^{(1)}(\rho, q) Mc_n^{(3)}(\rho', q)\ ;\ \rho \le \rho' \\ Mc_n^{(1)}(\rho', q) Mc_n^{(3)}(\rho, q)\ ;\ \rho' < \rho \end{cases} \right.$$
$$\left. + \sum_{n=1}^{\infty} se_n(\vartheta', q) se_n(\eta, q) \begin{cases} Ms_n^{(1)}(\rho, q) Ms_n^{(3)}(\rho', q)\ ;\ \rho \le \rho' \\ Ms_n^{(1)}(\rho', q) Ms_n^{(3)}(\rho, q)\ ;\ \rho' < \rho \end{cases} \right\} \tag{A.12}$$

# APPENDIX B: IDENTITIES OF TRIGONOMETRIC AND ANGULAR-MATHIEU INTEGRALS

Given $\varepsilon_m = \begin{cases} 1 \ ; \ m = 0 \\ 2 \ ; \ m > 0 \end{cases}$ and $\delta_{mn} = \begin{cases} 1 \ ; \ n = m \\ 0 \ ; \ n \neq m \end{cases}$, then identities of trigonometric and angular-Mathieu integrals can be proved as follows

(B.1) $\int_0^{\pi} \sin m\theta \cos n\theta \, d\theta = \frac{2m}{m^2-n^2}$ when $m + n =$ odd

$$\int_0^{\pi} \sin m\theta \cos n\theta \, d\theta = \int_0^{\pi} \frac{[\sin(m+n)\theta + \sin(m-n)\theta]}{2} d\theta$$

$$= -\frac{1}{2}\left[\frac{cos(m+n)\theta}{m+n} + \frac{cos(m-n)\theta}{m-n}\right]\Big|_0^{\pi}$$

$$= \frac{2m}{m^2-n^2}$$

(B.2) $\int_{-\pi/2}^{\pi/2} \cos(2m+1)\theta \cos 2n\theta \, d\theta = \frac{(-1)^{m-n}}{2m-2n+1} + \frac{(-1)^{m+n}}{2m+2n+1}$ when $m, n = 0,1,2, \ldots$

$$\int_{-\pi/2}^{\pi/2} \cos(2m+1)\theta \cos 2n\theta \, d\theta = \int_{-\pi/2}^{\pi/2} \frac{[\cos(2m-2n+1)\theta + \cos(2m+2n+1)\theta]}{2} d\theta$$

$$= \int_0^{\pi/2} [\cos(2m-2n+1)\theta + \cos(2m+2n+1)\theta] \, d\theta$$

$$= \left(\frac{sin(2m-2n+1)\theta}{2m-2n+1} + \frac{sin(2m+2n+1)\theta}{2m+2n+1}\right)\Big|_0^{\pi/2}$$

$$= \frac{(-1)^{m-n}}{2m-2n+1} + \frac{(-1)^{m+n}}{2m+2n+1}$$

(B.3) $\int_{-\pi/2}^{\pi/2} \sin(2m+2)\theta \sin(2n+1)\theta \, d\theta = \frac{(-1)^{m-n}}{2m-2n+1} + \frac{(-1)^{m+n}}{2m+2n+3}$ when $m, n = 0,1,2, \ldots$

$$\int_{-\pi/2}^{\pi/2} \sin(2m+2)\theta \sin(2n+1)\theta \, d\theta = \int_{-\pi/2}^{\pi/2} \frac{[\cos(2m-2n+1)\theta - \cos(2m+2n+3)\theta]}{2} d\theta$$

$$= \int_0^{\pi/2} [\cos(2m-2n+1)\theta - \cos(2m+2n+3)\theta] \, d\theta$$

$$= \left( \frac{sin(2m-2n+1)\theta}{2m-2n+1} - \frac{sin(2m+2n+3)\theta}{2m+2n+3} \right) \Big|_0^{\pi/2}$$

$$= \frac{(-1)^{m-n}}{2m-2n+1} + \frac{(-1)^{m+n}}{2m+2n+3}$$

(B.4) $\int_0^{\pi} ce_n(\vartheta, q) ce_m(\vartheta, q) \, d\vartheta = \frac{\pi}{2} \delta_{mn}$ when $m, n = 0,1,2, \ldots$

Since $ce_n(\vartheta, q) ce_m(\vartheta, q)$ is even function, then it is symmetric about 0; we obtain

$$\int_0^{\pi} ce_n(\vartheta, q) ce_m(\vartheta, q) \, d\vartheta = \frac{1}{2} \int_{-\pi}^{\pi} ce_n(\vartheta, q) ce_m(\vartheta, q) \, d\vartheta;$$

$$= \frac{1}{2} \int_0^{2\pi} ce_n(\vartheta', q) ce_m(\vartheta', q) \, d\vartheta'; \; \vartheta' = \vartheta + \pi$$

$$= \frac{\pi}{2} \delta_{mn}$$

(B.5) $\int_0^{\pi} se_n(\vartheta, q) se_m(\vartheta, q) \, d\vartheta = \frac{\pi}{2} \delta_{mn}$ when $m, n = 1,2,3, \ldots$

Since $se_n(\vartheta, q) se_m(\vartheta, q)$ is even function, then it is symmetric about 0; we obtain

$$\int_0^{\pi} se_n(\vartheta, q) se_m(\vartheta, q) \, d\vartheta = \frac{1}{2} \int_{-\pi}^{\pi} se(\vartheta, q) se_m(\vartheta, q) \, d\vartheta$$

$$= \frac{1}{2} \int_0^{2\pi} se_n(\vartheta', q) se_m(\vartheta', q) \, d\vartheta'; \; \vartheta' = \vartheta + \pi$$

$$= \frac{\pi}{2} \delta_{mn}$$

(B.6) $\int_{-\frac{\pi}{2}}^{\frac{\pi}{2}} ce_{2n}(\vartheta,q)ce_{2m}(\vartheta,q)\,d\vartheta = \frac{\pi}{2}\delta_{mn}$ when $m,n = 0,1,2,\ldots$

Since $ce_{2n}(\eta,q)$ is symmetric about 0 and $\pi/2$ (McLachlan, 1974), hence

$$\int_{-\frac{\pi}{2}}^{\frac{\pi}{2}} ce_{2n}(\vartheta,q)ce_{2m}(\vartheta,q)\,d\vartheta = 2\int_{0}^{\frac{\pi}{2}} ce_{2n}(\vartheta,q)ce_{2m}(\vartheta,q)\,d\vartheta$$

$$= \int_{0}^{\pi/2} ce_{2n}(\vartheta,q)ce_{2m}(\vartheta,q)\,d\vartheta + \int_{0}^{\pi/2} ce_{2n}(\vartheta,q)ce_{2m}(\vartheta,q)\,d\vartheta$$

$$= \int_{0}^{\pi/2} ce_{2n}(\vartheta,q)ce_{2m}(\vartheta,q)\,d\vartheta + \int_{\pi/2}^{\pi} ce_{2n}(\vartheta,q)ce_{2m}(\vartheta,q)\,d\vartheta$$

$$= \int_{0}^{\pi} ce_{2n}(\eta,q)ce_{2m}(\eta,q)\,d\eta = \frac{\pi}{2}\delta_{mn}$$

(B.7) $\int_{-\frac{\pi}{2}}^{\frac{\pi}{2}} ce_{2n+1}(\vartheta,q)ce_{2m+1}(\vartheta,q)\,d\vartheta = \frac{\pi}{2}\delta_{mn}$ when $m,n = 0,1,2,\ldots$

$ce_{2n+1}(\eta,q)$ is symmetric about 0, yet anti-symmetric about $\pi/2$ (McLachlan, 1974); hence the above product becomes symmetric about both 0, and $\pi/2$

$$\int_{-\frac{\pi}{2}}^{\frac{\pi}{2}} ce_{2n+1}(\vartheta,q)ce_{2m+1}(\vartheta,q)\,d\vartheta = 2\int_{0}^{\frac{\pi}{2}} ce_{2n}(\vartheta,q)ce_{2m}(\vartheta,q)\,d\vartheta$$

$$= \int_{0}^{\pi/2} ce_{2n+1}(\vartheta,q)ce_{2m+1}(\vartheta,q)\,d\vartheta + \int_{0}^{\pi/2} ce_{2n+1}(\vartheta,q)ce_{2m+1}(\vartheta,q)\,d\vartheta$$

$$= \int_{0}^{\pi/2} ce_{2n+1}(\vartheta,q)ce_{2m+1}(\vartheta,q)\,d\vartheta + \int_{\pi/2}^{\pi} ce_{2n+1}(\vartheta,q)ce_{2m+1}(\vartheta,q)\,d\vartheta$$

$$= \int_{0}^{\pi} ce_{2n+1}(\eta,q)ce_{2m+1}(\eta,q)\,d\eta = \frac{\pi}{2}\delta_{mn}$$

(B.8) $\int_{-\frac{\pi}{2}}^{\frac{\pi}{2}} se_{2n+1}(\vartheta,q)se_{2m+1}(\vartheta,q)\,d\vartheta = \frac{\pi}{2}\delta_{mn}$ when $m,n = 0,1,2,\ldots$

Since $se_{2n+1}(\vartheta,q)$ is symmetric $\pi/2$ and $se_{2n+1}(\vartheta,q)se_{2m+1}(\vartheta,q)$ is an even function (McLachlan, 1974), therefore

$$\int_{-\frac{\pi}{2}}^{\frac{\pi}{2}} se_{2n+1}(\vartheta,q)se_{2m+1}(\vartheta,q)\,d\vartheta = 2\int_{0}^{\frac{\pi}{2}} se_{2n+1}(\vartheta,q)se_{2m+1}(\vartheta,q)\,d\vartheta$$

$$= \int_{0}^{\pi/2} se_{2n+1}(\vartheta,q)se_{2m+1}(\vartheta,q)\,d\vartheta + \int_{0}^{\pi/2} se_{2n+1}(\vartheta,q)se_{2m+1}(\vartheta,q)\,d\vartheta$$

$$= \int_{0}^{\pi/2} se_{2n+1}(\vartheta,q)se_{2m+1}(\vartheta,q)\,d\vartheta + \int_{\pi/2}^{\pi} se_{2n+1}(\vartheta,q)se_{2m+1}(\vartheta,q)\,d\vartheta$$

$$= \int_{0}^{\pi} se_{2n+1}(\eta,q)se_{2m+1}(\eta,q)\,d\eta = \frac{\pi}{2}\delta_{mn}$$

(B.9) $\int_{-\frac{\pi}{2}}^{\frac{\pi}{2}} se_{2n+2}(\vartheta,q)se_{2m+2}(\vartheta,q)\,d\vartheta = \frac{\pi}{2}\delta_{mn}$ when $m,n = 0,1,2,\ldots$

$se_{2n+2}(\eta,q)$ and $se_{2m+2}(\eta,q)$ are anti-symmetric about both 0 and $\pi/2$. Then $se_{2n+2}(\vartheta,q)se_{2m+2}(\vartheta,q)$ is symmetric about 0 and $\pi/2$; therefore

$$\int_{-\frac{\pi}{2}}^{\frac{\pi}{2}} se_{2n+2}(\vartheta,q)se_{2m+2}(\vartheta,q)\,d\vartheta = 2\int_{0}^{\frac{\pi}{2}} se_{2n+2}(\vartheta,q)se_{2m+2}(\vartheta,q)\,d\vartheta$$

$$= \int_{0}^{\pi/2} se_{2n+2}(\vartheta,q)se_{2m+2}(\vartheta,q)\,d\vartheta + \int_{0}^{\pi/2} se_{2n+2}(\vartheta,q)se_{2m+2}(\vartheta,q)\,d\vartheta$$

$$= \int_{0}^{\pi/2} se_{2n+2}(\vartheta,q)se_{2m+2}(\vartheta,q)\,d\vartheta + \int_{\pi/2}^{\pi} se_{2n+2}(\vartheta,q)se_{2m+2}(\vartheta,q)\,d\vartheta$$

$$= \int_{0}^{\pi} se_{2n+2}(\eta,q)se_{2m+2}(\eta,q)\,d\eta = \frac{\pi}{2}\delta_{mn}$$

(B.10) $\int_{-\frac{\pi}{2}}^{\frac{\pi}{2}} \underbrace{ce_{2n}(\vartheta, q) se_{2m+1}(\vartheta, q)}_{odd\ function}\, d\vartheta = 0$ when $m, n = 0,1,2, \ldots$

Integral of odd function over $\left[-\frac{\pi}{2}, \frac{\pi}{2}\right]$ or $\left[\frac{\pi}{2}, -\frac{\pi}{2}\right]$ is equal to zero.

(B.11) $\int_{-\frac{\pi}{2}}^{\frac{\pi}{2}} \underbrace{ce_{2n+1}(\vartheta, q) se_{2m+2}(\vartheta, q)}_{odd\ function}\, d\vartheta = 0$

Integral of odd function over $\left[-\frac{\pi}{2}, \frac{\pi}{2}\right]$ or $\left[\frac{\pi}{2}, -\frac{\pi}{2}\right]$ is equal to zero.

# APPENDIX C: HALF-RANGE EXPANSION OF ANGULAR MATHIEU FUNCTIONS

Given $\varepsilon_m = \begin{cases} 1 \ ; \ m = 0 \\ 2 \ ; \ m > 0 \end{cases}$ and $\delta_{mn} = \begin{cases} 1 \ ; \ n = m \\ 0 \ ; \ n \neq m \end{cases}$, then the series expansion of Mathieu function can be proved as follows

(C.1) Expansion of the Mathieu functions over the range $[0, \pi]$ and $[-\pi, 0]$

Either $\{ce_n(\vartheta, q); n = 0,1,2, \ldots\}$ or $\{se_n(\vartheta, q); n = 1,2,3, \ldots\}$ can form a complete orthogonal set of functions over the prescribed ranges.

*The expansion of $se_m(\vartheta, q)$ in terms of $ce_n(\vartheta, q)$:*

$$se_m(\vartheta, q) = \sum_{n=0}^{\infty} \mathfrak{C}_{mn}\, ce_n(\vartheta, q) \tag{C.1}$$

Multiplying Equation (C.1) by $ce_p(\vartheta, q)$ and integrating over $[0, \pi]$ yield

$$\int_0^{\pi} se_m(\vartheta, q)\, ce_p(\vartheta, q) d\vartheta = \sum_{n=0}^{\infty} \mathfrak{C}_{mn} \int_0^{\pi} ce_n(\vartheta, q) ce_p(\vartheta, q)\, d\vartheta$$

Hence we may set

$$\mathfrak{C}_{mn} = \frac{\int_0^{\pi} se_m(\vartheta,q) ce_n(\vartheta,q) d\vartheta}{\|ce_n(\vartheta,q)\|^2} = \frac{2}{\pi} \int_0^{\pi} se_m(\vartheta, q)\, ce_n(\vartheta, q) d\vartheta \tag{C.2}$$

Next let expand $se_m(\vartheta, q)$ and $ce_n(\vartheta, q)$ by their Fourier form, Equation (2.13); therefore

$$\mathfrak{C}_{mn} = \frac{2}{\pi} \sum_{s=0}^{\infty} \sum_{r=1}^{\infty} A_s^{(n)} B_r^{(m)} \int_0^{\pi} \cos s\vartheta \sin r\vartheta \, d\vartheta$$

As shown in (B.1) of Appendix B, the above equation becomes

$$\mathfrak{C}_{mn} = \frac{4}{\pi}\sum_{\substack{r=1,s=0\\ r+s=odd}}^{\infty}\left(\frac{r}{r^2-s^2}\right)A_s^{(n)}B_r^{(m)}; 0 \le \vartheta \le \pi \quad \text{(C.3)}$$

Later the expansion of $se_m(\vartheta, q)$ over $[-\pi, 0]$ may follow the same procedure.

Equation (C.1) is still valid, except

$$\mathfrak{C}_{mn} = -\frac{4}{\pi}\sum_{\substack{r=1,s=0\\ r+s=odd}}^{\infty}\left(\frac{r}{r^2-s^2}\right)A_s^{(n)}B_r^{(m)}; -\pi \le \vartheta \le 0 \quad \text{(C.4)}$$

because of $\int_a^b f(\vartheta)\, d\vartheta = -\int_b^a f(\vartheta)\, d\vartheta$

*The expansion of $ce_m(\vartheta, q)$ in terms of $se_n(\vartheta, q)$:*

$$ce_m(\vartheta, q) = \sum_{n=1}^{\infty}\mathfrak{D}_{mn}\, se_n(\vartheta, q) \quad \text{(C.5)}$$

Multiplying Equation (C.4) by $se_p(\vartheta, q)$ and integrating over $[0, \pi]$ yield

$$\int_0^{\pi} ce_m(\vartheta, q)\, se_p(\vartheta, q) d\vartheta = \sum_{n=1}^{\infty}\mathfrak{D}_{mn}\int_0^{\pi} se_n(\vartheta, q) se_p(\vartheta, q)\, d\vartheta$$

Hence

$$\mathfrak{D}_{mn} = \frac{\int_0^{\pi} ce_m(\vartheta,q) se_n(\vartheta,q) d\vartheta}{\|se_n(\vartheta,q)\|^2} = \frac{2}{\pi}\int_0^{\pi} ce_m(\vartheta, q)\, se_n(\vartheta, q) d\vartheta \quad \text{(C.6)}$$

The integrands, except indices being switched, of Equations (C.2) and (C.6) are similar. Then without elaboration, Equation (C.6) becomes

$$\mathfrak{D}_{mn} = \frac{4}{\pi}\sum_{\substack{r=1,s=0\\ r+s=odd}}^{\infty}\left(\frac{r}{r^2-s^2}\right)A_s^{(m)}B_r^{(n)}; 0 \le \vartheta \le \pi \quad \text{(C.7)}$$

$$\mathfrak{D}_{mn} = -\frac{4}{\pi}\sum_{\substack{r=1,s=0\\ r+s=odd}}^{\infty}\left(\frac{r}{r^2-s^2}\right)A_s^{(m)}B_r^{(n)}; -\pi \le \vartheta \le 0 \quad \text{(C.8)}$$

(C.2) Expansion of the Mathieu functions over the range $\left[-\frac{\pi}{2},\frac{\pi}{2}\right]$ and $\left[\frac{\pi}{2},-\frac{\pi}{2}\right]$

Any angular function $f(\vartheta,q)$ over the half-ranges $\left[-\frac{\pi}{2},\frac{\pi}{2}\right]$ and $\left[\frac{\pi}{2},-\frac{\pi}{2}\right]$ may be expressed in a series expansion by the sets of $\{ce_{2n}(\vartheta,q), se_{2n+1}(\vartheta,q); n = 0,1,2,\dots\}$ or $\{ce_{2n+1}(\vartheta,q), se_{2n+2}(\vartheta,q); n = 0,1,2,\dots\}$ since they are the complete orthogonal sets over the prescribed ranges.

*The expansion of $ce_{2m+1}(\vartheta,q)$ in terms of $ce_{2n}(\vartheta,q)$:*

$$ce_{2m+1}(\vartheta,q) = \sum_{n=0}^{\infty} \mathfrak{M}_{mn}\, ce_{2n}(\vartheta,q) \tag{C.9}$$

Multiplying Equation (C.9) by $ce_{2p}(\vartheta,q)$ and integrating over $\left[-\frac{\pi}{2},\frac{\pi}{2}\right]$ yield

$$\int_{-\frac{\pi}{2}}^{\frac{\pi}{2}} ce_{2m+1}(\vartheta,q)\, ce_{2p}(\vartheta,q)d\vartheta = \sum_{n=0}^{\infty} \mathfrak{M}_{mn} \int_{-\frac{\pi}{2}}^{\frac{\pi}{2}} ce_{2n}(\vartheta,q) ce_{2p}(\vartheta,q)\, d\vartheta$$

Hence we may set

$$\mathfrak{M}_{mn} = \frac{\int_{-\frac{\pi}{2}}^{\frac{\pi}{2}} ce_{2m+1}(\vartheta,q) ce_{2n}(\vartheta,q)d\vartheta}{\|ce_{2n}(\vartheta,q)\|^2} = \frac{2}{\pi}\int_{-\frac{\pi}{2}}^{\frac{\pi}{2}} ce_{2m+1}(\vartheta,q)\, ce_{2n}(\vartheta,q)d\vartheta \tag{C.10}$$

Next let expand $ce_{2m+1}(\vartheta,q)$ and $ce_{2n}(\vartheta,q)$ by their Fourier form, Equation (2.13); therefore

$$\mathfrak{M}_{mn} = \frac{2}{\pi}\sum_{s=0}^{\infty}\sum_{r=1}^{\infty} A_{2r+1}^{(2m+1)} A_{2\mathrm{s}}^{(2n)} \int_{-\pi/2}^{\pi/2} \cos(2r+1)\vartheta \sin 2s\vartheta\, d\vartheta$$

As shown in (B.2) of Appendix B, the above equation becomes

$$\mathfrak{M}_{mn} = \frac{2}{\pi}\sum_{r=0}^{\infty}\sum_{s=0}^{\infty}\left[\frac{(-1)^{r-s}}{2r-2s+1} + \frac{(-1)^{r+s}}{2r+2s+1}\right] A_{2r+1}^{(2m+1)} A_{2s}^{(2n)}; -\pi/2 \le \vartheta \le \pi/2 \tag{C.11}$$

Later the expansion of $ce_{2m+1}(\vartheta, q)$ over $[\pi/2\,, -\pi/2]$ may follow the same procedure. Equation (C.9) is still valid, except

$$\mathfrak{M}_{mn} = -\frac{2}{\pi}\sum_{r=0}^{\infty}\sum_{s=0}^{\infty}\left[\frac{(-1)^{r-s}}{2r-2s+1} + \frac{(-1)^{r+s}}{2r+2s+1}\right] A_{2r+1}^{(2m+1)} A_{2s}^{(2n)}; \pi/2 \le \vartheta \le -\pi/2 \qquad \text{(C.12)}$$

because of $\int_a^b f(\vartheta)\, d\vartheta = -\int_b^a f(\vartheta)\, d\vartheta$

*The expansion of $se_{2m+2}(\vartheta, q)$ in terms of $se_{2n+1}(\vartheta, q)$:*

$$se_{2m+2}(\vartheta, q) = \sum_{n=0}^{\infty} \mathfrak{N}_{mn}\, se_{2n+1}(\vartheta, q) \qquad \text{(C.13)}$$

Multiplying Equation (C.13) by $se_{2p+1}(\vartheta, q)$ and integrating over $\left[-\frac{\pi}{2}, \frac{\pi}{2}\right]$ yield

$$\int_{-\frac{\pi}{2}}^{\frac{\pi}{2}} se_{2m+2}(\vartheta, q)\, se_{2p+1}(\vartheta, q) d\vartheta = \sum_{n=0}^{\infty} \mathfrak{N}_{mn} \int_{-\frac{\pi}{2}}^{\frac{\pi}{2}} se_{2n+1}(\vartheta, q) se_{2p+1}(\vartheta, q)\, d\vartheta$$

Hence we may set

$$\mathfrak{N}_{mn} = \frac{\int_{-\frac{\pi}{2}}^{\frac{\pi}{2}} se_{2m+2}(\vartheta,q) se_{2n+1}(\vartheta,q) d\vartheta}{\|se_{2n+1}(\vartheta,q)\|^2} = \frac{2}{\pi}\int_{-\frac{\pi}{2}}^{\frac{\pi}{2}} se_{2m+2}(\vartheta, q)\, se_{2n+1}(\vartheta, q) d\vartheta \qquad \text{(C.14)}$$

Next let expand $se_{2m+2}(\vartheta, q)$ and $se_{2n+1}(\vartheta, q)$ by their Fourier form, Equation (2.13); therefore

$$\mathfrak{N}_{mn} = \frac{2}{\pi}\sum_{s=0}^{\infty}\sum_{r=1}^{\infty} B_{2r+2}^{(2m+2)} B_{2s+1}^{(2n+1)} \int_{-\pi/2}^{\pi/2} \sin(2r+2)\vartheta \sin(2r+1)\vartheta\, d\vartheta$$

As shown in (B.3) of Appendix B, the above equation becomes

$$\mathfrak{N}_{mn} = \frac{2}{\pi}\sum_{r=0}^{\infty}\sum_{s=0}^{\infty}\left[\frac{(-1)^{r-s}}{2r-2s+1} + \frac{(-1)^{r+s}}{2r+2s+3}\right] B_{2r+2}^{(2m+2)} B_{2s+1}^{(2n+1)}; -\pi/2 \le \vartheta \le \pi/2 \qquad \text{(C.15)}$$

Later the expansion of $se_{2m+2}(\vartheta, q)$ over $[\pi/2\,, -\pi/2]$ may follow the same procedure. Equation (C.13) is still valid, except

$$\mathfrak{N}_{mn} = -\frac{2}{\pi}\sum_{r=0}^{\infty}\sum_{s=0}^{\infty}\left[\frac{(-1)^{r-s}}{2r-2s+1} + \frac{(-1)^{r+s}}{2r+2s+3}\right] B_{2r+2}^{(2m+2)} B_{2s+1}^{(2n+1)}; \pi/2 \le \vartheta \le -\pi/2 \qquad \text{(C.16)}$$

*The expansion of $ce_{2m}(\vartheta, q)$ in terms of $ce_{2n+1}(\vartheta, q)$:*

$$ce_{2m}(\vartheta, q) = \sum_{n=0}^{\infty} \mathfrak{Y}_{mn}\, ce_{2n+1}(\vartheta, q) \qquad \text{(C.17)}$$

Multiplying Equation (C.17) by $ce_{2p+1}(\vartheta, q)$ and integrating over $\left[-\frac{\pi}{2}, \frac{\pi}{2}\right]$ yield

$$\int_{-\frac{\pi}{2}}^{\frac{\pi}{2}} ce_{2m}(\vartheta, q)\, ce_{2p+1}(\vartheta, q) d\vartheta = \sum_{n=0}^{\infty} \mathfrak{Y}_{mn} \int_{-\frac{\pi}{2}}^{\frac{\pi}{2}} ce_{2n+1}(\vartheta, q) ce_{2p+1}(\vartheta, q)\, d\vartheta$$

Hence we may set

$$\mathfrak{Y}_{mn} = \frac{\int_{-\frac{\pi}{2}}^{\frac{\pi}{2}} ce_{2m}(\vartheta,q) ce_{2n+1}(\vartheta,q) d\vartheta}{\|ce_{2n+1}(\vartheta,q)\|^2} = \frac{2}{\pi}\int_{-\frac{\pi}{2}}^{\frac{\pi}{2}} ce_{2m}(\vartheta, q)\, ce_{2n+1}(\vartheta, q) d\vartheta \qquad \text{(C.18)}$$

The integrands, except indices being switched, of Equations (C.10) and (C.18) are similar. Then without elaboration, Equation (C.18) becomes

$$\mathfrak{Y}_{mn} = \frac{2}{\pi}\sum_{r=0}^{\infty}\sum_{s=0}^{\infty}\left[\frac{(-1)^{r-s}}{2r-2s+1} + \frac{(-1)^{r+s}}{2r+2s+1}\right] A_{2r+1}^{(2n+1)} A_{2s}^{(2m)}; -\pi/2 \le \vartheta \le \pi/2 \qquad \text{(C.19)}$$

$$\mathfrak{Y}_{mn} = -\frac{2}{\pi}\sum_{r=0}^{\infty}\sum_{s=0}^{\infty}\left[\frac{(-1)^{r-s}}{2r-2s+1} + \frac{(-1)^{r+s}}{2r+2s+1}\right] A_{2r+1}^{(2n+1)} A_{2s}^{(2m)}; \pi/2 \le \vartheta \le -\pi/2 \qquad \text{(C.20)}$$

*The expansion of $se_{2m+1}(\vartheta, q)$ in terms of $se_{2n+2}(\vartheta, q)$:*

$$se_{2m+1}(\vartheta, q) = \sum_{n=0}^{\infty} \mathfrak{Z}_{mn}\, se_{2n+2}(\vartheta, q) \qquad \text{(C.21)}$$

Multiplying Equation (C.21) by $se_{2p+2}(\vartheta, q)$ and integrating over $\left[-\frac{\pi}{2}, \frac{\pi}{2}\right]$ yield

$$\int_{-\frac{\pi}{2}}^{\frac{\pi}{2}} se_{2m+1}(\vartheta, q)\, se_{2p+2}(\vartheta, q) d\vartheta = \sum_{n=0}^{\infty} 3_{mn} \int_{-\frac{\pi}{2}}^{\frac{\pi}{2}} se_{2n+2}(\vartheta, q) se_{2p+2}(\vartheta, q)\, d\vartheta$$

Hence we may set

$$3_{mn} = \frac{\int_{-\frac{\pi}{2}}^{\frac{\pi}{2}} se_{2m+1}(\vartheta,q) se_{2n+2}(\vartheta,q) d\vartheta}{\|se_{2n+2}(\vartheta,q)\|^2} = \frac{2}{\pi} \int_{-\frac{\pi}{2}}^{\frac{\pi}{2}} se_{2m+1}(\vartheta, q)\, se_{2n+2}(\vartheta, q) d\vartheta \qquad \text{(C.22)}$$

The integrands, except indices being switched, of Equations (C.14) and (C.22) are similar. Then without elaboration, Equation (C.22) becomes

$$3_{mn} = \frac{2}{\pi} \sum_{r=0}^{\infty} \sum_{s=0}^{\infty} \left[\frac{(-1)^{r-s}}{2r-2s+1} + \frac{(-1)^{r+s}}{2r+2s+3}\right] B_{2r+2}^{(2n+2)} B_{2s+1}^{(2m+1)}; -\pi/2 \le \vartheta \le \pi/2 \qquad \text{(C.23)}$$

$$3_{mn} = -\frac{2}{\pi} \sum_{r=0}^{\infty} \sum_{s=0}^{\infty} \left[\frac{(-1)^{r-s}}{2r-2s+1} + \frac{(-1)^{r+s}}{2r+2s+3}\right] B_{2r+2}^{(2n+2)} B_{2s+1}^{(2m+1)}; \pi/2 \le \vartheta \le -\pi/2 \qquad \text{(C.24)}$$